

Acquisitions and Bibliographic Services Branch

395 Wellington Street Ottawa, Ontario K1A 0N4 Bibliothèque nationale du Canada

Direction des acquisitions et des services bibliographiques

395, rue Wellington Ottawa (Ontario) K1A 0N4

Your life Votre référence

Our lile Notre référence

NOTICE

The quality of this microform is heavily dependent upon the quality of the original thesis submitted for microfilming. Every effort has been made to ensure the highest quality of reproduction possible.

La qualité de cette microforme dépend grandement de la qualité de la thèse soumise au microfilmage. Nous avons tout fait pour assurer une qualité supérieure de reproduction.

AVIS

If pages are missing, contact the university which granted the degree.

S'il manque des pages, veuillez communiquer avec l'université qui a conféré le grade.

Some pages may have indistinct print especially if the original pages were typed with a poor typewriter ribbon or if the university sent us an inferior photocopy.

La qualité d'impression de certaines pages peut laisser à désirer, surtout si les pages originales ont été dactylographiées à l'aide d'un ruban usé ou si l'université nous a fait parvenir une photocopie de qualité inférieure.

Reproduction in full or in part of this microform is governed by the Canadian Copyright Act, R.S.C. 1970, c. C-30, and subsequent amendments. La reproduction, même partielle, de cette microforme est soumise à la Loi canadienne sur le droit d'auteur, SRC 1970, c. C-30, et ses amendements subséquents.



DYADIC MATRIX CONVERTER THEORY

Development, and Application to Voltage-Source-Converter Type Matrix Converter

Mehrdad Kazerani

B.Sc. Shiraz University, Iran, M.Eng. Concordia University, Canada

A Thesis submitted to the Faculty of Graduate Studies and Research in Partial fulfilment of the requirements for the degree of Doctor of Philosophy

Department of Electrical Engineering McGill University Montréal, Québec, Canada

February 1995

© Mehrdad Kazerani



Acquisitions and Bibliographic Services Branch

395 Wellington Street Ottawa, Ontario K1A 0N4 Bibliothèque nationale du Canada

Direction des acquisitions et des services bibliographiques

395, rue Wellington Ottawa (Ontario) K1A 0N4

Your file Votre référence

Our lile Notre référence

THE AUTHOR HAS GRANTED AN IRREVOCABLE NON-EXCLUSIVE LICENCE ALLOWING THE NATIONAL LIBRARY OF CANADA TO REPRODUCE, LOAN, DISTRIBUTE OR SELL COPIES OF HIS/HER THESIS BY ANY MEANS AND IN ANY FORM OR FORMAT, MAKING THIS THESIS AVAILABLE TO INTERESTED PERSONS.

L'AUTEUR A ACCORDE UNE LICENCE IRREVOCABLE ET NON EXCLUSIVE PERMETTANT A LA BIBLIOTHEQUE NATIONALE DU CANADA DE REPRODUIRE, PRETER, DISTRIBUER OU VENDRE DES COPIES DE SA THESE DE QUELQUE MANIERE ET SOUS QUELQUE FORME QUE CE SOIT POUR METTRE DES EXEMPLAIRES DE CETTE THESE A LA DISPOSITION DES PERSONNE INTERESSEES.

THE AUTHOR RETAINS OWNERSHIP OF THE COPYRIGHT IN HIS/HER THESIS. NEITHER THE THESIS NOR SUBSTANTIAL EXTRACTS FROM IT MAY BE PRINTED OR OTHERWISE REPRODUCED WITHOUT HIS/HER PERMISSION.

L'AUTEUR CONSERVE LA PROPRIETE DU DROIT D'AUTEUR QUI PROTEGE SA THESE, NI LA THESE NI DES EXTRAITS SUBSTANTIELS DE CELLE-CI NE DOIVENT ETRE IMPRIMES OU AUTREMENT REPRODUITS SANS SON AUTORISATION.

ISBN 0-612-05730-5



DYADIC MATRIX CONVERTER THEORY

Development, and Application to Voltage-Source-Converter Type Matrix Converter

Mehrdad Kazerani

B.Sc. Shiraz University, Iran M.Eng. Concordia University, Canada

A Thesis submitted to the Faculty of Graduate Studies and Research in partial fulfilment of the requirements for the degree of Doctor of Philosophy

Department of Electrical Engineering
McGill University
Montréal, Québec, Canada

February 1995

© Mehrdad Kazerani, 1995

For the past twenty years, the theoretical advance of the matrix converters has been impeded by the complexity arising from the time-varying trigonometric functions in their transformation matrix. In addition, the switching difficulties associated with the bidirectional switches have complicated the practical implementation of this class of converters.

In this thesis, the dyadic matrix structure and the a-b-c to d-q-0 transformation have been melded together to develop the dyadic matrix converter theory which is a generalized theory for the three-phase to three-phase matrix converters.

The thesis addresses the zero-sequence interaction in the matrix converters and the role of the zero-sequence elements in the Displacement Power Factor (DPF) correction on the utility-side, based on the Static VAR Controller (SVC) principle. Also, it is proved that using all the control degrees of freedom available, the dual condition of Unity Displacement Power Factor (UDPF) on side-1 and Field Vector Control (FVC) on side-2 can be established.

In this thesis, a new matrix converter topology, based on the three-phase voltage-source converters, has been proposed in which the switching difficulties reported in the conventional nine-bidirectional-switch topology have been bypassed.

The theoretical expectations have been verified by the simulation as well as experimental tests on a laboratory prototype of the new matrix converter topology composed of three units of voltage-source converters each rated at 1 kVA.

Bien que la modélisation des convertisseurs matriciels ait avancé depuis une vingtaine d'années, on se heurte toujours aux difficultés engendrées par les équations aux coéfficients variant trigonométriquement et par leur matrice de transformation. D'autre part, l'implantation de cette classe de convertisseurs est rendue difficile à cause des exigences sévères sur les commutateurs bidirectionnels.

Dans cette thèse nous contournons ces obstacles en développant d'une part une structure matricielle dyadique et d'autre part en appliquant la transformation a-L-c à d-q-0. Ces apports contribuent à une théorie généralisé des convertisseurs triphasé à triphasé.

On s'attaque à deux problèmes pratiques particuliers: l'influence des éléments homopolaires sur le comportement du convertisseur, et le rôle des éléments homopolaires dans la stratégie de correction du facteur de puissance de déplacement du coté de l'utilité publique. Cette dernière stratégie est basée sur les principes de correction utilisés par les compensateurs statiques. De plus, on peut maintenant prouver que le problème offre assez de degrés de liberté pour maintenir à la fois un facteur de puissance de déplacement unitaire au primaire et un asservissemnt du vecteur de champs au secondaire.

Une nouvelle topologie de convertisseur matricielle est proposé dans cette thèse, basée sur celle des convertisseurs triphasés de type source de tension. Celleci évite la plupart des difficultés associées à la topologie conventionnelle à neuf commutateurs bi-directionnels.

Les prédictions théoriques ont été vérifiées avec des simulations sur ordinateur, et avec des observations sur un appareil prototype composé de trois modules de convertisseurs de type source de tension dimensionnés de l'ordre du kVA.

ACKNOWLEDGEMENTS

Thank God for letting my dream of pursuing graduate study come true.

My sincere thanks go to Professor Dr. Boon-Teck Ooi, my knowledgable research supervisor, for his wise guidance, continuous encouragement, generous support, and warm friendship, throghout the course of this research. He kindly taught me to think hard and work hard and try to support new ideas with fundamental theory and experimentation. He eased my financial worries through offering an NSERC grant.

I am very thankful to Professor Dr. F.D. Galiana and Professor Dr. H.C. Lee for their kindness and support during my study. I would like to thank Professor Dr. Z. Wolanski for the very useful discussions I had with him.

I am grateful to my friends and colleagues in power group. I learnt a lot from Dr. X. Wang, Dr. Y. Gue, Prof. Z.C. Zhang, and Mr. B. Mwinyiwiwa. I also enjoyed the warm friendship of Mr. D. Olivera, Mr. S. Demassi, and Dr. H. Javidi. I would like to extend my thanks to the electric workshop technicians, especially Mr. J. Mui, and Electrical Engineering Department secretaries, especially Mrs. T. Hyland, Mrs. R. Pinzarrone, and Ms. C. Bethelmy for their unconditional help whenever I asked for it. Many thanks to Dr. M. Huneault for making an expert French translation of the Abstract.

I would like to thank the Iranian Ministry of Culture and Higher Education, for its support without which it would not be possible for me to start and continue my graduate studies.

I would like to thank my wonderful wife, Parichehr, and sons, Ali and Iman, without their love, support and sacrifices I would never be able to achieve my goals. My special thanks go to my father for his constant support and encouragement, and my mother for his never-ending love.

TABLE OF CONTENTS

	i
RÉSUMÉ	ii
ACKNOWLEDGEMENTS	iii
TABLE OF CONTENTS	iv
LIST OF ILLUSTRATIONS	viii
NOMENCLATURE	xi
CHAPTER 1 INTRODUCTION	1
1.1 An Introduction to Matrix Converters	1
1.2 Historical Background	11
1.2.1 Early History	11
1.2.2 Recent History	11
1.2.3 New Era	14
1.3 Organization, Scope, and Contributions	17
1.3.1 Dyadic Matrix Converter Theory	18
1.3.2 Voltage-Source-Converter Type Matrix Convert	ter 19
Under the Dyadic Matrix Converter Theory Co	ntrol
1.3.3 Implementation of the New Matrix Converter S	System 20
Under the Dyadic Matrix Converter Theory Co	ntrol
CHAPTER 2 DYADIC MATRIX CONVERTER THEORY	22
2.1 Introduction	22
2.2 Dyadic Matrix Transformation	24
2.2.1 Regrouping Inner Vector Products from Outer Product	Vector 25
2.3 Vector Spaces of Side-1 and Side-2 Voltages and Curr	rents 26
2.3.1 Orthonormal Properties of Base Vectors	27
2.4 Synthesis of the Transformation Matrix	28
2.4.1 Examples for Transformation Matrix Synthesis	29
2.4.1.1 Example 1	29
2.4.1.2 Example 2	30
2.4.1.3 Example 3	31
2.4.1.4 Example 4	32
2.4.1.5 Example 5	32
2.5 Park's Transformation	34

	TABLE OF CONTENTS	v
2.6 2.7	Transformation Matrix in D-Q-0 Frame Summary	35 38
CHAPTER 3	TRANSFORMATION MATRIX STRUCTURE	39
3.1	Introduction	39
3.2	Network of Side-1 as Viewed from Side-2	40
3.3	Integration of Side-1 and Side-2 Networks	45
3.4	Diagonal Structure	46
	$3.4.1 p_{11} = p_{22} = P_f$	48
	$3.4.2 p_{11} = -p_{22} = P_f$	49
	3.4.3 $p_{11} \neq \pm p_{22}$	51
3.5	Unity Displacement Power Factor with Diagonal $[P]_{2\times 2}$ -Matrix	52
3.6	Summary: Properties of Diagonal $[P]_{2\times 2}$ -Matrix	55
3.7	Full $[P]_{2\times 2}$ -Matrix	56
	3.7.1 Non-Conjugate Rotation	58
	3.7.2 Conjugate Rotation	59
	3.7.3 General Full $[P]_{2\times 2}$ -Matrix	61
3.8	Unity Displacement Power Factor (UDPF) with Full $[P]_{2\times 2}$ -Matrix	63
3.9	Summary: Properties of Full $[P]_{2\times 2}$ -Matrix	65
3.10	Summary	66
CHAPTER 4	ZERO-SEQUENCE INTERACTION IN MATRIX CONVERTED	RS 69
4.1	Introduction	69
4,2	System Equations Including Zero-Sequence	72
4.3	Decoupling the Zero-Sequence Interaction	75
	4.3.1 Polar Representation	77
4.4	Referring the Network of Side-1 to Side-2	78
	4.4.1 SVC Voltage	79
4.5	Integrating the Networks of Side-1 and Side-2	80
	4.5.1 Zero Components of Voltage and Current	83
4.6	$[H]$ -Matrix Associated with the $[P]_{2\times 3}$ -Matrix	84
4.7	Summary	86
CHAPTER 5	FEASIBILITY OF BOTH UNITY DISPLACEMENT POWER FACTOR AND FIELD VECTOR CONTROL	88
5.1	Introduction	88
5.2	Dual Condition of UDPF on Side-1 and FVC on Side-2	91
	5.2.1 Filter Capacitors Neglected	93

	TABLE OF CONTENTS	vi
5.3	5.2.2 Filter Capacitors Considered Summary	100 101
CHAPTER 6	VOLTAGE-SOURCE-CONVERTER TYPE MATRIX CONVERTER UNDER THE DYADIC MATRIX CONVERTER THEORY CONTROL	103
6.1	Introduction	103
6,2	Voltage-Source-Converter Type Matrix Converter	104
6.3	Mathematical Model	109
6.4		116
6.5	Matrix Converter Controllers	118
	6.5.1 M_f -Control	118
	6.5.2 γ-Control	119
	6.5.3 φ-Control	119
	6.5.4 <i>M</i> _a -Control	120
6.6	Unwanted Components in the Branch Currents	122
6.7	Elimination of Unwanted Components in the Branch Currents	125
	6.7.1 Principle of Operation	126
6.8	Summary	133
CHAPTER 7	RESULTS	134
7.1		134
7.2	DC Bias Voltage Control	135
7.3	Displacement Power Factor Control on Side-1	139
7.4	Unwanted Components in the Side-1 Branch Currents and the Side-2 AC Voltages	144
7.5	Dual Field Vector and Unity Displacement Power Factor	146
	Control 7.5.1 Open-Loop Experiment	147
	7.5.2 Closed-Loop Digital Simulation	150
7.6	Elimination of the Unwanted Components	151
	7.6.1 Branch Current Waveform	152
	7.6.2 Side-2 AC Voltage Waveform	153
	7.6.2.1 $f_1 = 60$ Hz and $f_2 = 30$ Hz	153
	7.6.2.2 $f_1 = 60$ Hz and $f_2 = 60$ Hz	155
	7.6.2.3 $f_1 = 60 \text{ Hz and } f_2 = 120 \text{ Hz}$	156
7.7	7.6.3 Dual Condition of UDPF on Side-1 and FVC on Side-2	158
7.7	Summary	159
	CONCLUSIONS	161
8.1	Development of Dyadic Matrix Converter Theory	161
8.2	Introduction of a New Matrix Converter Topology Based on the	163

	TABLE OF CONTENTS	<u>vii</u>
	Three-Phase Voltage-Source PWM Converters	
8.3	Implementation of Voltage-Source-Converter Type Matrix Converter under the Dyadic Matrix Converter Theory Control	163
8.4	Suggestions for Future Work	164
APPENDIX	A PROPERTIES OF $[P]_{2\times 2}$ -MATRIX WITH $p_{11} = p_{22} = 0$,	166
	$p_{12} \neq 0 \text{ AND } p_{21} \neq 0$	
APPENDIX	B [H]-MATRIX OF M. VENTURINI AND A. ALESINA'S MATRIX CONVERTER	170
APPENDIX	C $[H]$ -MATRIX OF L. HUBER AND D. BOROJEVIC'S MATRIX CONVERTER	173
APPENDIX	D CLOSED-LOOP CONTROL OF THE DC BIAS VOLTAGE ON SIDE-2	175
APPENDIX	E IMPLEMENTATION OF: VOLTAGE-SOURCE-CONVERTE TYPE MATRIX CONVERTER	R 183
E.1	Introduction	183
E.2	Power Circuit and Snubber Protection	184
E.3	Base Driver for the BJT Switches	185
E.4	Gating Signal Generation and Interlock Circuit	186
E.5		189
E.6		191
E.7	Synchronization Circuits	197
APPENDIX	F PARAMETERS OF THE SYSTEM OF FIG. 6-1	203
APPENDIX	G PARAMETERS OF THE SYSTEM OF FIG. 6-7	204
APPENDIX	THE PARAMETERS OF THE TRANSFORMERS $T_{aa},,T_{cc}$	205
REFEREN	CES	200

LIST OF ILLUSTRATIONS

CHAPTER 1	:	
Fig.1-1	Three-phase to three-phase static frequency changer.	2
Fig.1-2	Classes of static frequency changers.	2 4
Fig.1-3	Three-phase to three-phase NCC.	5
Fig.1-4	Three-phase to three-phase FCC.	5 6 7
Fig.1-5	Three-phase to three-phase matrix converter.	
Fig.1-6	Bidirectional switch realizations.	8
CHAPTER 2	:	
Fig.2-1	Three-phase to three-phase matrix converter.	23
Fig.2-2	Current and voltage transformations.	23
CHAPTER 3	:	
Fig.3-1	Matrix converter with the networks of side-1 and side-2.	41
CHAPTER 4	:	
Fig.4-1	Matrix converter with the networks of side-1 and side-2 including the side-2 capacitors.	70
Fig.4-2	Matrix converter with the networks of side-1 and side-2 (side-2 capacitors connected in four-wire wye).	71
Fig.4-3	Single-line equivalent circuit diagram of the system of Fig. 4-2 as viewed from side-2.	82
Fig.4-4	Phasor diagram of Fig. 4-3.	83
CHAPTER 5	:	
Fig.5-1	Single-line equivalent circuit diagram of side-1 of the system of Fig. 4-2.	89
Fig.5-2	Phasor diagram of Fig. 5-1.	89
Fig.5-3	Single-line equivalent circuit diagram of side-2 of the system of Fig. 4-2.	90
Fig.5-4	Phasor diagram of Fig. 5-3.	9:
Fig.5-5	Single-line equivalent circuit diagram of Fig. 4-3 with the filter capacitors neglected.	94
Fig.5-6	Phasor diagram of Fig. 5-5 for UDPF on side-1 and FVC on side-2.	99
Fig.5-7	Phasor diagram of Fig. 4-4 for UDPF on side-1 and FVC on side-2.	100

CHAPTER 6:

	LIST OF ILLUSTRATIONS	ix
Fig.6-1	Voltage-source-converter type matrix converter with the networks on side-1 and side-2.	105
Fig.6-2	Conventional nine-bidirectional-switch matrix converter with the networks on side-1 and side-2.	106
Fig.6-3	Typical waveform of the voltages on side-2 of the voltage-source-converter type matrix converter.	108
Fig.6-4	Equivalent circuit diagram of the system of Fig. 6-1.	114
Fig.6-5	Quadrature relationship of the side-1 current and the voltage projected on side-1 due to the dc bias voltages of side-2.	121
Fig.6-6	M_{\bullet} -control and its effect on DPF on side-1.	122
Fig.6-7	Voltage-source-converter type matrix converter with the trapping transformers.	127
Fig.6-8	Equivalent circuit diagram of the transformers used in Fig. 6-7.	128
CHAPTER	k 7:	
Fig.7-1	Quadrature relationship of $v_{1a\phi}$ and i_{1a} for UDPF on side-1.	137
Fig.7-2	Quadrature relationship of $v_{1a\phi}$ and i_{1a} for lagging DPF on side-1.	137
Fig.7-3	Step response of side-2 dc bias voltage.	138
Fig.7-4	Lagging DPF on side-1 for $M_f = 0$ and $M_{\varphi} = 0.2$.	139
Fig.7-5	UDPF on side-1 for $M_f = 0$ and $M_{\odot} = 0.55$.	140
Fig.7-6	Leading DPF on side-1 for $M_f = 0$ and $M_{\phi} = 0.6$.	140
Fig.7-7	Lagging DPF on side-1 for $M_f = 0.22$ and $M_{\infty} = 0.39$.	141
Fig.7-8	UDPF on side-1 for $M_f = 0.22$ and $M_{\odot} = 0.55$.	142
Fig.7-9	Leading DPF on side-1 for $M_f = 0.22$ and $M_{\phi} = 0.66$.	142
Fig.7-10	M_{\bullet} and I_{1r} vs. M_{f} for UDPF on side-1.	143
Fig.7-11	Unwanted components absent from the side-1 branch	145
Ü	currents for $M_f = 0$ and $M_{\phi} = 0.55$.	
Fig.7-12	Unwanted components present in the side-1 branch currents for $M_f = 0.44$ and $M_{\infty} = 0.33$.	146
Fig.7-13	Unwanted components present in the side-2 ac voltages.	147
Fig.7-14	Simulating the induced emf behind the reactance of	148
J	the synchronous motor.	
Fig.7-15	Dual condition of UDPF on side-1 and FVC on side-2.	149
Fig.7-16	Closed-loop control systems for UDPF on side-1 and FVC on side-2.	151
Fig.7-17	Simulation results: Dual condition of UDPF on side-1 and FVC on side-2.	152
Fig.7-18	Elimination of unwanted components in side-1 branch currents	. 153

	LIST OF ILLUSTRATIONS	<u>x</u>
Fig.7-19	Elimination of unwanted components in side-2 ac voltages.	154
•	for $f_1 = 60$ Hz, $f_2 = 30$ Hz, and $C = 50 \mu$ F.	
Fig.7-20	Elimination of unwanted components in side-2 ac voltages	155
-	for $f_1 = 60$ Hz, $f_2 = 30$ Hz, and $C = 200 \mu F$.	
Fig.7-21	Elimination of unwanted components in side-2 ac voltages	156
J	for $f_1 = 60$ Hz and $f_2 = 60$ Hz.	
Fig.7-22	Elimination of unwanted components in side-2 ac voltages	157
J	for $f_1 = 60$ Hz and $f_2 = 120$ Hz.	
Fig.7-23	Dual condition of UDPF on side-1 and FVC on side-2.	158
0		
APPENDIX	K D;	
Fig.D-1	Equivalent circuit diagram of Fig. 6-4 simplified for	176
	the case of pure dc voltages on side-2.	
Fig.D-2	Closed-loop control system of side-2 dc bias voltage.	181
Fig.D-3	Derivation of the side-2 dc bias voltage signal.	182
APPENDIX	K E:	
Fig.E-1	Overall view of the experimental set-up.	184
Fig.E-2	Control unit.	185
Fig.E-3	Power circuit and snubber protection scheme.	186
Fig.E-4	Base driver unit.	187
Fig.E-5	Gating signal generator and interlock circuit.	188
Fig.E-6	Dc bias voltage control system.	190
Fig.E-7	Elementary modulating signal generator circuit.	192
Fig.E-8	A/D converter, latch, and adder for φ-control.	194
Fig.E-9	A/D converter, latch, and adder for γ -control.	195
Fig.E-10	Total modulating signal generator circuit.	196
Fig.E-11	Synchronization circuit for $\cos \omega_1 t$ waveforms.	198
Fig.E-12	$\cos \omega_1 t$ waveforms generator circuit.	199
Fig.E-13	Synchronization signal generator for $\cos(\omega_1 + \omega_2)t$ waveforms.	201
Fig.E-14	Synchronization circuit for $\cos(\omega_1 + \omega_2)t$ waveforms.	202
	• • • • • • • • • • • • • • • • • • • •	

NOMENCLATURE

ω₁ Side-1 angular Frequency

 ω_2 Side-2 angular frequency

 P_1, P_2 Real power of side-1 and side-2

NCC Naturally-Commutated Cycloconverter

FCC Forced-Commutated Cycloconverter

GTO Gate-Turn-Off thyristor

BJT Bipolar Junction Transistor

MOSFET Metal Oxide Semiconductor Field Effect Transistor

IGBT Insulated-Gate Bipolar Transistor

 $SW_{aa}, ..., SW_{cc}$ Bidirectional switches of matrix converter

[S] Switching function matrix

 v_{1a}, v_{1b}, v_{1c} Instantaneous side-1 terminal voltages

 v_{2a}, v_{2b}, v_{2c} Instantaneous side-2 terminal voltages

 i_{1a}, i_{1b}, i_{1c} Instantaneous side-1 currents

 i_{2a}, i_{2b}, i_{2c} Instantaneous side-2 currents

[H] Transformation matrix of matrix converter in a-b-c frame

 $[H_r]$ Transformation matrix of rectifier block

 $[H_i]$ Transformation matrix of inverter block

SCR Silicon Controlled Rectifier

VSCF Variable-Speed Constant-Frequency

f_1	Side-1 frequency
f_2	Side-2 frequency
FCFC	Forced-Commutated Frequency Changer
SVC	Static VAR Controller (or Compensator)
VAR	Volt Ampere Reactive
$V_{dc,ref},V_{dc,fbk}$	Reference and feedback signals of side-2 dc bias voltage
ESR	Electro Static Resistance
$\underline{x}_1,\underline{x}_2$	Three-tuple vectors constructing dyadic $[H]$ -matrix
$\underline{v}_{1abc}, \underline{i}_{1abc}$	Side-1 voltage and current vectors in a-b-c frame
$\underline{\nu}_{2abc}$, \underline{i}_{2abc}	Side-2 voltage and current vectors in a-b-c frame
$\underline{b}_1(\omega_i),\underline{b}_2(\omega_i),\underline{b}_3(\omega_i)$	Base vectors of vector space of side-i $(i = 1, 2)$ voltages
	and currents
ω_i	Side-i $(i = 1, 2)$ angular frequency
v_{id}, v_{iq}, v_{io}	Side-i $(i = 1, 2)$ voltage d, q, and 0 components
i_{id}, i_{iq}, i_{io}	Side-i ($i = 1, 2$) current d, q, and 0 components
$[H_{jk}]$	Elementary dyadic matrix resulting from outer vector
	product of $\underline{b}_{j}(\omega_{1})$ and $\underline{b}_{k}(\omega_{2})$
p_{jk}	Weighting constants associated with $[H_{jk}]$
d, q, 0 components	Direct, quadrature, and zero components
V_{2d}	Steady-state value of the direct-axis component of side-2
	voltage
h_{ij}	ij^{th} element of $[H]$ -matrix
$[C(\omega_i)]$	d-q-0 to a-b-c Park's transformation matrix at

	angular fequency ω_i ($i = 1, 2$)
$\frac{v}{u_{idq0}}$, $\frac{i}{u_{idq0}}$	Side-i $(i = 1, 2)$ voltage and current vectors in d-q-0
	frame
\underline{v}_{iabc} , \underline{i}_{iabc}	Side-i $(i = 1, 2)$ voltage and current vectors in a-b-c
	frame
I	Identity matrix
[P]	Transformation matrix of marix converter in d-q-0 frame
$\underline{V}_{idq0},\underline{I}_{idq0}$	\underline{v}_{idq0} and \underline{i}_{idq0} at steady-state
<u>e</u> _{1abc}	Side-1 source voltage vector in a-b-c frame
e_{1a}, e_{1b}, e_{1c}	a, b, and c-axis components of \underline{e}_{1abc}
R_1	Per phase resistance of side-1 network
L_1	per phase inductance of side-1 network
$[R_1]$	Matrix of side-1 resistances
$[L_1]$	Matrix of side-1 induxtances
$\underline{v}_{1dq}, \underline{\dot{t}}_{1dq}$	Side-1 voltage and current vectors in d-q frame
<u>e</u> _{1dq}	Side-1 source voltage vector in d-q frame
$[G_1]$	Matrix of side-1 reactances in d-q frame
$\underline{v}_{2dq}, \underline{i}_{2dq}$	Side-2 voltage and current vectors in d-q frame
$rac{v}{2dq},rac{\dot{l}}{2dq}$ $rac{e'}{1dq}$	Side-1 source voltage vector in d-q frame as viewed
	from side-2
$\left[R_{1}^{\;\prime}\right]$	Matrix of side-1 resistances as viewed from side-2
$\left[L_1^{\ \prime}\right]$	Matrix of side-1 inductances as viewed from side-2

$\left[G_{_{1}}^{\prime}\right]$	Matrix of side-1 reactances as viewed from side-2
<u>e</u> _{2abc}	Side-2 load voltage vector in a-b-c frame
e_{2a}, e_{2b}, e_{2c}	a, b, and c-axis comonents of \underline{e}_{2abc}
R_2	per phase resitance of side-2 network
L_2	per phase inductanc of side-2 network
$[R_2]$	Matrix of side-2 resistances
$[L_2]$	Matrix of side-2 inductances
<u>e</u> _{2dq}	Side-2 load voltage vector in d-q frame
$[G_2]$	Matrix of side-2 reactances in d-q frame
CS(x)	Cosine function at angular frequency $\omega_1 + \omega_2$ with
	phase angle of x
CD(x)	Cosine function at angular frequency $\omega_1 - \omega_2$ with
	phase angle of x
e_{1d},e_{1q}	d and q-axis components of \underline{e}_{1dq}
P_f	Scaling factor
$e_{1a}^{},e_{1b}^{},e_{1c}^{}$	Instantaneous side-1 source voltages
$e_{1d}^{\prime},e_{1q}^{\prime}$	d and q-axis components of \underline{e}'_{1dq}
$e_{2d}^{},e_{2q}^{}$	d and q-axis components of \underline{e}_{2dq}
i_{2d}, i_{2q}	d and q-axis components of \underline{i}_{2dq}
$E_{1d}^{\prime},E_{1q}^{\prime}$	Steady-state values of e'_{1d} and e'_{1q}
E_{2d}, E_{2q}	Steady-state values of e_{2d} and e_{2q}
I_{2d}, I_{2q}	Steady-state values of i_{2d} and i_{2q}

E_{1d}, E_{1q}	Steady-state values of e_{1d} and e_{1q}
I_{1d}, I_{1q}	Steady-state values of i_{1d} and i_{1q}
Υ	Angle of rotation
E_1 , δ_1	Magnitude and phase of vector \underline{e}_{1dq}
P_{f1}, P_{f2}	Scaling factors
Υ1, Υ2	Angles of rotation
DPF	Displacement Power Factor
UDPF	Unity Displacement Power Factor
$\underline{\underline{E}}_{1dq},\underline{\underline{I}}_{1dq}$	\underline{e}_{1dq} and \underline{i}_{1dq} at steady-state
\underline{i}_C	Side-2 capacitor current vector in a-b-c frame
i_{Ca}, i_{Cb}, i_{Cc}	Instantaneous side-2 capacitor currents
<u>i'</u> 2abc	Side-2 load current vector in a-b-c frame
$i_{2a}^{\prime}, i_{2b}^{\prime}, i_{2c}^{\prime}$	Instantaneous side-2 load currents
$rac{ u'}{2abc}$	Vector of ac components of side-2 voltages in a-b-c
	frame
v_{zs}	Zero-sequence component of side-2 voltages
V_{dc}	DC component of side-2 voltages
v_{20}, i_{20}	Zero components of side-2 voltage and current
I_1 , η_1	Magnitude and phase of vector \underline{i}_{1dq}
$P_{_{f \phi}}$	Scaling factor, magnitude of vector $[p_{13} \ p_{23}]^T$
φ	Angle of rotation, phase of vector $[p_{13} \ p_{23}]^T$
<u>e</u> •dq	SVC voltage vector in d-q frame

$i_{2d}^{\prime},i_{2q}^{\prime}$	d and q-axis components of side-2 load currents
	in d-q frame
i_{Cd}, i_{Cq}, i_{C0}	d, q, and 0 components of side-2 capacitor
	currents in d-q-0 frame
С	Capacitance of side-2 capacitors
v_{Cd}, v_{Cq}	d and q-axis components of side-2 capacitor
	voltages in d-q frame
$I_{2d}^{\prime},I_{2q}^{\prime}$	Steady-state values of i'_{2d} and i'_{2q}
V_{20}	Steady-state value of v_{20}
$[H_f]$	Frequency changer part of [H]
$[H_{ullet}]$	SVC part of [H]
FVC	Field Vector Control
\hat{E}_1, \hat{I}_1	Phasor notations for \underline{E}_{1dq} and \underline{I}_{1dq}
\hat{E}_2, \hat{I}_2'	Phasor notations for \underline{E}_{2dq} and \underline{I}'_{2dq}
R_T	Total resistance as viewed from side-2
X_T	Total reactance as viewed from side-2
$E_{\phi d}, E_{\phi q}$	d and q-axis components of $\underline{e}_{\phi dq}$ at steady-state
E_2 , δ_2	Magnitude and phase of vector \underline{e}_{2dq}
K, K'	Positive proportionality constants
$i_{1aa},,i_{1cc}$	Instantaneous side-1 branch currents
ν _{1aa} ,, ν _{1cc}	Instantaneous side-1 terminal voltages
v_a, v_b, v_c	Instantaneous voltages at common coupling points

	of branches of phases a, b, and c on side-1
R_{sl}, L_{sl}	Side-1 source resistance and inductance
R_{s2}, L_{s2}	Side-1 branch resistance and inductance
PWM	Pulse Width Modulation
SPWM	Sinusoidal Pulse Width Modulation
$v_{\mathrm{mod},jk}$	Modulating signal of j^{th} phase $(j = a, b, c)$ of k^{th}
	converter $(k = a, b, c)$
v_{2k}	Instantaneous side-2 voltage of k^{th} converter $(k = a, b, c)$
V_{ι}	Peak value of triangular carrier signal
f_t	Frequency of triangular carrier signal
m_{jk}	Normalized modulating signal corresponding to $v_{\text{mod},jk}$
[M(t)]	Matrix of nomalized modulating signals
M_f	Scaling factor of frequency changer part of $[M(t)]$
$M_{oldsymbol{\phi}}$	Scaling factor of SVC part of $[M(t)]$
$\hat{\mathcal{E}}_1'$	Phasor notation for \underline{E}'_{1dq}
$\underline{v}_{2ac}, \underline{v}_{2dc}$	Vectors of ac and dc components of side-2 voltages
V_2	Amplitude of ac components of side-2 voltages
$\frac{v}{1}$	Vector of projected ac voltages on side-1 due
	to dc bias voltages on side-2
i_{2k}	Instantaneous side-2 current of k^{th} converter
	(k=a,b,c)
i_{1jk}	Instantaneous side-1 branch current of j^{th} phase

 i_{ij} Instantaneous side-1 source current of j^{th} phase

h, h' Integer multipliers

 T_{col} ..., T_{cc} Trapping transformers used in side-1 branches

T Ideal transformer

 R_o, L_o Shunt resistance and magnetizing inductance of

 $T_{aa},...,T_{cc}$

R, L Series resistance and leakage inductance of $T_{aa}, ..., T_{cc}$

 $n_1:n_2$ Primary to secondary turns ratio of $T_{aa}, ..., T_{cc}$

 $v_{aa1}, v_{aa2}, ..., v_{cc1}, v_{cc2}$ Primary voltages of $T_{aa}, ..., T_{cc}$ in the equivalent circuit

diagrams

 $v_{aa3}, v_{aa4}, ..., v_{cc3}, v_{cc4}$ Primary voltages of ideal transformers in equivalent

circuit diagrams of T_{aa} , ..., T_{cc}

 $v_{aa5}, v_{aa6}, ..., v_{cc5}, v_{cc6}$ Secondary voltages of ideal transformers in equivalent

circuit diagrams of T_{aa} , ..., T_{cc}

 $i_{2aa}, ..., i_{2cc}$ Primary currents of ideal transformers in equivalent

circuit diagrams of T_{aa} , ..., T_{cc}

i_{com} Common secondary current of ideal transformers in

equivalent circuit diagrams of T_{aa} , ..., T_{cc}

 $i_{\mu a}, i_{\mu b}, i_{\mu c}$ Magnetizing currents of T_{aa}, T_{ab}, T_{ac}

 $i_{\eta a}, i_{\eta b}, i_{\eta c}$ Currents through shunt resistances, R_o , of T_{aa}, T_{ab}, T_{ac}

 i_{oa}, i_{ob}, i_{oc} Total shunt currents of T_{aa}, T_{ab}, T_{ac}

kVA Kilo Volt Ampere

$v_{1a\phi}, v_{1b\phi}, v_{1c\phi}$	a, b, and c-axis components of $\underline{v}_{1\phi}$
I_{1m}, I_{1r}	Peak and rms values of side-1 source currents i_{1a} , i_{1b} , i_{1c}
E_{1m}, E_{1r}	Peak and rms values of side-1 source voltages e_{1a} , e_{1b} , e_{1c}
Q_1,Q_2	Instantaneous VARs on side-1 and side-2
<u>x</u>	Vector of state variables
<u>u</u>	Vector of control inputs
<u> </u>	Vector of derivatives of state variables with
	respect to time
$\Delta \underline{x}$	Vector of incremental state variables
$\Delta \underline{u}$	Vector of incremental control inputs
*	denotes steady-state value
l .	Denotes evaluation at steady-state operating point
f	Denotes function
d /dt	Denotes derivative with respect to time
∂ <u>f</u> /∂ <u>x</u>	Jacobian of system with respect to state variables
∂ <u>f</u> /∂ <u>u</u>	Jacobian of system with respect to control inputs
K_p, K_i	Proportional and integral coefficients of PI-controller
PI-controller	Proportional Integral controller
EPROM	Erasable Programmable Read Only Memory
D/A converter	Digital to Analog converter
A/D converter	Analog to Digital converter
MSB	Most Significant Bit
VCO	Voltage-Controlled-Oscillator
CLK	Clock

INTRODUCTION

1.1 An Introduction to Matrix Converters

In many industrial applications, the ac power needed is of a frequency other than the one which is available from the ac mains. For example, in variable-speed drives, in order to run an ac motor at different speeds, it is necessary to have a variable frequency ac power supply. There are also applications, in which, it is desirable to obtain ac power at a fixed frequency from an ac supply of variable or incompatible frequency. As an example for the case of variable frequency, the electric power generation in an aircraft or from a wind turbine can be considered. In both cases, the speed of the shaft of the alternator is not fixed; therefore, the frequency of the output voltage will be varying in direct proportion. A mechanical

solution would be using a hydraulic constant-speed coupling device for the regulation of the speed of the shaft of the alternator. As an example for the case of non-compatible frequency, one can consider the power generation from a high-speed turbine shaft with the alternator's shaft directly coupled to that of the turbine. A non-electrical solution would be a gear-box. The mechanical solutions usually demand frequent maintenance and periodic replacements. The wise solution in all the above applications is a Static Frequency Changer.

The term "Static Frequency Changer" applies to all electrical circuits composed of semiconductor switches, which are capable of converting electric power from one frequency, ω_1 , to another frequency, ω_2 . Fig. 1-1 shows the block diagram of a three-phase to three-phase static frequency changer. The three-phase ac power

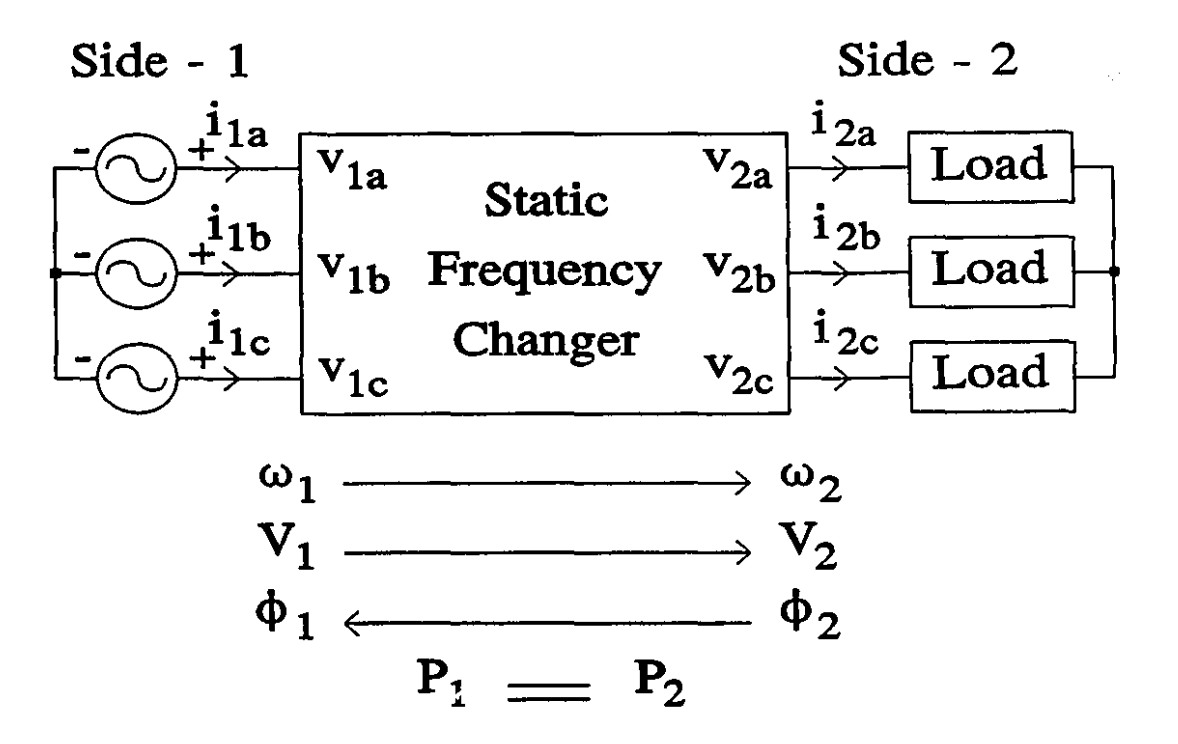


Fig. 1-1 Three-phase to three-phase static frequency changer.

supply is connected on side-1, while the three-phase load is connected on side-2. The three-phase balanced sinusoidal voltages at angular frequency ω_1 on side-1, are transformed to three-phase balanced sinusoidal voltages at angular frequency ω_2 on side-2. Static frequency changers, in general, can control the frequency and the magnitude of the voltage on side-2 and the phase angle of the current with respect to voltage on side-1. The only constraint is that of real power equality, i.e., $P_1 = P_2$ [1].

The static frequency changers are divided into two main classes. In the first class, the power conversion takes place in two stages with an intermediate dc link, as shown in Fig. 1-2(a). The ac power at angular frequency ω_1 on side-1 is first converted to dc power through a rectifier. Then, the dc power is converted back to ac power at the desired angular frequency ω_2 through an inverter. The main drawback of the two-stage or rectifier-inverter pair static frequency changer is the presence of dc link energy storage elements which add to the volume, weight, and cost of the system, as well as reducing the speed of response. In the second class of static frequency changers, the power conversion is performed directly in one stage, as shown in Fig. 1-2(b). The operation of single-stage static frequency changers is based on piecing together the voltage waveform of each phase on side-2 from selected segments of the voltage waveform on side-1 [1]. The first and the best-known member of this class is the classical "Cycloconverter" invented in the early 1930s [1]. A three-phase to three-phase "Naturally-Commutated Cycloconverter"

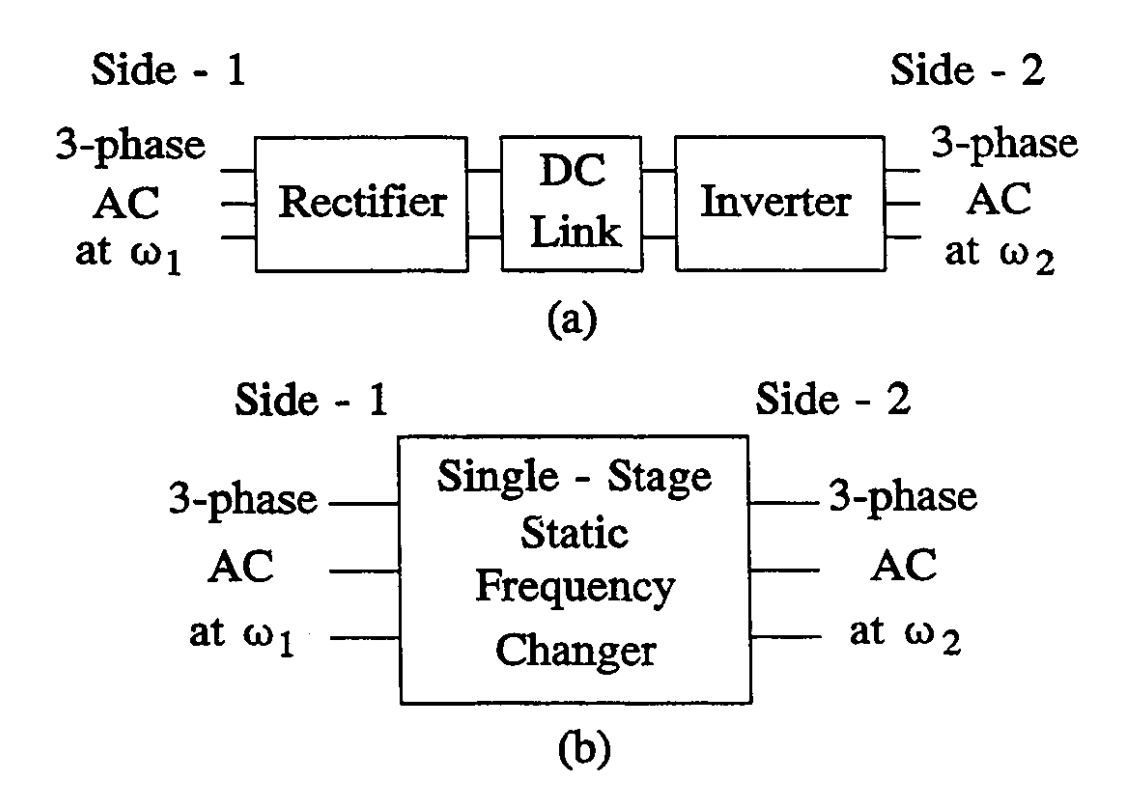


Fig. 1-2 Classes of static frequency changers.

(NCC)" [2] is shown in Fig. 1-3. As seen, for each phase on side-2, two back-to-back naturally-commutated three-phase thyristor bridge converters are required. Depending on the direction of the load current, the positive or the negative converter will be in operation. The mode of operation of each converter (rectification mode or inversion mode) is determined by the sign of the side-2 voltage to be realized. The attainable frequency on side-2 of the NCC is always below the supply frequency on side-1. The limit for ω_2 is about one third of ω_1 for an acceptable side-2 waveform with low harmonic content [2].

A more compact structure, with the total number of switching devices reduced

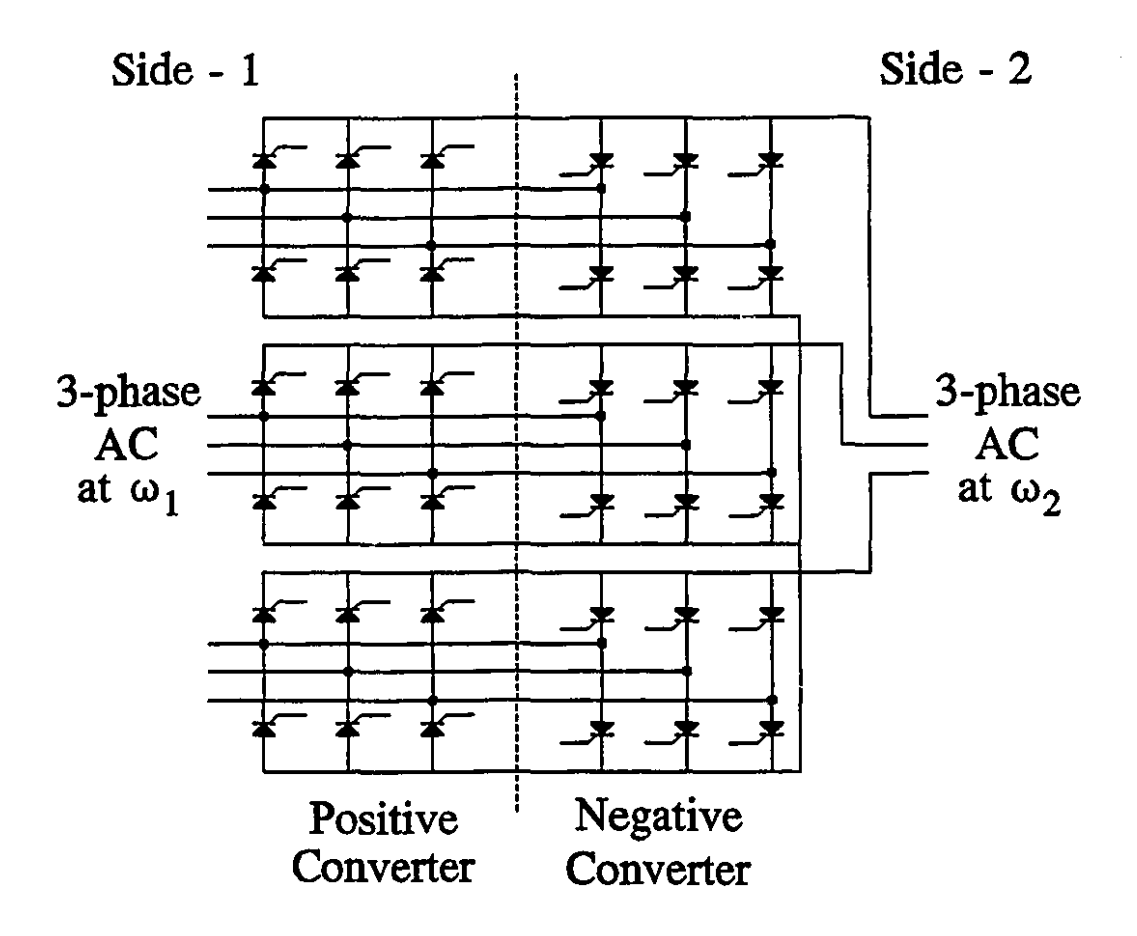


Fig. 1-3 Three-phase to three-phase NCC.

to half, can be found for the frequency changer, as shown in Fig. 1-4. The back-to-back connected thyristors have to be commutated forcibly. For this reason, the structure shown in Fig. 1-4 is called a "Forced-Commutated Cycloconverter (FCC)". To avoid the complications caused by employing force-commutating circuits, switches with inherent gate-turn-off capability (such as GTO, BJT, MOSFET, and IGBT) can be used instead of thyristors, if the devices with the required ratings are available. With the structure shown in Fig. 1-4, there is no limit on the allowable frequency on side-2. Since the frequency changer of Fig. 1-4 consists of an array of semiconductor

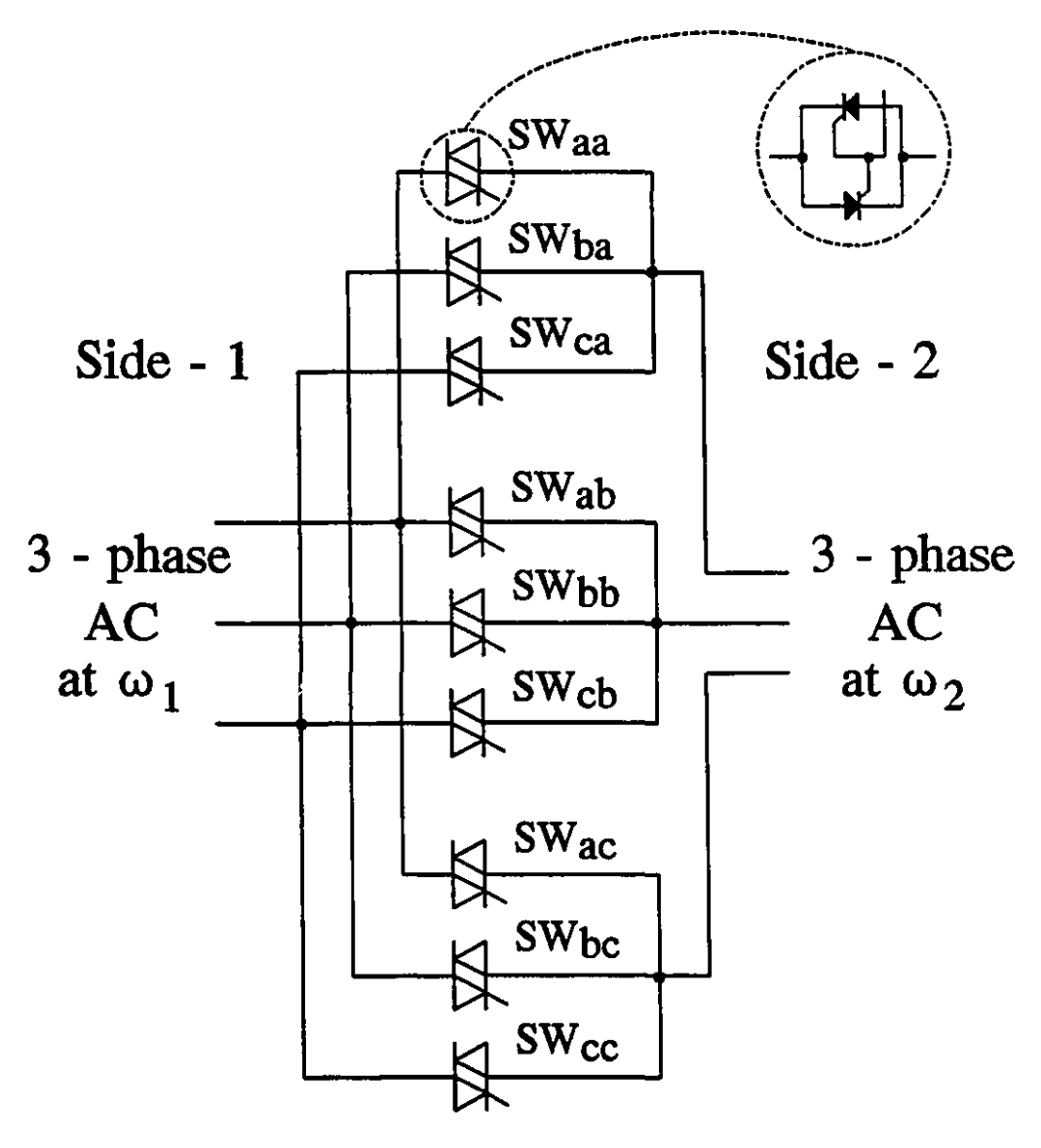


Fig. 1-4 Three-phase to three-phase FCC.

switches connected directly between the side-1 and side-2 terminals, this structure is also termed "Matrix Converter". Fig. 1-5 shows a three-phase to three-phase matrix converter with its 3×3 switching matrix of elements SW_{aa} , ..., SW_{cc} . As seen, each switch is responsible for connecting one phase of the system on side-1 to one phase

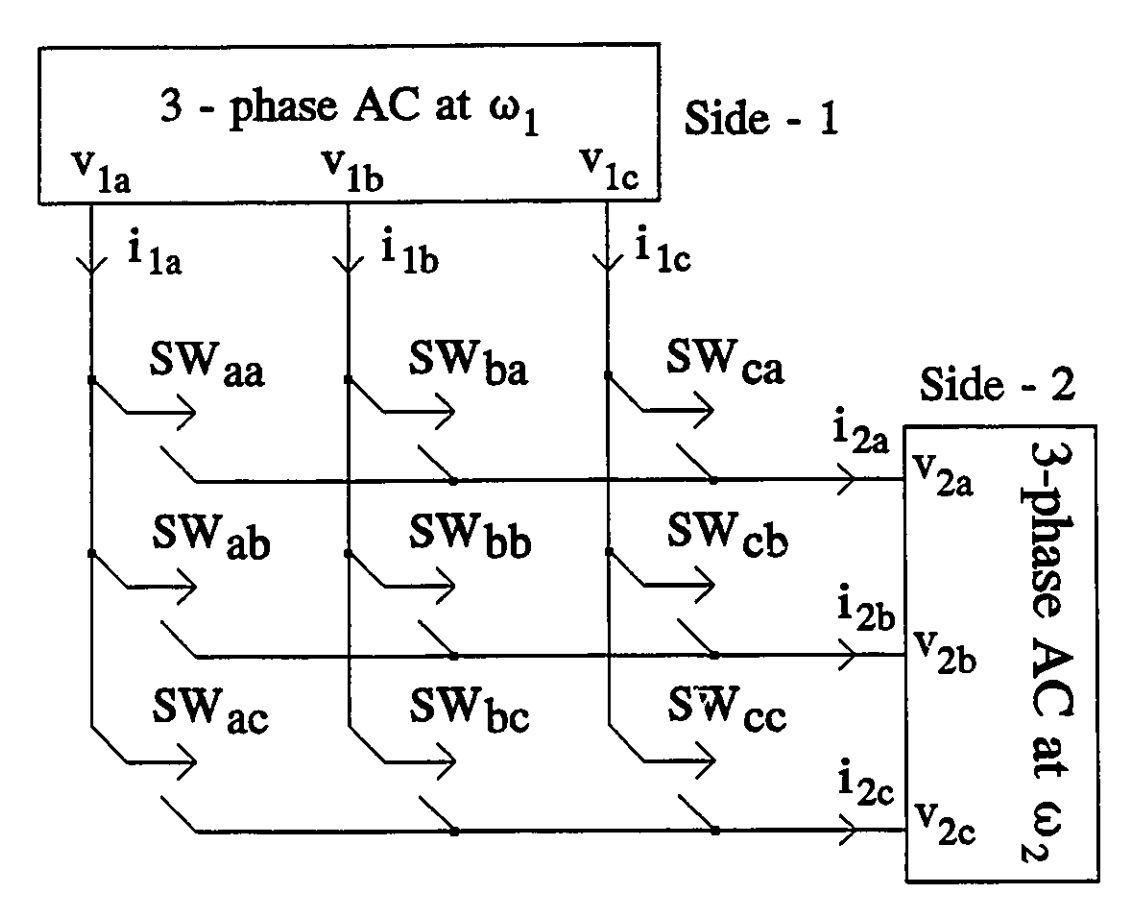


Fig. 1-5 Three-phase to three-phase matrix converter.

of the system on side-2.

In general, matrix converters employ four-quadrant or bidirectional switches $(SW_{aa}, ..., SW_{cc})$ in Fig. 1-5). Fig. 1-6 shows three ways of realizing bidirectional switches with BJTs. Bidirectional switches allow current in either direction while in ON-state and block the voltage of either polarity while in OFF-state [1].

The basic objective in the operation of matrix converters is to get balanced sinusoidal waveforms for the voltages on side-2 and currents on side-1 at the desired frequencies. Subfrequency and superfrequency components (i.e., components at

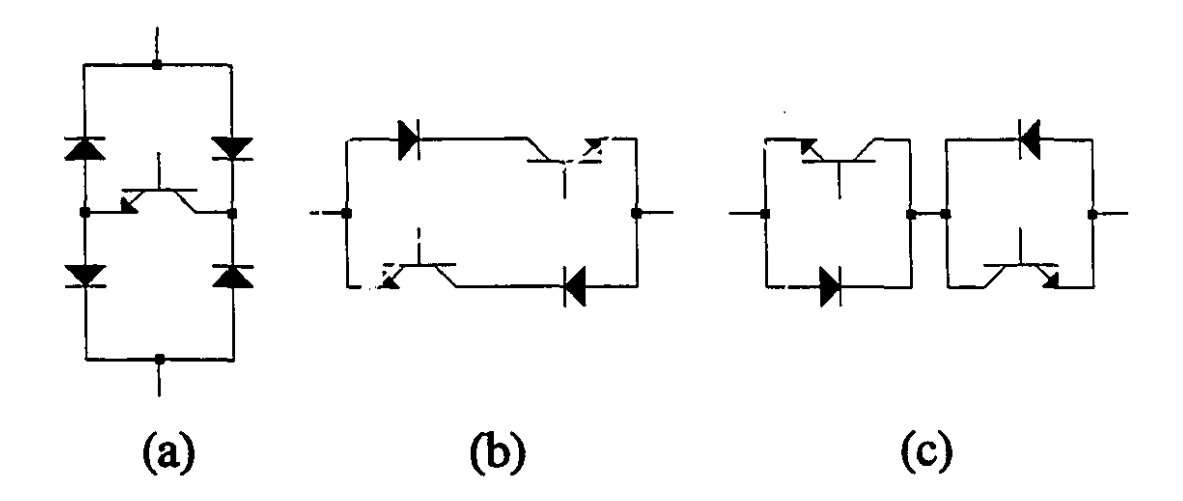


Fig. 1-6 Bidirectional switch realizations.

frequencies below and above the desired frequencies) are not allowed. Only high frequency switching harmonics are tolerated, since they can be filtered inexpensively. The key to the successful achievement of the above objectives is the proper choice of the ON and OFF periods of the switches SW_{aa} , ..., SW_{cc} , shown in Fig. 1-5. The bilevel functions governing the operation of the switches are called switching functions. The value 1 denotes the ON-command, while the value 0 means the OFF-command for the corresponding switch. The switching functions of the nine switches in Fig. 1-5 comprise a switching function matrix [S], also called the existence matrix [1]. The transformations of the voltages and the currents in Fig. 1-5, are performed according to the following equations:

$$\begin{bmatrix} v_{2a} \\ v_{2b} \\ v_{2c} \end{bmatrix} = \begin{bmatrix} S \end{bmatrix} \begin{bmatrix} v_{1a} \\ v_{1b} \\ v_{1c} \end{bmatrix} \qquad \begin{bmatrix} i_{1a} \\ i_{1b} \\ i_{1c} \end{bmatrix} = \begin{bmatrix} S \end{bmatrix}^T \begin{bmatrix} i_{2a} \\ i_{2b} \\ i_{2c} \end{bmatrix}$$

$$(1-1)$$

For the quantities on side-1 and side-2 of the matrix converter to contain the wanted fundamental component, the elements of [S]-matrix should be chosen properly. As far as the fundamental components of the quantities on both sides are concerned, [S] can be replaced by another matrix [H] whose elements are the local averages of the corresponding elements of the [S]-matrix. Equations (1-1) can therefore be rewritten as:

$$\begin{bmatrix} v_{2a} \\ v_{2b} \\ v_{2c} \end{bmatrix} = [H] \begin{bmatrix} v_{1a} \\ v_{1b} \\ v_{1c} \end{bmatrix} \qquad \begin{bmatrix} i_{1a} \\ i_{1b} \\ i_{1c} \end{bmatrix} = [H]^T \begin{bmatrix} i_{2a} \\ i_{2b} \\ i_{2c} \end{bmatrix}$$
(1-2)

Strictly speaking, the voltages and currents in (1-1) and (1-2) are not exactly the same. In fact, (1-1) relates the instantaneous values of the quantities of both sides, while (1-2) describes the relation of the instantaneous values of the dominant low-order fourier components of the same quantities. To avoid complications and comply with the standard representation styles, the same notations as in (1-1) have been used throughout this thesis for the dominant low-order fourier components.

The matrix [H] is in fact the "Transformation Matrix" of the matrix converter.

The elements of the [H]-matrix are typically composed of cosine functions at angular frequencies equal to the sum and difference of side-1 and side-2 angular frequencies, ω_1 and ω_2 . As an example, (1-5) gives the structure of a typical [H]-matrix:

$$M_{s} \begin{bmatrix} \cos(\omega_{1} + \omega_{2})t & \cos[(\omega_{1} + \omega_{2})t - 2\pi/3] & \cos[(\omega_{1} + \omega_{2})t - 4\pi/3] \\ \cos[(\omega_{1} + \omega_{2})t - 2\pi/3] & \cos[(\omega_{1} + \omega_{2})t - 4\pi/3] & \cos(\omega_{1} + \omega_{2})t \\ \cos[(\omega_{1} + \omega_{2})t - 4\pi/3] & \cos(\omega_{1} + \omega_{2})t & \cos[(\omega_{1} + \omega_{2})t - 2\pi/3] \end{bmatrix} \\ + M_{d} \begin{bmatrix} \cos(\omega_{1} - \omega_{2})t & \cos[(\omega_{1} - \omega_{2})t - 4\pi/3] & \cos[(\omega_{1} - \omega_{2})t - 2\pi/3] \\ \cos[(\omega_{1} - \omega_{2})t - 2\pi/3] & \cos(\omega_{1} - \omega_{2})t & \cos[(\omega_{1} - \omega_{2})t - 4\pi/3] \\ \cos[(\omega_{1} - \omega_{2})t - 4\pi/3] & \cos[(\omega_{1} - \omega_{2})t - 2\pi/3] & \cos(\omega_{1} - \omega_{2})t \end{bmatrix}$$

$$(1-5)$$

where M_s and M_d are constant scalars.

The direct synthesis of [H]-matrix from the desired specifications of side-1 and side-2 quantities is not straightforward. There is an indirect method for [H]-matrix synthesis which is more intuitive [3]. This method is based on modelling the matrix converter as two cascaded blocks, one of a rectifier and the other of an inverter, as in Fig. 1-2(a). First, a 1×3 row vector $[H_r]$ is designed that transforms the three-phase balanced sinusoidal voltages on side-1 to a dc voltage. To transform this dc voltage to a system of three-phase balanced sinusoidal voltages on side-2, a3×1 column vector $[H_i]$ will then be designed. The complete [H]-matrix will be the product of $[H_i]$ and $[H_r]$. Equation (1-3) can therefore be written as:

$$\begin{bmatrix} v_{2a} \\ v_{2b} \\ v_{2c} \end{bmatrix} = \begin{bmatrix} H_i \end{bmatrix} \begin{bmatrix} H_r \end{bmatrix} \begin{bmatrix} v_{1a} \\ v_{1b} \\ v_{1c} \end{bmatrix}$$
 (1-6)

1.2 Historical Background

1.2.1 Early History

The documented history of one-stage static frequency changers begins with the work of L.A. Hazeltine in 1923 [4]. He established the fundamental principle of constructing an ac voltage wave of chosen frequency from successive voltage waves of a multiphase ac supply of known frequency. However, his system could not be practically implemented because of the unavailability of electric valves with suitable characteristics and ratings [1].

During 1930s, thanks to the availability of mercury arc valves of adequate ratings, some practical experimental results were reported [5,6]. Variable output frequencies below the supply frequency and variable output amplitude were attained, just by controlling the firing angle of the valves.

In the second half of the 1930s, the mercury arc frequency converters were revisited and reviewed thoroughly by H. Rissik [7,8] and the now-familiar terms: "Cycloconversion" and "Cycloconverter" were introduced.

1.2.2 Recent History

In the late 1950s, the evolution of silicon controlled rectifier (SCR) or thyristor, together with the advantages they offered over mercury arc rectifiers, such as: smaller size, higher switching speed, lower ON-state voltage drop, and rugged construction, remotivated the research in the area of static frequency changers towards very useful applications such as: "Variable Speed Constant Frequency (VSCF)" power generating systems. References [9-14] reflect part of the effort made by researchers in the aforementioned area starting in the late 1950s.

By the middle of the 1960s, some researchers had advanced to the stage of addressing some of the wavefrom distortion problems associated with the frequency converters [15,16].

Until silicon devices with gate-turn-off capability became available at large ratings in the late 1970s, the advancement of static frequency changers was impeded by the inherent limitation of the thyristors due to the fact that they had gate-turn-on capability only and had to be turned off through natural (or line) commutation. However, researchers aware of the potentials of the cycloconverters, persisted in developing a technology based on line commutation and succeeded in realizing the great advantages it could offer in terms of amplitude and frequency control of the output voltage and bidirectionality. The major area of application was ac motor drives. The systems composed of a cycloconverter and an ac motor could fulfil the requirements expected from a dc motor, under armature voltage control, in terms of variable speed range, torque characteristics, and efficiency. The 1960s and early 1970s are marked by the efforts made by the researchers to develop practical systems with

cycloconverter-squirrel cage induction motor combination [17-31]. Cycloconverters were also perfect candidates for very large ac motor drives running at low speeds, such as ball mill drives and tube mill drives [32-37].

The 1970s are the years of flowering for the static frequency changers. Systems with new characteristics like controllable input displacement power factor and unity displacement power factor were invented [38-40], and new static power conversion and generation arrangements were discovered [41,42]. Two theoretical works were published by L. Gyugyi and B.R. Pelly [43,44] which covered the analysis of the terminal characteristics of different types of frequency changers including a thorough study of Naturally Commutated Cycloconverters (NCCs). These works were followed by another theoretical work by W. McMurray [45], covering the theory and design of cycloconverters. In 1976, L.Gyugyi and B.R. Pelly published their book: "Static Power Frequency Changers" [1]. The authors summarized the knowledge available at that time, in the area of one-stage static frequency changers, in a mathematical framework and made prophetic projections of new frequency changers based on forced-commutation. The novel concepts of "Existence Function" and "Existence Matrix", "Four-Quadrant or Bidirectional Switches", and "Generalized Transformer" were introduced. This book remained the main reference for most of the works to follow.

Since then, a new direction in frequency changers development has been under way. Further advances have been made thanks to the evolution of gate-turn-off silicon devices with large ratings, the invention of new topologies, and the

introduction of new control and modulation methods.

1.2.3 New Era

The new era actually began with two publications by M. Venturini and A. Alesina [46,47], in 1980. A new frequency converter capable of sinusoidal waveforms at both the input and the output, bidirectionality of power transfer, continuously controllable input power factor, and reactive power generation was proposed. Also, the condition imposed on the switching functions that the terminals on the voltagesource side are never to be short-circuited and the terminals on the current-source side are never to be left unconnected, received attention. Furthermore, the possibility of using Matrix Converters (another name for single-stage static frequency changers), for ac-to-ac $(f_1 \text{ and } f_2 \neq 0)$, dc-to-ac $(f_1 = 0 \text{ and } f_2 \neq 0)$, and dc-to-dc $(f_1 = f_2 = 0)$ conversions with the choice of having the voltage-sources on side-1 and currentsources on side-2 (buck topology) or current-sources on side-1 and voltage-sources on side-2 (boost topology) was mentioned. In the transformation matrix, cosine functions at both sum and difference of the side-1 and side-2 angular frequencies, i.e., $\omega_1+\omega_2$ and $\omega_1-\omega_2$ were used. The problem with large amplitude low-order harmonics present in the input current and output voltage, reported in [1], was solved to some extent. The maximum attainable output to input voltage ratio was reported to be 0.5.

Later, in 1985, P.D. Ziogas, S.I. Khan, and M.H. Rashid succeeded in

improving the harmonic distortion of the input current and output voltage, and reaching the output to input voltage ratio of 0.95, through improved frequency changer structures [48].

While the Forced Commutated Frequency Changers (FCFCs) were under constant improvement and advancement, the traditional Naturally Commutated Cycloconverter (NCC) continued to receive attention, in the area of application of new control techniques, especially for high power applications like: ice-breaker propulsion systems and rolling mill drives [49-57].

Reference [58] brought up the problem of severe unbalanced conditions caused by large single-phase loads connected directly to the ac mains, and suggested the use of a three-phase to single-phase matrix converter as the intermediate stage as a potential application for this class of converters.

In 1986, in their paper [59], P.D. Ziogas, S.I. Khan, and M.H. Rashid reported improvement on harmonic reduction and the increase of the output to input voltage ratio to 1.0. Their four-quadrant switch element was realized using the combination of a transistor switch and four diodes, as shown in Fig. 1-6(a).

The timing of the gating signals sent to the bidirectional switches is very critical. Inaccurate timing can lead to short-circuiting the input voltage sources or open-circuiting the load current [60-62]. The resulting current or voltage surges can be beyond the withstand limit of the switching devices. To protect their matrix converters against the hazardous conditions, some researchers have used snubber networks [58,59,64], while some others have implemented multi-step switching

algorithms [60,61,63,65,70]. Snubber circuits are usually bulky and dissipative and the multi-step switching techniques complicate the control circuitry. They require a feedback from the direction of load current or the polarity of the phase-to-phase supply voltages and can allow only the bidirectional switches of structures shown in Fig. 1-6(b) and 1-6(c) to be used.

Based on the great amount of knowledge available on the ac-to-ac converter topic, researchers continued to perfect the operational aspects of the system by introducing new control methods [61,62,66-69] and new modulation techniques, such as space vector modulation method by L.Huber and D. Borojevic [70].

Reference [64] showed that ac-to-ac matrix converters are suitable for high power application.

In 1992, D.G. Holmes and T.A. Lipo applied ac-to-ac matrix converter theory to controlled rectifiers and inverters [71,72]. This is part of the effort in the direction of integration of different applications in a single system. In this way, a single three-phase to three-phase ac-to-ac matrix converter can realize all major possible converter topologies, i.e., ac-to-ac, ac-to-dc, dc-to-ac, and dc-to-dc. Moving from one topology to another, does not need any hardware modification, but only some modifications in the software of the microprocessor-controlled system will be necessary.

In 1993, W.H. Kwon and G.H. Cho applied the a-b-c to d-q-0 transformation to the analysis of a boost-type nine-switch matrix converter [73]. In this way, the trigonometric functions in the a-b-c frame representation are replaced by time

invariant values in d-q-0 frame, simplifying the analysis to a great deal. Furthermore, for the first time, Kwon and Cho addressed, in the analysis, the inductances and the capacitances which form the energy buffers between the matrix of switches and the supply and the load. Until then, ideal current and voltage sources were traditionally used.

With enough theoretical background and satisfactory analytical, simulation, and laboratory experimental results in the literature, the trend in the development of ac-to-ac matrix converters seems to be in the direction of industrial prototyping and perfection of operational aspects.

1.3 Organization, Scope, and Contributions

This thesis is organized in three major parts:

Part I:

(Chapters 2-5, Appendices A,B, and C)

Theory: Development of Dyadic Matrix Converter Theory;

Part II:

(Chapter 6)

New Topology: Voltage-Source-Converter type Matrix Converter;

Application: Application of dyadic matrix converter theory to the new

matrix converter system; and

Part III:

(Chapter 7, Appendices D, E, F, G, and H)

Implementation: Implementation of the new matrix converter system

under the dyadic matrix converter theory control.

1.3.1 Dyadic Matrix Converter Theory (Chapters 2-5, Appendices A, B, and C)

The contributions of this thesis in the theory of matrix converters has been made possible by the synthesis of two central ideas:

- (1) The dyadic structure of the [H]-matrix (section 2.2); and
- (2) The a-b-c to d-q-0 transformation (section 2.5).

It should be mentioned that the dyadic matrix structure has been recognized by S.I. Khan, P.D. Ziogas, and M.H. Rashid [3,58,59], and L. Huber and D. Borojevic [70], as the indirect method of synthesis of [H]-matrix; but they were not aware of the convenience of the a-b-c to d-q-0 transformation. The advantages of the a-b-c to d-q-0 transformation were recognized by W.H. Kwon and G.H. Cho [73]; but they were not aware of the dyadic matrix structure. The progress made in the theory has to come from the melding together of the two central ideas (section 2.6). The outcome of this combination is a time-invariant equivalent, in d-q-0 frame, for the [H]-matrix, called [P]-matrix, which is a convenient design tool (section 2.6). By proper choice of the entries of the [P]-matrix, all possible [H]-matrix structures including the wellknown ones used by M. Venturini and A. Alesina [46], [47] and L.Huber and D. Borojevic [70] can be synthesized (sections 3.4, 3.5, 3.7, and 3.8, Appendices A,B, and C). Another outcome of the combination of dyadic matrix structure and a-b-c to d-q-0 transformation is the possibility of referring the network on one side of the matrix converter to the other side in the same way as it is done in the magnetic transformers, even though in this case the networks on the two sides of the matrix converter are generally excited at two different frequencies (section 3.2). Furthermore, the network of one side referred to the other side can be integrated with the network of that side resulting in a compact expression describing the dynamics of the whole system (section 3.3).

A significant contribution of this thesis to the matrix converter theory is the treatment of the phase angle rotation as a control element (section 3.7). Another important contribution is addressing the interaction of the zero-sequence components and the application of SVC concept to the matrix converters (chapter 4).

Finally, a complete [H]-matrix is synthesized which has all the necessary control levers to perform all aspects of: frequency changing, amplitude control of side-2 voltages, displacement power factor control on side-1, and field vector control on side-2 (section 4.6 and chapter 5).

1.3.2 Voltage-Source Converter Type Matrix Converter Under the Dyadic Matrix Converter Theory Control (chapter 6)

An important contribution of this thesis is introducing a new matrix converter topology. The new topology is composed of three modules of three-phase voltage-source converters (chapter 6). The advantage of the new topology over the conventional nine-bidirectional-switch topology is that it employs voltage-source-converter modules which are well known by the industry and there is no need for

switching precautions of the kind necessary in the conventional topology to be taken. The voltage-source converters can be protected against shoot-through simply by introducing a time delay between the gating pulses of the two switches in the same leg. Moreover, the total number of switches and diodes used are the same as those used in the conventional topology.

The contribution of the thesis in the area of application is in the form of applying the dyadic matrix converter theory developed in chapters 2-5 to the new matrix converter topology. The [H]-matrix governing the operation of the new matrix converter has been developed in section 4.6.

1.3.3 Implementation of the New Matrix Converter System Under the Dyadic Matrix Converter Theory Control (chapter 7, Appendices D, E, F, G, and H)

Experimental work constitutes a significant part of this thesis. Three existing modules of three-phase voltage-source converter were used to realize the voltage-source-converter type matrix converter topology. The control circuitry was designed and implemented using a combination of analog and digital circuit elements.

In deriving the $V_{dc,fbk}$ signal, the side-2 voltage signals of the three voltage-source converters were averaged, thus cancelling out the ac components without using a large filter.

The size of the capacitors on side-2 of the voltage-source converters, was reduced from several thousand microfarads, which is typical for pure dc outputs, to

 $50 \,\mu F$, reducing the size and weight of the system, without endangering the stability of the system.

Low ESR (Electro Static Resistance), non-electrolytic, capacitors were used on side-2 of the voltage-source converters to reduce the losses.

The simulation and experimental results presented in chapter 7, verify the correctness of the theoretical expectations.

DYADIC MATRIX CONVERTER THEORY

2.1 Introduction

The [H]-matrix in (1-5) contains trigonometric functions. The trigonometric functions make the analysis tedious and offer little insight into the mechanisms involved in the transformations. In this chapter, the [H]-matrix is assumed to be a dyadic matrix. The dyadic structure is formed by the outer vector product of two base vectors. This simplifies the matrix operations involving trigonometric functions. By using the a-b-c to d-q-0 transformation, the [H]-matrix is transformed to a time-invariant [P]-matrix. This offers a significant advantage from the design point of view.

The block diagram of a typical three-phase to three-phase matrix converter is shown in Fig. 2-1. The voltages and currents on side-1 and side-2 are assumed to

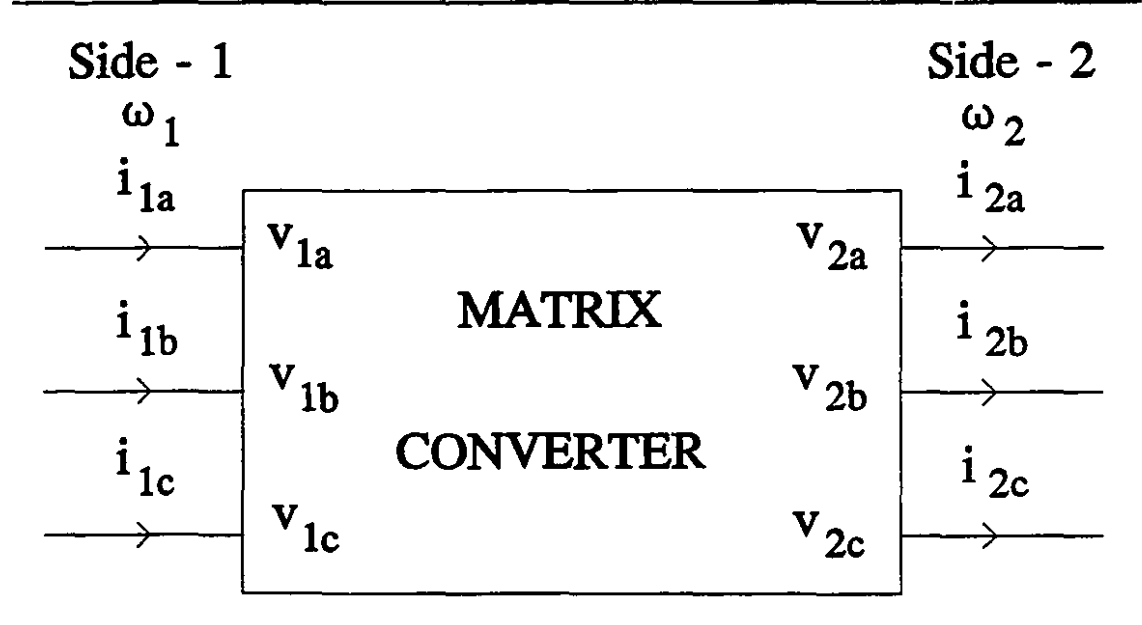


Fig. 2-1 Three-phase to three-phase matrix converter.

be balanced three-phase quantities. It is also assumed that the voltage sources are on side-2 and the current sources are on side-1. The transformations of the voltages and currents of side-1 and side-2 are performed through the [H]-matrix, as shown in Fig. 2-2. The key factor in a successful transformation is the proper choice of the [H]-matrix.

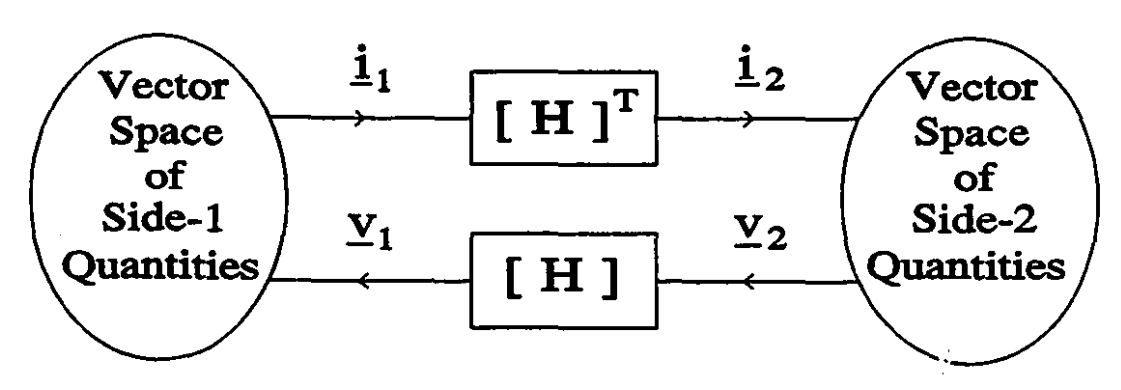


Fig. 2-2 Current and voltage transformations.

This chapter proceeds with an introduction to the dyadic matrix concept. Then, a review of the vector space of the three-phase sinusoidal voltages and currents will be presented. The orthonormal base vectors are the columns of the transformation matrix relating d-q-0 and a-b-c frames. Due to the orthonormal properties of the base vectors, [H]-matrix can be viewed as the superposition of nine weighted outer vector products of all possible combinations of the base vectors of side-1 and side-2. The design task, then boils down to the choice of proper weights according to the desired applications. The chapter continues with a review of Park's Transformation, and finally, the [H]-matrix in the d-q-0 frame is derived.

2.2 Dyadic Matrix Transformation

A 3×3 dyadic matrix, [H], is defined [74] to be a matrix formed by the outer vector product of two three-tuple vectors, \underline{x}_1 and \underline{x}_2 :

$$[H] = \underline{x}_1 \, \underline{x}_2^T \tag{2-1}$$

The ij^{th} element of the matrix [H] is:

$$h_{ii} = x_{1i} x_{2i} (2-2)$$

where x_{1i} and x_{2j} are the i^{th} element of \underline{x}_1 and the j^{th} element of \underline{x}_2 , respectively.

On expansion, for the case of i = a, b, c and j = a, b, c, (2-1) becomes:

$$[H] = \begin{bmatrix} x_{1a} \\ x_{1b} \\ x_{1c} \end{bmatrix} \begin{bmatrix} x_{2a} & x_{2b} & x_{2c} \end{bmatrix} = \begin{bmatrix} x_{1a} & x_{2a} & x_{1a} & x_{2b} & x_{1a} & x_{2c} \\ x_{1b} & x_{2a} & x_{1b} & x_{2b} & x_{1b} & x_{2c} \\ x_{1c} & x_{2a} & x_{1c} & x_{2b} & x_{1c} & x_{2c} \end{bmatrix}$$
(2-3)

2.2.1 Regrouping Inner Vector Products from Outer Vector Product

In Fig. 2.1, the side-1 voltage and current vectors are:

$$\underline{v}_{1abc}^{T} = \begin{bmatrix} v_{1a} & v_{1b} & v_{1c} \end{bmatrix}$$
 (2-4)

$$\mathbf{i}_{1abc}^{T} = \begin{bmatrix} i_{1a} & i_{1b} & i_{1c} \end{bmatrix}$$
(2-5)

Similarly, the side-2 voltage and current vectors are:

$$\underline{v}_{2abc}^{T} = \begin{bmatrix} v_{2a} & v_{2b} & v_{2c} \end{bmatrix} \tag{2-6}$$

The voltage transformation, shown in Fig. 2-2, is described as:

$$\underline{y}_{1abc} = [H] \underline{y}_{2abc} \tag{2-8}$$

Premultiplying both sides of (2-8) by \underline{i}_{labc}^{T} , yields:

$$i_{1abc}^T \underline{y}_{1abc} = i_{1abc}^T [H] \underline{y}_{2abc}$$
 (2-9)

From the power invariance principle for an ideal matrix converter,

$$i_{1abc}^T \underline{y}_{1abc} = i_{2abc}^T \underline{y}_{2abc}$$
 (2-10)

Equating the right-hand-side of (2-9) and (2-10), the current transformation, as shown

in Fig. 2-2, results:

Substituting (2-1) in (2-8) and (2-11), and regrouping the last two vectors to form an inner vector product,

$$\underline{\mathbf{y}}_{1abc} = \left(\underline{\mathbf{x}}_{1} \underline{\mathbf{x}}_{2}^{T}\right) \underline{\mathbf{y}}_{2abc} = \underline{\mathbf{x}}_{1} \left(\underline{\mathbf{x}}_{2}^{T} \underline{\mathbf{y}}_{2abc}\right) \tag{2-12}$$

$$i_{2abc} = (x_2 x_1^T) i_{1abc} = x_2 (x_1^T i_{1abc})$$
 (2-13)

From (2-12) it can be seen that v_{1a} , v_{1b} , and v_{1c} can be made to take the same functional forms as x_{1a} , x_{1b} , and x_{1c} if and only if the inner vector product $\left(\underline{x}_{2}^{T}\,\underline{v}_{2abc}\right)$, is a constant scalar. Also, (2-13) shows that \underline{i}_{2abc} can be made to be linearly dependent on \underline{x}_{2} if and only if $\left(\underline{x}_{1}^{T}\,\underline{i}_{1abc}\right)$, is a constant scalar. The only way for the above inner products to result in constant scalars, is that \underline{x}_{1} and \underline{x}_{2} be chosen from the base vectors of the vector spaces of side-1 and side-2 currents and voltages, respectively. This is the essence of the indirect method of constructing the transformation matrix [H], using the concept of fictitious rectifier and inverter contained in the ac-to-ac matrix converter [3, 58, 59, 70].

2.3 Vector Spaces of Side-1 and Side-2 Voltages and Currents

The voltage and current vector spaces of side-1 and side-2 can be spanned by

the following base vectors:

$$\underline{b}_{1}(\omega_{i}) = \sqrt{\frac{2}{3}} \begin{bmatrix} \cos \omega_{i} t \\ \cos (\omega_{i} t - 2\pi/3) \\ \cos (\omega_{i} t - 4\pi/3) \end{bmatrix}$$
(2-14)

$$\underline{b}_{2}(\omega_{i}) = \sqrt{\frac{2}{3}} \begin{bmatrix} -\sin \omega_{i} t \\ -\sin (\omega_{i} t - 2\pi/3) \\ -\sin (\omega_{i} t - 4\pi/3) \end{bmatrix}$$
(2-15)

$$\underline{b}_{3}(\omega_{i}) = \sqrt{\frac{1}{3}} \begin{bmatrix} 1\\1\\1 \end{bmatrix} \tag{2-16}$$

where i = 1 denotes side-1 and i = 2 indicates side-2. In fact, any voltage or current vector belonging to the side-1 and side-2 vector spaces, can be represented by a linear combination of the above base vectors:

$$\underline{v}_{iabc} = v_{id} \, \underline{b}_1(\omega_i) + v_{iq} \, \underline{b}_2(\omega_i) + v_{i0} \, \underline{b}_3(\omega_i) \tag{2-17}$$

$$i_{iabc} = i_{id} \underline{b}_1(\omega_i) + i_{iq} \underline{b}_2(\omega_i) + i_{i0} \underline{b}_3(\omega_i)$$
 (2-18)

where v_{id} , v_{iq} , v_{i0} , i_{id} , i_{iq} , and i_{i0} are the coordinates using the base vectors as the axes. Under steady-state, balanced, three-phase operation at a single angular frequency ω_i , v_{id} , v_{iq} , i_{id} , and i_{iq} are time-invariant scalars. The remaining coordinates, i.e., v_{i0} and i_{i0} , can be time-dependent or time-invariant scalars.

2.3.1 Orthonormal Properties of Base Vectors

From (2-14) - (2-16), it can be deduced that:

$$\left[\underline{b}_{j}(\omega_{i}) \right]^{T} \left[\underline{b}_{k}(\omega_{i}) \right] = 0 \qquad \text{for } j \neq k$$

$$\neq 0 \qquad \text{for } j = k$$

$$(2-19)$$

for j = 1, 2, 3 and k = 1, 2, 3. Thus, the base vectors $\underline{b}_1(\omega_i)$, $\underline{b}_2(\omega_i)$, and $\underline{b}_3(\omega_i)$ are orthonormal. The constant coefficients $\sqrt{2/3}$ and $\sqrt{1/3}$ used in (2-14) - (2-16) have been chosen intentionally in order to make

$$\left[\underline{b}_{j}(\omega_{i})\right]^{T}\left[\underline{b}_{k}(\omega_{i})\right] = 1$$
 for $j = k$ (2-20)

2.4 Synthesis of the Transformation Matrix

As mentioned earlier in subsection 2.2.1, the criterion for choosing \underline{x}_1 and \underline{x}_2 is that they must belong to the vector spaces of the currents and voltages of side-1 and side-2 of the matrix converter, respectively. Therefore, any of the base vectors $\underline{b}_1(\omega_i)$, $\underline{b}_2(\omega_i)$, and $\underline{b}_3(\omega_i)$ is a candidate for the choice of \underline{x}_1 and \underline{x}_2 provided that the proper angular frequency, ω_i , is used.

In general, by choosing \underline{x}_1 to be $\underline{b}_j(\omega_1)$, j=1,2,3, and \underline{x}_2 to be $\underline{b}_k(\omega_2)$, k=1,2,3, a feasible dyadic matrix $[H_{jk}]$ can be formed:

$$[H_{jk}] = p_{jk} \underline{b}_{j}(\omega_{1}) [\underline{b}_{k}(\omega_{2})]^{T}$$
(2-21)

where p_{ik} is any weighting constant. Overall, nine different dyadic matrices can be

constructed in this way, out of which some are significant from engineering point of view, while the others are not useful. Any combination of the above nine elementary dyadic matrices is also possible. The most general expression for the combination of different feasible dyadic matrices is:

$$[H] = \sum_{j=1}^{3} \sum_{k=1}^{3} p_{jk} \underline{b}_{j}(\omega_{1}) [\underline{b}_{k}(\omega_{2})]^{T}$$
 (2-22)

Because of the trigonometric nature of the elements of the vectors $\underline{b}_1(\omega_i)$ and $\underline{b}_2(\omega_i)$, the expansion of (2-22) to the form of (2-3) will be complicated and yields no analytical insight. This is the main reason for transforming to d-q-0 frame.

At this point, it will be enlightening to explore the structure of some of the numerous transformation matrices [H], that can be obtained using (2-21) and (2-22).

2.4.1 Examples for Transformation Matrix Synthesis

For all of the following examples, the side-2 voltage vector is assumed to be:

$$\underline{v}_{2abc} = V_{2d} \, \underline{b}_1(\omega_2) \tag{2-23}$$

2.4.1.1 Example 1

Let $\underline{x}_1 = \underline{b}_1(\omega_1)$ and $\underline{x}_2 = \underline{b}_1(\omega_2)$. Then, from (2-21),

$$[H_{11}] = p_{11} \underline{b}_{1}(\omega_{1})[\underline{b}_{1}(\omega_{2})]^{T}$$
 (2-24)

As a result of the transformation, the side-1 voltage becomes:

$$\underline{\mathbf{v}}_{1abc} = [H_{11}]\underline{\mathbf{v}}_{2abc} = p_{11} V_{2d} \underline{\mathbf{b}}_{1}(\omega_{1})[\underline{\mathbf{b}}_{1}^{T}(\omega_{2})\underline{\mathbf{b}}_{1}(\omega_{2})]$$
 (2-25)

According to (2-20), the inner vector product inside the brackets in (2-25) equals 1. Therefore,

$$\underline{\mathbf{v}}_{1abc} = p_{11} \, V_{2d} \, \underline{b}_{1}(\omega_{1}) \tag{2-26}$$

It can be seen that the balanced three-phase voltages on side-2, with amplitude $\sqrt{2/3}\ V_{2d}$, at angular frequency ω_2 , have been transformed to the balanced three-phase voltages, with amplitude $\sqrt{2/3}\ p_{11}V_{2d}$, at angular frequency ω_1 , on side-1. The side-1 voltages have cosine functional form, determined by $\underline{b}_1(\omega_1)$ in (2-14).

The ij^{th} element of $[H_{11}]$ is given by (2-2) and (2-14) to be:

$$h_{ij} = \frac{2}{3} p_{11} \cos \left[\omega_1 t - (i-1) \frac{2\pi}{3} \right] \cos \left[\omega_2 t - (j-1) \frac{2\pi}{3} \right]$$

$$= \frac{1}{3} p_{11} \cos \left[(\omega_1 + \omega_2) t - (i+j-2) \frac{2\pi}{3} \right]$$

$$+ \frac{1}{3} p_{11} \cos \left[(\omega_1 - \omega_2) t - (i-j) \frac{2\pi}{3} \right]$$
(2-27)

with cosine functions at angular frequencies $(\omega_1 + \omega_2)$ and $(\omega_1 - \omega_2)$.

2.4.1.2 Example 2

Let $\underline{x}_1 = \underline{b}_2(\omega_1)$ and $\underline{x}_2 = \underline{b}_1(\omega_2)$. Then, from (2-21),

$$[H_{21}] = p_{21} \underline{b}_{2}(\omega_{1}) [\underline{b}_{1}(\omega_{2})]^{T}$$
 (2-28)

The side-1 voltage vector becomes:

$$\underline{V}_{1abc} = p_{21} V_{2d} \, \underline{b}_2(\omega_2) \tag{2-29}$$

As seen, the same side-2 voltage vector as in Example 1, has been transformed to a side-1 voltage vector at angular frequency ω_1 , but the side-1 voltage has acquired sine functional form of $\underline{b}_2(\omega_1)$ in (2-15). This means that a phase angle shift of $\pi/2$ has been introduced to the side-1 voltages compared to the case of Example-1. The elements of $[H_{21}]$ -matrix will contain sine functions at angular frequencies: $(\omega_1 + \omega_2)$ and $(\omega_1 - \omega_2)$.

2.4.1.3 Example 3

When the $[H_{11}]$ of Example 1 and $[H_{21}]$ of Example-2 are combined, the resulting [H]-matrix is:

$$[H] = p_{11} \underline{b}_1(\omega_1) [\underline{b}_1(\omega_2)]^T + p_{21} \underline{b}_2(\omega_1) [\underline{b}_1(\omega_2)]^T \qquad (2-30)$$

and the side-1 voltage vector becomes:

$$\underline{\mathbf{v}}_{1abc} = V_{2d} [p_{11} \underline{b}_{1} (\omega_{1}) + p_{21} \underline{b}_{2} (\omega_{1})]$$
 (2-31)

It can be seen that the side-1 voltages are weighted sums of cosine and sine functions

which can be represented as sine or cosine functions with some phase shift. The phase shift can be adjusted by choosing appropriate values for p_{11} and p_{21} . For example, if p_{11} and p_{21} are chosen in such a way that $p_{11} = \cos \alpha$ and $p_{21} = \sin \alpha$, then

$$\underline{v}_{1abc} = \sqrt{\frac{2}{3}} V_{2d} \begin{bmatrix} \cos(\omega_1 t + \alpha) \\ \cos(\omega_1 t + \alpha - 2\pi/3) \\ \cos(\omega_1 t + \alpha - 4\pi/3) \end{bmatrix}$$
(2-32)

In the structure of the [H]-matrix, cosine and sine functions at angular frequencies $(\omega_1 + \omega_2)$ and $(\omega_1 - \omega_2)$ exist.

2.4.1.4 Example 4

Let $\underline{x}_1 = f(t)\underline{b}_3$ and $\underline{x}_2 = \underline{b}_1(\omega_2)$, where f(t) is a scalar function of time and \underline{b}_3 is given in (2-16). Then, the $[H_{31}]$ -matrix becomes:

$$[H_{31}] = p_{31} f(t) \underline{b}_{3} [\underline{b}_{1}(\omega_{2})]^{T}$$
 (2-33)

and the side-1 voltage vector is:

$$\underline{v}_{1abc} = p_{31} f(t) V_{2d} \underline{b}_{3} \tag{2-34}$$

As seen, the side-2 voltages which constitute a balanced three-phase system are transformed into zero-sequence voltages on side-1.

2.4.1.5 Example 5

As the last example, let $\underline{x}_1 = \underline{b}_3$ and $\underline{x}_2 = \underline{b}_3$. Then, the $[H_{33}]$ -matrix becomes:

$$[H_{33}] = p_{33} \, \underline{b}_3 \, \underline{b}_3^T = \frac{1}{3} \, p_{33} \begin{bmatrix} 1 & 1 & 1 \\ 1 & 1 & 1 \\ 1 & 1 & 1 \end{bmatrix}$$
 (2-35)

and the side-1 voltage vector will become:

$$\underline{v}_{1abc} = p_{33} V_{2d} \underline{b}_{3} \left[\underline{b}_{3}^{T} \underline{b}_{1} (\omega_{2}) \right] = \underline{0}$$
 (2-36)

Of course, such a transformation is of no engineering significance.

Now, let us combine $[H_{11}]$ and $[H_{33}]$. The resulting [H]-matrix will contain elements like:

$$h_{ij} = \frac{1}{3} p_{11} \cos \left[\left(\omega_1 + \omega_2 \right) t - (i + j - 2) \frac{2\pi}{3} \right]$$

$$+ \frac{1}{3} p_{11} \cos \left[\left(\omega_1 - \omega_2 \right) t - (i - j) \frac{2\pi}{3} \right]$$

$$+ \frac{1}{3} p_{33}$$
(2-37)

As far as the side-1 voltages are concerned, there will be no change in comparison with Example-1 and $\underline{\nu}_{1abc}$ will be exactly the same as in (2-26). But, the inclusion of constant scalars $1/3 p_{33}$ in the elements of the [H]-matrix, makes the rank of the matrix to be 3 (instead of 2 for the [H]-matrix of Example-1), and therefore it will be invertible.

The invertibility of [H]-matrix, helps in the analysis, in the sense that as

transforming $\underline{\nu}_{2abc}$ to $\underline{\nu}_{1abc}$ can be expressed by $\underline{\nu}_{1abc} = [H]\underline{\nu}_{2abc}$, the inverse transformation, i.e., the transformation of $\underline{\nu}_{1abc}$ to $\underline{\nu}_{2abc}$ can also be stated by $\underline{\nu}_{2abc} = [H]^{-1} \underline{\nu}_{1abc}$. In the operation of the matrix converter, however, the inclusion of the constant scalars p_{33} in the [H]-matrix has no effect.

It is interesting to note that the [H]-matrix obtained as a combination of $[H_{11}]$ and $[H_{33}]$, is identical to the [H]-matrix used for the first time, in 1980, by M. Venturini and A. Alesina [46], as shown in Appendix B. The above mentioned authors have used $[H_{33}]$ to keep the values of the entries of the [H]-matrix between 0 and 1, so that the [H]-matrix is the local-averaged representation of the existence matrix which is governing the transformations, as mentioned in chapter 1.

2.5 Park's Transformation

The base vectors given in (2-14) - (2-16), are, in fact, the columns of the well-known Park's transformation matrix [75], which maps a set of three-phase quantities from d-q-0 frame to a-b-c frame, as shown in (2-17) and (2-18). The 3×3 Park's transformation matrix is therefore

$$\left[C(\omega_i)\right]_{3\times3} = \left[\underline{b}_1(\omega_i) : \underline{b}_2(\omega_i) : \underline{b}_3(\omega_i)\right] \tag{2-38}$$

Defining the d-q-0 voltage and current vectors on side-i (i = 1, 2) as

$$\underline{v}_{idg0}^{T} = \begin{bmatrix} v_{id} & v_{iq} & v_{i0} \end{bmatrix} \tag{2-39}$$

$$i_{idq0}^{T} = [i_{id} \ i_{iq} \ i_{i0}]$$
 (2-40)

(2-17) and (2-18) can be rewritten as:

$$\underline{v}_{iabc} = \left[C(\omega_i) \right]_{3 \times 3} \underline{v}_{ida0} \tag{2-41}$$

$$\underline{i}_{iabc} = [C(\omega_i)]_{3\times3} \underline{i}_{idq0}$$
 (2-42)

From the orthogonal properties of the base vectors stated in (2-19) and (2-20), it can be deduced that:

$$[C(\omega_i)]^T [C(\omega_i)] = I$$
 (2-43)

where I is the Identity Matrix.

2.6 Transformation Matrix in D-Q-0 Frame

In order to move from the a-b-c frame to the d-q-0 frame, in which the matrix converter is to be studied, the transformations of (2-41) and (2-42) are used. Substituting (2-22) in (2-8) yields:

$$\underline{\underline{v}}_{1abc} = \left[\sum_{j=1}^{3} \sum_{k=1}^{3} p_{jk} \, \underline{b}_{j} \left(\omega_{1} \right) \left[\underline{b}_{k} \left(\omega_{2} \right) \right]^{T} \right] \underline{\underline{v}}_{2abc} \tag{2-44}$$

Replacing \underline{v}_{1abc} and \underline{v}_{2abc} in (2-44) by their equivalents from (2-41),

$$\left[C(\omega_1)\right]_{3\times3}\underline{\nu}_{1dq0} = \left[\sum_{j=1}^3\sum_{k=1}^3p_{jk}\,\underline{b}_j(\omega_1)\left[\underline{b}_k(\omega_2)\right]^T\right]\left[C(\omega_2)\right]_{3\times3}\underline{\nu}_{2dq0} \quad (2-45)$$

Premultiplying both sides of (2-45) by $\left[C(\omega_1)\right]_{3\times 3}^T$,

$$\underline{\underline{v}}_{1dq0} = \begin{bmatrix} \sum_{j=1}^{3} \sum_{k=1}^{3} p_{jk} \begin{bmatrix} \underline{b}_{1}^{T}(\omega_{1}) \\ \underline{b}_{2}^{T}(\omega_{1}) \\ \underline{b}_{3}^{T}(\omega_{1}) \end{bmatrix} \underline{b}_{j}(\omega_{1}) \\
= \begin{bmatrix} [\underline{b}_{k}(\omega_{2})]^{T} [\underline{b}_{1}(\omega_{2}) : \underline{b}_{2}(\omega_{2}) : \underline{b}_{3}(\omega_{3})]] \underline{\underline{v}}_{2dq0} \\
= [P]_{3 \times 3} \underline{\underline{v}}_{2dq0}$$
(2-46)

where $[P]_{3\times3}$ contains only the weighting constants p_{jk} introduced in (2-21):

$$[P]_{3\times3} = \begin{bmatrix} p_{11} & p_{12} & p_{13} \\ p_{21} & p_{22} & p_{23} \\ p_{31} & p_{32} & p_{33} \end{bmatrix}$$
(2-47)

The simplification in the evaluation of (2-46) is the result of orthonormality of the base vectors. As an example for the method of carrying out the operations involved in (2-46), consider the case of j = 3 and k = 2. The corresponding 3×3 matrix will be found using (2-19) and (2-20), as follows:

$$p_{32} \begin{bmatrix} 0 \\ 0 \\ 1 \end{bmatrix} \begin{bmatrix} 0 & 1 & 0 \end{bmatrix} = \begin{bmatrix} 0 & 0 & 0 \\ 0 & 0 & 0 \\ 0 & p_{32} & 0 \end{bmatrix}$$
 (2-48)

Equation (2-46) is the voltage transformation in d-q-0 frame:

$$\underline{\mathbf{v}}_{1dq0} = [P]_{3\times3} \ \underline{\mathbf{v}}_{2dq0} \tag{2-49}$$

A similar relation can be derived for the current transformation in d-q-0 frame. Premultiplying both sides of (2-49) by \underline{i}_{1dq0}^{T}

$$i_{1dq0}^{T} \mathcal{Y}_{1dq0} = i_{1dq0}^{T} [P]_{3 \times 3} \mathcal{Y}_{2dq0}$$
 (2-50)

From power invariance principle, for an ideal matrix converter, one can write:

$$\underline{i}_{1dq0}^{T} \underline{y}_{1dq0} = \underline{i}_{2dq0}^{T} \underline{y}_{2dq0}$$
 (2-51)

Equating the right-hand-sides of (2-50) and (2-51),

$$i_{2dq0}^T = i_{1dq0}^T [P]_{3x3}$$
 (2-52)

By transposing both sides of (2-52), one gets:

$$\underline{i}_{2dq0} = [P]_{3\times3}^T \, \underline{i}_{1dq0}$$
(2-53)

which is the current transformation in d-q-0 frame.

As a result of the matrix manipulations in this section, the relationship between [H] and $[P]_{3\times 3}$ matrices can be derived as follows:

$$[P]_{3\times3} = [C(\omega_1)]^T [H] [C(\omega_2)]$$
 (2-54)

$$[H] = [C(\omega_1)][P]_{3\times3}[C(\omega_2)]^T$$
 (2-55)

Under steady-state operating conditions, \underline{v}_{idq0} and \underline{i}_{idq0} (i=1,2) are time-invariant vectors \underline{V}_{idq0} and \underline{I}_{idq0} in the d-q-0 vector space of side-i. All the controls performed by the matrix converter can therefore be studied in terms of mapping the constant vectors on one side to the other side, by the constant matrix $[P]_{3\times3}$.

After the analysis and design in the d-q-0 frame is completed, and the entries of the $[P]_{3\times3}$ -matrix are determined, (2-55) can be used to evaluate matrix [H] which is necessary for the implementation of the matrix converter.

2.7 Summary

In this chapter, it was shown that the frequency changing can be interpreted as a linear transformation through a dyadic matrix. The base vectors are taken from the d-q-0 to a-b-c Park's transformation matrix. It was shown that the dyadic matrix [H] in the a-b-c frame, has an equivalent dyadic matrix [P] in the d-q-0 frame. Because of the time-invariance, [P]-matrix is the preferred means for the analysis of the matrix converter as the [H]-matrix, in general, has sum of sine or cosine functions at angular frequencies $(\omega_1 + \omega_2)$ and $(\omega_1 - \omega_2)$ in each of its nine elements.

CHAPTER THREE

TRANSFORMATION MATRIX STRUCTURE

3.1 Introduction

In chapter 2, it was shown that the generalized transformation matrix in a-b-c frame is of the following structure:

$$[H] = [C(\omega_1)][P]_{3\times 3}[C(\omega_2)]^T$$
 (3-1)

where $C(\omega_1)$ and $C(\omega_2)$ are the well-known d-q-0 to a-b-c Park's transformation matrices at angular frequencies ω_1 and ω_2 , respectively, and

$$[P]_{3\times3} = \begin{bmatrix} p_{11} & p_{12} & p_{13} \\ p_{21} & p_{22} & p_{23} \\ p_{31} & p_{32} & p_{33} \end{bmatrix}$$
(3-2)

is the transformation matrix in the d-q-0 frame consisting of constant entries.

The objective of this chapter is to explore the roles played by the elements p_{jk} (j=1,2,3) and k=1,2,3 of the [P]-matrix of (3-2). With this understanding, the engineering design can then follow.

This chapter considers the case where zero-sequence components do not exist in the networks of either side of the matrix converter. The chapter proceeds with looking at the network of side-1 as viewed from side-2. Then, the side-1 network, referred to side-2, will be integrated with the network of side-2. From the resulting system, the properties of different [P]-matrix structures can be clearly understood. The analysis of this chapter is general and, as will be shown, covers the transformation matrices used by the predecessors: M. Venturini and A. Alesina [46, 47], P.D. Ziogas, S.I. Khan, and M.H. Rashid [59], and L.Huber and D. Borojevic [70]. Because the exhaustive study of all the possibilities would take more than one thesis, only the most important ones are considered here. The cases not considered are open for further exploration.

3.2 Network of Side-1 as Viewed from Side-2

Fig 3-1 shows the block diagram representation of the matrix converter and

the circuit diagram of the networks on side-1 and side-2. The circuits on both sides of the matrix converter have three-wire wye connection and therefore, the zero-sequence components do not exist. This reduces the order of the systems of equations in d-q-0 frame from 3 to 2, and as a result, makes the transformation of circuit equations from one side to the other side easier.

As a result of neglecting the zero-sequence components on both sides of the matrix converter, [P] will be a 2×2 matrix:

$$[P]_{2\times 2} = \begin{bmatrix} p_{11} & p_{12} \\ p_{21} & p_{22} \end{bmatrix}$$
 (3-3)

Equation (3-1) is therefore modified to:

$$[H] = [C(\omega_1)]_{3 \times 2} [F]_{2 \times 2} [C(\omega_2)]_{3 \times 2}^T$$
 (3-4)

where $\left[C(\omega_1)\right]_{3\times 2}$ and $\left[C(\omega_2)\right]_{3\times 2}$ are the Park's transformation matrices with the

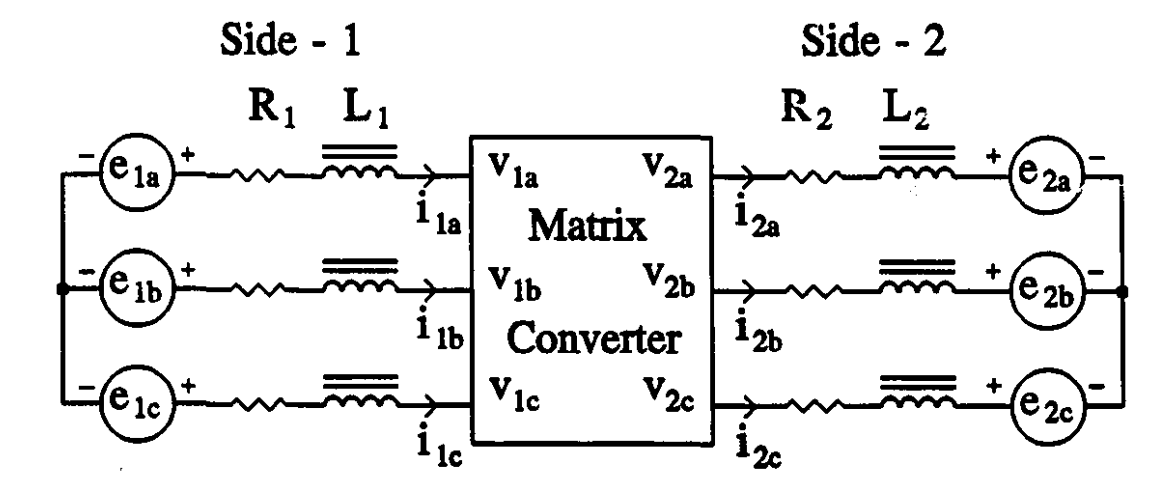


Fig. 3-1 Matrix converter with the networks of side-1 and side-2.

columns corresponding to the zero-sequence components omitted. The modified Park's transformation matrices have the following structures:

$$[C(\omega_1)]_{3\times 2} = [\underline{b}_1(\omega_1) : \underline{b}_2(\omega_1)]$$
 (3-5)

$$\left[C(\omega_2)\right]_{3\times 2} = \left[\underline{b}_1(\omega_2) : \underline{b}_2(\omega_2)\right] \tag{3-6}$$

where $\underline{b}_1(\omega_i)$ and $\underline{b}_2(\omega_i)$ are defined in (2-14) and (2-15), respectively.

From Kirchhoff's voltage law on side-1,

$$\underline{v}_{1abc} = \underline{e}_{1abc} - [R_1] \underline{i}_{1abc} - [L_1] \frac{d}{dt} \underline{i}_{1abc}$$
(3-7)

where

$$\underline{v}_{1abc} = \begin{bmatrix} v_{1a} \\ v_{1b} \\ v_{1c} \end{bmatrix} ; \underline{e}_{1abc} = \begin{bmatrix} e_{1a} \\ e_{1b} \\ e_{1c} \end{bmatrix} ; \underline{i}_{1abc} = \begin{bmatrix} i_{1a} \\ i_{1b} \\ i_{1c} \end{bmatrix}
\begin{bmatrix} R_1 \end{bmatrix} = \begin{bmatrix} R_1 & 0 & 0 \\ 0 & R_1 & 0 \\ 0 & 0 & R_1 \end{bmatrix} ; \underline{[L_1]} = \begin{bmatrix} L_1 & 0 & 0 \\ 0 & L_1 & 0 \\ 0 & 0 & L_1 \end{bmatrix}$$
(3-8)

Equation (3-7) in d-q frame is:

$$\underline{y}_{1dq} = \underline{e}_{1dq} - [R_1] \underline{i}_{1dq} - [L_1] \frac{d}{dt} \underline{i}_{1dq} - [G_1] \underline{i}_{1dq}$$
 (3-9)

where

$$\underline{v}_{1dq} = \begin{bmatrix} v_{1d} \\ v_{1q} \end{bmatrix} \quad ; \quad \underline{e}_{1dq} = \begin{bmatrix} e_{1d} \\ e_{1q} \end{bmatrix} \quad ; \quad \underline{i}_{1dq} = \begin{bmatrix} i_{1d} \\ i_{1q} \end{bmatrix} \\
[R_1] = \begin{bmatrix} R_1 & 0 \\ 0 & R_1 \end{bmatrix} \quad ; \quad [L_1] = \begin{bmatrix} L_1 & 0 \\ 0 & L_1 \end{bmatrix} \quad ; \quad [G_1] = \begin{bmatrix} 0 & -\omega_1 L_1 \\ \omega_1 L_1 & 0 \end{bmatrix}$$
(3-10)

The voltage and current transformation equations in d-q frame, equivalent to (2-8) and (2-11) are:

$$\underline{y}_{1dq} = [P]_{2 \times 2} \, \underline{y}_{2dq} \tag{3-11}$$

$$\underline{i}_{2dq} = [P]_{2\times 2}^T \underline{i}_{1dq}$$
(3-12)

The inverse transformation equations are:

$$\underline{\mathbf{v}}_{2da} = [P]_{2\times 2}^{-1} \, \underline{\mathbf{v}}_{1da} \tag{3-13}$$

$$i_{1dq} = ([P]_{2\times 2}^T)^{-1} i_{2dq} = ([P]_{2\times 2}^{-1})^T i_{2dq}$$
 (3-14)

where

$$[P]_{2\times2}^{-1} = \frac{1}{p_{11}p_{22} - p_{12}p_{21}} \begin{bmatrix} p_{22} & -p_{12} \\ -p_{21} & p_{11} \end{bmatrix}$$
(3-15)

Premultiplying both sides of (3-9) by $[P]_{2\times 2}^{-1}$ and substituting for $[P]_{2\times 2}^{-1} \underline{\nu}_{1dq}$ and \underline{i}_{1dq} from (3-13)and (3-14), respectively,

$$\underline{y}_{2dq} = \underline{e}'_{1dq} - \left[R'_1\right] \underline{i}_{2dq} - \left[L'_1\right] \frac{d}{dt} \underline{i}_{2dq} - \left[G'_1\right] \underline{i}_{2dq}$$
 (3-16)

where

$$\underline{e}'_{1dq} = [P]_{2 \times 2}^{-1} \ \underline{e}_{1dq} \tag{3-17}$$

$$[R_1'] = R_1 [P]_{2 \times 2}^{-1} ([P]_{2 \times 2}^{-1})^T$$
 (3-18)

$$[L_1'] = L_1[P]_{2\times 2}^{-1} ([P]_{2\times 2}^{-1})^T$$
 (3-19)

$$\left[G_1' \right] = \omega_1 L_1 \left[P \right]_{2 \times 2}^{-1} \begin{bmatrix} 0 & -1 \\ 1 & 0 \end{bmatrix} \left(\left[P \right]_{2 \times 2}^{-1} \right)^T$$
 (3-20)

Equation (3-16) describes the dynamics of side-1 network as viewed from side-2. As seen from (3-17) - (3-20), side-1 quantities have undergone quite significant transformations after being referred to side-2. Equations (3-16) - (3-20) clearly define the transformations of the source and terminal voltages, the currents, the resistances, the inductances, and the reactances of side-1. However, the results will still be quite undigestible for the case when $[P]_{2\times 2}$ is a full matrix. For this reason, this chapter will consider the simpler case of the diagonal matrix, before going to the full [P]-matrix.

To have an overall view of the whole system, the network of side-1, referred to side-2, and the side-2 network will be integrated into a single system. The integration of the networks of side-1 and side-2 which are, in general, excited at two different frequencies, has been made possible by the virtue of the transformation to

the d-q-0 frame.

3.3 Integration of Side-1 and Side-2 Networks

From Kirchhoff's voltage law on side-2 of Fig. 3-1,

$$\underline{v}_{2abc} = \underline{e}_{2abc} + [R_2] \underline{i}_{2abc} + [L_2] \frac{d}{dt} \underline{i}_{2abc}$$
(3-21)

where

$$\underline{v}_{2abc} = \begin{bmatrix} v_{2a} \\ v_{2b} \\ v_{2c} \end{bmatrix} ; \quad \underline{e}_{2abc} = \begin{bmatrix} e_{2a} \\ e_{2b} \\ e_{2c} \end{bmatrix} ; \quad \underline{i}_{2abc} = \begin{bmatrix} i_{2a} \\ i_{2b} \\ i_{2c} \end{bmatrix}
[R_{2}] = \begin{bmatrix} R_{2} & 0 & 0 \\ 0 & R_{2} & 0 \\ 0 & 0 & R_{2} \end{bmatrix} ; \quad [L_{2}] = \begin{bmatrix} L_{2} & 0 & 0 \\ 0 & L_{2} & 0 \\ 0 & 0 & L_{2} \end{bmatrix}$$
(3-22)

Remembering that on side-2, as on side-1, the zero-sequence components do not exist, (3-21) can be rewritten in d-q frame as:

$$y_{2dq} = e_{2dq} + [R_2]i_{2dq} + [L_2]\frac{d}{dt}i_{2dq} + [G_2]i_{2dq}$$
 (3-23)

where

$$\underline{v}_{2dq} = \begin{bmatrix} v_{2d} \\ v_{2q} \end{bmatrix} \quad ; \quad \underline{e}_{2dq} = \begin{bmatrix} e_{2d} \\ e_{2q} \end{bmatrix} \quad ; \quad \underline{i}_{2dq} = \begin{bmatrix} i_{2d} \\ i_{2q} \end{bmatrix} \\
\begin{bmatrix} R_2 \end{bmatrix} = \begin{bmatrix} R_2 & 0 \\ 0 & R_2 \end{bmatrix} \quad ; \quad \begin{bmatrix} L_2 \end{bmatrix} = \begin{bmatrix} L_2 & 0 \\ 0 & L_2 \end{bmatrix} \quad ; \quad \begin{bmatrix} G_2 \end{bmatrix} = \begin{bmatrix} 0 & -\omega_2 L_2 \\ \omega_2 L_2 & 0 \end{bmatrix}$$
(3-24)

The network of side-2 can now be integrated with the network of side-1 referred to side-2 by equating the right-hand-sides of (3-16) and (3-23). After some rearrangements, the resulting equation will be:

$$\underline{e}'_{1dq} = \underline{e}_{2dq} + ([R'_1] + [R_2])\underline{i}_{2dq} + ([L'_1] + [L_2])\frac{d}{dt}\underline{i}_{2dq} + ([G'_1] + [G_2])\underline{i}_{2dq}$$

$$+ ([G'_1] + [G_2])\underline{i}_{2dq}$$
(3-25)

Equation (3-25) describes the dynamics of the system of Fig. 3.1 from the point of view of side-2. Having obtained a complete image of the system, the properties of some transformation matrix structures can now be examined.

3.4 Diagonal Structure

This section is concerned with the $[P]_{2\times 2}$ -matrix of diagonal structure:

$$[P]_{2\times 2} = \begin{bmatrix} p_{11} & 0 \\ 0 & p_{22} \end{bmatrix}$$
 (3-26)

Three different cases will be considered:

(1)
$$p_{11} = p_{22} = P_f$$

(2)
$$p_{11} = -p_{22} = P_f$$

(3)
$$p_{11} \neq \pm p_{22}$$

With $[P]_{2\times 2}$ defined as in (3-26), (3-4) gives upon expansion:

$$[H] = \frac{p_{11} - p_{22}}{3} \begin{bmatrix} CS(0) & CS(-2\pi/3) & CS(-4\pi/3) \\ CS(-2\pi/3) & CS(-4\pi/3) & CS(0) \\ CS(-4\pi/3) & CS(0) & CS(-2\pi/3) \end{bmatrix}$$

$$+ \frac{p_{11} + p_{22}}{3} \begin{bmatrix} CD(0) & CD(-4\pi/3) & CD(-2\pi/3) \\ CD(-2\pi/3) & CD(0) & CD(-4\pi/3) \\ CD(-4\pi/3) & CD(-2\pi/3) & CD(0) \end{bmatrix}$$
(3-27)

where

$$CS(x) = \cos[(\omega_1 + \omega_2)t + x]$$
 (3-28)

and

$$CD(x) = \cos[(\omega_1 - \omega_2)t + x]$$
 (3-29)

Also, for the case of diagonal $[P]_{2\times 2}$ -matrix, (3-17) - (3-20) can be rewritten as:

$$\underline{e}'_{1dq} = \begin{bmatrix} \frac{e_{1d}}{p_{11}} \\ \frac{e_{1q}}{p_{22}} \end{bmatrix}$$
 (3-30)

$$\begin{bmatrix} R_1' \end{bmatrix} = \begin{bmatrix} \frac{R_1}{p_{11}^2} & 0 \\ 0 & \frac{R_1}{p_{22}^2} \end{bmatrix}$$
 (3-31)

$$\begin{bmatrix} L_1' \end{bmatrix} = \begin{bmatrix} \frac{L_1}{p_{11}^2} & 0 \\ 0 & \frac{L_1}{p_{22}^2} \end{bmatrix}$$
 (3-32)

$$[G_1'] = \frac{1}{p_{11}p_{22}} \begin{bmatrix} 0 & -\omega_1 L_1 \\ \omega_1 L_1 & 0 \end{bmatrix}$$
 (3-33)

3.4.1
$$p_{11} = p_{22} = P_f$$

In this case, the [H]-matrix of (3-27) becomes:

$$[H] = \frac{2}{3} P_f \begin{bmatrix} CD(0) & CD(-4\pi/3) & CD(-2\pi/3) \\ CD(-2\pi/3) & CD(0) & CD(-4\pi/3) \\ CD(-4\pi/3) & CD(-2\pi/3) & CD(0) \end{bmatrix}$$
(3-34)

where CD(x) is given by (3-29). As seen, each of the nine elements in the [H]matrix, contains a single cosine function at the angular frequency $\omega_1 - \omega_2$, i.e., the
difference of the side-1 and side-2 angular frequencies. This case offers less
complexity from the implementation point of view, compared to the more general
cases where there are two cosine functions at $\omega_1 + \omega_2$ and $\omega_1 - \omega_2$ in each element
of the [H]-matrix.

In the case of $p_{11} = p_{22} = P_f$, (3-30) - (3-33) can be rewritten as:

$$\underline{e}_{1dq}^{\prime} = \frac{1}{P_f} \underline{e}_{1dq} \tag{3-35}$$

$$[R_1'] = \frac{1}{P_f^2} [R_1]$$
 (3-36)

$$\left[L_1'\right] = \frac{1}{P_f^2} \left[L_1\right] \tag{3-37}$$

$$\left[G_{1}^{\prime}\right] = \frac{1}{P_{f}^{2}} \left[G_{1}\right] \tag{3-38}$$

where \underline{e}_{1dq} , $[R_1]$, $[L_1]$, and $[G_1]$ have been defined in (3-10). As seen, upon referring to side-2, the side-i voltages are divided by P_f and the resistances, inductances, and reactances are divided by P_f^2 .

3.4.2
$$p_{11} = -p_{22} = P_f$$

In this case, the [H]-matrix of (3-27) becomes:

$$[H] = \frac{2}{3} P_f \begin{bmatrix} CS(0) & CS(-2\pi/3) & CS(-4\pi/3) \\ CS(-2\pi/3) & CS(-4\pi/3) & CS(0) \\ CS(-4\pi/3) & CS(0) & CS(-2\pi/3) \end{bmatrix}$$
(3-39)

where CS(x) is defined by (3-28). Each element of the [H]-matrix, in this case, contains a single cosine function at the angular frequency $\omega_1 + \omega_2$, i.e., the sum of the side-1 and side-2 angular frequencies.

The referred quantities, from (3-30) - (3-33), are:

$$\underline{e}'_{1dq} = \frac{1}{P_f} \begin{bmatrix} e_{1d} \\ -e_{1q} \end{bmatrix} \tag{3-40}$$

$$[R_1'] = \frac{1}{P_f^2} [R_1] \tag{3-41}$$

$$\left[L_{1}'\right] = \frac{1}{P_{f}^{2}} \left[L_{1}\right] \tag{3-42}$$

$$\left[G_1'\right] = -\frac{1}{P_f^2} \left[G_1\right] \tag{3-43}$$

where $[R_1]$, $[L_1]$, and $[G_1]$ have been defined in (3-10). From (3-40) - (3-43), it can be seen that by referring to side-2, the magnitude of the side-1 source voltage is divided by P_f and the magnitudes of the resistances, inductances, and reactances are divided by P_f^2 . In this sense, the case of diagonal $[P]_{2\times 2}$ -matrix with $p_{11} = -p_{22} = P_f$ is not different from the case with $p_{11} = p_{22} = P_f$. Thus, as far as the transformation of the magnitudes of the quantities is concerned, P_f has the same effect in a matrix converter governed by a $[P]_{2\times 2}$ -matrix of diagonal structure as the primary to secondary turns ratio in a magnetic transformer. The matrix converter, as a frequency changer, adds to the capabilities of a magnetic transformer by being able to transform frequency, as well (realizing the idea of "Generalized Transformer").

The only difference between the results of the transformations in the two diagonal [P]-matrices studied, is that in the second case, i.e., $p_{11} = -p_{22} = P_f$, the complex voltages and impedances on side-1 are changed to complex conjugate quantities when referred to side-2. As will be seen later on, in section 3.5, this "Conjugate Property" offers the attractive practical advantage of reducing the total reactance of both sides through "Series Reactance Compensation". This will ease the task of displacement power factor correction. Because of this conjugate property, the case $p_{11} = -p_{22}$ is preferred to $p_{11} = p_{22}$.

3.4.3 $p_{11} \neq \pm p_{22}$

In this case, the [H]-matrix takes the complete form of (3-27) and the side-1 voltages, resistances, inductances, and reactances referred to side-2 are described by (3-30) - (3-33). The [H]-matrix elements contain cosine functions at angular frequencies $\omega_1 + \omega_2$ and $\omega_1 - \omega_2$, i.e., both sum and difference of the side-1 and side-2 angular frequencies. This is because the general diagonal $[P]_{2\times 2}$ -matrix is a linear combination of the $[P]_{2\times 2}$ -matrices in the two previous cases:

$$\begin{bmatrix} p_{11} & 0 \\ 0 & p_{22} \end{bmatrix} = \frac{p_{11} + p_{22}}{2} \begin{bmatrix} 1 & 0 \\ 0 & 1 \end{bmatrix} + \frac{p_{11} - p_{22}}{2} \begin{bmatrix} 1 & 0 \\ 0 & -1 \end{bmatrix}$$
(3-44)

The implementation is not as simple as in the last two cases. The referred quantities

assume more complex forms compared to the previous cases, as well.

For the sake of completeness, the case where the diagonal elements of the $[P]_{2\times 2}$ -matrix are zero $(p_{11}=p_{22}=0)$ and the off-diagonal elements are nonzero $(p_{12}\neq 0 \text{ and } p_{21}\neq 0)$ is studied in Appendix A.

An issue which has been attracting a lot of attention ever since static frequency changers were introduced, is the "Displacement Power Factor Control". In most of the cases, one is specially interested in getting "Unity Displacement Power Factor" at the interface of the matrix converter with the ac mains. The next section will explore the capabilities of the matrix converter governed by the diagonal $[P]_{2\times 2}$ -matrix, in this respect.

3.5 Unity Displacement Power Factor with Diagonal $[P]_{2\times 2}$ -Matrix

In Fig. 3.1, Unity Displacement Power Factor (UDPF) on the source side, corresponds to the in-phase relationship between the side-1 currents i_{1a} , i_{1b} , and i_{1c} , and the source voltages e_{1a} , e_{1b} , and e_{1c} , respectively. In d-q-0 frame, this translates to collinearity of the side-1 current and source voltage vectors, \underline{i}_{1dq} and \underline{e}_{1dq} .

The Displacement Power Factor (DPF) on side-1 is affected by all the parameters of the system. Therefore, the equation describing the behaviour of the integrated system, i.e., (3-25) will be used in the study carried out in this section. For

the general case of the diagonal $[P]_{2\times 2}$ -matrix $(p_{11} \neq \pm p_{22})$, (3-25) can be presented

as:

$$\begin{bmatrix} e'_{1d} \\ e'_{1q} \end{bmatrix} = \begin{bmatrix} e_{2d} \\ e_{2q} \end{bmatrix} + \begin{bmatrix} \frac{R_1}{p_{11}^2} + R_2 & 0 \\ 0 & \frac{R_1}{p_{22}^2} + R_2 \end{bmatrix} \begin{bmatrix} i_{2d} \\ i_{2q} \end{bmatrix}$$

$$+ \begin{bmatrix} \frac{L_1}{p_{11}^2} + L_2 & 0 \\ 0 & \frac{L_1}{p_{22}^2} + L_2 \end{bmatrix} \frac{d}{dt} \begin{bmatrix} i_{2d} \\ i_{2q} \end{bmatrix}$$

$$+ \begin{bmatrix} 0 & -\frac{\omega_1 L_1}{p_{11} p_{22}} - \omega_2 L_2 \\ \frac{\omega_1 L_1}{p_{11} p_{22}} + \omega_2 L_2 & 0 \end{bmatrix} \begin{bmatrix} i_{2d} \\ i_{2q} \end{bmatrix}$$
(3-45)

Under steady-state operating conditions, (3-45) can be written in the following decomposed form:

$$E'_{1d} = E_{2d} + \left(\frac{R_1}{p_{11}^2} + R_2\right) I_{2d} - \left(\frac{\omega_1 L_1}{p_{11} p_{22}} + \omega_2 L_2\right) I_{2q}$$
 (3-46)

$$E'_{1q} = E_{2q} + \left(\frac{R_1}{p_{22}^2} + R_2\right) I_{2q} + \left(\frac{\omega_1 L_1}{p_{11} p_{22}} + \omega_2 L_2\right) I_{2d}$$
 (3-47)

where E_{1d}' , E_{1q}' , E_{2d} , E_{2q} , I_{2d} , and I_{2q} are steady-state quantities, and the terms

containing d/dt have been omitted because of the fact that i_{2d} and i_{2q} are constants $(I_{2d} \text{ and } I_{2q}, \text{ respectively})$ at steady-state. Let us assume, for simplicity, that $E_{1q}=0$ $(E_{1q} \text{ being the steady-state value of } e_{1q})$. Therefore, from (3-30), $E_{1q}'=0$. Also, let $E_{2d}=E_{2q}=0$, i.e., let the network on side-2 be passive. UDPF on side-1 necessitates that $I_{1q}=0$ $(I_{1q} \text{ being the steady-state value of } i_{1q})$. From (3-12) and (3-26), $I_{1q}=0$ translates to $I_{2q}=0$ on side-2. Since $I_{2d}\neq 0$, in order for (3-47) to be satisfied, the following condition must hold:

$$\frac{\omega_1 L_1}{p_{11} p_{22}} + \omega_2 L_2 = 0 ag{3-48}$$

Substituting (3-48) in (3-46), one gets:

$$E_{1d}' = \left(\frac{R_1}{p_{11}^2} + R_2\right) I_{2d} \tag{3-49}$$

which from (3-12), (3-17), and (3-26), on side-1 is:

$$E_{1d} = (R_1 + p_{11}^2 R_2) I_{1d} ag{3-50}$$

Equation (3-50) clearly shows the resistance emulation or UDPF on side-1.

 p_{11} , which is the current gain of the matrix converter $(p_{11} = I_{2d}/I_{1d})$, can be found from (3-49) given the desired value of I_{2d} or the power demand on side-2, as:

$$p_{11} = \sqrt{\frac{R_1 I_{2d}}{E'_{1d} - R_2 I_{2d}}}$$
 (3-51)

Then, (3-48) can be used to find the value of p_{22} , corresponding to the choice of p_{11} , that maintains UDPF on side-1, in the following way:

$$p_{22} = -\frac{\omega_1 L_1}{p_{11} \omega_2 L_2} \tag{3-52}$$

If $p_{11} = -p_{22} = P_f$ is used or the network on side-2 is active, (i.e., $E_{2d} \neq 0$ and $E_{2q} \neq 0$), then there will not be enough degrees of freedom to achieve UDPF on side-1 and real power control.

The possibility of DPF correction and attaining UDPF on side-1 of the frequency changers, have been explained well by L.Gyugyi and B.R. Pelly in [1]. M. Venturini and A. Alesina incorporated this capability in the [H]-matrix of their matrix converter [46, 47], which was followed by the researchers thereafter. Appendix B shows that the [H]-matrix used by Venturini and Alesina has the same structure as given in (3-27), except for the constant terms.

Before directing attention towards the off-diagonal elements, let us summarize the properties of the diagonal $[P]_{2\times 2}$ -matrix.

3.6 Summary: Properties of Diagonal $[P]_{2\times 2}$ -Matrix

- The special cases for which $p_{11} = p_{22} = P_f$ and $p_{11} = -p_{22} = P_f$, offer less complexity in terms of implementation than the general case $(p_{11} \neq \pm p_{22})$.
- The general case $(p_{11} \neq \pm p_{22})$ and the case with $p_{11} = -p_{22} = P_f$, offer conjugate property. This property can be taken advantage of, in reactance compensation and as a result, in DPF correction. Equation (3-48) shows that reactance compensation can be carried out by proper choice of the inductances on one or both sides (if applicable), as well as by proper choice of p_{11} and p_{22} .
- In the case of general diagonal $[P]_{2\times 2}$ -matrix, (3-51) and (3-52) offer control levers p_{11} and p_{22} , for active and reactive power control, respectively.

3.7 Full $[P]_{2\times 2}$ -Matrix

As revealed by section 3.5, the diagonal $[P]_{2\times 2}$ -matrix, with the diagonal terms p_{11} and p_{22} , offers at most two degrees of freedom for control purposes. In this section, it will be shown that the inclusion of the off-diagonal elements in the $[P]_{2\times 2}$ -matrix will add to the control degrees of freedom, the control effect being that of "Phase Angle Rotation". Three different cases will be studied. In the first two cases, a single cosine function will appear in each element of the [H]-matrix, while in the

third case, each element in the [H]-matrix will have two cosine functions.

In subsection 3.7.1, the $[P]_{2\times 2}$ -matrix will be designed to result in cosine functions at angular frequency equal to the difference of the side-1 and side-2 angular frequencies, in the [H]-matrix. This case lacks the conjugate property and thus reactance compensation cannot be performed. Except for the rotation control, this case is similar to the case of the diagonal $[P]_{2\times 2}$ -matrix with $p_{11} = p_{22} = P_f$ of subsection 3.4.1.

Subsection 3.7.2 considers the case which results in an [H]-matrix containing cosine functions at angular frequency equal to the sum of the side-1 and side-2 angular frequencies. This case is similar to the case of diagonal $[P]_{2\times 2}$ -matrix with $p_{11} = -p_{22} = P_f$ of subsection 3.4.2. It offers the conjugate property plus the rotation control.

Subsection 3.7.3 considers, for the sake of completeness, the case which results in an [H]-matrix containing elements composed of cosine functions at angular frequencies equal to the sum and difference of the side-1 and side-2 angular frequencies. This case is similar to the case of general diagonal $[P]_{2\times 2}$ -matrix with $p_{11} \neq \pm p_{22}$ of subsection 3.4.3.

3.7.1 Non-Conjugate Rotation

In this case, $[P]_{2\times 2}$ -matrix is:

$$[P]_{2\times 2} = P_f \begin{bmatrix} \cos \gamma & \sin \gamma \\ -\sin \gamma & \cos \gamma \end{bmatrix}$$
 (3-53)

which is recognized as a rotational transformation matrix in Cartesian Coordinates. The angle of rotation is equal to γ . The corresponding [H]-matrix can be derived from (3-4) and has the formula exactly like (3-34), where

$$CD(x) = \cos \left[\left(\omega_1 - \omega_2 \right) t - \gamma + x \right] \tag{3-54}$$

The inverse of the rotational transformation matrix of (3-53) is:

$$[P]_{2\times2}^{-1} = \frac{1}{P_f} \begin{bmatrix} \cos\gamma & -\sin\gamma \\ \sin\gamma & \cos\gamma \end{bmatrix}$$
 (3-55)

Let

$$\underline{e}_{1dq} = \begin{bmatrix} e_{1d} \\ e_{1q} \end{bmatrix} = E_1 \begin{bmatrix} \cos \delta_1 \\ \sin \delta_1 \end{bmatrix}$$
 (3-56)

Substituting (3-55) and (3-56) in (3-17), then gives:

$$\underline{e}'_{1dq} = \frac{E_1}{P_f} \begin{bmatrix} \cos(\gamma + \delta_1) \\ \sin(\gamma + \delta_1) \end{bmatrix}$$
 (3-57)

According to (3-57), the vector \underline{e}_{1dq} is rotated by an angle γ , specified in the $[P]_{2\times 2}$ -

matrix, when it is referred to side-2.

In the case of the full $[P]_{2\times 2}$ -matrix under study, $[R_1']$, $[L_1']$, and $[G_1']$ of (3-18) - (3-20) will take exactly the same forms as (3-36) - (3-38).

It is gratifying to see that the angle of rotation, γ , appears only in the source voltage referred to side-2, given in (3-57), and the resistances, inductances, and reactances are not affected by γ .

It is quite clear that the full $[P]_{2\times 2}$ -matrix of this subsection, is a general form for the special case of the diagonal $[P]_{2\times 2}$ -matrix with $p_{11} = p_{22} = P_f$ of subsection 3.4.1. In fact, the latter can be obtained from the former, by just equating γ to zero.

3.7.2 Conjugate Rotation

In this case, $[P]_{2\times 2}$ -matrix is:

$$[P]_{2\times 2} = P_f \begin{bmatrix} \cos \gamma & \sin \gamma \\ \sin \gamma & -\cos \gamma \end{bmatrix}$$
 (3-58)

Equation (3-58) shares with (3-53), the scaling by the factor P_f and the rotation by the angle γ . The corresponding [H]-matrix can be found using (3-4), to be exactly like (3-39), where

$$CS(x) = \cos[(\omega_1 + \omega_2)t + \gamma + x]$$
 (3-59)

The inverse of the $[P]_{2\times 2}$ -matrix of (3-58) is:

$$[P]_{2\times2}^{-1} = \frac{1}{P_f} \begin{bmatrix} \cos\gamma & \sin\gamma \\ \sin\gamma & -\cos\gamma \end{bmatrix}$$
 (3-60)

Letting \underline{e}_{1dq} be as in (3-56), (3-17) then yields:

$$\underline{e}'_{1dq} = \frac{E_1}{P_f} \begin{bmatrix} \cos(\gamma - \delta_1) \\ \sin(\gamma - \delta_1) \end{bmatrix}$$
 (3-61)

Equation (3-61) indicates a rotation by an angle γ as a result of referring \underline{e}_{1dq} to side-2. Also, from (3-61), it is observed that upon referring, \underline{e}_{1dq} becomes conjugated prior to being rotated by γ . The conjugate property is similar to the one in the case of diagonal $[P]_{2\times 2}$ -matrix with $p_{11} = -p_{22} = P_f$.

In the case of the full $[P]_{2\times 2}$ -matrix under study, $[R_1']$, $[L_1']$, and $[G_1']$ of (3-18) - (3-20) will take exactly the same forms as (3-41) - (3-43). Equation (3-43) shows that in this case, the impedance of side-1 is conjugated when referred to side-2, offering the possibility of reactance compensation and DPF correction.

The case of full $[P]_{2\times 2}$ -matrix studied in this section, is the general form for the special case of diagonal $[P]_{2\times 2}$ -matrix with $P_{11} = -P_{22} = P_f$ of subsection 3.4.2. The

latter can be obtained from the former, by just putting γ equal to zero. In this way, only the phase rotation property vanishes, but all other properties are preserved.

3.7.3 General Full $[P]_{2\times 2}$ -Matrix

Just in the same way as the general diagonal $[P]_{2\times 2}$ -matrix of subsection 3.4.3 was described as the superposition of two elementary cases of subsections 3.4.1 and 3.4.2, the general full $[P]_{2\times 2}$ -matrix can be represented as the weighted sum of the two elementary cases of subsections 3.7.1 and 3.7.2:

$$[P]_{2\times 2} = \begin{bmatrix} p_{11} & p_{12} \\ p_{21} & p_{22} \end{bmatrix} = P_{f1} \begin{bmatrix} \cos\gamma_1 & \sin\gamma_1 \\ -\sin\gamma_1 & \cos\gamma_1 \end{bmatrix} + P_{f2} \begin{bmatrix} \cos\gamma_2 & \sin\gamma_2 \\ \sin\gamma_2 & -\cos\gamma_2 \end{bmatrix}$$
(3-62)

From (3-62),

$$\begin{split} P_{f1}\cos\gamma_1 + P_{f2}\cos\gamma_2 &= p_{11} \\ P_{f1}\sin\gamma_1 + P_{f2}\sin\gamma_2 &= p_{12} \\ P_{f1}\sin\gamma_1 - P_{f2}\sin\gamma_2 &= -p_{21} \\ P_{f1}\cos\gamma_1 - P_{f2}\cos\gamma_2 &= p_{22} \end{split} \tag{3-63}$$

 P_{fl} , P_{f2} , γ_1 , and γ_2 can be easily found from (3-63), in terms of p_{11} , p_{12} , p_{21} , and p_{22} as:

$$P_{f1} = \frac{1}{2} \sqrt{(p_{11} + p_{22})^2 + (p_{12} - p_{21})^2}$$

$$\gamma_1 = \arctan \frac{p_{12} - p_{21}}{p_{11} + p_{22}}$$
(3-64)

$$P_{f2} = \frac{1}{2} \sqrt{(p_{11} - p_{22})^2 + (p_{12} + p_{21})^2}$$

$$\gamma_2 = \arctan \frac{p_{12} + p_{21}}{p_{11} - p_{22}}$$
(3-65)

The explicit solutions for P_{f1} , γ_1 , P_{f2} , and γ_2 show that any 2×2 [P]-matrix can be decoupled into two 2×2 elementary matrices of the form given in (3-62).

Using (3-4), the [H]-matrix can be found to have the same structure as in (3-27), except that $(p_{11} - p_{22})/3$ is replaced by $2/3P_{f2}$ and $(p_{11} + p_{22})/3$ by $2/3P_{f1}$. CD(x) and CS(x) are as defined by (3-54) and (3-59), respectively. As seen, the general full $[P]_{2\times 2}$ -matrix of (3-62) results in an [H]-matrix whose elements contain cosine functions at the sum and difference of side-1 and side-2 angular frequencies. By putting $\gamma_1 = \gamma_2 = 0$, the case of general diagonal $[P]_{2\times 2}$ -matrix of subsection 3.4.3 results.

Equations (3-17) - (3-20), in the case of full $[P]_{2\times 2}$ -matrix of (3-63), take more complex forms than in the case of subsections 3.7.1 and 3.7.2, due to the presence of the angles of rotation, γ_1 and γ_2 , in the referred resistances, inductances, and

reactances, as well as in the referred voltages. The physical meaning, in this case, is not clear.

3.8 Unity Displacement Power Factor (UDPF) with Full $[P]_{2\times 2}$ -Matrix

The general full $[P]_{2\times2}$ -matrix is supposed to be able to perform both DPF correction on side-1 and real power control even with a three-phase active load connected on side-2; but the complexity of structure and lack of clear physical insight makes its use inconvenient. The two special cases of subsections 3.7.1 and 3.7.2 offer two control degrees of freedom, each. Therefore, as discussed in section 3.5, for a general active load on side-2, DPF control on side-1 and satisfying the power demand on side-2 is not possible.

Consider the case of full $[P]_{2\times 2}$ -matrix with conjugate rotation of subsection 3.7.2. Equation (3-25) can be presented in the following form:

$$\begin{bmatrix} e'_{1d} \\ e'_{1q} \end{bmatrix} = \begin{bmatrix} e_{2d} \\ e_{2q} \end{bmatrix} + \begin{bmatrix} \frac{R_1}{P_f^2} + R_2 & 0 \\ 0 & \frac{R_1}{P_f^2} + R_2 \end{bmatrix} \begin{bmatrix} i_{2d} \\ i_{2q} \end{bmatrix} + \begin{bmatrix} \frac{L_1}{P_f^2} + L_2 & 0 \\ 0 & \frac{L_1}{P_f^2} + L_2 \end{bmatrix} \frac{d}{dt} \begin{bmatrix} i_{2d} \\ i_{2q} \end{bmatrix} + \begin{bmatrix} 0 & \frac{\omega_1 L_1}{P_f^2} - \omega_2 L_2 \\ -\frac{\omega_1 L_1}{P_f^2} + \omega_2 L_2 & 0 \end{bmatrix} \begin{bmatrix} i_{2d} \\ i_{2q} \end{bmatrix}$$

(3-66)

In the steady-state, (3-66) can be rewritten in the following decomposed form:

$$E'_{1d} = E_{2d} + \left(\frac{R_1}{p_f^2} + R_2\right) I_{2d} + \left(\frac{\omega_1 L_1}{p_f^2} - \omega_2 L_2\right) I_{2q}$$
 (3-67)

$$E'_{1q} = E_{2q} + \left(\frac{R_1}{p_f^2} + R_2\right) I_{2q} - \left(\frac{\omega_1 L_1}{p_f^2} - \omega_2 L_2\right) I_{2d}$$
 (3-68)

Let us consider a simple case where $E_{2q}=0$. In (3-61), γ can be chosen equal to δ_1 resulting in $E_{1q}'=0$. Also, the coefficient of I_{2d} in (3-68) can be made zero by appropriate choice of P_f . Then from (3-68), one can deduce that $I_{2q}=0$; thus (3-67) becomes:

$$E'_{1d} = E_{2d} + \left(\frac{R_1}{P_f^2} + R_2\right) I_{2d}$$
 (3-69)

From (3-69), one can see that UDPF has been attained on side-2. Using (3-12), I_{1dq} can be found in the following way:

$$I_{1dq} = \begin{bmatrix} I_{1d} \\ I_{1q} \end{bmatrix} = \left([P]_{2\times 2}^{-1} \right)^T \begin{bmatrix} I_{2d} \\ 0 \end{bmatrix} = \frac{1}{P_f} \begin{bmatrix} \cos\gamma & \sin\gamma \\ \sin\gamma & -\cos\gamma \end{bmatrix} \begin{bmatrix} I_{2d} \\ 0 \end{bmatrix} = \frac{I_{2d}}{P_f} \begin{bmatrix} \cos\gamma \\ \sin\gamma \end{bmatrix}$$
(3-70)

Comparing (3-56) and (3-70), one can see that for the previous choice of $\gamma = \delta_1$, \underline{I}_{1dq} and \underline{E}_{1dq} are collinear, i.e., UDPF condition has been established on side-1.

It is noteworthy that UDPF condition has been established on both sides of

the matrix converter using the full $[P]_{2\times 2}$ -matrix. The significance of this dual situation will be discussed later in chapter 5.

As can be seen, because of the lack of enough degrees of freedom, I_{2d} or the side-2 power demand cannot be controlled at this point.

It is interesting to point out that the $[P]_{2\times 2}$ -matrix equivalent of the [H]-matrices used by the researchers like P.D. Ziogas, S.I. Khan, and M.H. Rashid [59], and L. Huber and D. Borojevic [70], is of the structure given in (3-62). This has been shown in Appendix C.

Before closing the discussion on the full $[P]_{2\times 2}$ -matrix, let us summarize the properties of this structure.

3.9 Summary: Properties of Full $[P]_{2\times 2}$ -Matrix

- The special cases studied (i.e., non-conjugate rotation and conjugate rotation) offer more physical insights into the mechanism of operation and less complexity from implementation point of view, compared to the general case.
- The conjugate rotation case of section 3.7.2 offers conjugate property which helps correct the displacement power factor on side-1.
- The conjugate rotation version of the full $[P]_{2\times 2}$ -matrix offers both the

scaling factor, P_f , and the rotation angle, γ . P_f defines the gain of the matrix converter and γ -control can be used to align the referred side-1 source voltage vector along the desired direction. Adjustments of P_f and γ can result in UDPF on side-1 and even on side-2, but real power control cannot be performed due to the lack of enough degrees of freedom.

- In the case of a passive network on side-2, UDPF can be established on both sides by just adjusting P_f . In this case, γ -control is dormant.
- The general full $[P]_{2\times 2}$ -matrix, with four control degrees of freedom is supposed to be able to perform DPF control on side-1 and real power control with a general active load on side-2. But, the complexity of the structure does not offer proper physical insight into the mechanism of operation.

3.10 Summary

The criteria for the choice of a proper $[P]_{2\times 2}$ -matrix are:

- Clear physical insight;
- Sufficient control levers or degrees of freedom;

and

- A corresponding [H]-matrix of acceptable degree of complexity from the implementation point of view.

Following the above line of thinking, from the special cases studied in this chapter, the selection is:

$$[P]_{2\times 2} = P_f \begin{bmatrix} \cos\gamma & \sin\gamma \\ \sin\gamma & -\cos\gamma \end{bmatrix}$$
 (3-71)

and

$$[H] = \frac{2}{3} P_f \begin{bmatrix} CS(0) & CS\left(-\frac{2\pi}{3}\right) & CS\left(-\frac{4\pi}{3}\right) \\ CS\left(-\frac{2\pi}{3}\right) & CS\left(-\frac{4\pi}{3}\right) & CS(0) \\ CS\left(-\frac{4\pi}{3}\right) & CS(0) & CS\left(-\frac{2\pi}{3}\right) \end{bmatrix}$$
(3-72)

where

$$CS(x) = \cos[(\omega_1 + \omega_2)t + \gamma + x]$$
 (3-73)

One sees that besides the inherent frequency changing capability (from ω_1 to ω_2), the matrix converter has two independent levers of control:

- (1) Scaling by the factor P_f ;
- (2) Phase Rotation by the angle γ .

Furthermore, it offers the conjugate property, which can be used for reactance compensation with the goal of Unity Displacement Power Factor (UDPF). UDPF on both sides is attainable for both passive and active networks on side-2. However, the power demand or the motor torque (in the case of a motor load) cannot be

controlled, simultaneously, because this will require another degree of freedom in the control.

The next chapter will study the zero-sequence interaction in the matrix converters and will use it to add more degrees of freedom in the control.

ZERO-SEQUENCE INTERACTION IN MATRIX CONVERTERS

4.1 Introduction

In the matrix converter of Fig. 3.1, there was no zero-sequence component, because the networks on side-1 and side-2 were connected in three-wire wye configuration. The three-wire wye and delta are the configurations used by almost all researchers. In either case, there is no need to worry about the zero-sequence components.

In the derivation of the system equations (3-25), (3-45), and (3-66), the effect of the filter capacitors at side-2 terminals of the matrix converter (Fig. 4-1) was neglected, because the inclusion of the capacitors would complicate the system equations. Since the filter capacitors are fairly small, ignoring them in the derivations would not alter the results considerably. Taking the capacitors into consideration, will

not result in any zero-sequence components, if they are connected in three-wire wye or delta configuration, as shown in Figs. 4-1(a) and 4-1(b), respectively.

This chapter deals with the case where zero-sequence components are present. In Fig. 4-2, the capacitors on side-2 of the matrix converter are connected in four-wire wye configuration. Because of the return path to the converter, provided for the charging currents of the capacitors, the presence of the zero-sequence components on side-2 cannot be ignored. Since the voltage sources on both sides of the matrix

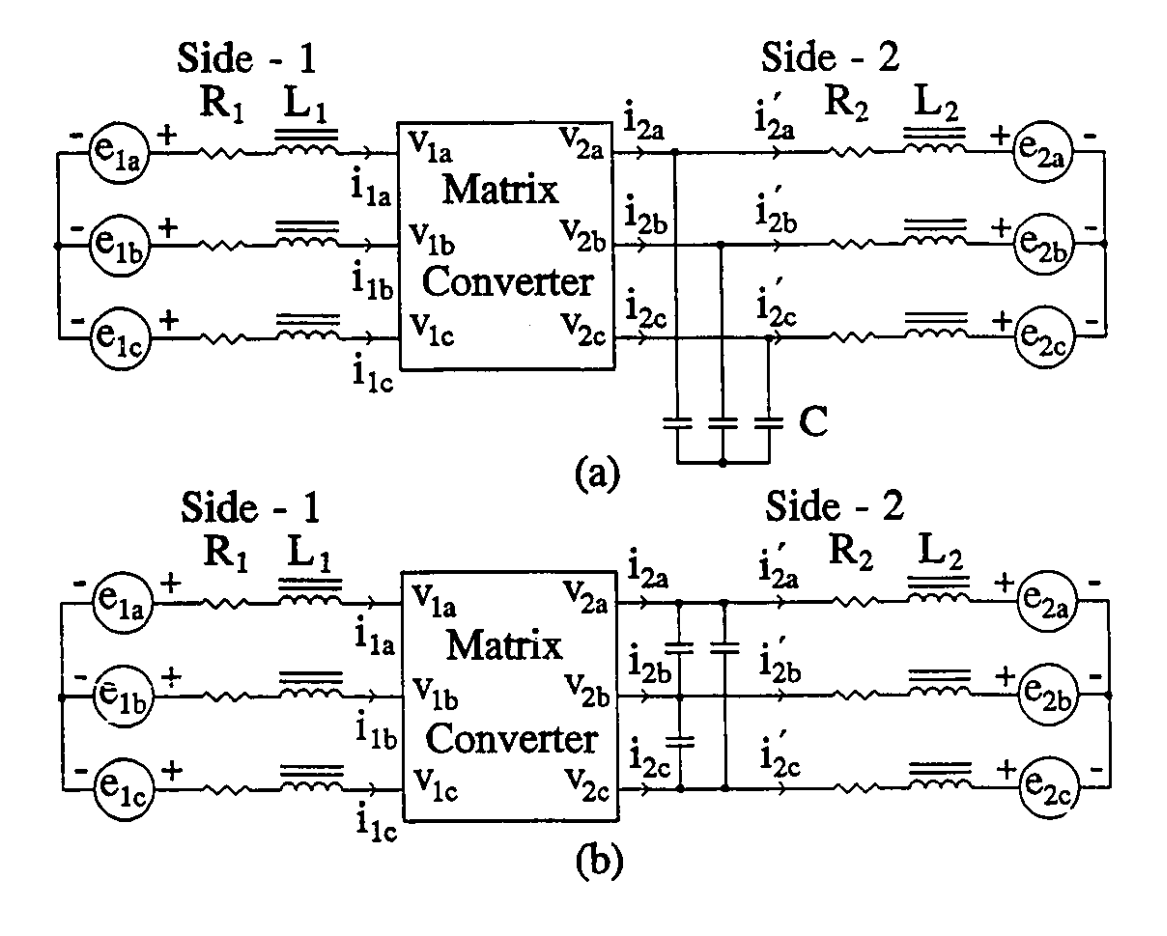


Fig. 4-1 Matrix converter with the networks of side-1 and side-2 including the side-2 capacitors.

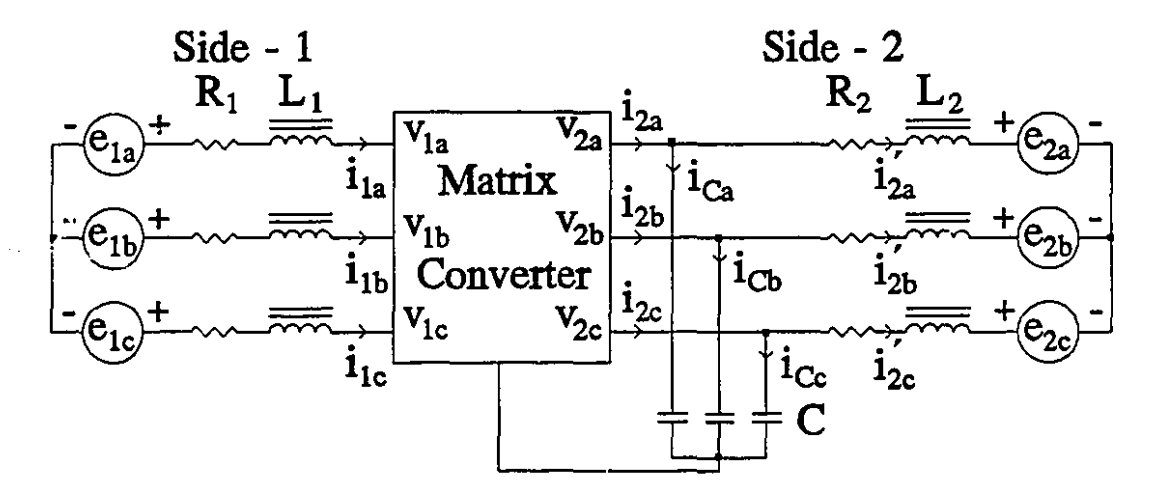


Fig. 4-2 Matrix converter with the networks of side-1 and side-2 (Side-2 capacitors connected in four-wire wye).

converter are connected in three-wire wye configuration, the zero-sequence currents can only flow through the capacitors, and return to the converter through the neutral line. Likewise, the zero-sequence voltages can exist only across the capacitors.

There are basically three reasons why this chapter is dedicated to the study of the zero-sequence interaction in matrix converters:

- (1) Basic Research: Zero-sequence components can exist in matrix converters; therefore, it is reasonable to study their effects and explore some ways in which they can be exploited.
- (2) Search for more control levers: It was concluded in chapter 3 that the favourable $[P]_{2\times 2}$ -matrix of subsection 3.7.2, with rotation and conjugate properties, is in need of more degrees of freedom or control levers to accomplish real power control together with Displacement

Power Factor (DPF) control on side-1. This chapter will investigate the possibility of using the zero-sequence components to create additional control levers.

(3) Laying the theoretical foundation for the study of a matrix converter based on three-phase voltage-source converters in chapter 6.

This chapter contains the following important contributions of this thesis:

- SVC control: A static VAR controller (SVC) has been included in the body of the matrix converter which uses the zero-sequence components of the voltages on side-2 to control DPF on side-1.
- Dual Unity Displacement Power Factor (UDPF) on side-1 and Field

 Vector Control on side-2: With adequate number of control levers

 made available, the matrix converter can enjoy UDPF on both sides.

This chapter will proceed with the derivation of the mathematical model of the matrix converter with the zero-sequence components present. The complete [P] and [H] matrices will be presented and finally the control levers and their control actions will be explained.

4.2 System Equations Including Zero-Sequence

In Fig. 4.2, the capacitor currents are:

$$\dot{i}_{C} = \begin{bmatrix} i_{Ca} \\ i_{Cb} \\ i_{Cc} \end{bmatrix}$$
(4-1)

and the currents through the network on the right-hand-side of the capacitors are defined as:

$$\dot{i}'_{2abc} = \begin{vmatrix} i'_{2a} \\ i'_{2b} \\ i'_{2c} \end{vmatrix}$$
(4-2)

where the side-2 terminal currents, \underline{i}_{2abc} , the capacitor currents, \underline{i}_{C} , and the load currents, \underline{i}'_{2abc} are related in the following way:

$$\underline{i}'_{2abc} = \underline{i}_{2abc} - \underline{i}_{C} \tag{4-3}$$

Since the zero-sequence components exist on side-2, a 2×3 [P]-matrix and the 3×3 Park's transformation matrix $[C(\omega_2)]_{3\times3}$, given by (2-38) must be used. The $[P]_{2\times3}$ -matrix has the following structure:

$$[P]_{2\times3} = \begin{bmatrix} p_{11} & p_{12} & p_{13} \\ p_{21} & p_{22} & p_{23} \end{bmatrix}$$
 (4-4)

and the [H]-matrix can be evaluated as follows:

$$[H] = [C(\omega_1)]_{3\times 2} [F]_{2\times 3} [C(\omega_2)]_{3\times 3}^T$$
 (4-5)

Equation (4-5) can be presented in more detailed form as:

$$[H] = \left[\underline{b}_{1}(\omega_{1}) : \underline{b}_{2}(\omega_{1})\right] \begin{bmatrix} p_{11} & p_{12} & p_{13} \\ p_{21} & p_{22} & p_{23} \end{bmatrix} \begin{bmatrix} \underline{b}_{1}^{T}(\omega_{2}) \\ \underline{b}_{2}^{T}(\omega_{2}) \\ \underline{b}_{3}^{T}(\omega_{2}) \end{bmatrix}$$
(4-6)

In the voltage transformation,

$$\underline{v}_{1abc} = [H] \underline{v}_{2abc} = [C(\omega_1)]_{3\times 2} [P]_{2\times 3} ([C(\omega_2)]_{3\times 3}^T \underline{v}_{2abc})$$
(4-7)

the term in parentheses, is the side-2 voltage vector in d-q-0 frame containing all three d, q, and 0 components:

$$\begin{bmatrix} v_{2d} \\ v_{2q} \\ v_{20} \end{bmatrix} = \begin{bmatrix} \underline{b}_{1}^{T}(\omega_{2}) \\ \underline{b}_{2}^{T}(\omega_{2}) \\ \underline{b}_{3}^{T}(\omega_{2}) \end{bmatrix} \underline{v}_{2abc}$$

$$(4-8)$$

The side-2 terminal voltages with respect to the common connection point of the capacitors are:

$$\underline{v}_{2abc} = \underline{v}'_{2abc} + v_{zs} \begin{bmatrix} 1 \\ 1 \\ 1 \end{bmatrix}$$
 (4-9)

where

$$\underline{y}'_{2abc} = \underline{e}_{2abc} + [R_2] \underline{i}'_{2abc} + [L_2] \frac{d}{dt} \underline{i}'_{2abc}$$
 (4-10)

and

$$v_{zs} = \frac{v_{2a} + v_{2b} + v_{2c}}{3} \tag{4-11}$$

is the zero-sequence component of the voltages of side-2. Substituting (4-10) in (4-9) and the resulting equation in (4-8), and using (3-23),

$$\begin{bmatrix} v_{2d} \\ v_{2q} \\ v_{20} \end{bmatrix} = \begin{bmatrix} e_{2d} \\ e_{2q} \end{bmatrix} + \begin{bmatrix} R_2 & 0 \\ 0 & R_2 \end{bmatrix} \begin{bmatrix} i'_{2d} \\ i'_{2q} \end{bmatrix} + \begin{bmatrix} L_2 & 0 \\ 0 & L_2 \end{bmatrix} \frac{d}{dt} \begin{bmatrix} i'_{2d} \\ i'_{2q} \end{bmatrix} + \begin{bmatrix} 0 & -\omega_2 L_2 \\ \omega_2 L_2 & 0 \end{bmatrix} \begin{bmatrix} i'_{2d} \\ i'_{2q} \end{bmatrix}$$

$$(4-12)$$

$$\sqrt{3} v_{zs}$$

At steady-state, \underline{v}_{2dq0} is a constant vector; therefore, v_{zs} is a constant scalar, V_{dc} . The dc voltages of the capacitors on side-2 are set up at the start-up and maintained during the operation of the system, through a negative feedback control loop [78]. The control loop ensures that the zero-sequence component of \underline{i}_{2abc} is equal to zero. This control loop will be explained in chapter 6 and Appendix D.

4.3 Decoupling the Zero-Sequence Interaction

Based on the conclusions made in section 3.10 of chapter 3, the $[P]_{2\times 2}$ -matrix of (3-71) is used here as a submatrix in the $[P]_{2\times 3}$ -matrix:

$$[P]_{2\times3} = \begin{bmatrix} P_f \begin{bmatrix} \cos\gamma & \sin\gamma \\ \sin\gamma & -\cos\gamma \end{bmatrix} & \vdots & \begin{bmatrix} p_{13} \\ p_{23} \end{bmatrix} \end{bmatrix}$$
(4-13)

Therefore, the voltage transformation equation

$$\underline{v}_{1da} = [P]_{2 \times 3} \, \underline{v}_{2da0} \tag{4-14}$$

becomes

$$\begin{bmatrix} v_{1d} \\ v_{1q} \end{bmatrix} = P_f \begin{bmatrix} \cos \gamma & \sin \gamma \\ \sin \gamma & -\cos \gamma \end{bmatrix} \begin{bmatrix} v_{2d} \\ v_{2q} \end{bmatrix} + \begin{bmatrix} p_{13} \\ p_{23} \end{bmatrix} v_{20}$$
(4-15)

Equation (4-15) can be changed to power balance equation through multiplication of both sides by $\begin{bmatrix} i_{1d} & i_{1q} \end{bmatrix}$:

$$\begin{bmatrix} i_{1d} & i_{1q} \end{bmatrix} \begin{bmatrix} v_{1d} \\ v_{1q} \end{bmatrix} = \begin{bmatrix} i_{1d} & i_{1q} \end{bmatrix} P_f \begin{bmatrix} \cos \gamma & \sin \gamma \\ \sin \gamma & -\cos \gamma \end{bmatrix} \begin{bmatrix} v_{2d} \\ v_{2q} \end{bmatrix} + \begin{bmatrix} i_{1d} & i_{1q} \end{bmatrix} \begin{bmatrix} p_{13} \\ p_{23} \end{bmatrix} v_{20}$$
(4-16)

The zero component of the side-2 currents can be defined from the second term on the right-hand-side of (4-16) to be:

$$i_{20} = p_{13} i_{1d} + p_{23} i_{1g} (4-17)$$

The elements p_{13} and p_{23} of $[P]_{2\times 3}$ -matrix can be controlled in order to make sure that i_{20} will be zero after the capacitors on side-2 have been charged to their dc bias level. Therefore, according to (4-16), all the power from side-1 will go to the first

term on the right-hand-side and from power balance principle,

$$\begin{bmatrix} i_{2d} \\ i_{2q} \end{bmatrix} = P_f \begin{bmatrix} \cos \gamma & \sin \gamma \\ \sin \gamma & -\cos \gamma \end{bmatrix} \begin{bmatrix} i_{1d} \\ i_{1q} \end{bmatrix}$$
(4-18)

which is in the same form as (3-12).

4.3.1 Polar Representation

In order to decouple the d-q variables from the zero-axis variables, one can start with the polar representation of $\begin{bmatrix} i_{1d} & i_{1q} \end{bmatrix}^T$ and $\begin{bmatrix} p_{13} & p_{23} \end{bmatrix}^T$:

$$\begin{bmatrix} i_{1d} \\ i_{1q} \end{bmatrix} = I_1 \begin{bmatrix} \cos \eta_1 \\ \sin \eta_1 \end{bmatrix} \tag{4-19}$$

$$\begin{bmatrix} p_{13} \\ p_{23} \end{bmatrix} = P_{\varphi} \begin{bmatrix} \cos \varphi \\ \sin \varphi \end{bmatrix} \tag{4-20}$$

Substituting (4-19) and (4-20) in (4-17),

$$i_{20} = P_{\varphi} I_1 \cos(\varphi - \eta_1)$$
 (4-21)

From (4-21), $i_{20} = 0$ necessitates that $\varphi - \eta_1 = \pm \pi/2$. As will be seen in chapter 6, sections 6.5.3 and 6.5.4, based on the closed-loop control system employed for dc bias voltage regulation on side-2 and the role of P_{φ} in DPF control on side-1, for both positive and negative values of P_{φ} the following relation will hold:

$$\varphi - \eta_1 = -\frac{\pi}{2} \tag{4-22}$$

This is just another way of expressing the condition of quadrature relationship between the side-1 current vector, $\begin{bmatrix} i_{1u} & i_{1q} \end{bmatrix}^T$, and the voltage vector projected by the zero component of side-2 voltage vector on side-1, $\begin{bmatrix} p_{13} & p_{23} \end{bmatrix}^T \nu_{20}$. The magnitude of the projected voltage on side-1 due to the zero component of the voltage on side-2 is $|P_{\varphi}|\nu_{20}$. The negative feedback loop adjusts the phase angle φ to set up the condition given by (4-22), while P_{φ} controls the size of the projected voltage.

4.4 Referring the Network of Side-1 to Side-2

The side-1 equations in the d-q frame is given in (3-9). Replacing \underline{v}_{1dq} in (3-9) by its equivalent from (4-15),

$$P_{f}\begin{bmatrix} \cos \gamma & \sin \gamma \\ \sin \gamma & -\cos \gamma \end{bmatrix} \begin{bmatrix} v_{2d} \\ v_{2q} \end{bmatrix} + P_{\varphi} \begin{bmatrix} \cos \varphi \\ \sin \varphi \end{bmatrix} v_{20} = \begin{bmatrix} e_{1d} \\ e_{1q} \end{bmatrix}$$

$$- \begin{bmatrix} R_{1} & 0 \\ 0 & R_{1} \end{bmatrix} \begin{bmatrix} i_{1d} \\ i_{1q} \end{bmatrix} - \begin{bmatrix} L_{1} & 0 \\ 0 & L_{1} \end{bmatrix} \frac{d}{dt} \begin{bmatrix} i_{1d} \\ i_{1q} \end{bmatrix} - \begin{bmatrix} 0 & -\omega_{1} L_{1} \\ \omega_{1} L_{1} & 0 \end{bmatrix} \begin{bmatrix} i_{1d} \\ i_{1q} \end{bmatrix}$$

$$(4-23)$$

Equation (4-18), upon inversion, yields:

$$\begin{bmatrix} i_{1d} \\ i_{1q} \end{bmatrix} = \frac{1}{P_f} \begin{bmatrix} \cos \gamma & \sin \gamma \\ \sin \gamma & -\cos \gamma \end{bmatrix} \begin{bmatrix} i_{2d} \\ i_{2q} \end{bmatrix}$$
(4-24)

Substituting (4-24) in (4-23) and premultiplying both sides by $[P]_{2\times 2}^{-1}$ given in (3-60) and rearranging terms,

$$\begin{bmatrix} v_{2d} \\ v_{2q} \end{bmatrix} = \frac{1}{P_f} \begin{bmatrix} \cos \gamma & \sin \gamma \\ \sin \gamma & -\cos \gamma \end{bmatrix} \begin{bmatrix} e_{1d} \\ e_{1q} \end{bmatrix} - \frac{1}{P_f^2} \begin{bmatrix} R_1 & 0 \\ 0 & R_1 \end{bmatrix} \begin{bmatrix} i_{2d} \\ i_{2q} \end{bmatrix} - \frac{1}{P_f^2} \begin{bmatrix} L_1 & 0 \\ 0 & L_1 \end{bmatrix} \frac{d}{dt} \begin{bmatrix} i_{2d} \\ i_{2q} \end{bmatrix}$$

$$- \frac{1}{P_f^2} \begin{bmatrix} 0 & \omega_1 L_1 \\ -\omega_1 L_1 & 0 \end{bmatrix} \begin{bmatrix} i_{2d} \\ i_{2q} \end{bmatrix} - \frac{P_{\varphi}}{P_f} v_{20} \begin{bmatrix} \cos (\gamma - \varphi) \\ \sin (\gamma - \varphi) \end{bmatrix}$$
(4-25)

4.4.1 SVC Voltage

The additional term in (4-25), due to the zero component of the side-2 voltages, which is given the name "Static VAR Controller (SVC) voltage", is the subject of this subsection. The SVC voltage is:

$$\underline{e}_{\varphi dq} = \frac{P_{\varphi}}{P_{f}} \nu_{20} \begin{bmatrix} \cos(\gamma - \varphi) \\ \sin(\gamma - \varphi) \end{bmatrix}$$
 (4-26)

The two additional control degrees of freedom resulting from the introduction of p_{13} and p_{23} , are:

- The angle of rotation φ;
- The scaling factor P_{Φ} .

The angle φ is adjusted by the negative feedback control loop (regulating V_{dc}) to ensure the quadrature relationship between the voltage vector $\underline{e}_{\varphi dq}$ and the

current vector $\begin{bmatrix} i_{2d} & i_{2q} \end{bmatrix}^T$. The above condition is the restatement of the quadrature relationship between the voltage vector $\begin{bmatrix} p_{13} & p_{23} \end{bmatrix}^T v_{20}$ and the current vector $\begin{bmatrix} i_{1d} & i_{1q} \end{bmatrix}^T$ on side-1, explained in subsection 4.3.1.

The scaling factor P_{φ} controls the size of the SVC voltage, $\underline{e}_{\varphi dq}$, which is in quadrature with the side-2 current vector $\begin{bmatrix} i_{2d} & i_{2q} \end{bmatrix}^T$. The effect of this voltage on side-2 is the same as a controllable inductive or capacitive reactance. The SVC voltage will be used for DPF correction purposes.

4.5 Integrating the Networks of Side-1 and Side-2

Because of the presence of the filter capacitors in Fig. 4.2, the current vector \underline{i}_{2do0} consists of two parts:

$$\begin{bmatrix} i_{2d} \\ i_{2q} \\ i_{20} \end{bmatrix} = \begin{bmatrix} i'_{2d} \\ i'_{2q} \\ 0 \end{bmatrix} + \begin{bmatrix} i_{Cd} \\ i_{Cq} \\ i_{C0} \end{bmatrix}$$
(4-27)

The three-wire wye connected network on the right-hand-side of the capacitors in F.g. 4-2 does not have zero-sequence components so that only i'_{2d} and i'_{2q} exist. The zero-sequence components exist only through the return path of the filter capacitors.

This section deals with the d and q components only. Subsection 4.5.1 is a treatment of the zero component.

If the left-hand-side of (4-25) is replaced by its equivalent from the first two lines of (4-12), after some rearrangements, the following equation is obtained:

$$\begin{bmatrix} e'_{1d} \\ e'_{1q} \end{bmatrix} = \frac{1}{P_f} \begin{bmatrix} \cos \gamma & \sin \gamma \\ \sin \gamma & -\cos \gamma \end{bmatrix} \begin{bmatrix} e_{1d} \\ e_{1q} \end{bmatrix} = \begin{bmatrix} e_{2d} \\ e_{2q} \end{bmatrix} + \frac{1}{P_f^2} \begin{bmatrix} R_1 & 0 \\ 0 & R_1 \end{bmatrix} \begin{bmatrix} i_{2d} \\ i_{2q} \end{bmatrix}$$

$$+ \begin{bmatrix} R_2 & 0 \\ 0 & R_2 \end{bmatrix} \begin{bmatrix} i'_{2d} \\ i'_{2q} \end{bmatrix} + \frac{1}{P_f^2} \begin{bmatrix} L_1 & 0 \\ 0 & L_1 \end{bmatrix} \frac{d}{dt} \begin{bmatrix} i_{2d} \\ i_{2q} \end{bmatrix}$$

$$+ \begin{bmatrix} L_2 & 0 \\ 0 & L_2 \end{bmatrix} \frac{d}{dt} \begin{bmatrix} i'_{2d} \\ i'_{2q} \end{bmatrix} + \frac{1}{P_f^2} \begin{bmatrix} 0 & \omega_1 L_1 \\ -\omega_1 L_1 & 0 \end{bmatrix} \begin{bmatrix} i_{2d} \\ i_{2q} \end{bmatrix}$$

$$+ \begin{bmatrix} 0 & -\omega_2 L_2 \\ \omega_2 L_2 & 0 \end{bmatrix} \begin{bmatrix} i'_{2d} \\ i'_{2q} \end{bmatrix} + \frac{P_{\varphi}}{P_f} v_{20} \begin{bmatrix} \cos (\gamma - \varphi) \\ \sin (\gamma - \varphi) \end{bmatrix}$$

$$+ \frac{1}{2} \begin{bmatrix} v_{2d} \\ v_{2d} \end{bmatrix} + \frac{1}{2} \begin{bmatrix}$$

Equation (4-28) describes the dynamics of the system, including side-2 capacitors, as viewed from side-2. The current vectors \underline{i}_{2dq} and \underline{i}'_{2dq} are related in the following way:

$$\begin{bmatrix} i'_{2d} \\ i'_{2q} \end{bmatrix} = \begin{bmatrix} i_{2d} \\ i_{2q} \end{bmatrix} - \begin{bmatrix} i_{Cd} \\ i_{Cq} \end{bmatrix}$$

$$(4-29)$$

where $\underline{i}_{Cdq} = [i_{Cd} \ i_{Cq}]^T$ is the vector of the d and q components of the capacitor charging current governed by the equation

$$\begin{bmatrix} i_{Cd} \\ i_{Cq} \end{bmatrix} = \begin{bmatrix} C & 0 \\ 0 & C \end{bmatrix} \frac{d}{dt} \begin{bmatrix} v_{Cd} \\ v_{Cq} \end{bmatrix} + \begin{bmatrix} 0 & -\omega_2 C \\ \omega_2 C & 0 \end{bmatrix} \begin{bmatrix} v_{Cd} \\ v_{Cq} \end{bmatrix}$$
(4-30)

with $\begin{bmatrix} v_{Cd} & v_{Cq} \end{bmatrix}^T$ being the capacitor voltage vector which is equal to $\begin{bmatrix} v_{2d} & v_{2q} \end{bmatrix}^T$.

In steady-state, (4-28) becomes:

$$\begin{bmatrix} E'_{1d} \\ E'_{1q} \end{bmatrix} = \frac{1}{P_f} \begin{bmatrix} \cos \gamma & \sin \gamma \\ \sin \gamma & -\cos \gamma \end{bmatrix} \begin{bmatrix} E_{1d} \\ E_{1q} \end{bmatrix} = \begin{bmatrix} E_{2d} \\ E_{2q} \end{bmatrix} + \frac{1}{P_f^2} \begin{bmatrix} R_1 & 0 \\ 0 & R_1 \end{bmatrix} \begin{bmatrix} I_{2d} \\ I_{2q} \end{bmatrix}
+ \begin{bmatrix} R_2 & 0 \\ 0 & R_2 \end{bmatrix} \begin{bmatrix} I'_{2d} \\ I'_{2q} \end{bmatrix} + \frac{1}{P_f^2} \begin{bmatrix} 0 & \omega_1 L_1 \\ -\omega_1 L_1 & 0 \end{bmatrix} \begin{bmatrix} I_{2d} \\ I_{2q} \end{bmatrix}
+ \begin{bmatrix} 0 & -\omega_2 L_2 \\ \omega_2 L_2 & 0 \end{bmatrix} \begin{bmatrix} I'_{2d} \\ I'_{2q} \end{bmatrix} + \frac{P_{\phi}}{P_f} V_{20} \begin{bmatrix} \cos (\gamma - \phi) \\ \sin (\gamma - \phi) \end{bmatrix}$$
(4-31)

Fig. 4-3 shows the equivalent circuit diagram of the system of Fig. 4-2, with the network of side-1 referred to side-2 and integrated with the network of side-2, based on (4-31).

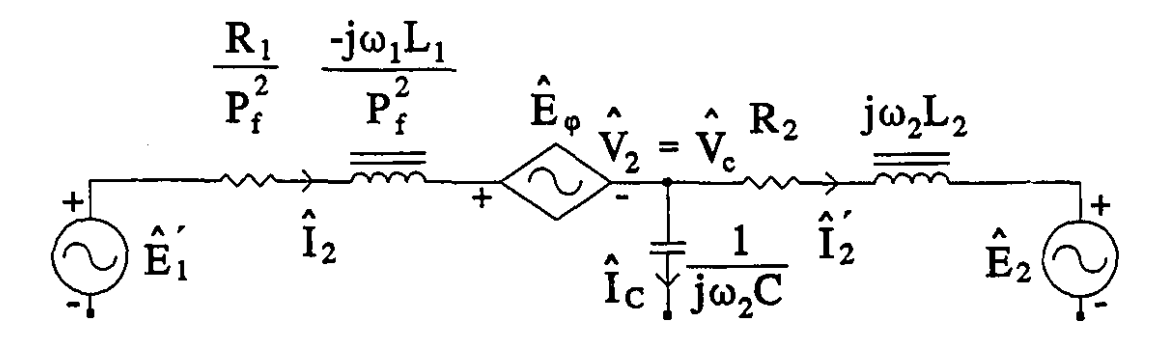


Fig. 4-3 Equivalent circuit diagram of the syustem of Fig. 4-2 as viewed from side-2.

The phasor diagram of the voltages and currents in Fig. 4-3 is shown in Fig. 4-4.

4.5.1 Zero Components of Voltage and Current

The zero component of the charging current, i_{20} , is given by (4-21). The zero component of the voltage, v_{20} , is charged by i_{20} according to the equation:

$$v_{20}(t) = \frac{1}{C} \int_{-\infty}^{0} i_{20} d\tau + \frac{1}{C} \int_{0}^{t} i_{20} d\tau$$
 (4-32)

Prior to t=0, the capacitor has been charged to the voltage V_{20} ($V_{20} rianlge t$ the steady-state value of v_{20}):

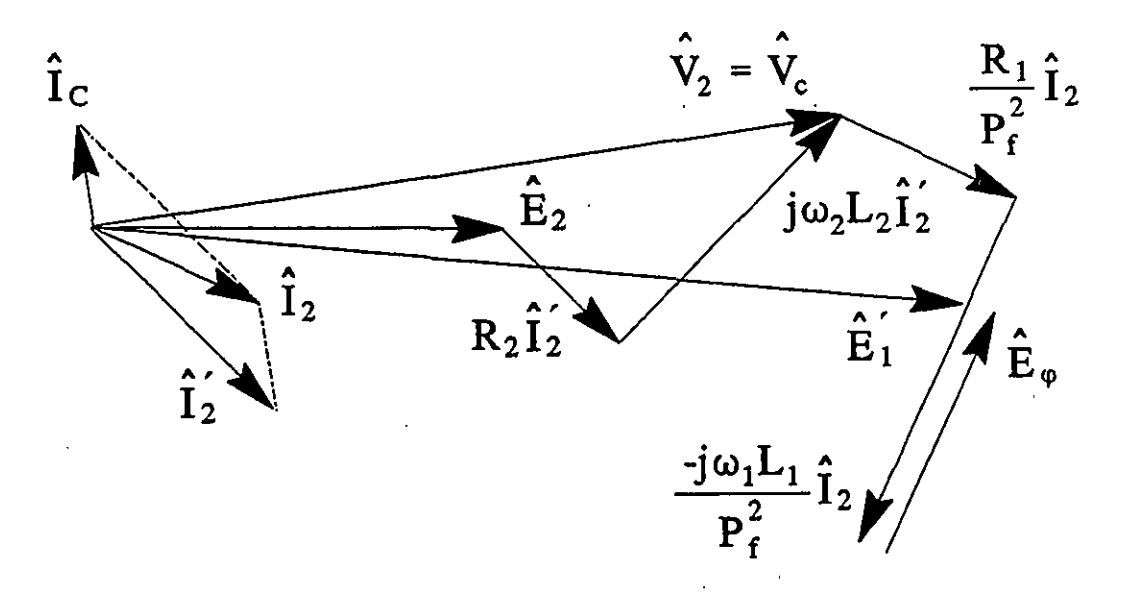


Fig. 4-4 Phasor diagram of Fig. 4-3.

$$V_{20} = \frac{1}{C} \int_{-\infty}^{0} i_{20}(\tau) d\tau$$
 (4-33)

Thereafter, the SVC control keeps $i_{20} = 0$ by making $\varphi - \eta_1 = -\pi/2$, so that

$$\frac{1}{C} \int_{0}^{t} i_{20}(\tau) d\tau = 0 (4-34)$$

and

$$v_{20}(t) = V_{20} \tag{4-35}$$

4.6 [H]-Matrix Associated with the $[P]_{2\times 3}$ -Matrix

The $[P]_{2\times 3}$ -matrix of (4-4) can be represented as:

$$[P]_{2\times 3} = [[P]_{2\times 2} : [P]_{2\times 1}]$$
 (4-36)

where the $[P]_{2\times 2}$ and $[P]_{2\times 1}$ matrices are defined in (3-58) and (4-20), respectively.

The matrix [H] is then found using (4-5) as follows:

$$[H] = [C(\omega_{1})]_{3\times2}[[P]_{2\times2} : [P]_{2\times1}]_{2\times3}[C(\omega_{2})]_{3\times3}^{T}$$

$$= [C(\omega_{1})]_{3\times2}[[P]_{2\times2} : [P]_{2\times1}]_{2\times3}\begin{bmatrix} [C(\omega_{2})]_{3\times2}^{T} \\ \dots \\ b_{3}^{T}(\omega_{2}) \end{bmatrix}$$

$$= [C(\omega_{1})]_{3\times2}[P]_{2\times2}[C(\omega_{2})]_{3\times2}^{T} + [C(\omega_{1})]_{3\times2}[P]_{2\times1}\underline{b}_{3}^{T}(\omega_{2})$$

$$= [H_{f}] + [H_{\phi}]$$

$$(4-37)$$

The first term on the right-hand-side of (4-37), $[H_f]$, is the Frequency Changer Matrix, with the same structure as in (3-39):

$$[H_f] = \frac{2P_f}{3} \begin{bmatrix} CS(0) & CS(-2\pi/3) & CS(-4\pi/3) \\ CS(-2\pi/3) & CS(-4\pi/3) & CS(0) \\ CS(-4\pi/3) & CS(0) & CS(-2\pi/3) \end{bmatrix}$$
(4-38)

where CS(x) is defined in the same way as in (3-59):

$$CS(x) = \cos[(\omega_1 + \omega_2)t + \gamma + x]$$
 (4-39)

The second term on the right-hand-side of (4-37), $[H_{\varphi}]$, is called the SVC Matrix, with the following structure:

$$[H_{\varphi}] = \frac{\sqrt{2}}{3} P_{\varphi} \begin{bmatrix} C(0) & C(0) & C(0) \\ C(-2\pi/3) & C(-2\pi/3) & C(-2\pi/3) \\ C(-4\pi/3) & C(-4\pi/3) & C(-4\pi/3) \end{bmatrix}$$
 (4-40)

where

$$C(x) = \cos(\omega_1 t + \varphi + x) \tag{4-41}$$

The complete [H]-matrix is capable of:

- Frequency changing from ω_1 to ω_2 ;
- Magnitude control of Side-2 voltage by P_f ;
- Rotating the side-1 source voltage by γ, as viewed from side-2;
- Maintaining a regulated dc bias voltage, V_{dc} , across the side-2 filter capacitors through adjustments of angle φ ; and
- DPF control on side-1 by P_{∞} .

4.7 Summary

In this chapter, the zero-sequence interaction in matrix converters has been studied. The $[P]_{2\times 2}$ -matrix of chapter 3 has been modified to a $[P]_{2\times 3}$ -matrix, due to the presence of zero-sequence components on side-2. In this way, two control degrees of freedom are added to the system. The first control lever is the angle φ , that regulates the zero-sequence voltage on side-2 which is a dc voltage. The second control lever is the scaling factor P_{φ} , that is used to control the Displacement Power Factor (DPF) on side-1. The DPF control method used in this thesis is based on varying the size of a voltage called SVC voltage which acts like a controllable inductive or capacitive reactance and will be explained in chapter 5. This chapter has also provided the theoretical base for the application of dyadic matrix converter

theory to a new matrix converter system composed of three three-phase voltagesource converters to be studied in chapter 6.

FEASIBILITY OF BOTH UNITY DISPLACEMENT POWER FACTOR AND FIELD VECTOR CONTROL

5.1 Introduction

In this chapter, it will be shown that the two desirable features of Unity Displacement Power Factor (UDPF) at the ac supply end [1,46,65,70,80,81] and Field Vector Control (FVC) at the motor end [76,77,80,81] can be realized, at the same time, using the matrix converter of Fig. 4-2.

Fig. 5-1 shows the single-line equivalent circuit diagram of the network on side-1 of the system of Fig. 4-2. For UDPF condition to exist at the interface with the ac mains, the side-1 source voltage vector, \hat{E}_1 , and current vector, \hat{I}_1 , must be collinear, as shown in the phasor diagram of Fig. 5-2. In doing this, the matrix

converter behaves like a Static VAR Compensator (SVC), besides acting as a frequency changer.

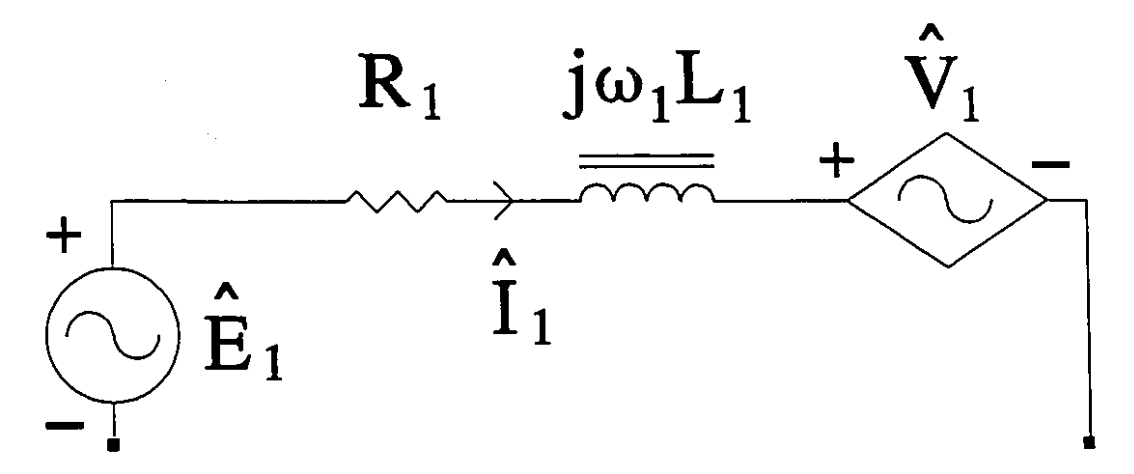


Fig. 5-1 Single-line equivalent circuit diagram of side-1 of system of Fig. 4-2.

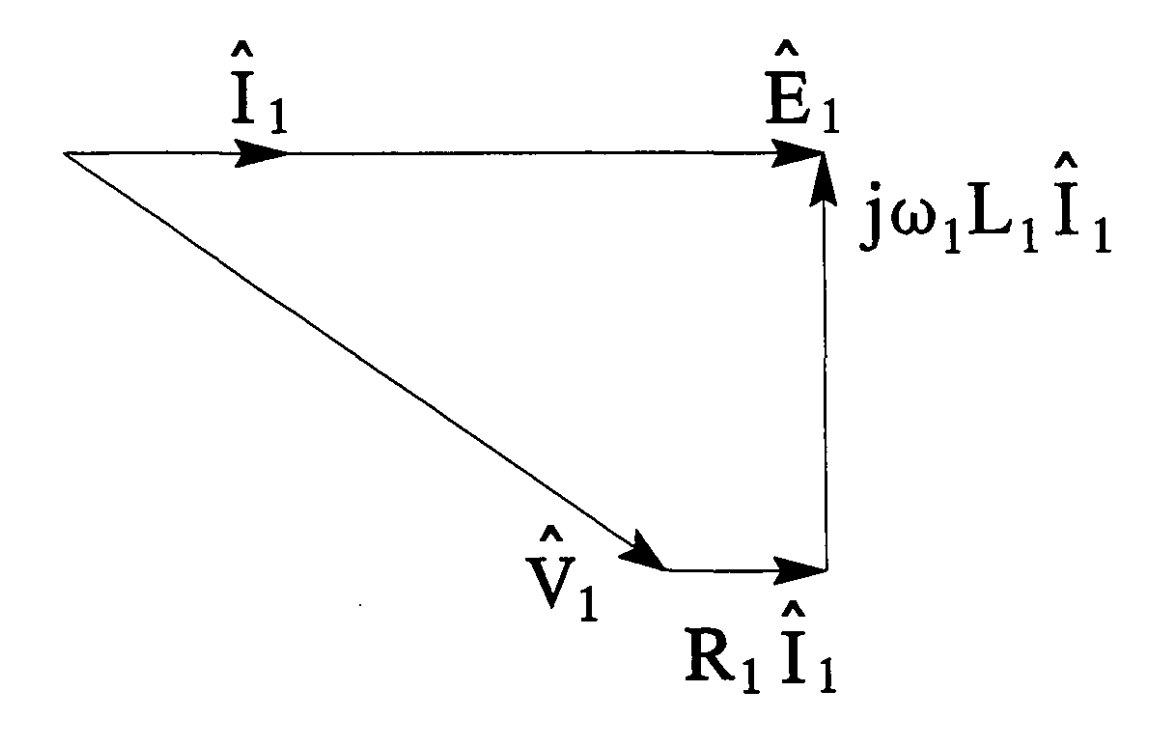


Fig. 5-2 Phasor diagram of Fig. 5-1.

Fig. 5-3 shows the single-line equivalent circuit diagram of the network on side-2 of the system of Fig. 4.2. For Field Vector Control (FVC) condition to exist at the interface with the ac motor (synchronous motor) on side-2, the axes of the magnetic fluxes produced by the stator and the rotor currents of the motor must be kept at space quadrature. In the time domain, the above requirement translates into the alignment of the stator current phasor, \hat{I}'_2 , and the phasor of the induced voltage behind the synchronous reactance, \hat{E}_2 , as shown in the phasor diagram of Fig. 5-4.

This chapter shows that the matrix converter of Fig. 4-2, under the control of $[P]_{2\times 3}$ -matrix, presented in chapter 4, can function as a high performance variable-speed ac motor drive by offering UDPF on side-1 and FVC on side-2, at the same time.

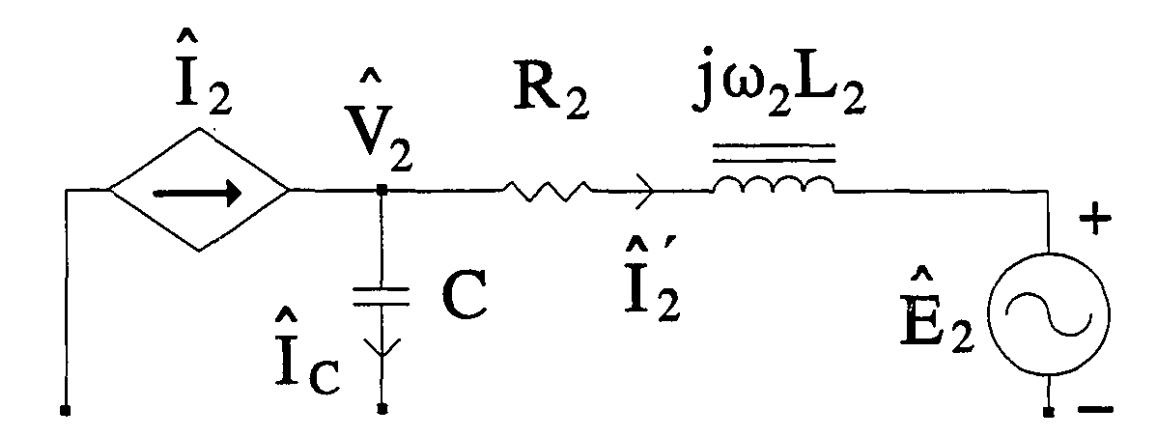


Fig. 5-3 Single-line equivalent circuit diagram of side-2 of system of Fig. 4-2.

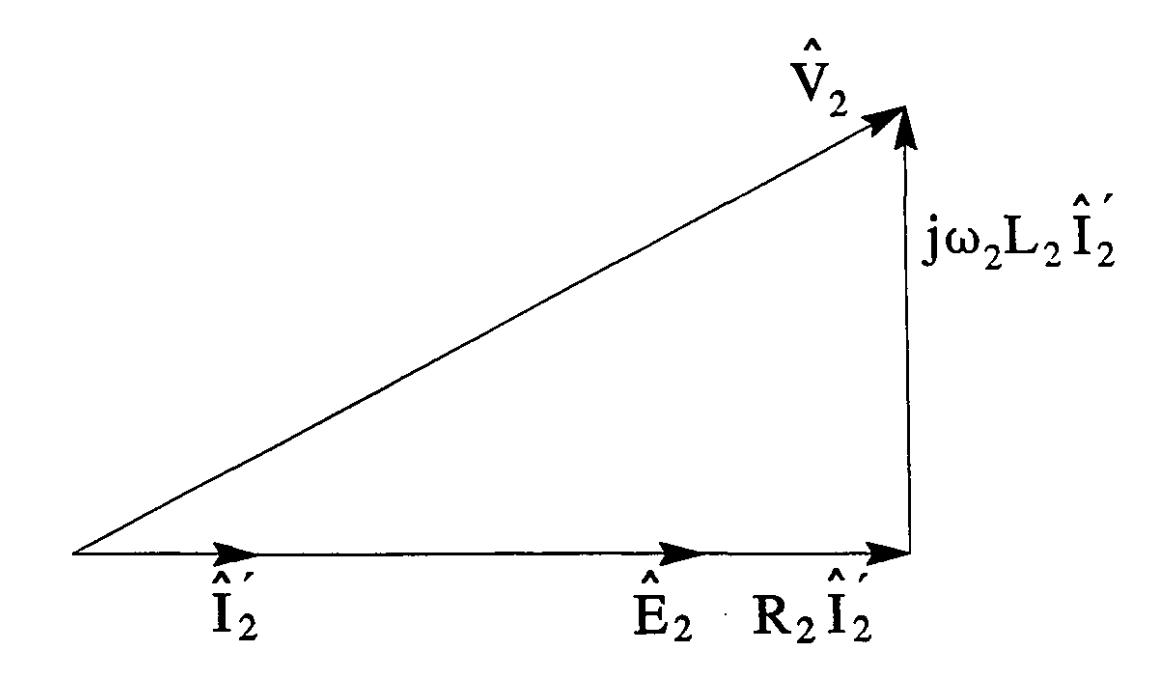


Fig. 5-4 Phasor diagram of Fig. 5-3.

5.2 Dual Condition of UDPF on Side-1 and FVC on Side-2

In this section, the procedure of reaching at the dual condition of UDPF on side-1 and FVC on side-2 and the role of different control levers in accomplishing the above task are explained.

The mathematical model of the integrated system, given by (4-31), is used as the working tool for the study carried out in this section. Since (4-31) is in terms of the side-2 quantities, in order to be able to use it for UDPF study on side-1, a clear relationship between the current and voltage vectors of side-1, and the referred current and voltage vectors on side-2 must be established. From (3-12), (3-17), (3-56), (3-58), and (4-19), it can be deduced that in referring side-1 source voltage vector,

 \underline{E}_{1dq} , and current vector, \underline{I}_{1dq} , to side-2, they will be both conjugated and rotated through the same angle, γ :

$$I_{2dq} = [P]_{2x2} I_{1dq} = P_f \begin{bmatrix} \cos \gamma & \sin \gamma \\ \sin \gamma & -\cos \gamma \end{bmatrix} I_1 \begin{bmatrix} \cos \eta_1 \\ \sin \eta_1 \end{bmatrix}$$

$$= P_f I_1 \begin{bmatrix} \cos (\gamma - \eta_1) \\ \sin (\gamma - \eta_1) \end{bmatrix}$$
(5-1)

$$\underline{E}'_{1dq} = [P]_{2x2}^{-1} \underline{E}_{1dq} = \frac{1}{P_f} \begin{bmatrix} \cos \gamma & \sin \gamma \\ \sin \gamma & -\cos \gamma \end{bmatrix} E_1 \begin{bmatrix} \cos \delta_1 \\ \sin \delta_1 \end{bmatrix} \\
= \frac{E_1}{P_f} \begin{bmatrix} \cos (\gamma - \delta_1) \\ \sin (\gamma - \delta_1) \end{bmatrix} \tag{5-2}$$

Therefore, the phase relationship between the side-1 source voltage and current vectors will remain unchanged after referring to side-2 and the phase relationship of \underline{E}'_{1dq} and \underline{I}_{2dq} can be studied instead of that of \underline{E}_{1dq} and \underline{I}_{1dq} . More specifically, \underline{I}_{2dq} being in phase with \underline{E}'_{1dq} automatically implies that UDPF exists on side-1.

Due to the complexity of (4-31), the role played by each control input and the way the conditions of UDPF on side-1 and FVC on side-2 are established cannot be clearly seen. For this reason, the analysis of this section will be performed in two parts. In the first part, subsection 5.2.1, the filter capacitors on side-2 will be neglected to clarify the main ideas. Since the side-2 terminal capacitors are small, the effect of neglecting them will not be considerably large. In practice, taking care of

the effect of the presence of the capacitors is a matter of fine adjustment of the control inputs, after the desired conditions have been approached through coarse adjustments. In the second part of this section, subsection 5.2.2, the effect of the capacitors will be considered.

5.2.1 Filter Capacitors Neglected

When the filter capacitors on side-2 of Fig. 4-2 are neglected,

$$i_{2abc}^{\prime} = i_{2abc} \tag{5-3}$$

In this case, the single-line equivalent circuit diagram of the system as viewed from side-2 shown in Fig. 4-3, will be modified to that of Fig. 5-5, where

$$R_T = \frac{R_1}{P_f^2} + R_2 {(5-4)}$$

$$X_T = \frac{-\omega_1 L_1}{P_f^2} + \omega_2 L_2 \tag{5-5}$$

and (4-31) can be rewritten as:

$$\begin{bmatrix} E'_{1d} \\ E'_{1q} \end{bmatrix} = \begin{bmatrix} E_{2d} \\ E_{2q} \end{bmatrix} + \begin{bmatrix} R_T - X_T \\ X_T R_T \end{bmatrix} \begin{bmatrix} I_{2d} \\ I_{2q} \end{bmatrix} + \frac{P_{\varphi}}{P_f} V_{20} \begin{bmatrix} \cos(\gamma - \varphi) \\ \sin(\gamma - \varphi) \end{bmatrix}$$
(5-6)

Equation (5-6) can be written as two simultaneous equations:

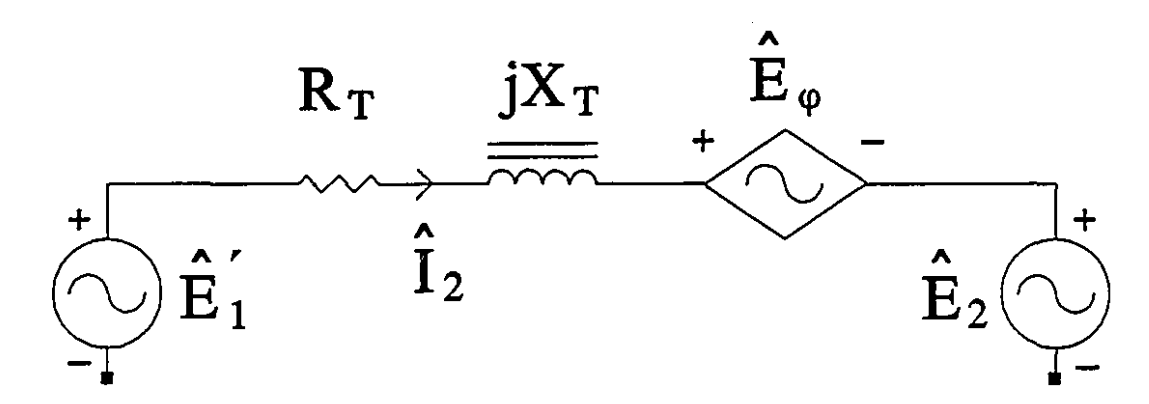


Fig. 5-5 Sigle-line equivalent circuit diagram of Fig. 4-3 with the filter capacitors neglected.

$$E'_{1d} = E_{2d} + R_T I_{2d} - X_T I_{2g} + E_{\varphi d}$$
 (5-7)

$$E'_{1q} = E_{2q} + X_T I_{2d} + R_T I_{2q} + E_{\omega q}$$
 (5-8)

where

$$E_{\varphi d} = \frac{P_{\varphi}}{P_f} V_{20} \cos(\gamma - \varphi) \tag{5-9}$$

and

$$E_{\varphi q} = \frac{P_{\varphi}}{P_f} V_{20} \sin(\gamma - \varphi) \tag{5-10}$$

For UDPF on side-1 and FVC on side-2, both \underline{E}'_{1dq} and \underline{E}_{2dq} should be in phase with \underline{I}_{2dq} . This dual condition can be resolved into the following two conditions:

(1) \underline{E}'_{1dq} should be aligned with \underline{E}_{2dq} ;

(2) \underline{I}_{2dq} should be aligned with \underline{E}'_{1dq} (which implies alignment with \underline{E}_{2dq} , as well).

The first condition can be described as:

$$\begin{bmatrix} E'_{1d} \\ E'_{1q} \end{bmatrix} = \frac{E_1}{P_f} \begin{bmatrix} \cos(\gamma - \delta_1) \\ \sin(\gamma - \delta_1) \end{bmatrix} = K \begin{bmatrix} E_{2d} \\ E_{2q} \end{bmatrix}$$
 (5-11)

where K is a positive proportionality constant. Assuming

$$\underline{E}_{2dq} = E_2 \begin{bmatrix} \cos \delta_2 \\ \sin \delta_2 \end{bmatrix} \tag{5-12}$$

the condition for the alignment of \underline{E}'_{1dq} to \underline{E}_{2dq} can be found from (5-11) as:

$$\gamma = \delta_1 + \delta_2 \tag{5-13}$$

Let us assume, for simplicity of the results, that

$$E_{2dq} = \begin{bmatrix} E_2 \\ 0 \end{bmatrix} \tag{5-14}$$

i.e., $\delta_2 = 0$. In this case, the condition given in (5-13) simplifies to:

$$\gamma = \delta_1 \tag{5-15}$$

Substituting (5-15) in (5-11), one gets:

$$E'_{1d} = \frac{E_1}{P_f}$$

$$E'_{1g} = 0$$
(5-16)

The second condition, i.e., the alignment of the \underline{I}_{2dq} with \underline{E}'_{1dq} can be described as:

$$\begin{bmatrix} I_{2d} \\ I_{2q} \end{bmatrix} = K' \begin{bmatrix} E_{1d}' \\ E_{1q}' \end{bmatrix}$$
 (5-17)

K', being a positive proportionality constant. Substituting (5-16) in (5-17), one gets:

$$I_{2d} = K' \frac{E_1}{P_f}$$

$$I_{2q} = 0$$
(5-18)

The alignment of \underline{I}_{2dq} to \underline{E}'_{1dq} can be accomplished through the adjustments of P_{ϕ} which controls the magnitude of the SVC voltage vector $\underline{E}_{\phi dq}$ of Fig. 5.5, given by (5-9) and (5-10). As mentioned in section 4.4 of chapter 4, the dc bias voltage regulation loop keeps quadrature relationship between the SVC voltage vector and \underline{I}_{2dq} . Since $I_{2q} = 0$, the d-axis component of SVC voltage, $E_{\phi d}$, will be zero. Therefore, from (5-9), $\gamma - \phi = \pm \pi/2$. Using (4-22) and the fact that $\gamma = \delta_1$ for FVC on side-2 and $\delta_1 - \eta_1 = 0$ for UDPF on side-1,

$$\gamma - \varphi = \frac{\pi}{2} \tag{5-19}$$

The SVC voltage responsible for the alignment of \underline{I}_{2dq} to \underline{E}'_{1dq} will then be E_{qq} given by (5-10).

Substituting $E'_{1q} = E_{2q} = I_{2q} = 0$ and $\gamma - \varphi = \pi/2$ in (5-7) and (5-8), and rearranging terms, the following interesting relations result:

$$I_{2d} = \frac{\frac{E_1}{P_f} - E_2}{R_T} \tag{5-20}$$

$$P_{\varphi} = -\frac{P_f X_T I_{2d}}{V_{2o}} = -\frac{P_f I_{2d}}{V_{2o}} \left(\frac{-\omega_1 L_1}{P_f^2} + \omega_2 L_2 \right)$$
 (5-21)

Equation (5-20) shows that when the dual condition of UDPF on side-1 and FVC on side-2 are satisfied, the integrated system as viewed from side-2, shown in Fig. 5-5, behaves as a purely resistive network. In this case, the SVC voltage, E_{eq} , has compensated for the voltage drop across the total reactance, i.e., jX_TI_{2d} . Equation (5-20) also illustrates clearly the role of P_f in real power control.

Equation (5-21) gives the value of P_{ϕ} necessary to get UDPF on side-1. The sign of P_{ϕ} is opposite of that of X_T . This is the way P_{ϕ} controls the magnitude and sign of the SVC voltage to compensate for the voltage drop across X_T to establish

UDPF on side-1. The range, in which P_{ϕ} can be varied, is limited. The limit on P_{ϕ} is imposed by the fact that the total modulating signal which is the weighted sum of $2/3P_f$ CS(x) of (4-39) and $\sqrt{2/3}$ P_{ϕ} C(x) of (4-41) must not exceed the saturation limit of the Pulse Width Modulation (PWM) control of the matrix converter. In the case of the Sinusoidal Pulse Width Modulation (SPWM) strategy, the saturation limit is the peak value of the triangular carrier waveform. Equation (5-21) offers the possibility of conjugate reactance compensation, through $-\omega_1 L_1/P_f^2$. With ω_1 , ω_2 , and L_2 being fixed, L_1 and/or P_f can be adjusted to minimize $X_T = -\omega_1 L_1/P_f^2 + \omega_2 L_2$. This, when possible, ensures that the excursion of P_{ϕ} in trying to maintain UDPF on side-1 is modest. In this way, the saturation of the control circuitry is avoided and more room is left for the manoeuvre of P_f , within the range restricted by the peak value of the triangular carrier signal.

Fig. 5-6 shows the phasor diagram of the system of Fig. 5-5, for the dual condition of UDPF on side-1 and FVC on side-2, when filter capacitors on side-2 are neglected and $\underline{E}_{2dq} = E_{2d} = E_2$. Fig. 5-6(a) illustrates the case when $X_T < 0$ and $E_{\phi q} > 0$ ($P_{\phi} > 0$), while Fig. 5-6(b) shows the case of $X_T > 0$ and $E_{\phi q} < 0$ ($P_{\phi} < 0$). In both cases, the voltage drop across X_T has been compensated completely by $E_{\phi q}$.

Based on the above discussions, the complete scenario of establishing UDPF

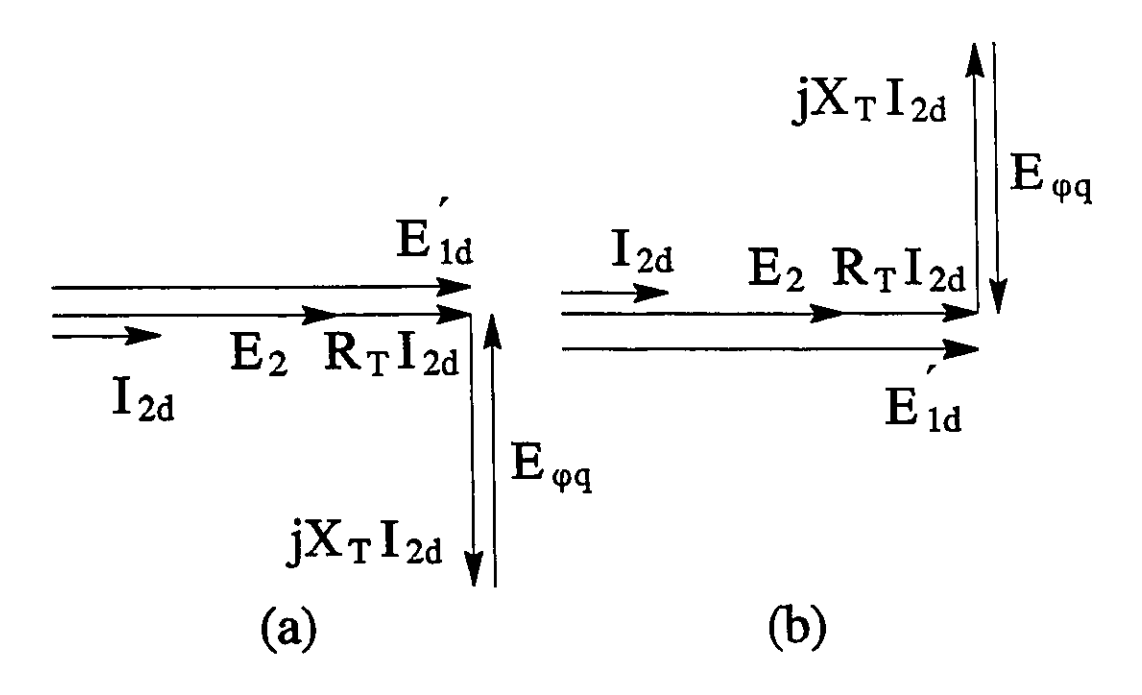


Fig. 5-6 Phasor diagram of Fig. 5-5 for UDPF on side-1 and FVC on side-2.

on side-1 and FVC on side-2 can be summarized in the following way:

- γ is adjusted to δ_1 , according to (5-15);
- P_f is adjusted for the desired real power or motor torque, according to (5-20);
- P_{φ} is adjusted, according to (5-21) such that $E_{\varphi q} = P_{\varphi}/P_f V_{2o}$ cancels jX_TI_{2d} , as shown in Fig. 5-6.
- φ is adjusted by the SVC feedback control loop, regulating the dc bias
 voltage on side-2, according to (5-19).

5.2.2 Filter Capacitors Considered

Fig. 4-2 shows the complete system including the filter capacitors on side-2. The single-line equivalent circuit diagram of the system of Fig. 4-2, as viewed from side-2, is shown in Fig. 4-3. The mathematical model of the integrated system is given by (4-31). When the dual condition of UDPF on side-1 and FVC on side-2 are established, the phasor diagram of Fig. 4-4 will be modified to that shown in Fig. 5-7.

The scenario of establishing the conditions of Fig. 5-7 is almost the same as that for the case of subsection 5.2.1, where the filter capacitors on side-2 were

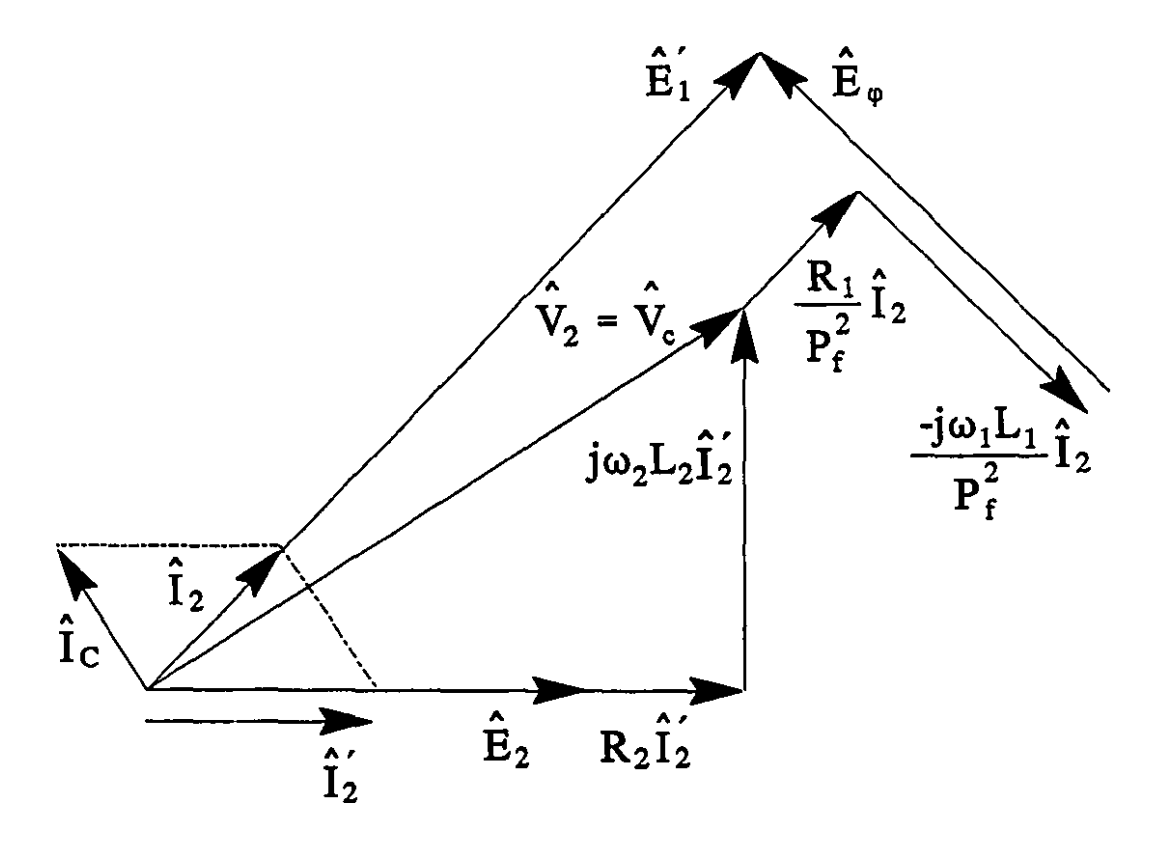


Fig. 5-7 Phasor diagram of Fig. 4-4 for UDPF on side-1 and FVC on side-2.

neglected. The procedure is repeated here with the slight changes included:

- γ is adjusted until \underline{I}'_{2dq} is aligned with \underline{E}_{2dq} ;
- P_f is adjusted for the desired real power or motor torque;
- P_{Φ} is adjusted until \underline{I}_{2dq} is aligned with \underline{E}'_{1dq} ;
- ϕ is adjusted by the dc bias voltage regulation control loop until $\underline{E}_{\phi dq}$ is at right angles with \underline{I}_{2dq} .

If the filter capacitors are small, which is usually the case, by slight modifications of the adjustments suggested in subsection 5.2.1, the dual condition of UDPF and FVC for the real case, where the filter capacitors on side-2 are present, can be satisfied.

5.3 Summary

In this chapter, it has been shown that the matrix converter system of Fig. 4-2 governed by the $[P]_{2\times 3}$ -matrix introduced in chapter 4, with four control levers: P_f , γ , P_{φ} , and φ can be used to achieve the following objectives:

- DC bias voltage regulation on side-2 through φ -control;
- Real power control or motor torque control through P_f -control;
- Simultaneous Unity Displacement Power Factor (UDPF) on side-1 and

Field Vector Control (FVC) on side-2 through $P_{_{\mathbf{\phi}}}$ and $_{\mathbf{\gamma}}$ controls.

In the next chapter, a new matrix converter topology based on three-phase voltage-source converter modules will be introduced. Then the dyadic matrix converter theory developed in chapters 2-to-5 will be applied to the system and the capabilities of the matrix converter will be investigated.

VOLTAGE-SOURCE-CONVERTER TYPE MATRIX CONVERTER UNDER THE DYADIC MATRIX CONVERTER THEORY CONTROL

6.1 Introduction

In the interest of extending the frontier of research, in this chapter, a new matrix converter based on voltage-source converters is introduced [79-81] which is distinct from the conventional nine-switch topology [47]. Then, the dyadic matrix converter theory, developed in chapters 2-5, will be applied to the proposed matrix converter. It will be shown that:

- Frequency changing,
- Amplitude control of the side-2 voltage,

- Displacement Power Factor control on side-1 [1], and
- Field Vector Control on side-2 [76,77]

can be realized by the new matrix converter.

The proposed matrix converter, shown in Fig. 6-1, is composed of three identical modules of the three-phase voltage-source converters, connected between the networks of side-1 and side-2. This is an alternative to the original direct ac to ac matrix converter employing nine bidirectional switches, shown in Fig. 6-2. The total number of valves and diodes employed in the proposed matrix converter is the same as in the nine-bidirectional-switch topology, assuming that each bidirectional switch is realized by two switches and two diodes (Fig. 1-6(b) and (c)).

As mentioned earlier in section 1.2 of chapter 1 on the historical background, the bidirectional or 4-quadrant switches have serious switching problems and the main motive for the new circuit topology is to bypass the switching difficulties at the power circuit.

6.2 Voltage-Source-Converter Type Matrix Converter

The voltage-source-converter type matrix converter, shown in Fig. 6.1, offers the following advantages:

- The three-phase voltage-source converters constituting the building blocks of the proposed matrix converter, are well-known and proven technologies and the industries have a lot of know-how about them. The existing voltage-source converter units can be used in modular form, without any

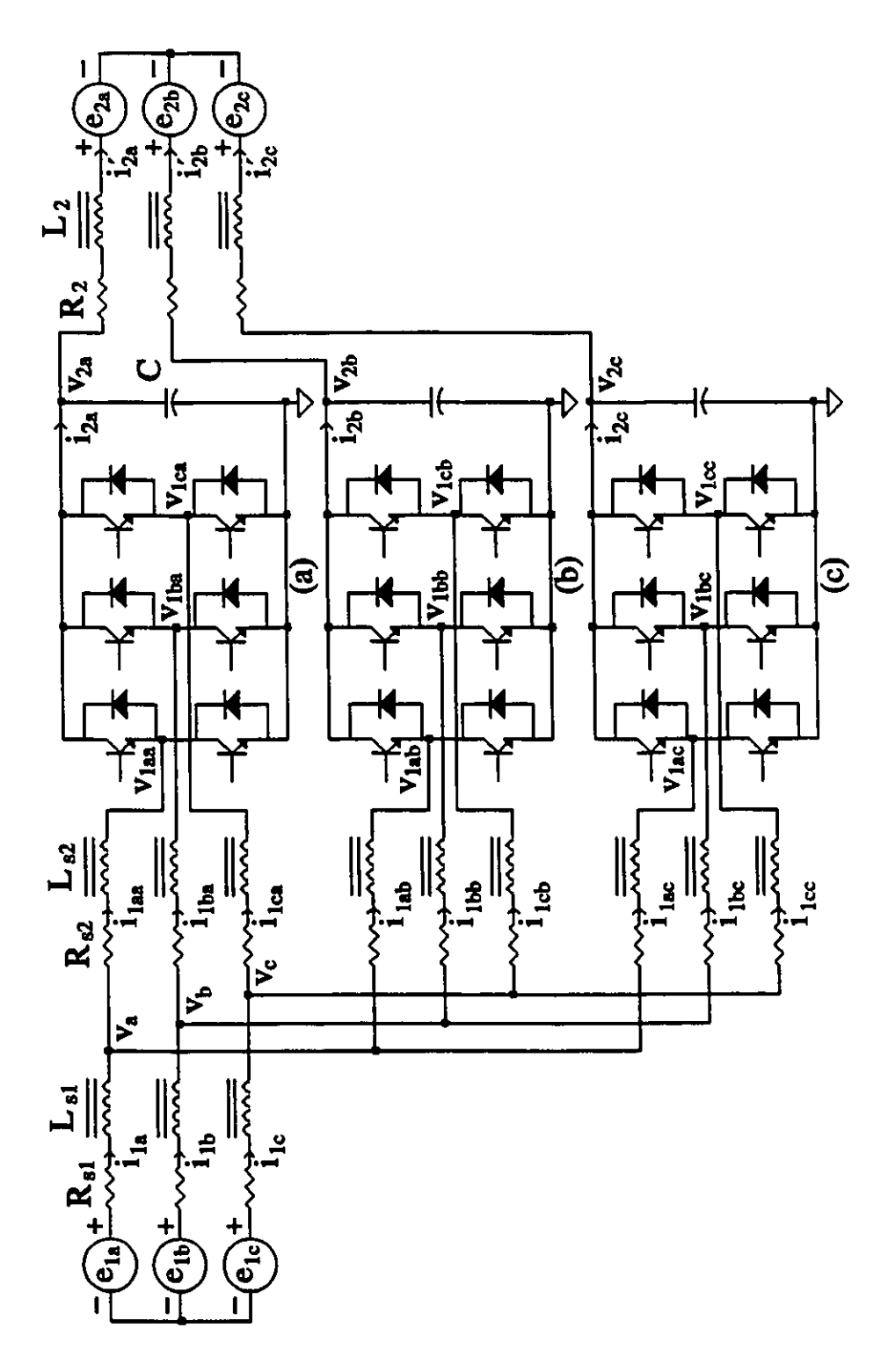


Fig. 6-1 Voltage-source-converter type matrix converter with the networks of side-1 and side-2.

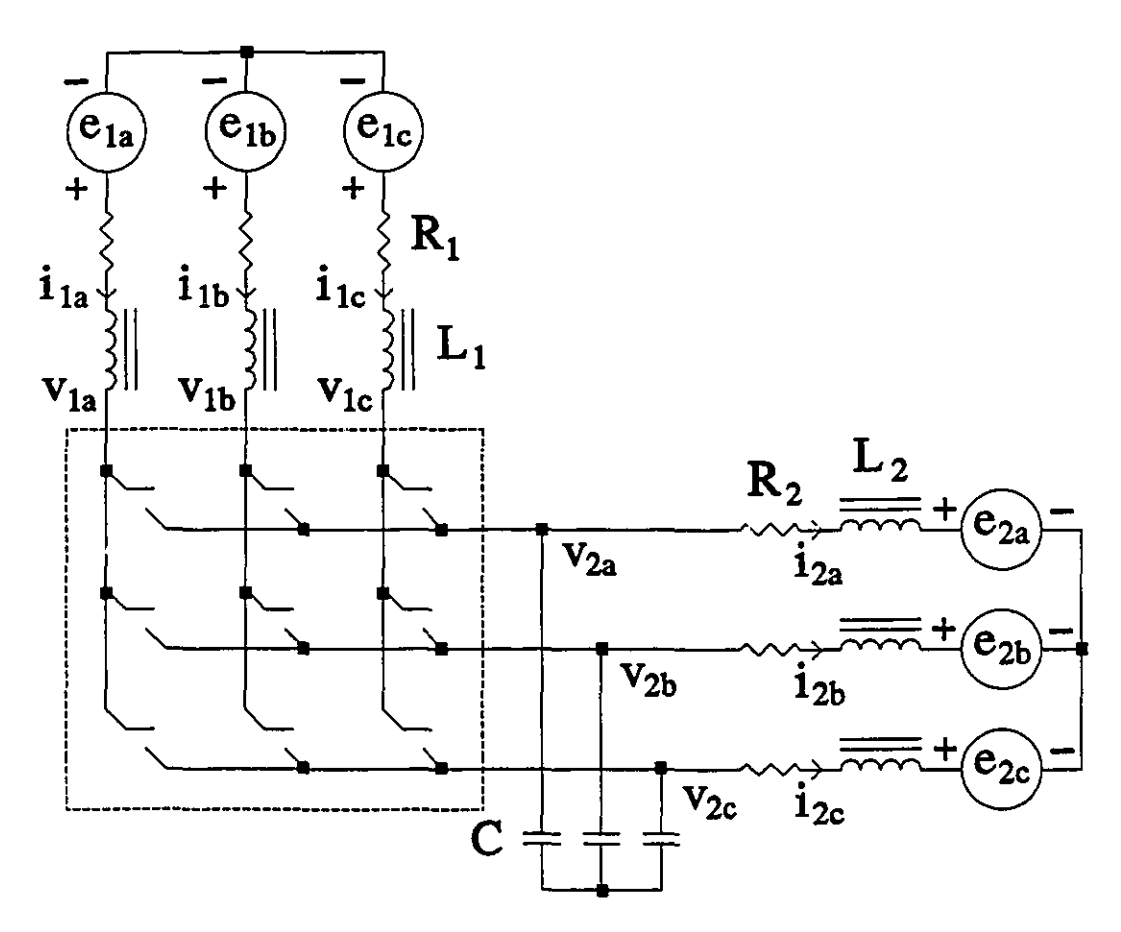


Fig. 6-2 Conventional nine-bidirectional-switch matrix converter with the networks of side-1 and side-2.

modifications, to construct the matrix converter.

- The dc-link capacitor and the anti-parallel diodes in a voltage-source converter provide a natural overvoltage protection for the switches. The overcurrent protection (known also as "shoot-through" protection), can be simply added by designing a time delay between the complementary OFF and ON signals of every two switches in the same leg. The voltage-source-converter type matrix converter is free of the switching difficulties

associated with the nine-bidirectional-switch matrix converter.

- In the nine-bidirectional-switch matrix converter, the conduction losses are attributed to the forward voltage drops of two four-quadrant switches at the rated current. Noting that each bidirectional switch is equivalent to two semiconductor devices in series (one switch and one diode), the conduction losses are those of 2 diodes and 2 switches in series at the rated current. The voltage-source-converter type matrix converter enjoy the advantage of having conduction losses due to forward voltage drops of six semiconductor devices at one third of the rated current. This is equivalent to two semiconductor devices at rated current. The reduction of conduction losses is an imprtant consideration in high power applications.

The voltage-source-converter type matrix converter has the following drawbacks:

- A dc bias voltage must always be kept as part of the capacitor voltages of the three voltage-source converters (Fig. 6-3). This is because the dc link voltage must never become negative. In fact, a negative voltage on the dc link can forward bias the anti-parallel diodes of the converter legs and as a result, the converter legs will be short circuited. The presence of some dc voltage on the filter capacitors on side-2 is also necessary at start-up, since otherwise the converter valves cannot start switching. The necessity to have a dc bias voltage means that the valves have to be rated at least at twice the peak value of the largest ac voltage on side-2. Experimental tests on the

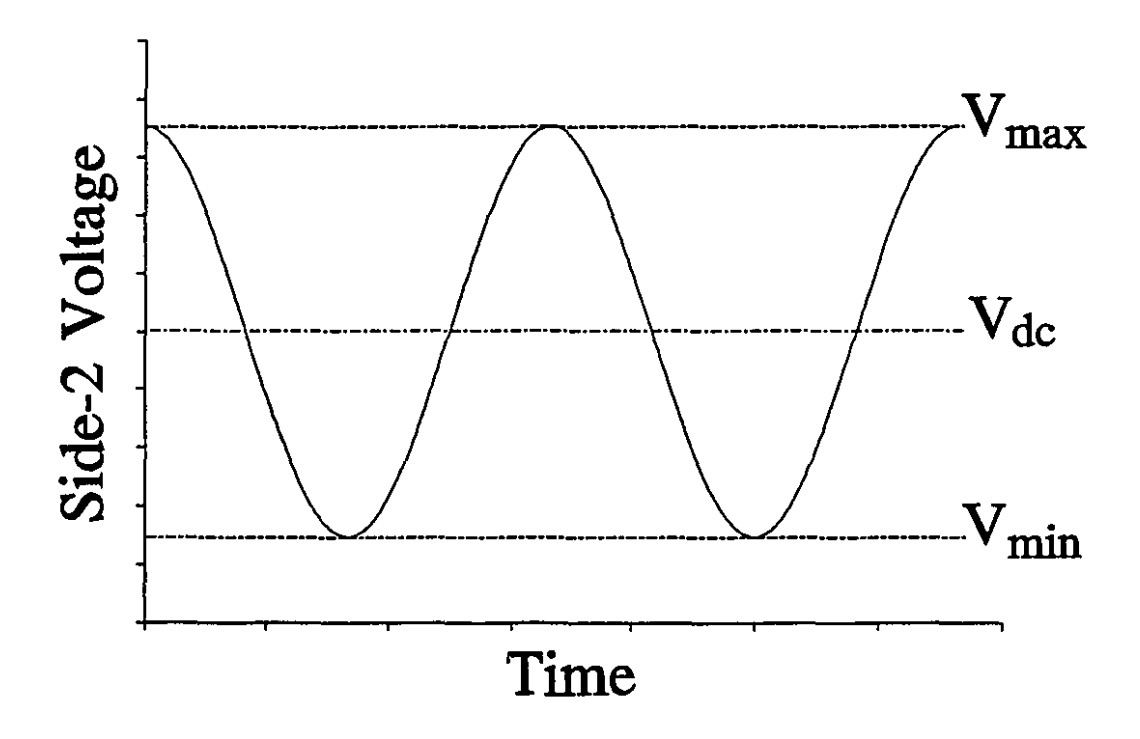


Fig. 6-3 Typical waveform of the voltages on side-2 of the voltage-source-converter type matrix converter.

matrix converter show that the lower limit for the minimum of the side-2 voltages, V_{min} , is approximately zero. According to these tests, a voltage with near zero value on side-2 does not disturb the switching of the valves at all. Therefore, the minimum for the dc bias voltage that can be chosen is approximately equal to the peak value of the ac component of the voltages on side-2.

- As will be made clear later on in section 6.6, the branch currents i_{1aa} , ..., i_{1cc} , as designated in Fig. 6-1, will contain subfrequency components (i.e., components at angular frequencies below ω_1) and superfrequency

components (i.e., components at angular frequencies above ω_1). These frequencies do not appear in the source currents i_{1a} , i_{1b} , and i_{1c} , but will affect the quality of the ac voltages on side-2. The problem of waveform distortion will be revisited later in this chapter and a novel method to overcome this problem will be presented.

6.3 Mathematical Model

In this section, the mathematical model of the matrix converter of Fig. 6-1 will be derived. First, let us make familiar with the notations used in Fig. 6-1. In this figure, from left to right, the side-1 network, the matrix converter consisting of three voltage-source converter modules, and the side-2 network can be distinguished. e_{1a} , e_{1b} , and e_{1c} denote three-phase balanced sinusoidal source voltages at angular frequency ω_1 , and i_{1a} , i_{1b} , and i_{1c} are the corresponding source currents. The three-phase balanced sinusoidal load voltages are designated e_{2a} , e_{2b} , and e_{2c} , and the corresponding load currents are i'_{2a} , i'_{2b} and i'_{2c} . The voltage source converters are labeled according to the side-2 phases to which they are connected, i.e., from top to the bottom, converter (a), converter (b), and converter (c). On side-1, the currents i_{1aa} , ..., i_{1cc} are termed branch currents, and the voltages v_{1ac} , ..., v_{1cc} are called side-1 terminal voltages. In subscript, they share a 1, denoting side-1. The two letters

following 1, correspond to the side-1 phase and the converter to which they are related, respectively; e.g., i_{1ab} is a branch of i_{1a} connected to converter b. i_{2a} , i_{2b} , and i_{2c} are side-2 currents of the converters (a), (b), and (c), respectively, and v_{2a} , v_{2b} , and v_{2c} denote side-2 terminal voltages of converters (a), (b), and (c), respectively. v_a , v_b , and v_c are the voltages at the common coupling points of the branches of phases a, b, and c on side-1, respectively. R_{s1} and L_{s1} are the source resistance and inductance, while R_{s2} and L_{s2} are the branch resistance and inductance. Finally, R_2 and L_2 are the load resistance and inductance.

The switchings of the valves in each leg of the voltage-source converter of Fig. 6-1 are based on the well-known Sinusoidal Pulse Width Modulation (SPWM) strategy [2]. Assuming that the modulating signal of the j^{th} phase (j = a, b, c) of the k^{th} converter (k = a, b, c) is $v_{\text{mod},jk}$, and the side-2 voltage of the k^{th} converter is v_{2k} , and the peak value of the triangular carrier waveform is V_t , the general form of the terminal voltages on side-1 $(v_{1aa}, ..., v_{1cc})$ will be [2]:

$$v_{1jk} = \frac{v_{mod,jk} v_{2k}}{2V_{*}} \tag{6-1}$$

Defining the normalized modulating signal as:

$$m_{jk} = \frac{v_{mod,jk}}{V_t} \tag{6-2}$$

(6-1) can be written as:

$$v_{1jk} = \frac{1}{2} m_{jk} v_{2k} \tag{6-3}$$

From (6-3), the three-phase voltages at the side-1 terminals of the k^{th} converter can then be found:

- for converter k = a

$$v_{1aa} = \frac{1}{2} m_{aa} v_{2a}$$

$$v_{1ba} = \frac{1}{2} m_{ba} v_{2a}$$

$$v_{1ca} = \frac{1}{2} m_{ca} v_{2a}$$
(6-4)

- for converter k = b

$$v_{1ab} = \frac{1}{2} m_{ab} v_{2b}$$

$$v_{1bb} = \frac{1}{2} m_{bb} v_{2b}$$

$$v_{1cb} = \frac{1}{2} m_{cb} v_{2b}$$
(6-5)

- for converter k = c

$$v_{1ac} = \frac{1}{2} m_{ac} v_{2c}$$

$$v_{1bc} = \frac{1}{2} m_{bc} v_{2c}$$

$$v_{1cc} = \frac{1}{2} m_{cc} v_{2c}$$
(6-6)

From KVL on side-1

$$e_{1a} - v_{a} = R_{s1}i_{1a} + L_{s1}\frac{d}{dt}i_{1a}$$

$$e_{1b} - v_{b} = R_{s1}i_{1b} + L_{s1}\frac{d}{dt}i_{1b}$$

$$e_{1c} - v_{c} = R_{s1}i_{1c} + L_{s1}\frac{d}{dt}i_{1c}$$
(6-7)

$$v_{a} - v_{1aa} = R_{s2} i_{1aa} + L_{s2} \frac{d}{dt} i_{1aa}$$

$$v_{b} - v_{1ba} = R_{s2} i_{1ba} + L_{s2} \frac{d}{dt} i_{1ba}$$

$$v_{c} - v_{1ca} = R_{s2} i_{1ca} + L_{s2} \frac{d}{dt} i_{1ca}$$
(6-8)

$$v_{a} - v_{1ab} = R_{s2} i_{1ab} + L_{s2} \frac{d}{dt} i_{1ab}$$

$$v_{b} - v_{1bb} = R_{s2} i_{1bb} + L_{s2} \frac{d}{dt} i_{1bb}$$

$$v_{c} - v_{1cb} = R_{s2} i_{1cb} + L_{s2} \frac{d}{dt} i_{1cb}$$
(6-9)

$$v_{a} - v_{1ac} = R_{s2} i_{1ac} + L_{s2} \frac{d}{dt} i_{1ac}$$

$$v_{b} - v_{1bc} = R_{s2} i_{1bc} + L_{s2} \frac{d}{dt} i_{1bc}$$

$$v_{c} - v_{1cc} = R_{s2} i_{1cc} + L_{s2} \frac{d}{dt} i_{1cc}$$
(6-10)

Adding the first lines of (6-8), (6-9) and (6-10),

$$v_a = \frac{1}{3} R_{s2} i_{1a} + \frac{1}{3} L_{s2} \frac{d}{dt} i_{1a} + v_{1a}$$
 (6-11)

where

$$v_{1a} = \frac{v_{1aa} + v_{1ab} + v_{1ac}}{3} \tag{6-12}$$

and

$$i_{1a} = i_{1aa} + i_{1ab} + i_{1ac} ag{6-13}$$

Repeating the same procedure for the second and the third lines of (6-8), (6-9), and (6-10),

$$v_b = \frac{1}{3} R_{s2} i_{1b} + \frac{1}{3} L_{s2} \frac{d}{dt} i_{1b} + v_{1b}$$
 (6-14)

and

$$v_c = \frac{1}{3} R_{s2} i_{1c} + \frac{1}{3} L_{s2} \frac{d}{dt} i_{1c} + v_{1c}$$
 (6-15)

where

$$v_{1b} = \frac{v_{1ba} + v_{1bb} + v_{1bc}}{3} \tag{6-16}$$

$$i_{1b} = i_{1ba} + i_{1bb} + i_{1bc} ag{6-17}$$

$$v_{1c} = \frac{v_{1ca} + v_{1cb} + v_{1cc}}{3}$$
 (6-18)

and

$$i_{1c} = i_{1cc} + i_{1cb} + i_{1cc} ag{6-19}$$

Substituting (6-11), (6-14), and (6-15) in (6-7),

$$e_{1a} - v_{1a} = \left(R_{s1} + \frac{R_{s2}}{3}\right)i_{1a} + \left(L_{s1} + \frac{L_{s2}}{3}\right)\frac{d}{dt}i_{1a}$$
 (6-20)

$$e_{1b} - v_{1b} = \left(R_{s1} + \frac{R_{s2}}{3}\right)i_{1b} + \left(L_{s1} + \frac{L_{s2}}{3}\right)\frac{d}{dt}i_{1b}$$
 (6-21)

$$e_{1c} - v_{1c} = \left(R_{s1} + \frac{R_{s2}}{3}\right)i_{1c} + \left(L_{s1} + \frac{L_{s2}}{3}\right)\frac{d}{dt}i_{1c}$$
 (6-22)

Fig. 6-4 shows the equivalent circuit diagram of the networks on side-1 and side-2 of the matrix converter of Fig. 6-1 based on (6-20)-(6-22), where

$$R_{1} = R_{s1} + \frac{R_{s2}}{3}$$

$$L_{1} = L_{s1} + \frac{L_{s2}}{3}$$
(6-23)

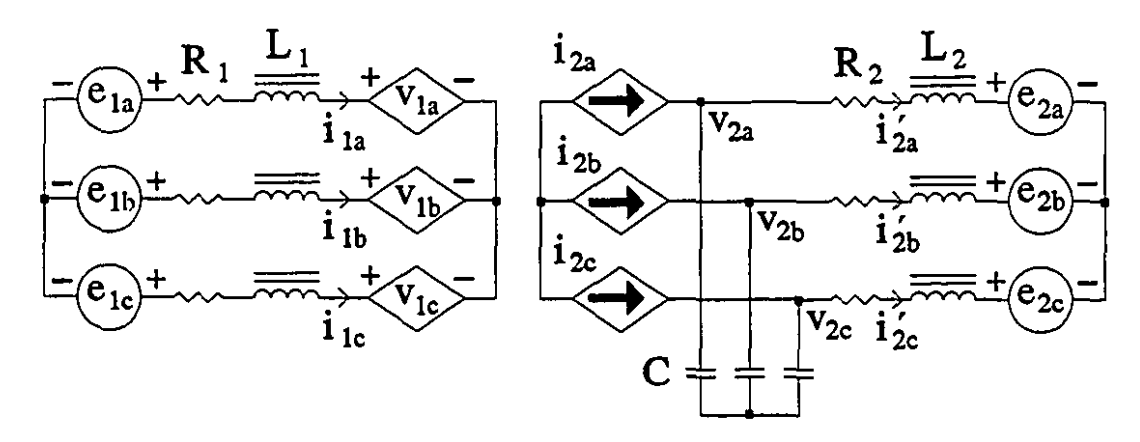


Fig. 6-4 Equivalent circuit diagram of the system of Fig. 6-1.

Substituting (6-4), (6-5), and (6-6) in (6-12), (6-16), and (6-18), the following matrix equation for the voltage transformation results:

$$\begin{bmatrix} v_{1a} \\ v_{1b} \\ v_{1c} \end{bmatrix} = \frac{1}{6} \begin{bmatrix} m_{aa} & m_{ab} & m_{ac} \\ m_{ba} & m_{bb} & m_{bc} \\ m_{ca} & m_{cb} & m_{cc} \end{bmatrix} \begin{bmatrix} v_{2a} \\ v_{2b} \\ v_{2c} \end{bmatrix}$$
(6-24)

Based on power invariance principle in the system of Fig. 6.4, the following matrix equation will be found for current transformation:

$$\begin{bmatrix} i_{2a} \\ i_{2b} \\ i_{2c} \end{bmatrix} = \frac{1}{6} \begin{bmatrix} m_{aa} & m_{ba} & m_{ca} \\ m_{ab} & m_{bb} & m_{cb} \\ m_{ac} & m_{bc} & m_{cc} \end{bmatrix} \begin{bmatrix} i_{1a} \\ i_{1b} \\ i_{1c} \end{bmatrix}$$
(6-25)

Equations (6-24) and (6-25) can be rewritten in the following more formal form:

$$\underline{y}_{1abc} = [H] \underline{y}_{2abc}
 \underline{i}_{2abc} = [H]^T \underline{i}_{1abc}$$
(6-26)

where

$$\underline{v}_{1abc} = \begin{bmatrix} v_{1a} \\ v_{1b} \\ v_{1c} \end{bmatrix} \qquad ; \qquad \underline{v}_{2abc} = \begin{bmatrix} v_{2a} \\ v_{2b} \\ v_{2c} \end{bmatrix}
\underline{i}_{1abc} = \begin{bmatrix} i_{1a} \\ i_{1b} \\ i_{1c} \end{bmatrix} \qquad ; \qquad \underline{i}_{2abc} = \begin{bmatrix} i_{2a} \\ i_{2b} \\ i_{2c} \end{bmatrix}$$
(6-27)

and

$$[H] = \frac{1}{6} \begin{bmatrix} m_{aa} & m_{ab} & m_{ac} \\ m_{ba} & m_{bb} & m_{bc} \\ m_{ca} & m_{cb} & m_{cc} \end{bmatrix}$$
(6-28)

with [H] being the transformation matrix of the matrix converter.

6.4 The [H]-Matrix

As mentioned in section 4.6 of chapter 4, the [H]-matrix is chosen to be the sum of two matrices:

$$[H] = [H_f] + [H_{\varphi}] \tag{6-29}$$

where

$$[H_f] = \frac{2}{3} P_f \begin{bmatrix} CS(0) & CS(-2\pi/3) & CS(-4\pi/3) \\ CS(-2\pi/3) & CS(-4\pi/3) & CS(0) \\ CS(-4\pi/3) & CS(0) & CS(-2\pi/3) \end{bmatrix}$$
(6-30)

and

$$[H_{\varphi}] = \frac{\sqrt{2}}{3} P_{\varphi} \begin{bmatrix} C(0) & C(0) & C(0) \\ C(-2\pi/3) & C(-2\pi/3) & C(-2\pi/3) \\ C(-4\pi/3) & C(-4\pi/3) & C(-4\pi/3) \end{bmatrix}$$
(6-31)

with CS(x) and C(x) defined as follows:

$$CS(x) = \cos[(\omega_1 + \omega_2)t + \gamma + x]$$
 (6-32)

$$C(x) = \cos(\omega_1 t + \varphi + x) \tag{6-33}$$

From (6-28) - (6-31), the matrix of the normalized modulating signals, [M(t)], is:

$$[M(t)] = \begin{bmatrix} m_{aa} & m_{ab} & m_{ac} \\ m_{ba} & m_{bb} & m_{bc} \\ m_{ca} & m_{cb} & m_{cc} \end{bmatrix} = 6 [H]$$

$$= M_f \begin{bmatrix} CS(0) & CS(-2\pi/3) & CS(-4\pi/3) \\ CS(-2\pi/3) & CS(-4\pi/3) & CS(0) \\ CS(-4\pi/3) & CS(0) & CS(-2\pi/3) \end{bmatrix}$$

$$= M_{\phi} \begin{bmatrix} C(0) & C(0) & C(0) \\ C(-2\pi/3) & C(-2\pi/3) & C(-2\pi/3) \\ C(-4\pi/3) & C(-4\pi/3) & C(-4\pi/3) \end{bmatrix}$$
(6-34)

where

$$M_f = 4 P_f \tag{6-35}$$

$$M_{\omega} = 2\sqrt{2} P_{\omega} \tag{6-36}$$

and CS(x) and C(x) are defined by (6-32) and (6-33), respectively.

In SPWM strategy, the maximum value of the modulating signal must not exceed the peak value of the triangular carrier signal, i.e., V_t . Therefore, the maximum value of the normalized modulating signals m_{aa} , ..., m_{cc} , defined by (6-2) is limited to 1. This restricts the magnitude of M_f and M_{ϕ} , since from (6-34), a typical normalized modulating signal is the sum of $M_f CS(x)$, $(x = 0, -2\pi/3, -4\pi/3)$

and $M_{\varphi}C(y)$, $(y=0,-2\pi/3,-4\pi/3)$. Letting M_f vary in a wide range, reduces the room for the maneuver of M_{φ} and vice versa. The main objective of using a matrix converter being frequency changing and control of the amplitude of the ac voltage on side-2, M_f is given higher priority in having the freedom to vary within a wider range than M_{φ} . In subsection 5.2.1 of chapter 5, a method based on reactance compensation was recommended which enables the task of displacement power factor control on side-1 to be performed by varying P_{φ} and therefore M_{φ} in a narrow range.

6.5 Matrix Converter Controllers

By looking at the structure of the matrix [M(t)] given in (6-34), one can readily see that there exist four control levers available in the proposed matrix converter: M_f , γ , φ , and M_{φ} .

6.5.1 M_f - Control

The scaling factor M_f is the multiplier of the frequency changing component of [M(t)]-matrix. It is used to control the amplitude of the ac component of the voltages on side-2 of the matrix converter.

6.5.2 y - Control

The angle γ is used to rotate the side-1 source voltage vector as viewed from side-2, \hat{E}_1' , in order to align the load current vector, \hat{I}_2' , to the load voltage vector, \hat{E}_2 , for field vector control purposes.

6.5.3 φ - Control

The angle φ is varied automatically by a closed loop control system which regulates the side-2 dc bias voltage. The φ -control rotates the ac voltages projected on side-1 due to the dc bias voltages on side-2, until the quadrature relationship with respect to the side-1 currents is established. Assuming that the side-2 voltage vector, \underline{v}_{2abc} , is expressed as:

$$\underline{\mathbf{v}}_{2abc} = \underline{\mathbf{v}}_{2ac} + \underline{\mathbf{v}}_{2dc} \tag{6-37}$$

where

$$\underline{v}_{2ac} = V_2 \begin{bmatrix} \cos(\omega_2 t + \alpha) \\ \cos(\omega_2 t - \frac{2\pi}{3} + \alpha) \\ \cos(\omega_2 t - \frac{4\pi}{3} + \alpha) \end{bmatrix}$$
 (6-38)

and

$$\underline{\underline{v}}_{2dc} = \begin{bmatrix} V_{dc} \\ V_{dc} \\ V_{dc} \end{bmatrix} \tag{6-39}$$

the reflected voltage vector on side-1 due to the side-2 voltage vector will be:

$$\underline{\underline{v}}_{1abc} = [H] \underline{\underline{v}}_{2abc} = ([H_f] + [H_{\varphi}]) (\underline{\underline{v}}_{2ac} + \underline{\underline{v}}_{2dc})$$

$$= [H_f] \underline{\underline{v}}_{2ac} + [H_f] \underline{\underline{v}}_{2dc} + [H_{\varphi}] \underline{\underline{v}}_{2ac} + [H_{\varphi}] \underline{\underline{v}}_{2dc}$$

$$= [H_f] \underline{\underline{v}}_{2ac} + [H_{\varphi}] \underline{\underline{v}}_{2dc}$$
(6-40)

since

$$[H_f] \underline{y}_{2dc} = \underline{0} \tag{6-41}$$

and

$$\left[H_{\varphi}\right]\underline{v}_{2ac}=\underline{0}\tag{6-42}$$

The component of the projected voltage on side-1 that can be rotated by the φ -control is $\underline{\nu}_{1\varphi} = [H_{\varphi}]\underline{\nu}_{2dc}$. The phasor diagram of Fig. 6-5 shows the quadrature relationship of phase-a components of $\underline{\nu}_{1\varphi}$ and side-1 source current, \underline{i}_{1abc} , set up by φ -control.

6.5.4 M_{\bullet} - Control

The scaling factor M_{φ} is used to vary the size of the reflected voltage vector $\underline{v}_{1\varphi} = [H_{\varphi}] \underline{v}_{2dc}$ to adjust the displacement angle of the side-1 source current, \underline{i}_{1abc} ,

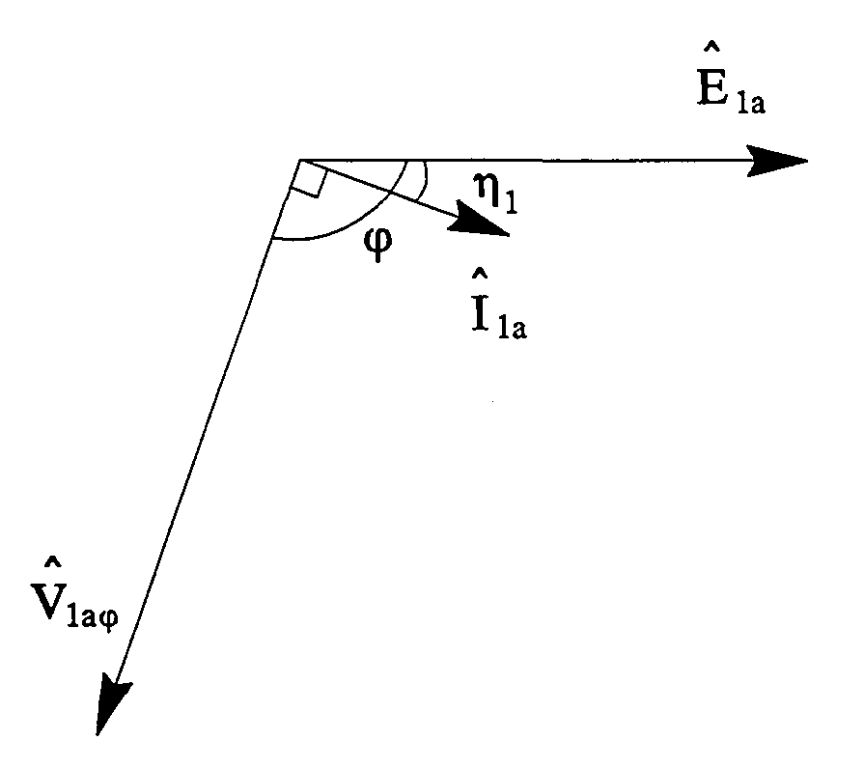


Fig. 6-5 Quadrature relationship of the side-1 current and the voltage projected on side-1 due to the dc bias voltages of side-2.

with respect to the side-1 source voltage, \underline{e}_{1abc} (see Fig. 6-6). Therefore, M_{φ} is the control lever for the side-1 displacement power factor correction.

Even though the four controllers explained above are not completely decoupled, they can work with one another, in a range, to set up the desired conditions.

From (6-41) and (6-42), two interesting observations can be made:

- (1) The presence of the dc bias voltages on side-2 does not interfere with the frequency changing;
- (2) The VAR controller matrix $[H_{\varphi}]$ does not couple with the ac voltages

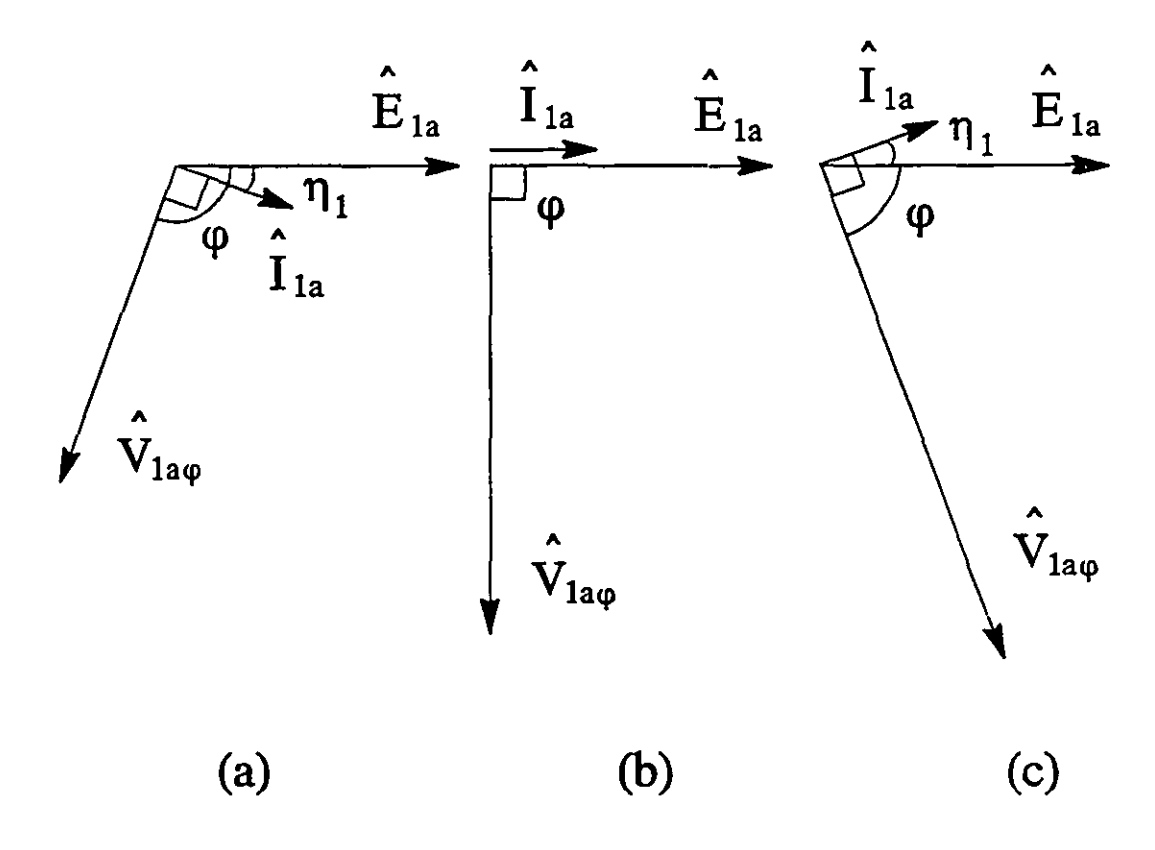


Fig. 6-6 M_p -control and its effect on DPF on side-1.

of side-2.

The simulation and experimental results obtained for the system of Fig. 6-1 are presented in chapter 7.

6.6 Unwanted Components in the Branch Currents

In the system of Fig. 6.1, the terminal voltages of side-1, v_{1aa} , ..., v_{1cc} , contain unwanted subfrequency and superfrequency components as a result of the multiplication of trigonometric functions in the voltage transformation equations (6-4)

- (6-6). Therefore, the branch currents i_{1aa} , ..., i_{1cc} , will be contaminated by the components at the same unwanted frequencies, according to (6-8) - (6-10).

From the power invariance principle for the k^{th} converter (k = a, b, c) in Fig. 6-1,

$$i_{2k} = \frac{1}{2} \sum_{j=a,b,c} m_{jk} i_{1jk}$$
 (6-43)

Therefore, the individual side-2 currents are:

$$i_{2a} = \frac{1}{2} \left(m_{aa} i_{1aa} + m_{ba} i_{1ba} + m_{ca} i_{1ca} \right)$$

$$i_{2b} = \frac{1}{2} \left(m_{ab} i_{1ab} + m_{bb} i_{1bb} + m_{cb} i_{1cb} \right)$$

$$i_{2c} = \frac{1}{2} \left(m_{ac} i_{1ac} + m_{bc} i_{1bc} + m_{cc} i_{1cc} \right)$$
(6-44)

From (6-44), one can see that side-2 currents i_{2a} , i_{2b} , and i_{2c} , will contain unwanted components as a result of the trigonometric multiplications involved in the current transformations. Therefore, side-2 voltages v_{2a} , v_{2b} , and v_{2c} and the load currents i_{2a}' , i_{2b}' , and i_{2c}' , will contain unwanted components at the same frequencies.

Comparing (6-44) and (6-25), one can see that the above two equations will be identical if and only if the branch currents and the source currents on side-1 are linearly dependent through the proportionality constant 1/3, i.e.,

$$i_{1jk} = \frac{1}{3}i_{1j} \tag{6-45}$$

for j = a, b, c and k = a, b, c.

As a result of voltage transformations of (6-4) - (6-6), the side-1 terminal voltages and branch currents will contain components at angular frequencies:

$$(\omega_1),(\omega_1+\omega_2),(\omega_1-\omega_2),(\omega_1+2\,\omega_2),(\omega_1-2\,\omega_2),(\omega_1+3\,\omega_2),...$$

or in general form, $\omega_1 \pm h \omega_2$, where h = 0, 1, Note that $\omega_1 \pm h \omega_2 = 0$ implies the presence of a dc component. The resulting components in side-2 currents and voltages will be at:

$$0, \omega_2, 2\omega_2, 3\omega_2, \dots$$

or in general form, $h'\omega_2$, where h'=0,1,... The presence of the unwanted components is associated with additional losses in the system, especially in the branch resistances R_{s2} (see Fig. 6.1) as well as waveform distortion.

As the angular frequencies of the unwanted components on side-1 and side-2 increase, they are attenuated due to the filtering effects of side-1 branch inductances, L_{s2} , and side-2 filter capacitors, C. The dominant components will therefore be the first few low frequency ones.

For any phase-j (j=a,b,c) on side-1, the branch currents i_{1jk} (k=a,b,c) contain unwanted components which are cosine functions, phase-shifted by $2\pi/3$ with respect to one another, at each frequency. Therefore, in the sum, they add up to zero

and the source currents, i_{1a} , i_{1b} , and i_{1c} , are single frequency cosine functions. This implies that, according to (6-45), for (6-25) to be the exact model of the current transformations of the matrix converter system of Fig. 6-1, the branch currents must not contain any unwanted components.

Using large filtering elements (inductances on side-1 and capacitors on side-2) is not a proper solution to the problem of unwanted components on side-1 and side-2. One way, through which the unwanted components in side-1 branch currents and therefore in side-2 voltages can be attenuated, is to limit the range of variation of M_{\bullet} , thus reducing the magnitude of the unwanted components which are proportional to M_{\bullet} . Earlier, in chapter 5, subsection 5.2.1, a method based on 100% reactance compensation at the desired ω_2 , by adjustment of the inductances on one side or on both sides (if applicable) was proposed. This method is effective if the side-2 frequency is not supposed to vary in a wide range.

A novel technique for eliminating the subfrequency and superfrequency components of side-1 branch currents, and as a result, the unwanted components in side-2 voltages, will be presented in the next section.

6.7 Elimination of Unwanted Components in the Branch Currents

The problem of presence of undesired components in the side-1 branch currents, resulting in additional losses and waveform distortion in side-2 voltages was explained in section 6.6. In this section, a novel technique based on using nine

identical single-phase transformers with the primary circuits in the path of side-1 branch currents, i_{1aa} , ..., i_{1cc} , as shown in Fig. 6-7, is proposed. The secondary circuits of the transformers are connected in delta configuration so that the unwanted components are trapped in the secondary circuits, leaving the branch currents virtually free of any unwanted component.

6.7.1 Principle of Operation

Fig. 6-7 shows the schematic diagram of the voltage-source-converter type matrix converter with the trapping transformers installed. To clarify the way in which the scheme shown in Fig. 6-7 succeeds in trapping the unwanted components in the side-1 branch currents, the detailed equivalent circuit diagram of the transformers T_{aa} , T_{ab} , and T_{ac} whose secondaries are connected in delta configuration, has been shown in Fig. 6-8.

In Fig. 6-8, each transformer has been represented by its equivalent circuit diagram consisting of an ideal transformer, T, a shunt inductance, L_o , representing the magnetizing inductane, a shunt resistance, R_o , representing the iron loss, a series resistance, R, representing the copper loss, and a series inductance, L, representing the leakage inductance. The values for L_o , R_o , R, and L, can be easily measured through open circuit and short circuit tests on the actual transformers.

In the ideal transformers of Fig. 6-8,

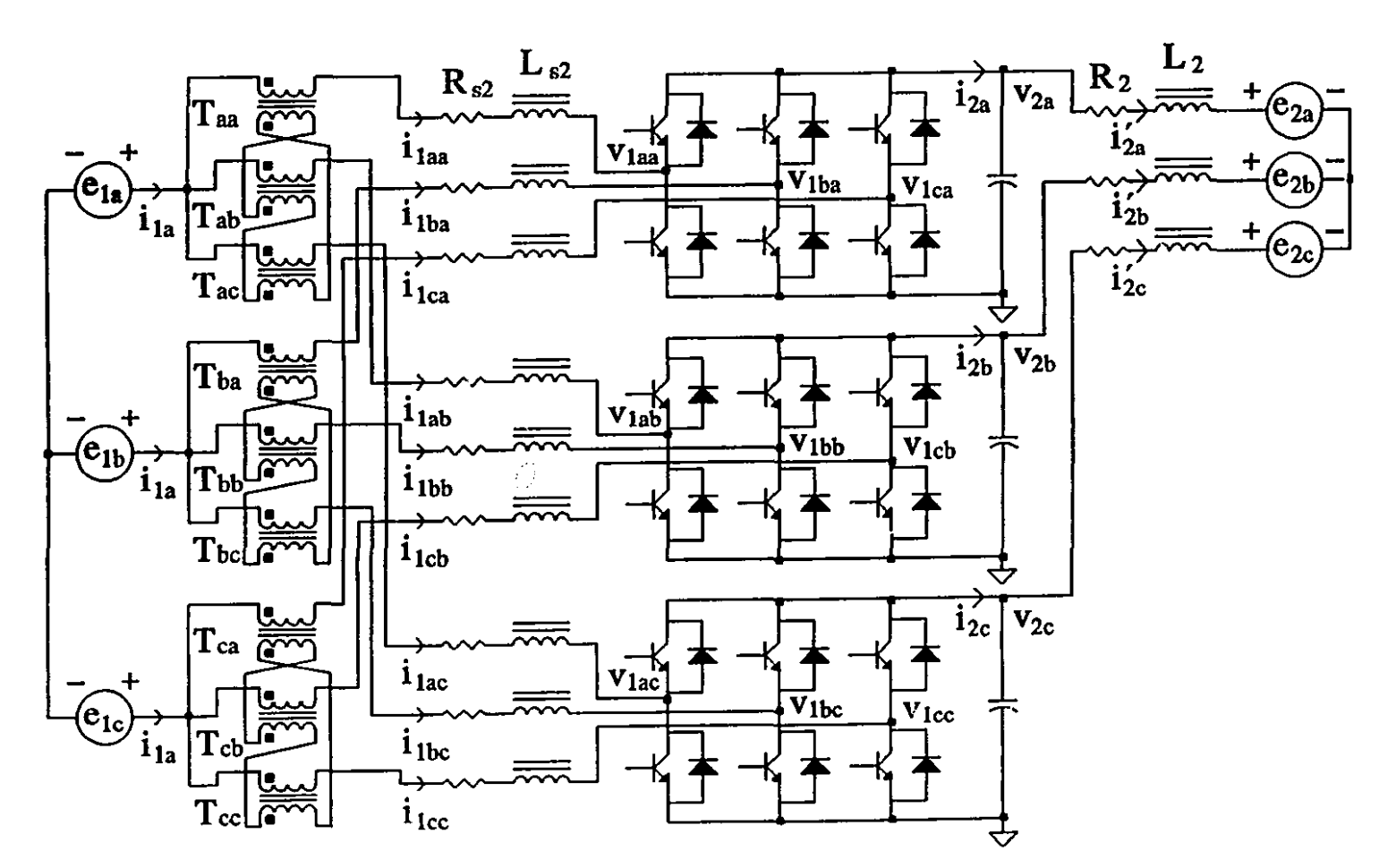


Fig. 6-7 transformers. Voltage-source-converter type matrix converter with the trapping

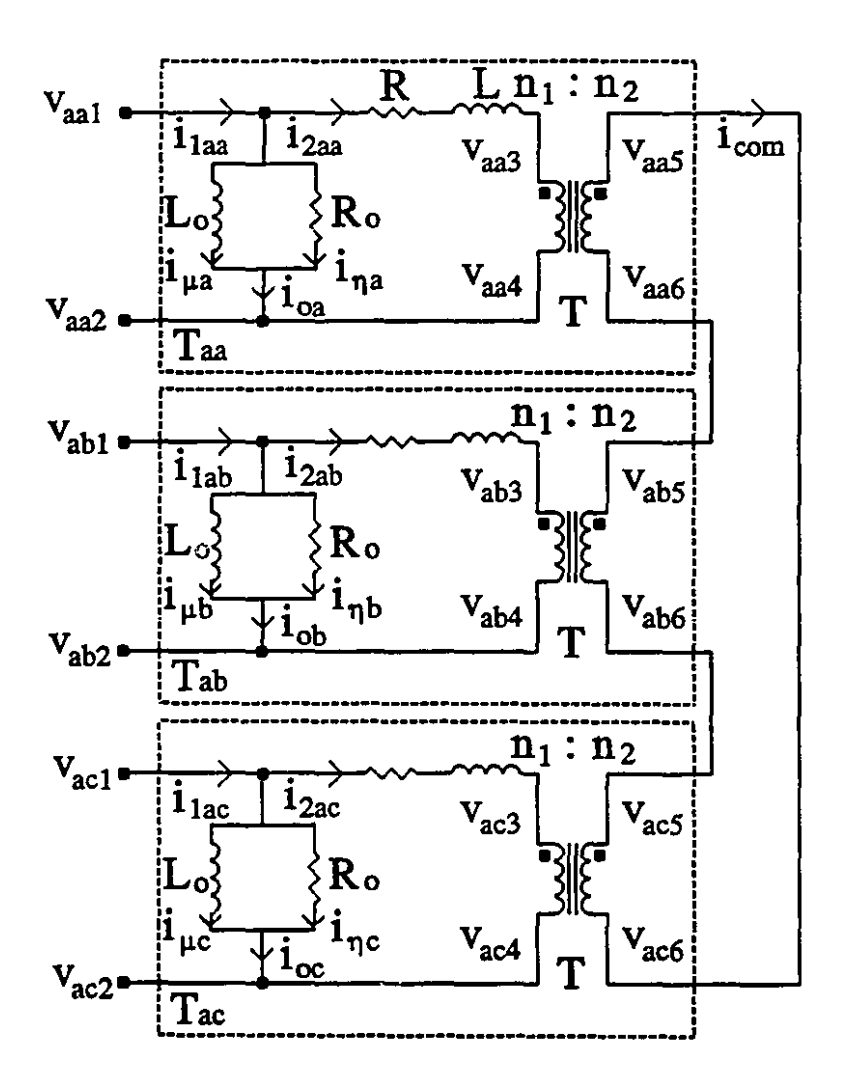


Fig. 6-8 Equivalent circuit diagram of the transformers used in Fig. 6-7.

$$\frac{v_{aa3} - v_{aa4}}{v_{aa5} - v_{aa6}} = \frac{v_{ab3} - v_{ab4}}{v_{ab5} - v_{ab6}} = \frac{v_{ac3} - v_{ac4}}{v_{ac5} - v_{ac6}} = \frac{n_1}{n_2}$$
 (6-46)

Also,

$$\frac{i_{2aa}}{i_{com}} = \frac{i_{2ab}}{i_{com}} = \frac{i_{2ac}}{i_{com}} = \frac{n_2}{n_1}$$
 (6-47)

From (6-47), one can conclude that

$$i_{2aa} = i_{2ab} = i_{2ac} = \frac{n_2}{n_1} i_{com}$$
 (6-48)

Also, since in the delta connected secondary circuits, by KVL

$$(v_{aa5} - v_{aa6}) + (v_{ab5} - v_{ab6}) + (v_{ac5} - v_{ac6}) = 0$$
 (6-49)

from (6-46),

$$(v_{aa3} - v_{aa4}) + (v_{ab3} - v_{ab4}) + (v_{ac3} - v_{ac4}) = 0$$
 (6-50)

In the primary-side of T_{aa} , one can write:

$$\frac{di_{\mu a}}{dt} = \frac{v_{aa1} - v_{aa2}}{L_a} \tag{6-51}$$

$$i_{\eta a} = \frac{v_{aa1} - v_{aa2}}{R_a} \tag{6-52}$$

$$i_{oa} = i_{\mu a} + i_{\eta a} \tag{6-53}$$

and

$$\frac{di_{2aa}}{dt} = \frac{(v_{aa1} - v_{aa2}) - Ri_{2aa} - (v_{aa3} - v_{aa4})}{I}$$
 (6-54)

Similarly, in the primary-side of T_{ab} ,

$$\frac{di_{\mu b}}{dt} = \frac{v_{ab1} - v_{ab2}}{L_a} \tag{6-55}$$

$$i_{\eta b} = \frac{v_{ab1} - v_{ab2}}{R_o} \tag{6-56}$$

$$i_{ob} = i_{\mu b} + i_{\eta b} \tag{6-57}$$

and

$$\frac{di_{2ab}}{dt} = \frac{(v_{ab1} - v_{ab2}) - Ri_{2ab} - (v_{ab3} - v_{ab4})}{L}$$
(6-58)

Likewise, in the primary-side of T_{ac} ,

$$\frac{di_{\mu c}}{dt} = \frac{v_{ac1} - v_{ac2}}{L_a} \tag{6-59}$$

$$i_{\eta c} = \frac{v_{ac1} - v_{ac2}}{R_o} \tag{6-60}$$

$$i_{oc} = i_{\mu c} + i_{\eta c}$$
 (6-61)

and

$$\frac{di_{2ac}}{dt} = \frac{(v_{ac1} - v_{ac2}) - Ri_{2ac} - (v_{ac3} - v_{ac4})}{L}$$
 (6-62)

Adding both sides of (6-54), (6-58), and (6-62), and using (6-48) and (6-50), one gets:

$$\frac{di_{com}}{dt} = \frac{\frac{1}{3} \frac{n_1}{n_2} \left[\left(v_{aa1} - v_{aa2} \right) + \left(v_{ab1} - v_{ab2} \right) + \left(v_{ac1} - v_{ac2} \right) \right] - Ri_{com}}{L}$$
(6-63)

From Fig. 6-7,

$$v_{aa1} = v_{ab1} = v_{ac1} = e_{1a} ag{6-64}$$

Therefore, (6-63) can be rewritten as:

$$\frac{di_{com}}{dt} = \frac{\frac{1}{3} \frac{n_1}{n_2} \left[3e_{1a} - \left(v_{aa2} + v_{ab2} + v_{ac2} \right) \right] - Ri_{com}}{L}$$
 (6-65)

The voltage sum: $v_{aa2} + v_{ab2} + v_{ac2}$ does not contain any unwanted components, since the unwanted components in v_{1aa} , v_{1ab} , and v_{1ac} , and therefore in v_{aa2} , v_{ab2} , and v_{ac2} , at any frequency, are equal in magnitude and phase shifted by $2\pi/3$ with respect to one another and upon adding, they cancel out. The fundamental components of v_{1aa} , v_{1ab} , and v_{1ac} , and therefore of v_{aa2} , v_{ab2} , and v_{ac2} , at angular frequency ω_1 , are equal in magnitude and in phase so they add up. The result is that from (6-65), i_{com} is a single-frequency cosine waveform at angular frequency ω_1 . From (6-48), then, one can conclude that i_{2aa} , i_{2ab} , and i_{2ac} are free of unwanted components. According to Fig. (6-8),

$$i_{1aa} = i_{oa} + i_{2aa}$$
 $i_{1ab} = i_{ob} + i_{2ab}$
 $i_{1ac} = i_{oc} + i_{2ac}$
(6-66)

But, i_{oa} , i_{ob} , and i_{oc} are very small, since L_o and R_o are very large; therefore, to a very good approximation, one can write (6-66) as:

$$i_{1aa} = i_{2aa}$$
 $i_{1ab} = i_{2ab}$
 $i_{1ac} = i_{2ac}$
(6-67)

The conclusion is that since i_{2aa} , i_{2ab} , and i_{2ac} are free of subfrequency and superfrequency components, the branch currents i_{1aa} , i_{1ab} , and i_{1ac} will be free of unwanted components, as well. The same is true for the remaining branch currents.

The above discussion shows clearly that by using the transformers in the body of the matrix converter, it is guaranteed that the unwanted components in the side-1 branch currents are eliminated and as a result, the waveforms of the side-2 currents and voltages will be free of unwanted components.

As mentioned in section 6.6, there might be an unwanted dc component in the branch currents on side-1. The dc components cancel upon addition and do not appear in the source currents; but they can cause problems such as additional losses and saturation in the transformers. Unfortunately, the transformers used cannot eliminate the dc components and this problem remains to be solved. However, the dc component can be avoided by making sure that the frequency of the components in the branch currents, i.e., $\omega_1 \pm h \omega_2$ (h = 0, 1, 2, ...), never becomes equal to zero.

A similar problem exists for very low frequency components of the branch currents. In fact, these components, can flow through L_o and as a result, they cannot be trapped in the transformers. Apart from the dc and very low frequency unwanted components, the operation is expected to be quite satisfactory. The experimental results obtained for the system of Fig. 6-7 are presented in chapter 7.

It should be noted that the trapping transformers can replace the inductors in the side-1 branches of the system of Fig. 6-7. In this way, the size, weight, and cost of the system of Fig. 6-7 will be approximately the same as those of the system of Fig. 6-1.

6.8 Summary

In this chapter, a new matrix converter composed of three modules of the three-phase voltage-source converter, has been introduced and the dyadic matrix converter theory, developed in chapters 2-5, has been applied to the proposed matrix converter. The voltage-source-converter type matrix converter offers advantages in terms of: bypassing the switching difficulties associated with the bidirectional switches, reduction of the conduction losses, as well as taking advantage of a well-known technology. The problem of presence of unwanted components in the side-1 branch currents and therefore side-2 ac voltages has been addressed. Finally, a novel technique to overcome the above problem has been proposed.

SIMULATION AND EXPERIMENTAL TEST RESULTS

7.1 Introduction

In chapter 6, the voltage-source-converter type matrix converter (Fig. 6-1) was introduced and its capabilities under the application of the dyadic matrix converter theory were explained. This chapter presents the simulation and experimental results obtained from the matrix converter systems of Figs. 6-1 and 6-7. For the laboratory implementation, three identical voltage-source-converter units, each rated at 1 kVA, have been employed as the matrix of nine switches. A hybrid (analog and digital) electronic control circuit has been designed and constructed to realize the transformation matrix [H] of (6-29)-(6-33).

The program of simulation and experimental tests has been constructed to verify the predictions of the characteristics described in the previous chapters.

The results will be presented in the following order:

- (1) DC bias voltage control;
- (2) Displacement power factor control on side-1;
- (3) Unwanted components in the side-1 branch currents and the side-2 ac voltages;
- (4) Dual Field Vector and Unity Displacement Power Factor control;
- (5) Elimination of the unwanted components.

The parameters of the systems of Figs. 6-1 and 6-7 are given in Appendices F and G, respectively. The parameters of the equivalent circuits of the transformers in Fig. 6-7 are given in Appendix H.

7.2 DC Bias Voltage Control

The dc bias voltage on side-2 of the matrix converter of Fig. 6-1 is regulated by a closed-loop control system through adjusting the angle φ . The control system is explained in Appendix D and the detailed circuit diagrams are given in Appendix E.

In this section, the objective is to check the behaviour of the dc bias voltage control loop; therefore, M_f is set to zero. The modulating signals will then be of the

form: $M_{\varphi}\cos(\omega_1 t + \varphi + x)$, where x = 0, $-2\pi/3$, $-4\pi/3$. As a result, the side-2 voltages will contain only dc components, V_{dc} . The dc bias voltage control system adjusts φ until the quadrature relationship between the ac voltages projected on side-1 due to the dc bias voltages on side-2 and the side-1 source currents is established. The phase-a component of the projected voltage on side-1 due to the dc bias voltages on side-2, $v_{1a\varphi}$, can be expressed as:

$$v_{1a\varphi} = \frac{1}{2} M_{\varphi} V_{dc} \cos(\omega_1 t + \varphi)$$
 (7-1)

and the side-1 source current, i_{1a} , as:

$$i_{1a} = I_{1m} \cos\left(\omega_1 t + \eta_1\right) \tag{7-2}$$

For $v_{1a\phi}$ and i_{1a} to have quadrature relationship, the following relation must hold:

$$\varphi - \eta_1 = -\frac{\pi}{2} \tag{7-3}$$

Figs. 7-1 and 7-2 illustrate the above condition by showing the waveforms of i_{1a} for $\eta_1 = 0$ and $\eta_1 = -\pi/4$, and the modulating signal $v_{\text{mod}, aa}$:

$$v_{\text{mod},aa} = M_{\phi} \cos(\omega_1 t + \varphi) \tag{7-4}$$

which is proportional to $v_{1a\phi}$. As seen, in both cases, the condition given in (7-3) has been fulfilled in steady-state, after the desired dc bias voltage has been set up on side-2.

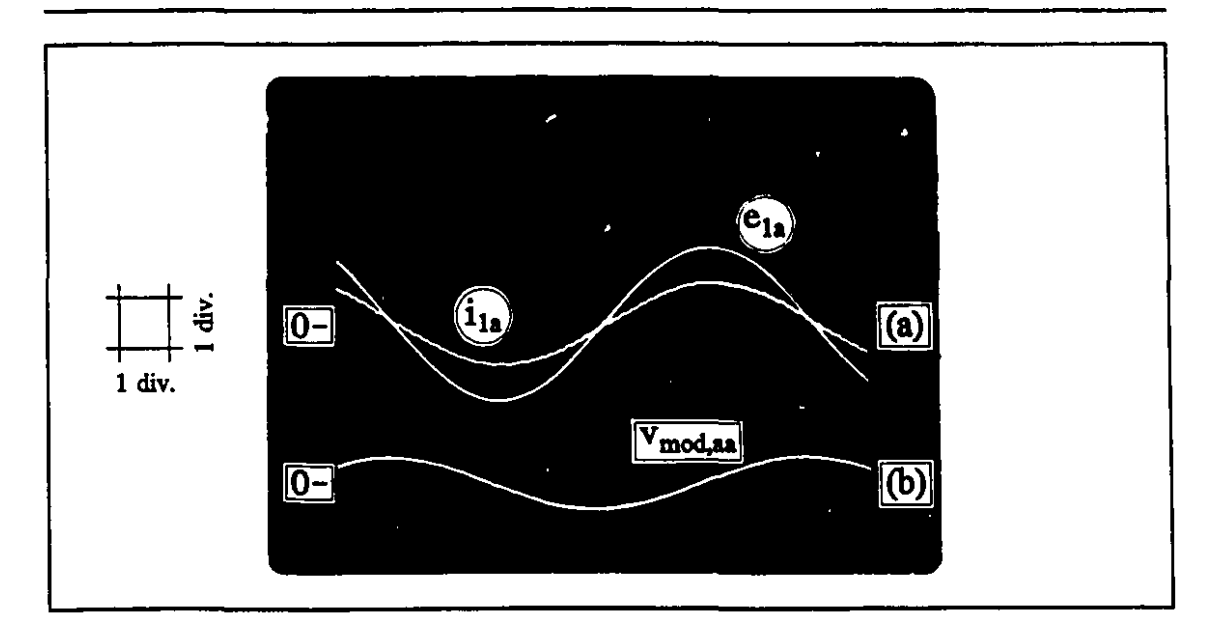


Fig. 7-1 Quadrature relationship of $v_{1a\phi}$ and i_{1a} for $M_f = 0$, $M_{\phi} = 0.5$, $V_{dc} = 65$ V, $e_{2a} = e_{2b} = e_{2c} = 0$, and $\eta_1 = 0$ (UDPF on side-1): (a) $e_{1a} = 10$ V/div, $i_{1a} = 25$ A/div, t = 2 ms/div (b) $v_{mod,aa} = 5$ V/div.

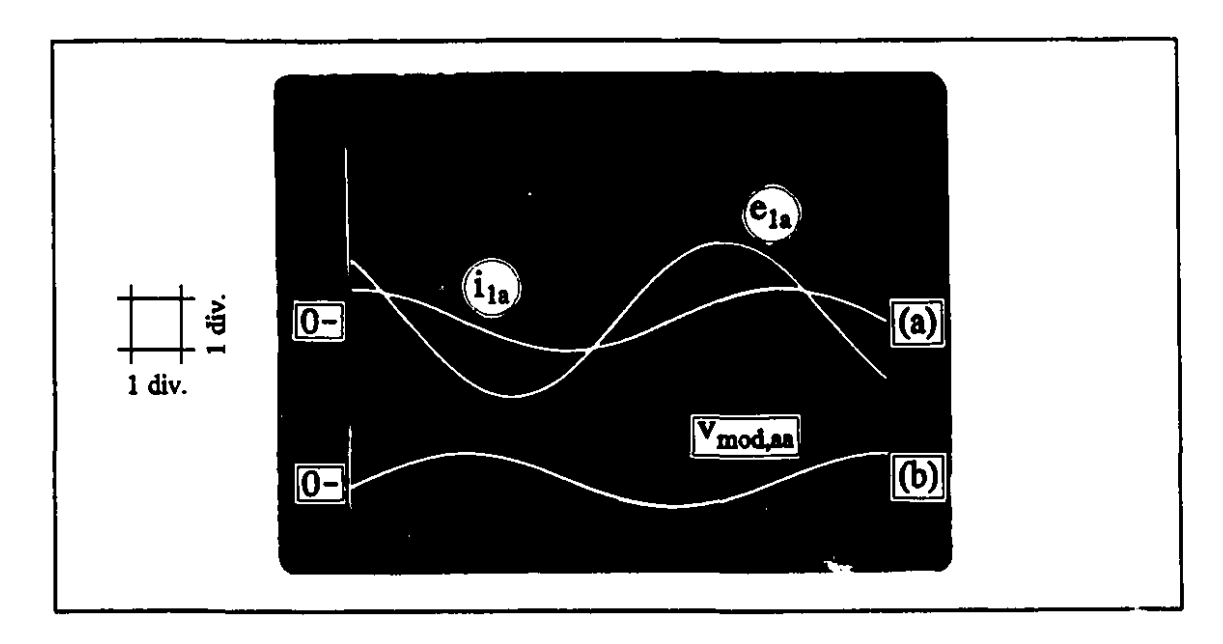


Fig. 7-2 Quadrature relationship of $v_{1a\phi}$ and i_{1a} for $M_f = 0$, $M_{\phi} = 0.2$, $V_{dc} = 20$ V, $e_{2a} = e_{2b} = e_{2c} = 0$, and $\eta_1 = -\pi/4$ (lagging DPF on side-1): (a) $e_{1a} = 10$ V/div, $i_{1a} = 25$ A/div, t = 2 ms/div (b) $v_{mod,aa} = 2$ V/div.

To demonstrate the transient behaviour of the dc bias voltage control loop, Fig. 7-3 shows the response of the side-2 dc bias voltage to a step change of 50% in the dc bias voltage reference. As seen, it takes only few cycles of 60 Hz (with the period T = 16.67 ms) for the side-2 dc bias voltage to reach the new steady-state level.

In the experimental results to follow, the side-2 dc bias voltages have been kept at the minimum possible level, i.e., approximately equal to the peak of the ac component of the side-2 voltages. Lowering the dc bias voltage level below this value, results in flattening the bottom of the waveforms of the side-2 voltages due to the forward biasing of the antiparallel diodes of the voltage-source converters and short circuiting the converter legs.

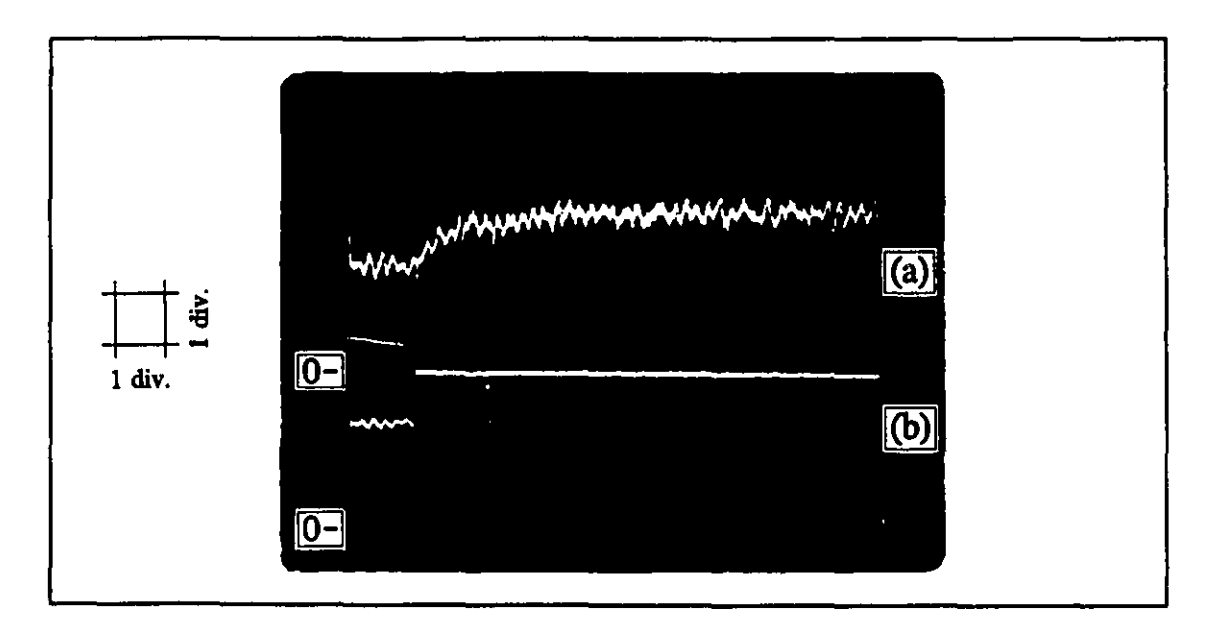


Fig. 7-3 Step response of side-2 dc bias voltage for $M_f = 0$, $M_{\phi} = 0.2$, $E_{1r} = 10$ V, and $e_{2a} = e_{2b} = e_{2c} = 0$: (a) $V_{dc} = 20$ V/div, t = 50 ms/div (b) $V_{dc,ref} = 20$ V/div.

7.3 Displacement Power Factor Control on Side-1

The displacement power factor on side-1 is controlled by adjusting M_{ϕ} , thus varying the magnitude of the ac voltages: $v_{1a\phi}$, $v_{1b\phi}$, and $v_{1c\phi}$, projected on side-1 due to the dc bias voltages on side-2. As shown in subsection 6.5.4 of chapter 6, positive M_{ϕ} values have leading effect on the DPF on side-1. Likewise, negative M_{ϕ} values have lagging effect on the DPF on side-1.

Figs. 7-4, 7-5, and 7-6 show the experimental results for the side-1 source voltage e_{1a} , source current i_{1a} , and side-2 voltage v_{2a} , for different values of M_{ϕ} for the case where $M_f = 0$ and therefore the side-2 voltages are purely dc. The dc bias

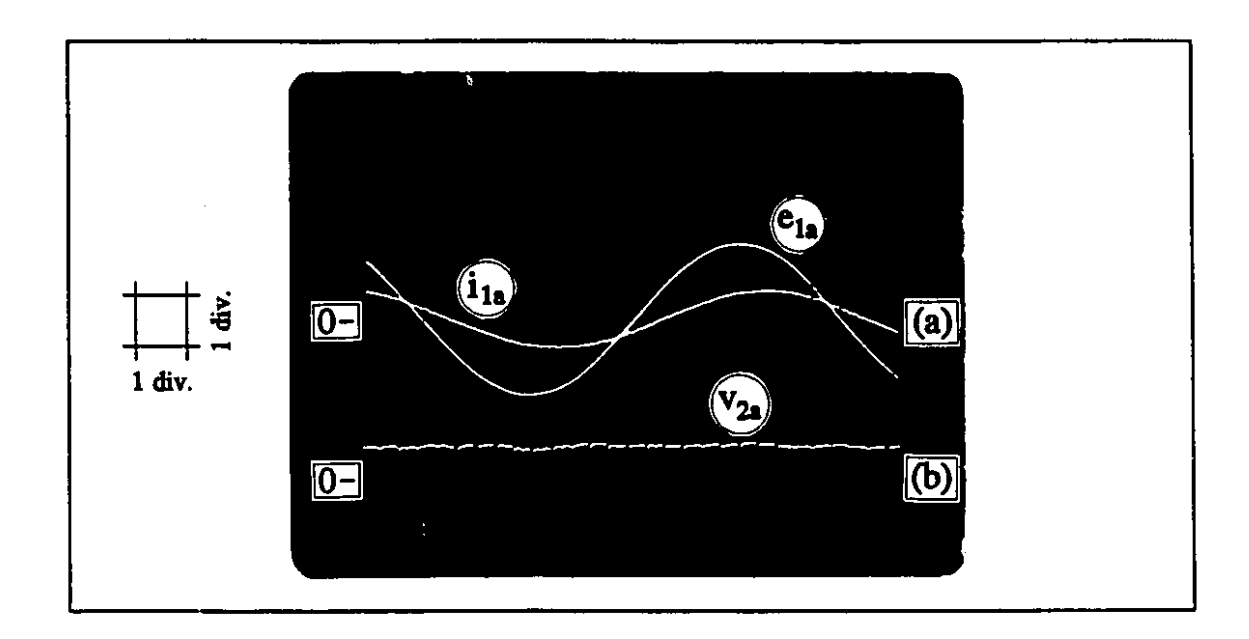


Fig. 7-4 Lagging DPF on side-1 for $M_f = 0$, $M_{\phi} = 0.2$, and $e_{2a} = e_{2b} = e_{2c} = 0$: (a) $e_{1a} = 10 \text{ V/div}$, $i_{1a} = 25 \text{ A/div}$, t = 2 ms/div (b) $v_{2a} = 100 \text{ V/div}$.

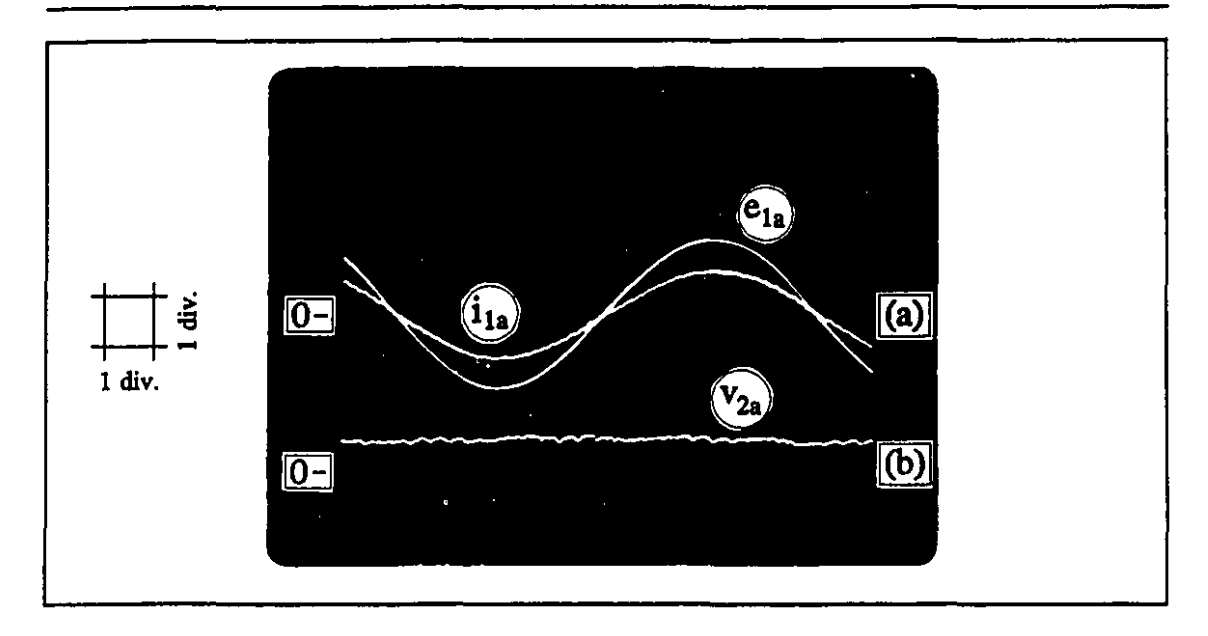


Fig. 7-5 UDPF on side-1 for $M_f = 0$, $M_{\phi} = 0.55$, and $e_{2a} = e_{2b} = e_{2c} = 0$: (a) $e_{1a} = 10 \text{ V/div}$, $i_{1a} = 25 \text{ A/div}$, t = 2 ms/div (b) $v_{2a} = 100 \text{ V/div}$.

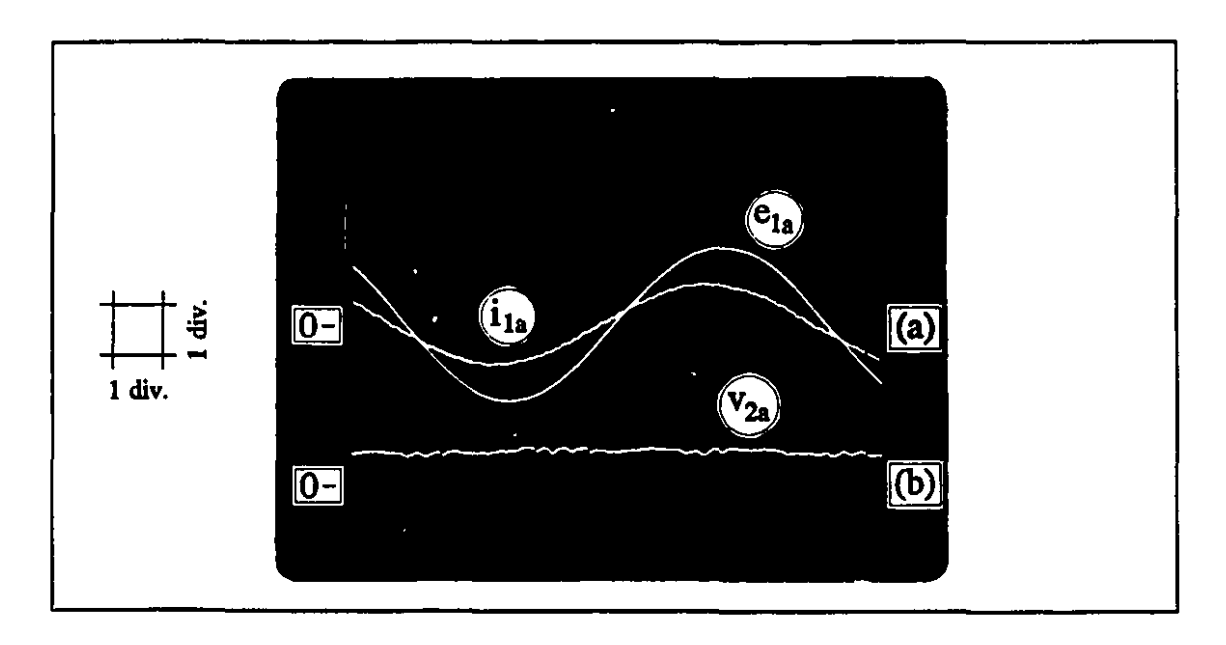


Fig. 7-6 Leading DPF on side-1 for $M_f = 0$, $M_{\phi} = 0.6$, and $e_{2a} = e_{2b} = e_{2c} = 0$:
(a) $e_{1a} = 10 \text{ V/div}$, $i_{1a} = 25 \text{ A/div}$, t = 2 ms/div (b) $v_{2a} = 100 \text{ V/div}$.

voltage is regulated at $V_{dc} = 65$ V. As seen, the displacement angles range from lagging to leading passing through zero degree corresponding to UDPF. There will be no current flowing in the loads simply because the neutral point of the wye-connected three-phase load is at the potential V_{dc} . Also, in this case, there will be no unwanted components in the side-1 branch currents, as will be seen later in section 7-4.

Figs. 7-7, 7-8, and 7-9 show the experimental results for the side-1 source voltage, e_{1a} , and source current, i_{1a} , for $M_f = 0.22$ and different values of M_{ϕ} . The dc bias voltage is kept at $V_{dc} = 65$ V using a closed-loop control system. The results are obtained at $f_2 = 120$ Hz. As seen, the displacement angles on side-1 assume a

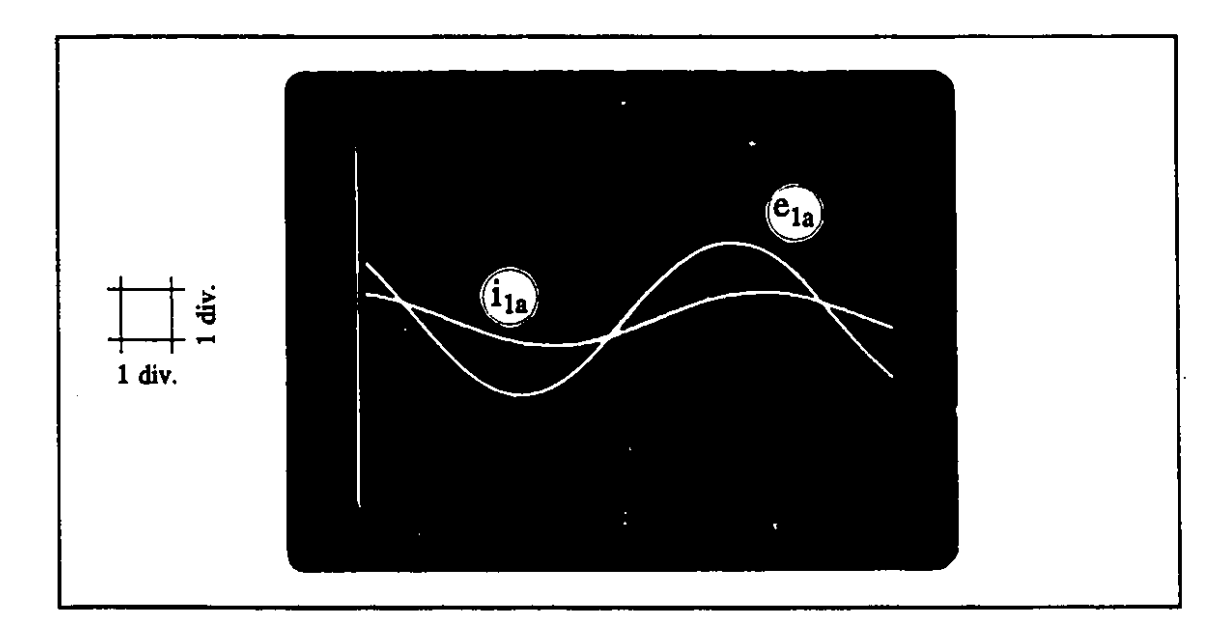


Fig. 7-7 Lagging DPF on side-1 for $M_f = 0.22$, $M_{\phi} = 0.39$, $V_{dc} = 65 \text{ V}$, $e_{2a} = e_{2b} = e_{2c} = 0$, and $f_2 = 120 \text{ Hz}$: $e_{1a} = 10 \text{ V/div}$, $i_{1a} = 25 \text{ A/div}$, t = 2 ms/div.

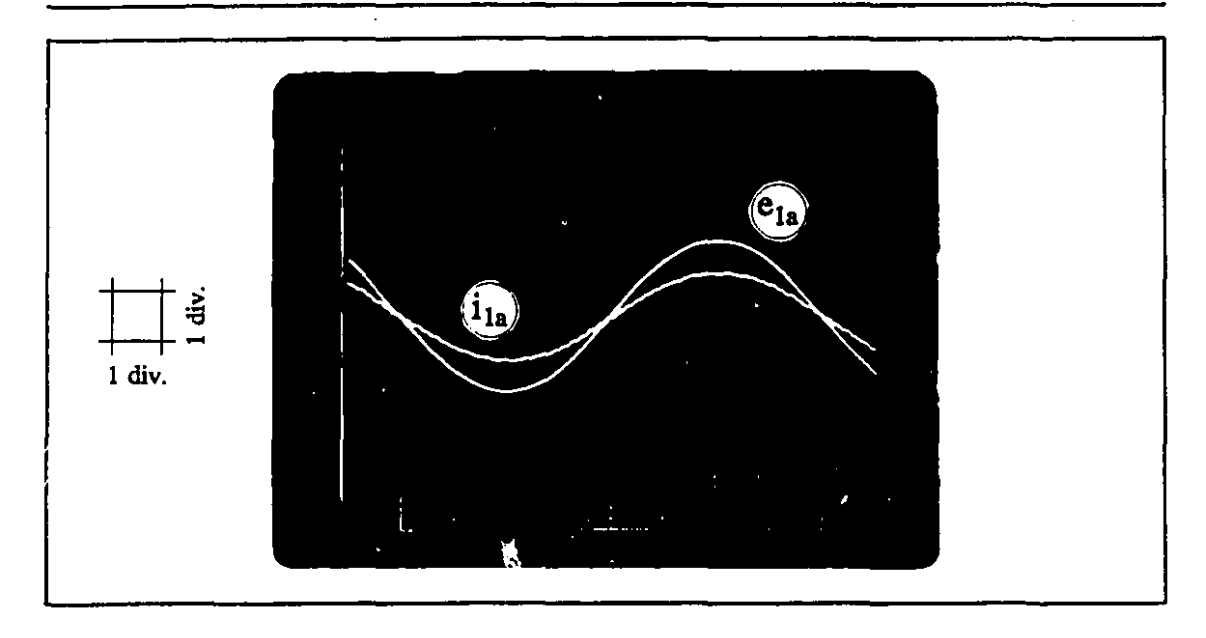


Fig. 7-8 UDPF on side-1 for $M_f = 0.22$, $M_{\phi} = 0.55$, $V_{dc} = 65$ V, $e_{2a} = e_{2b} = e_{2c} = 0$, and $f_2 = 120$ Hz: $e_{1a} = 10$ V/div, $i_{1a} = 25$ A/div, t = 2 ms/div.

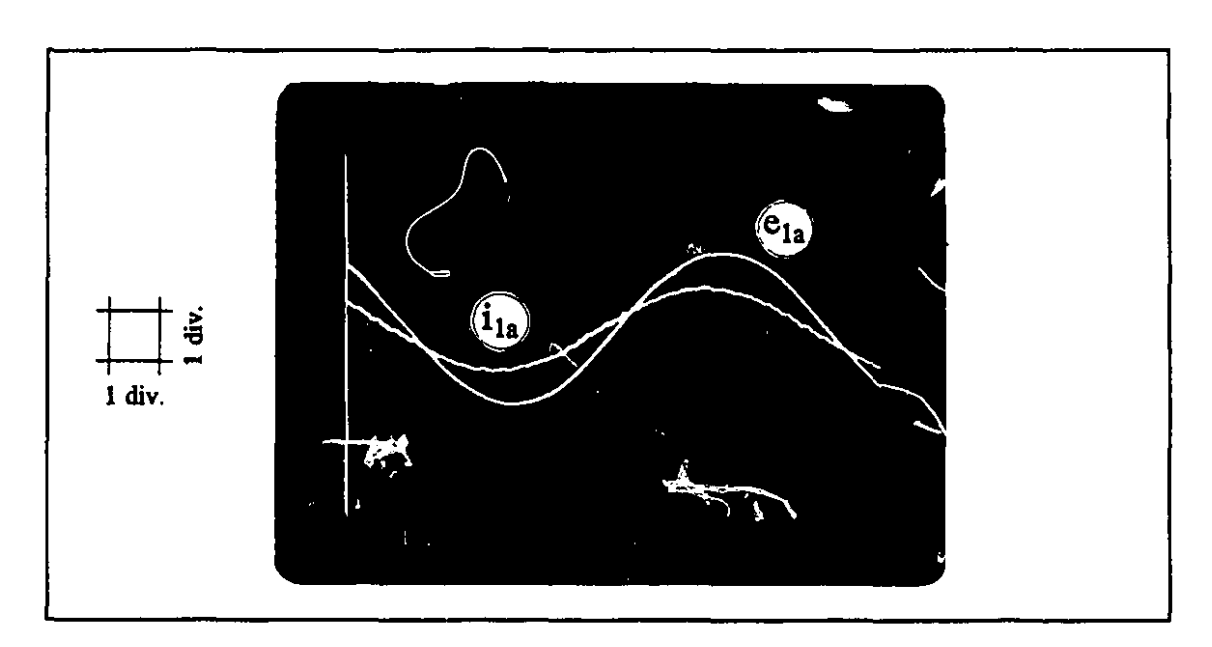


Fig. 7-9 Leading DPF on side-1 for $M_f = 0.22$, $M_{\phi} = 0.66$, $V_{dc} = 65$ V, $e_{2a} = e_{2b} = e_{2c} = 0$, and $f_2 = 120$ Hz: $e_{1a} = 10$ V/div, $i_{1a} = 25$ A/div, t = 2 ms/div.

wide range of leading and lagging values including zero degrees which corresponds to UDPF.

In order to demonstrate that UDPF does not occur only at a single combination of M_f and M_{ϕ} values, Fig. 7-10 shows the experimental results obtained for M_{ϕ} and I_{1r} (rms value of i_{1a}) vs. M_f , for E_{1r} = 10 V, V_{dc} = 65 V, and f_2 = 120 Hz under the UDPF condition on side-1. As seen, the desired condition of UDPF on side-1 can be satisfied in a wide range of M_f variations, corresponding to a wide

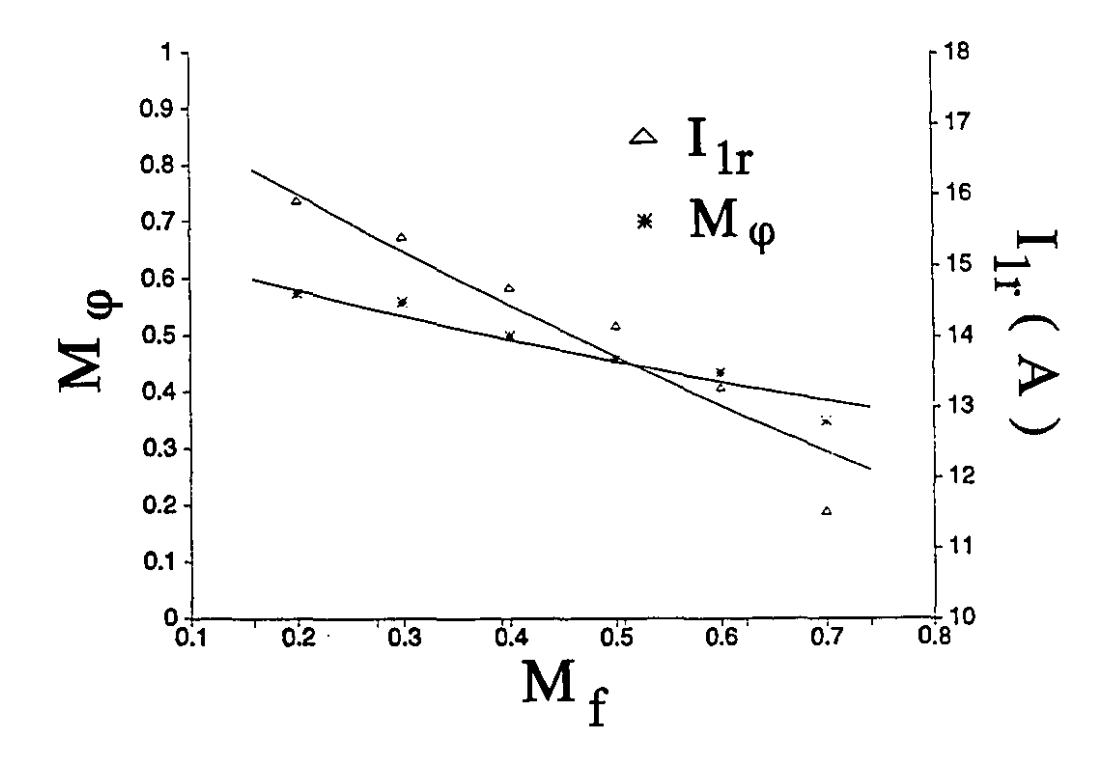


Fig. 7-10 Experimental results: M_{ϕ} and I_{1r} vs. M_f for UDPF on side-1, $E_{1r} = 10$ V, $V_{dc} = 65$ V, $f_2 = 120$ Hz, and $e_{2a} = e_{2b} = e_{2c} = 0$.

range of side-2 ac voltages and load currents. This is promising for variable-speed ac motor drive applications, where the motor torque has to be controlled by varying the side-2 current. Another significant conclusion is that the changes in the range considered are monotonic. This implies that negative feedback control can be employed.

7.4 Unwanted Components in the Side-1 Branch Currents and the Side-2 AC Voltages

The experimental results presented in this section, back up the discussion made in section 6.6 of chapter 6, over the presence of the unwanted components in the side-1 branch currents and side-2 ac voltages of the system of Fig. 6-1.

Fig. 7-11 shows the waveform of the modulating signal $v_{\text{mod},aa}$, and the corresponding side-1 branch current i_{1aa} , for $M_f = 0$ and $M_{\phi} = 0.55$. As seen, no low-frequency unwanted component is sensed in the branch current waveform. This is because the side-2 voltages are purely dc and the modulating signals are of the form: $M_{\phi}\cos(\omega_1 t + \phi + x)$, where $x = 0, -2\pi/3, -4\pi/3$.

Comparing Figs. 7-11 and 7-5, which have been produced under identical conditions, one can see that $i_{1aa} = 1/3 i_{1a}$. This backs up the discussion made in section 6.6 of chapter 6 leading to the conclusion that when the branch currents are free of unwanted harmonics, they are equal to 1/3 of the corresponding source current; i.e., in Fig. 6-1,

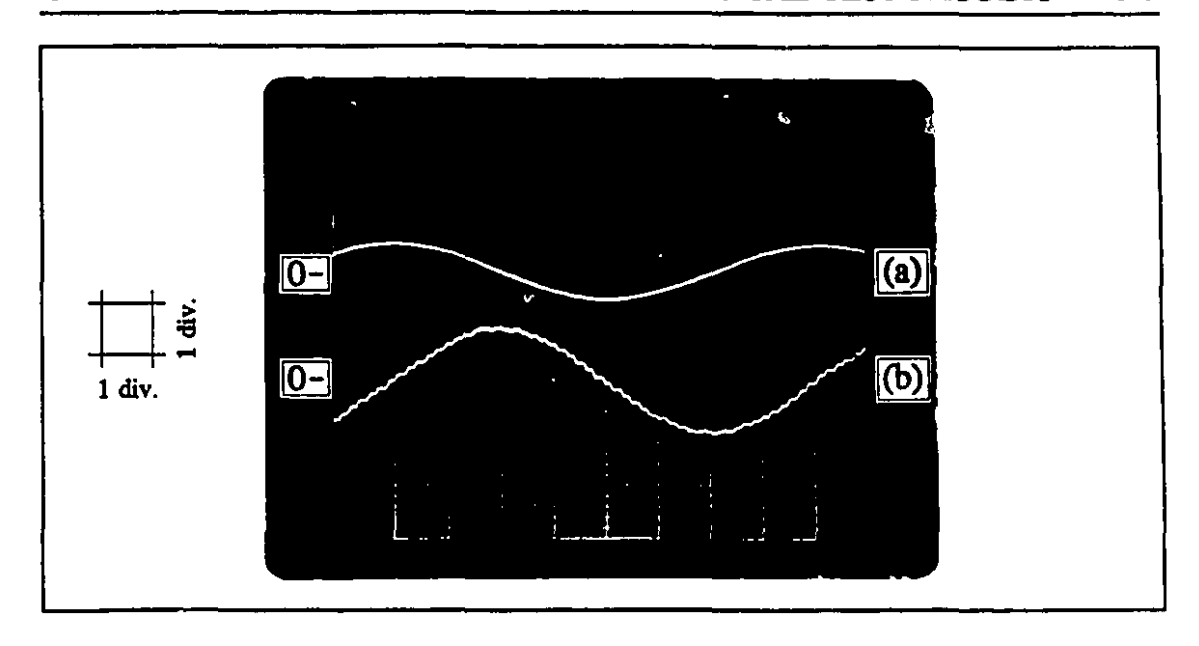


Fig. 7-11 Unwanted components absent from the side-1 branch currents for $f_1 = 60$ Hz, $M_f = 0$, $M_{\phi} = 0.55$, $E_{1r} = 10$ V, $e_{2a} = e_{2b} = e_{2c} = 9$, $V_{dc} = 65$ V: (a) $v_{mod,aa} = 5.5$ V/div, t = 2 ms/div (b) $i_{1aa} = 5$ A/div.

$$i_{1aa} = i_{1ab} = i_{1ac} = \frac{1}{3}i_{1a}$$

$$i_{1ba} = i_{1bb} = i_{1bc} = \frac{1}{3}i_{1b}$$

$$i_{1ca} = i_{1cb} = i_{1cc} = \frac{1}{3}i_{1c}$$
(7-5)

Fig. 7-12 shows the waveform of the modulating signal $v_{\text{mod},aa}$, and the corresponding side-1 branch current for $M_f = 0.44$, $M_{\phi} = 0.33$, and $f_2 = 120$ Hz. The presence of low-frequency unwanted components is clearly seen in the side-1 branch current. One can see, by inspection, that the dominant component is the third harmonic at the angular frequency of $3\omega_1$. According to the discussion in section 6.6 of chapter 6, this corresponds to the component at the angular frequency of $\omega_1 + \omega_2 = \omega_1 + 2\omega_1 = 3\omega_1$.

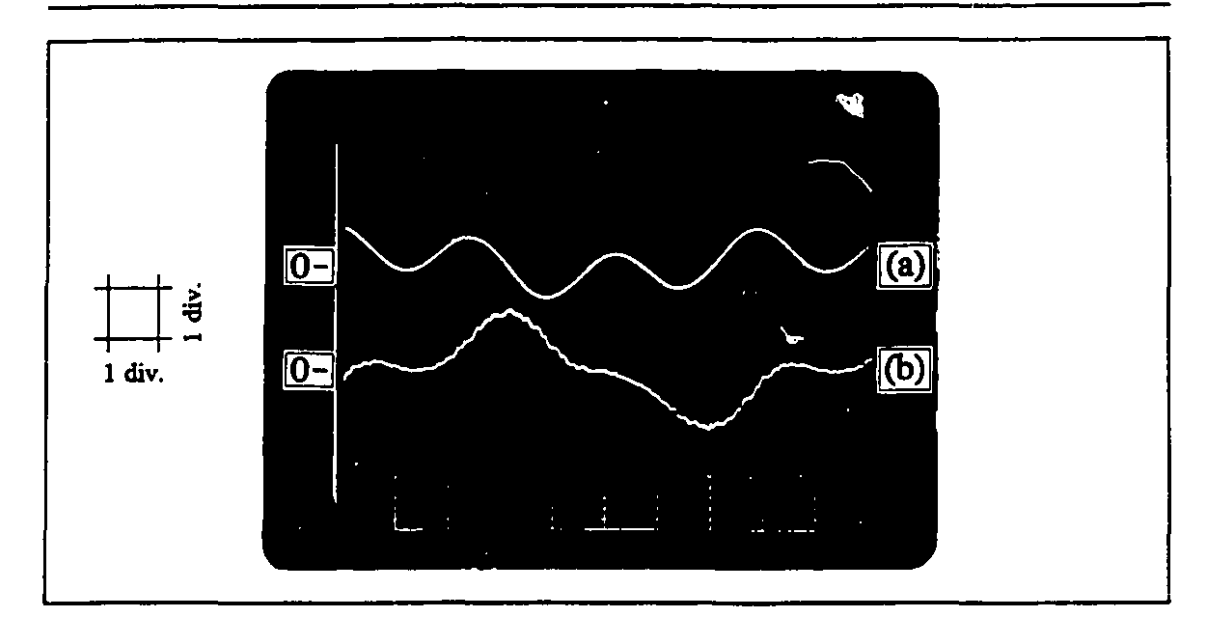


Fig. 7-12 Unwanted components present in the side-1 branch currents for $f_1 = 60$ Hz, $f_2 = 120$ Hz, $M_f = 0.44$, $M_{\phi} = 0.33$, $E_{1r} = 10$ V, $e_{2a} = e_{2b} = e_{2c} = 0$, and $V_{dc} = 65$ V: (a) $v_{mod,aa} = 5.5$ V/div, t = 2 ms/div (b) $i_{1aa} = 5$ A/div.

Fig. 7-13 shows the side-1 source voltage, e_{1a} , source current, i_{1a} , the ac component of side-2 voltage, v_{2a} , and side-2 load current, i_{2a}' . The low-frequency unwanted components in v_{2a} and i_{2a}' waveforms are visible.

By inspecting the waveforms in Figs. 7-12 and 7-13, one can clearly see that even though the side-1 branch currents and side-2 ac voltages contain unwanted components, the source currents are clean and free of unwanted components as pointed out in section 6.6 of chapter 6.

7-5 Dual Field Vector and Unity Displacement Power Factor Control

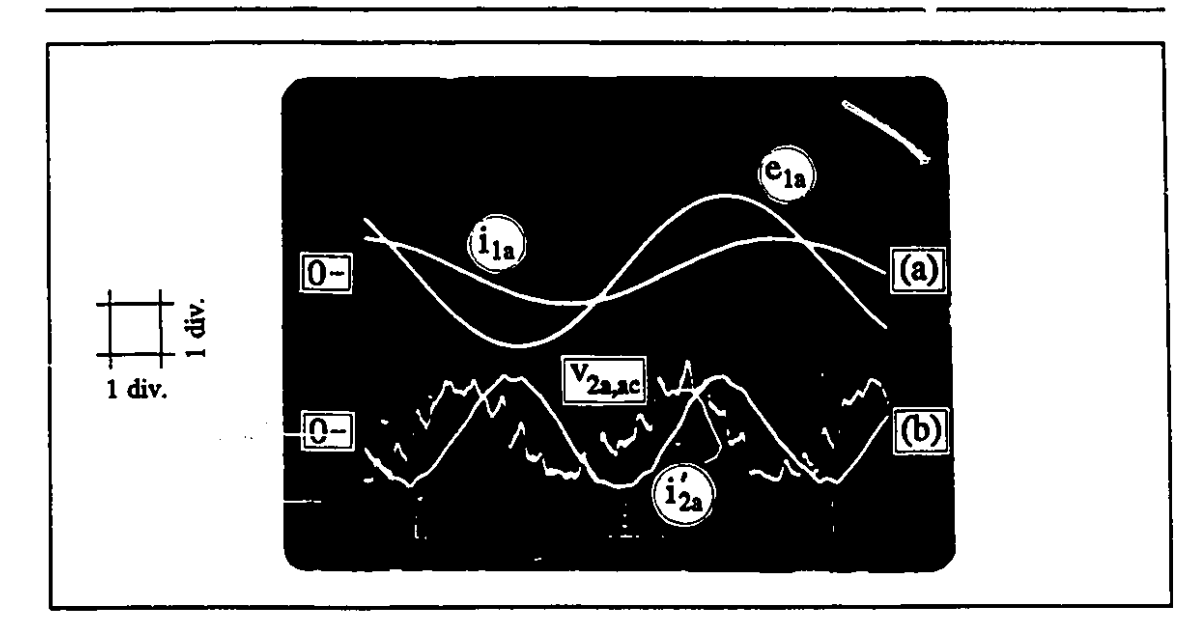


Fig. 7-13 Unwanted components present in the side-2 ac voltage for $f_1 = 60$ Hz, $f_2 = 120$ Hz, $M_f = 0.7$, $M_{\phi} = 0.2$, $V_{dc} = 20$ V, and $e_{2a} = v_{2b} = v_{2c} = 0$: (a) $e_{1a} = 10$ V/div, $i_{1a} = 25$ A/div, t = 2 ms/div (b) $v_{2a, ac} = 20$ V/div, $i'_{2a} = 0.5$ A/div.

In this section, it is demonstrated, through an open-loop experiment and a closed-loop digital simulation, that simultaneous occurrence of UDPF on side-1 and FVC on side-2 is feasible. The dual condition can be satisfied using the existing control levers of the matrix converter (i.e., M_f , γ , φ , and M_{φ}).

7.5.1 Open-Loop Experiment

In the experiment performed, all the controls are open-loop except for the dc bias voltage control which is closed-loop. Because of the complexity of the system and the multiplicity of the control variables, an open-loop experiment is not easy to perform. Nevertheless, a demonstration experiment was managed through which a "proof of principle" has been achieved.

The source voltages are at 60 Hz and the load voltages are at 120 Hz. The reason for using f_2 = 120 Hz has been that at low values of f_2 , the presence of the unwanted components in the side-1 branch currents and side-2 ac voltages is more pronounced.

It is desirable to be able to observe the induced voltage behind the reactance in an ac motor to make sure that the condition of FVC has been satisfied. That is why in the experiment performed, a three-phase ac source is needed to represent e_{2a} , e_{2b} , and e_{2c} . Since no three-phase supply at 120 Hz was available in the lab, the arrangement shown in Fig. 7-14 was set up. As shown in Fig. 7-14, the side-2 load voltages: e_{2a} , e_{2b} , and e_{2c} of Fig. 6-1, have been taken from the rotor terminals of

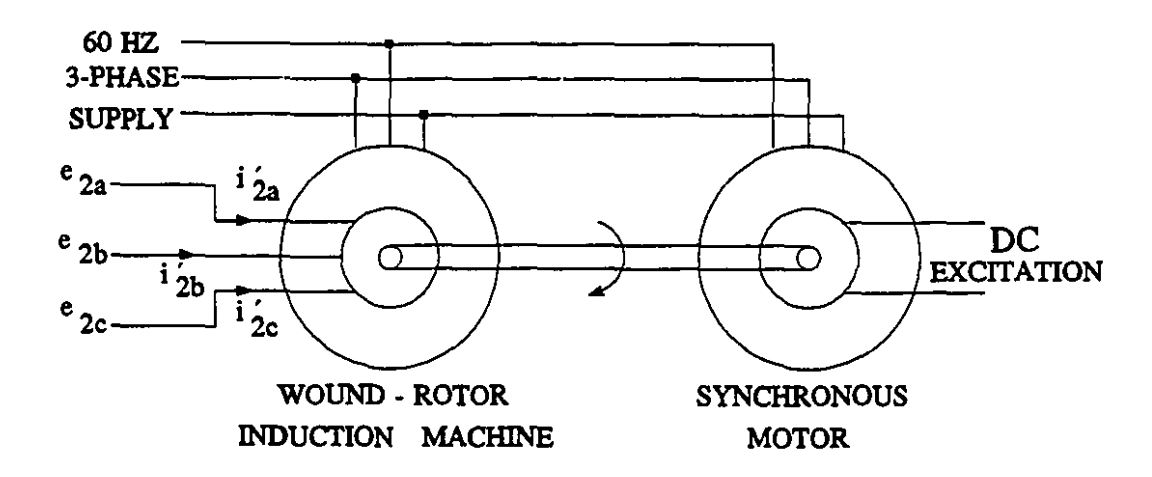


Fig. 7-14 Simulation of the induced emf behind the reactance of the synchronous motor at $f_2 = 120$ Hz.

a wound-rotor induction machine. The rotor of the induction machine is driven by a synchronous motor against the counter rotating magnetic flux of the induction machine stator. The stator of the induction machine is excited by the 60 Hz supply with the phase sequence reversed. The 120 Hz rotor voltages of the induction machine represent the voltages induced by the dc field winding of a synchronous motor which would be driven by the matrix converter. The side-2 currents i_{2a}^{\prime} , i_{2b}^{\prime} , and i_{2c}^{\prime} represent the stator currents of the above synchronous motor.

Fig. 7-15 shows the experimental results for the condition of UDPF on side-1 and FVC on side-2. The zero displacement angle of the load current i'_{2a} , with respect

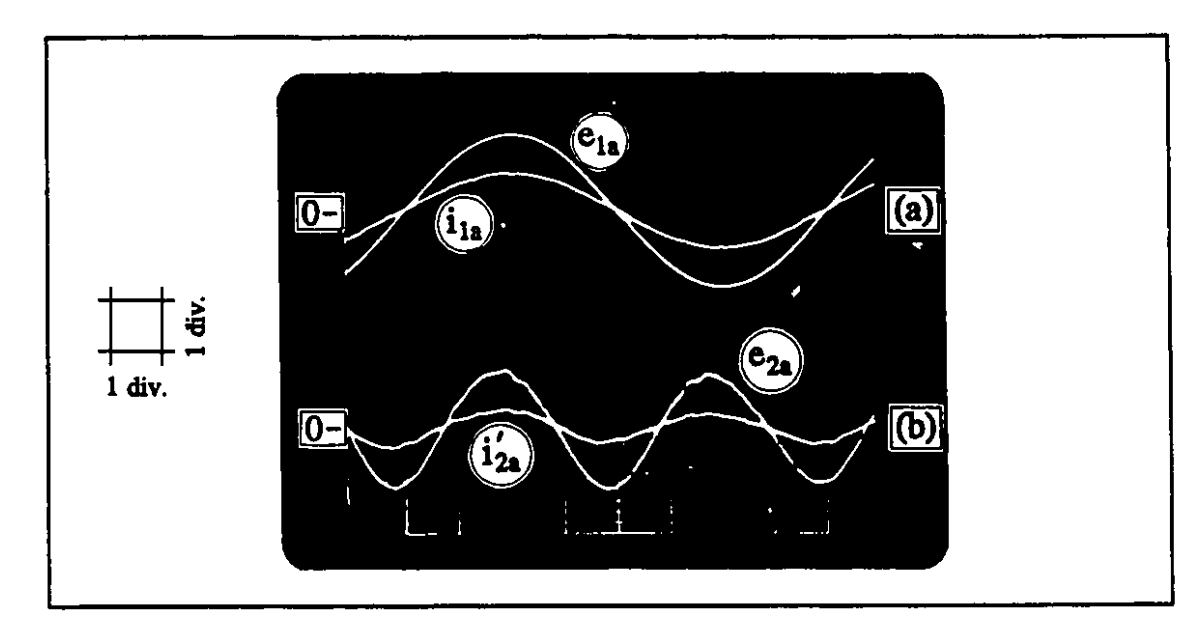


Fig. 7-15 Dual condition of UDPF on side-1 ($f_1 = 60 \text{ Hz}$) and FVC on side-2 ($f_2 = 120 \text{ Hz}$) for $V_{dc} = 48 \text{ V}$: (a) $e_{1a} = 10 \text{ V/div}$, $i_{1a} = 25 \text{ A/div}$, t = 2 ms/div (b) $e_{2a} = 4.33 \text{ V/div}$, $i'_{2a} = 1.25 \text{ A/div}$.

to the load voltage e_{2a} , illustrated in Fig. 7-15, corresponds to the space quadrature relationship of the magnetic fluxes of the rotor and the stator of the fictitious synchronous motor. This is the desired criterion in the Field Vector Control.

It was observed, during the experiment, that the alignment of the current i_{2a}' and the voltage e_{2a} is strongly dependent on the γ -control, while the alignment of the current i_{1a} and the voltage e_{1a} is strongly dependent on the M_{ϕ} -control.

Fig. 7-15 shows that by making use of all available degrees of freedom, the involved task of simultaneous establishment of UDPF on side-1 and FVC on side-2 of the matrix converter, can be performed.

7.5.2 Closed-Loop Digital Simulation

In this subsection, it is shown that converging towards the condition of UDPF on side-1 and FVC on side-2 is feasible by closed-loop control. The block diagram of the closed-loop control systems used are shown in Fig. 7-16.

In the first closed-loop control system, Fig. 7-16(a), the instantaneous VAR on side-1, Q_1 , is measured. Then, the control system tries to null Q_1 through M_{ϕ} -control.

In the second closed-loop control system, Fig. 7-16(b), the instantaneous VAR on side-2, Q_2 , is measured and the control system tries to null Q_2 through γ -control.

The dc bias voltage on side-2 is regulated by φ-control, as before.

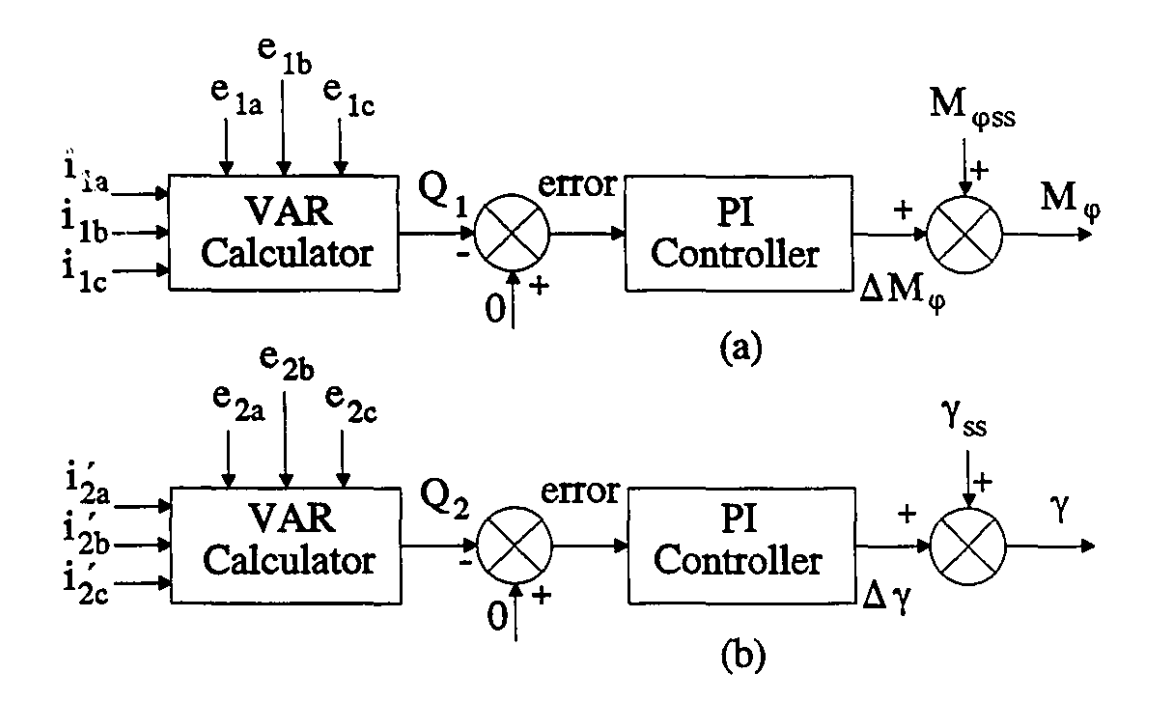


Fig. 7-16 Closed-loop control systems of: (a) UDPF on side-1 (b) FVC on side-2.

Fig. 7-17 shows the digital simulation results for the dual condition of UDPF on side-1 and FVC on side-2. The convergence to the desired conditions on both sides is achieved quickly and automatically, as a result of employing the closed-loop control systems described above.

7.6 Elimination of the Unwanted Components

In chapter 6, section 6.7, a novel method for eliminating the unwanted components in the side-1 branch currents and thus in the side-2 ac voltages was proposed. The proposed method was based on using trapping transformers on side-1

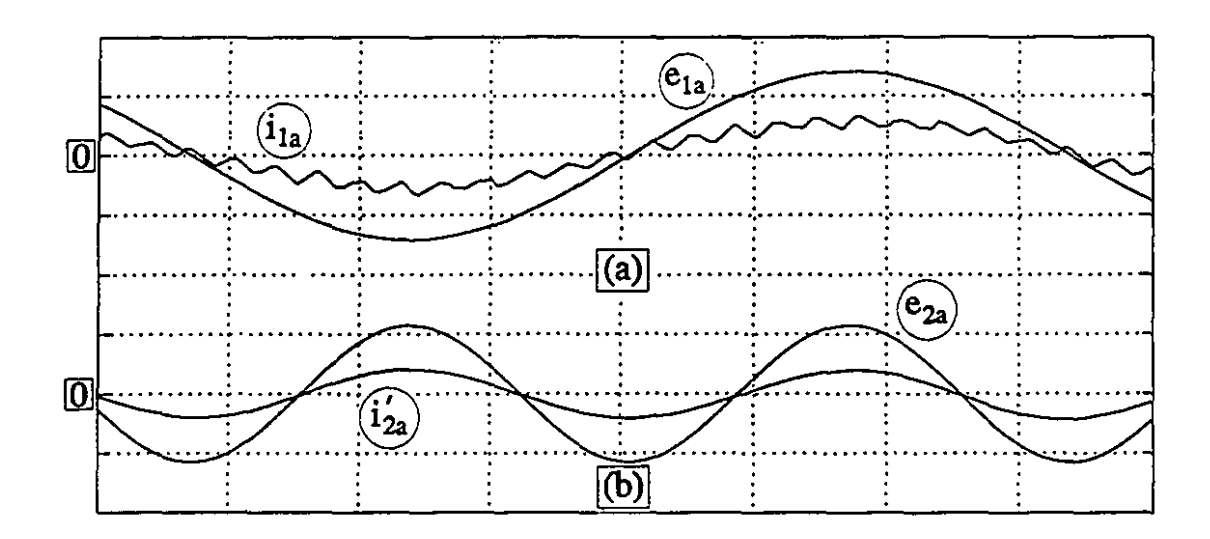


Fig. 7-17 Dual condition of UDPF on side-1 ($f_1 = 60 \text{ Hz}$) and FVC on side-2 ($f_2 = 120 \text{ Hz}$) for $R_1 = 0.399 \,\Omega$, $L_1 = 0.00399 \,H$, $R_2 = 4 \,\Omega$, $L_2 = 0.015 \,H$, $C = 80 \,\mu\text{F}$, $V_{dc} = 140 \,\text{V}$: (a) $e_{1a} = 20 \,\text{V/div}$, $i_{1a} = 80 \,\text{A/div}$, $t = 2.5 \,\text{ms/div}$ (b) $e_{2a} = 80 \,\text{V/div}$, $i_{2a}' = 20 \,\text{A/div}$.

of the matrix converter (Fig. 6-7) and proved anatically to be effective. In this section, selected experimental results are used to highlight the extent of the improvement made possible by employing the above technique.

7.6.1 Branch Current Waveform

Fig. 7-18 shows the waveform of the side-1 source current, i_{1a} , and that of the side-1 branch current, i_{1aa} . As seen, the branch current i_{1aa} is a sine wave of the same quality as the side-1 source current, i_{1a} . Moreover, i_{1aa} is in phase with i_{1a} with the amplitude equal to 1/3 of that of i_{1a} . This indicates that the condition given by

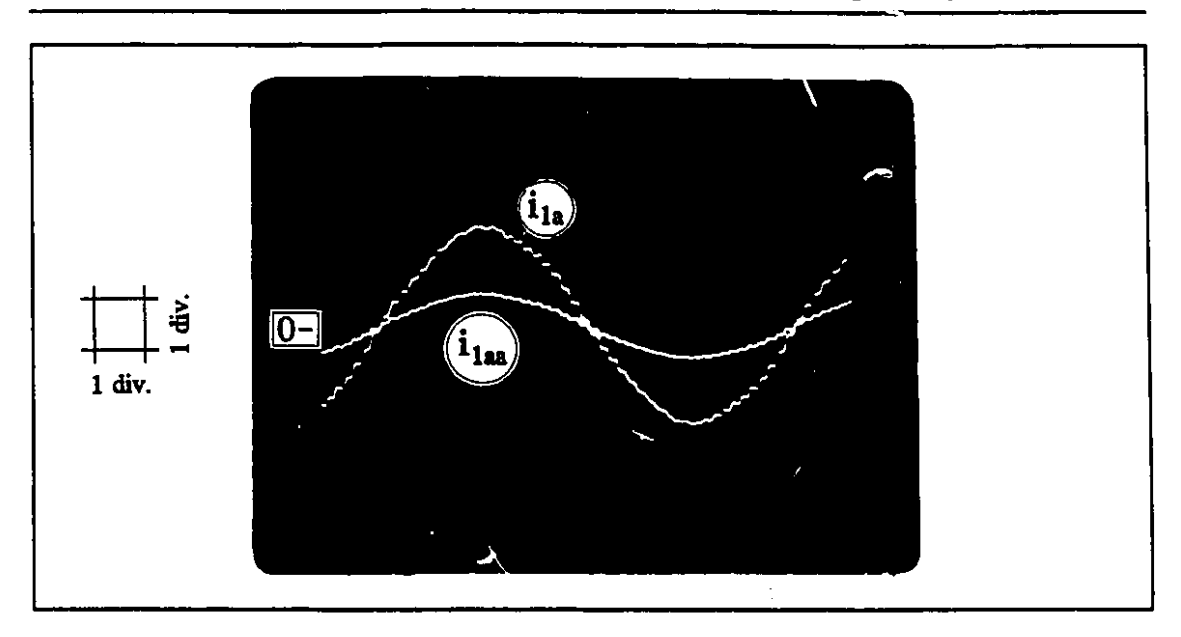


Fig. 7-18 Elimination of unwanted components in side-1 branch currents for E_{1r} = 10 V, V_{dc} = 50 V, e_{2a} = e_{2b} = e_{2c} = 0, M_f = 0.14, M_{ϕ} = 0.4, η_1 = 0 (UDPF on side-1), f_1 = 60 Hz, and f_2 = 120 Hz: i_{1a} = 5A/div, i_{1aa} = 5A/div, t_{1aa} = 5A/div, t_{1aa}

(6-45) has been met and as mentioned in section 6.6 of chapter 6, (6-25) represents the exact model of the current transformation in the voltage-source-converter type matrix converter system.

7.6.2 Side-2 AC Voltage Waveform

7.6.2.1 $f_1 = 60$ Hz and $f_2 = 30$ Hz

Fig. 7-19 shows the side-1 and side-2 current and voltage waveforms of the matrix converter system of Fig. 6-7 at UDPF on side-1 and f_2 = 30 Hz. The distortion noticed in the side-2 voltage and current waveforms, is due to the fact that according

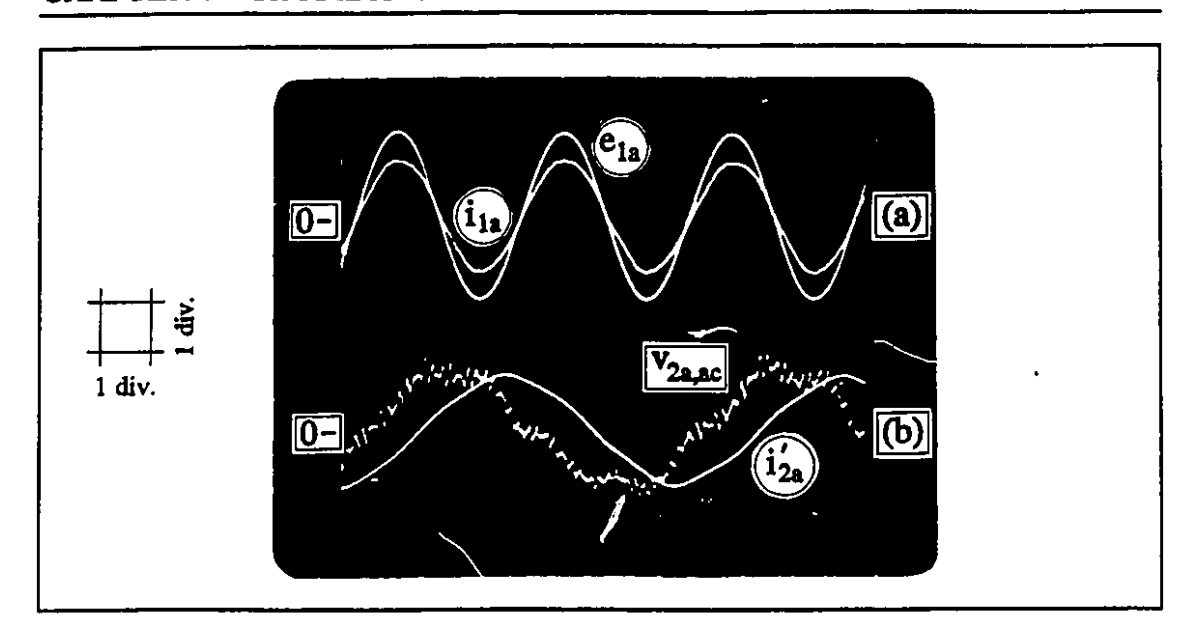


Fig. 7-19 Elimination of unwanted components in side-2 ac voltages for $E_{1r} = 10 \text{ V}$, $V_{dc} = 34.7 \text{ V}$, $e_{2a} = e_{2b} = e_{2c} = 0$, $M_f = 0.95$, $M_{\phi} = 0.175$, $\eta_1 = 0$ (UDPF on side-1), $f_1 = 60 \text{ Hz}$, $f_2 = 30 \text{ Hz}$, and $C = 50 \mu\text{F}$: (a) $e_{1a} = 9 \text{ V/div}$, $i_{1a} = 10.9 \text{ A/div}$, t = 5 ms/div (b) $v_{2a,ac} = 20 \text{ V/div}$, $i'_{2a} = 2.36 \text{ A/div}$.

to the discussion in section 6.6 of chapter 6, at f_1 = 60 Hz and f_2 = 30 Hz, the component having the angular frequency $\omega_1 - 2\omega_2$ in the branch currents is a dc component which cannot be eliminated by the proposed method. The result is the presence of unwanted components at angular frequencies $\omega_1 + \omega_2$ and ω_1 , equivalent to 90 Hz and 60 Hz, which can be observed in the waveform of the side-2 ac voltage.

Fig. 7-20 shows that by increasing the size of the side-2 capacitors from $50 \,\mu F$ to $200 \,\mu F$, the waveform of the side-2 ac voltage is improved to a great extent, as a result of the attenuation of the unwanted components.

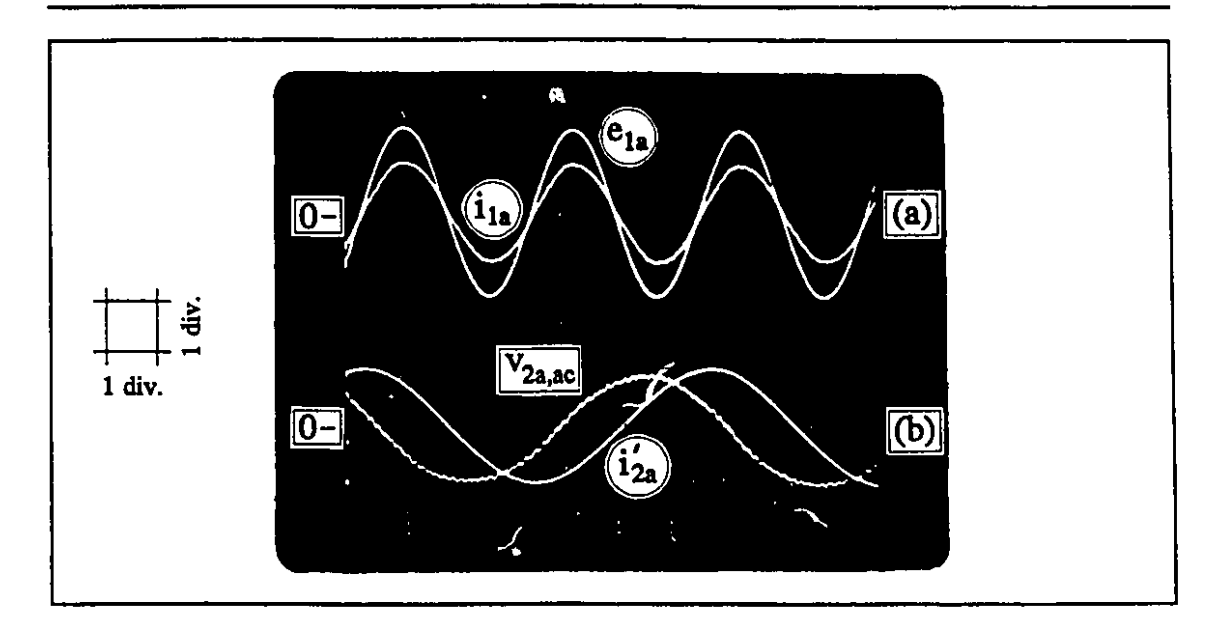


Fig. 7-20 Elimination of unwanted components in side-2 ac voltages for $E_{1r} = 10 \text{ V}$, $V_{dc} = 34.9 \text{ V}$, $e_{2a} = e_{2b} = e_{2c} = 0$, $M_f = 0.925$, $M_{\phi} = 0.09$, $\eta_1 = 0$ (UDPF on side-1), $f_1 = 60 \text{ Hz}$, $f_2 = 30 \text{ Hz}$, and $C = 200 \mu\text{F}$: (a) $e_{1a} = 9 \text{ V/div}$, $i_{1a} = 10.9 \text{ A/div}$, $t_{1a} = 5 \text{ ms/div}$ (b) $v_{2a,ac} = 20 \text{ V/div}$, $i_{2a} = 2.69 \text{ A/div}$.

7.6.2.2 $f_1 = 60$ Hz and $f_2 = 60$ Hz

Fig. 7-21 shows the side-1 and side-2 current and voltage waveforms of the matrix converter system of Fig. 6-7 at UDPF on side-1 and f_2 = 60 Hz. The side-2 ac voltage waveform is of a good quality. In fact, according to section 6.6 of chapter 6, for $f_2 = f_1$ = 60 Hz, the component with the angular frequency $\omega_1 - \omega_2$ in the branch currents is a dc component which is not supposed to be eliminated using the proposed method. This dc component which is generated by the $M_{\phi}\cos(\omega_1 t + \phi)$ terms in the modulating signals, is small and does not result in observable distortion

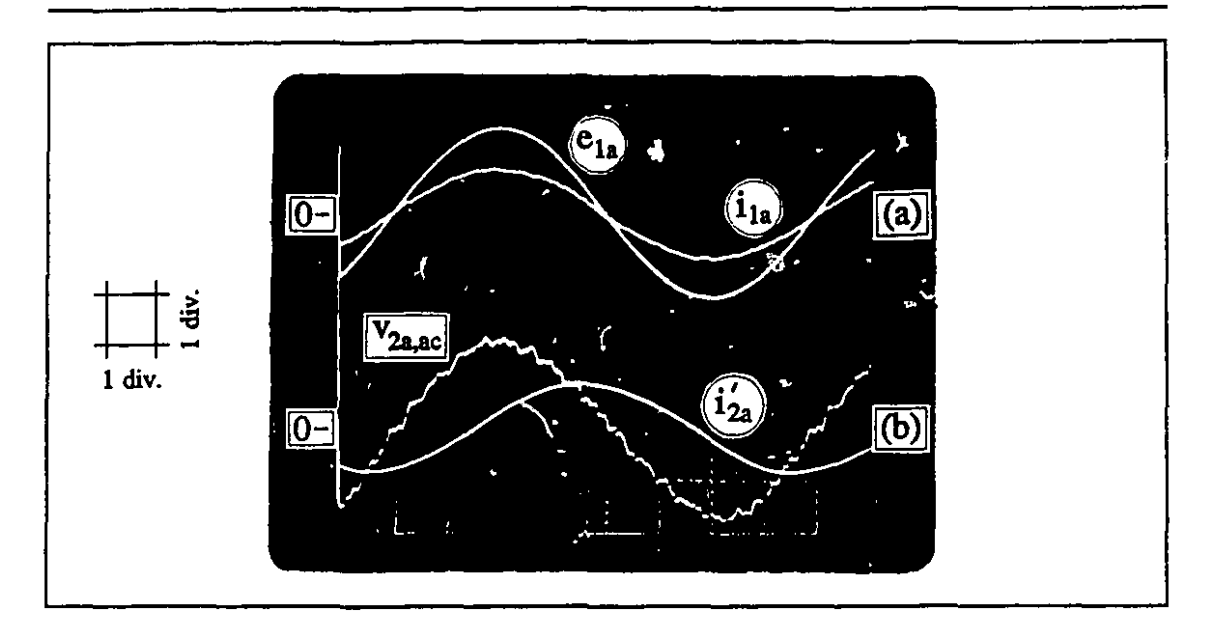


Fig. 7-21 Elimination of unwanted components in side-2 ac voltages for $E_{1r} = 10 \text{ V}$, $V_{dc} = 36.5 \text{ V}$, $e_{2a} = e_{2b} = e_{2c} = 0$, $M_f = 0.75$, $M_{\phi} = 0.075$, $\eta_1 = 0$ (UDPF on side-1), $f_1 = 60 \text{ Hz}$, $f_2 = 60 \text{ Hz}$, and $C = 50 \mu\text{F}$: (a) $e_{1a} = 9 \text{ V/div}$, $i_{1a} = 10.9 \text{ A/div}$, t = 2 ms/div (b) $v_{2a,ac} = 20 \text{ V/div}$, $i'_{2a} = 2.48 \text{ A/div}$.

in the side-2 ac voltage waveform of Fig. 7-21 since M_{\bullet} is very small in this case. The condition of UDPF on side-1 at a very low value of M_{\bullet} has been achieved as a result of reactance compensation due to the conjugate property offered by the $[H_f]$ part of the [H]-matrix.

7.6.2.3 $f_1 = 60$ Hz and $f_2 = 120$ Hz

Fig. 7-22 shows the side-1 and side-2 current and voltage waveforms of the matrix converter system of Fig. 6-7 at UDPF on side-1 and f_2 = 120 Hz. As seen, the

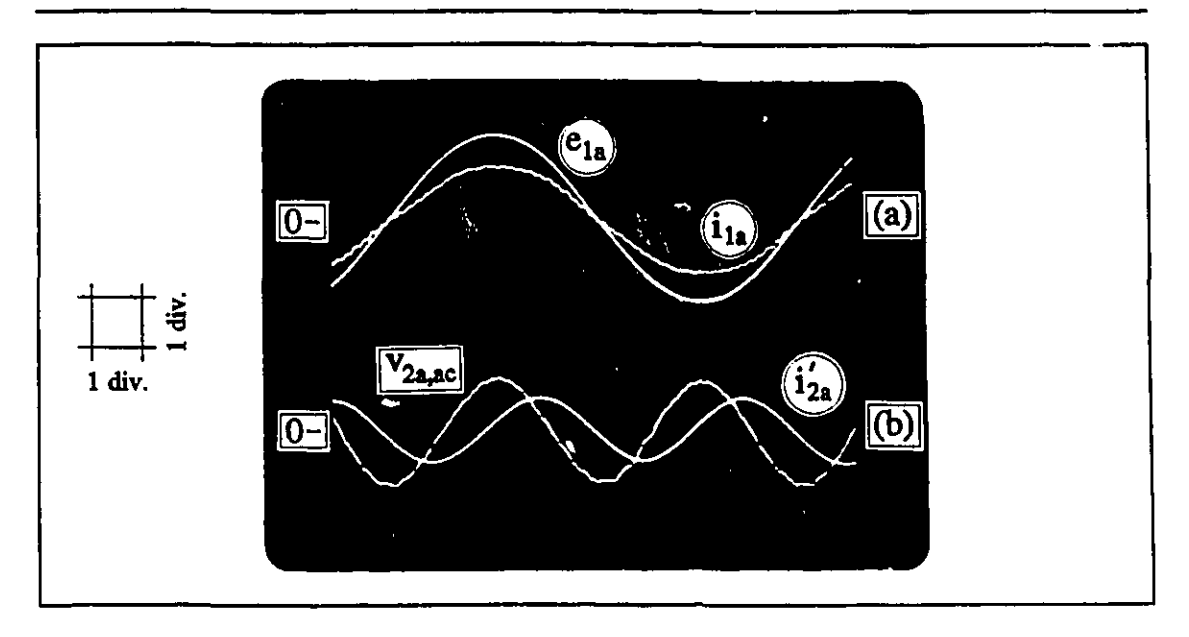


Fig. 7-22 Elimination of unwanted components in side-2 ac voltages for $E_{1r} = 10 \text{ V}$, $V_{dc} = 50 \text{ V}$, $e_{2a} = e_{2b} = e_{2c} = 0$, $M_f = 0.14$, $M_{\phi} = 0.4$, $\eta_1 = 0$ (UDPF on side-1), $f_1 = 60 \text{ Hz}$, $f_2 = 120 \text{ Hz}$, and $C = 50 \mu\text{F}$: (a) $e_{1a} = 9 \text{ V/div}$, $i_{1a} = 10.5 \text{ A/div}$, $i_{2a} = 2.4 \text{ A/div}$.

side-2 ac voltage is a good quality sine wave. Comparing the side-2 ac voltage of Fig. 7-22 with that of Fig. 7-13, one can see that the unwanted components (except for the switching harmonics) have been eliminated, proving the effectiveness of the proposed method. According to section 6.6 of chapter 6, no dc or low frequency unwanted components exists in the branch currents. Therefore, the method proposed in section 6.7 of chapter 6, can effectively eliminate all the unwanted components in the branch currents and the side-2 ac voltages will also be free of unwanted components.

As a matter of fact, the method presented in section 6.7 of chapter 6, is quite

effective if $f_2 > f_1$. The higher the difference of f_1 and f_2 , the more effective the method is. This means that the voltage-source-converter type matrix converter of Fig. 6-7, is very suitable for ac drives operating at $f_2 > f_1$.

7.6.3 Dual Condition of UDPF on Side-1 and FVC on Side-2

Fig. 7-23 is an improved version of Fig. 7-15. In Fig. 7-23, the side-1 and side-2 current and voltage waveforms are shown where UDPF exists on side-1 (at $f_1 = 60$ Hz) and FVC is achieved on side-2 (at $f_2 = 120$ Hz). The waveforms are of much better quality due to the employment of the new method for the elimination of the

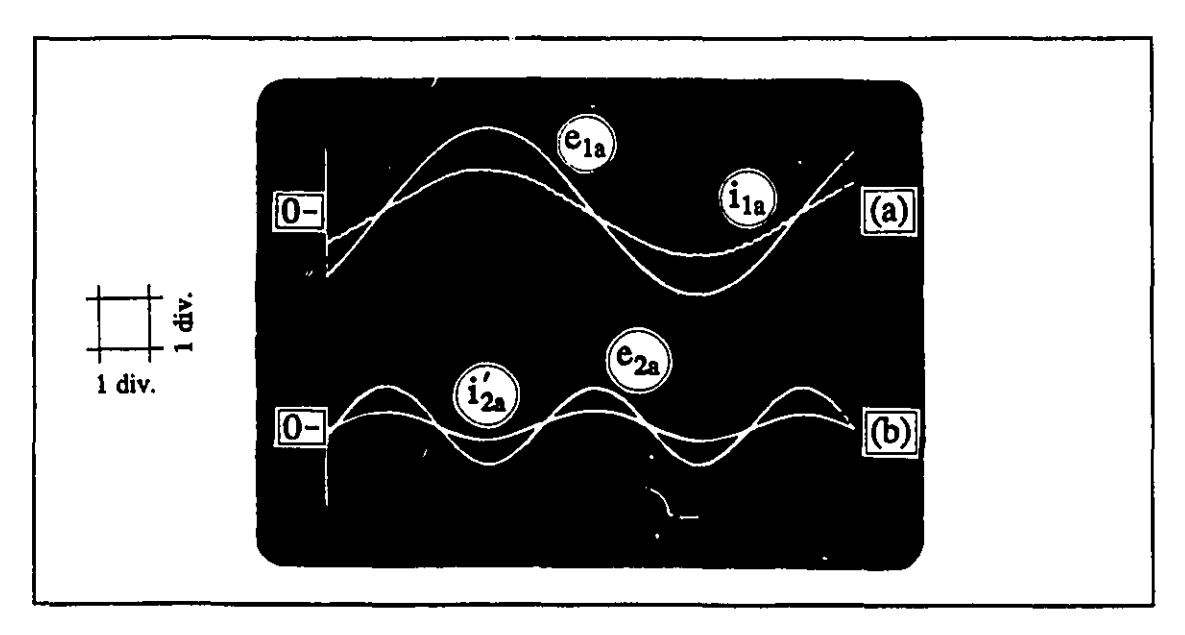


Fig. 7-23 Dual condition of UDPF on side-1 ($f_1 = 60 \text{ Hz}$), and FVC on side-2 ($f_2 = 120 \text{ Hz}$) for $E_{1r} = 10 \text{ V}$, $V_{dc} = 50 \text{ V}$, $M_f = 0.31$, $M_{\phi} = 0.33$, and $C = 50 \mu\text{F}$: (a) $e_{1a} = 9 \text{ V/div}$, $i_{1a} = 10.5 \text{ A/div}$, t = 2 ms/div (b) $e_{2a} = 34 \text{ V}$, $i'_{2a} = 3.4 \text{ A/div}$.

unwanted components.

7-7 Summary

In this chapter, first the results obtained from the implementation of the voltage-source-converter type matrix converter of Fig. 6-1 have been presented. The capability of the system in: frequency changing, side-2 dc bias voltage control, side-1 DPF control, and dual condition of UDPF on side-1 and FVC on side-2 have been tested and verified. Also, the issue of the presence of the unwanted components in side-1 branch currents and side-2 ac voltages have been addressed by presenting illustrative experimental results.

In the second part of the chapter, the improvements made possible through the implementation of the method proposed in section 6.7 of chapter 6 have been appreciated by presenting the improved waveforms of the side-1 branch currents and side-2 ac voltages.

It can be deduced that the voltage-source-converter type matrix converter equipped with the trapping transformers (Fig. 6-7), as it stands, is very suitable for the ac drive applications where $f_2 > f_1$. In these cases, UDPF on side-1 can be achieved with no fear about the distortions caused by large M_{φ} values. For low f_2 values, where a dc or a very low-frequency component might be present in the side-1 branch currents, the distortion of the side-2 ac voltage waveforms can be avoided by using the conjugate property offered by the $[H_f]$ part of the [H]-matrix, resulting in

reactance compensation and asking for less effort for DPF correction by M_{φ} . Of course, if DPF correction or achieving UDPF on side-1 is not an issue, the operation and the results will be quite satisfactory, since in this case M_{φ} will be minimal, i.e., just big enough for the dc bias voltage control loop to be able to do its job.

CHAPTER EIGHT

CONCLUSIONS

This thesis has contributed to the advancement of the theory and engineering design of matrix converters in the following ways:

- (1) Development of the Dyadic Matrix Converter Theory;
- (2) Introduction of a new Matrix Converter topology based on the voltagesource PWM converters;
- (3) Implementation of the voltage-source-converter type matrix converter under the dyadic matrix converter theory control.

In this chapter, the conclusions will be reported in the same order as above.

8.1 Development of Dyadic Matrix Converter Theory (Chapters 2-5, Appendices A, B, and C)

The Dyadic Matrix Converter Theory has been developed and has been shown to be an important tool in engineering design. Prior to this work, the complexity arising from the time-varying trigonometric functions in the transformation matrix, [H], has been a stumbling block for the past 20 years, impeding theoretical advance. The time-invariant transformation matrix, [P], derived from the theory, is a breakthrough. The significance of this break-through can be seen in the illustration example of the variable-speed ac motor drive, chosen in the thesis. Using the analytical insights offered by the [P]-matrix, it is possible now to operate it so that: (1) the utility supply side operates at Unity Displacement Power Factor (UDPF) and (2) the motor operates as under Field Vector Control (FVC).

Apart from its importance as a design tool, the Dyadic Matrix Converter Theory provides the framework for understanding the operation of matrix converters as a linear mapping from the d-q-0 reference frame at one frequency to the d-q-0 reference frame at another frequency. The thesis has outlined the structures for achieving:

- (1) Scaling,
- (2) Phase Rotation, and
- (3) Complex Conjugation

in the controls.

In addition, the Dyadic Matrix Converter Theory has shown that the zerosequence components can be gainfully employed. In the variable ac drive in the illustrative example, this consists of using the zero-sequence dc voltages to project reactive voltages for Displacement Power Factor (DPF) correction.

8.2 Introduction of a New Matrix Converter Topology Based on the Three-Phase Voltage-Source PWM Converters (Chapter 6)

Three identical modules of three-phase voltage-source converters have been shown to be capable of operating as a matrix converter. The advantages of this new topology over the conventional topology based on nine bidirectional switches are:

- (1) Reduced Conduction Losses: The conduction losses are half of those in the topology using bidirectional switches; and
- (2) Established Switching Technology: The voltage-source PWM converters represent established technologies of industrial practice in contrast to bidirectional switches which still belong in research laboratories.

Along with the advantages mentioned above, there is a drawback associated with the voltage-source-converter type matrix converter topology: A dc bias voltage with a magnitude of at least equal to the peak value of the side-2 ac voltage must be kept as part of the side-2 voltages. This requires the voltage ratings of the switches to be raised. On the other hand, the dc bias voltage can be put to use to generate the Static VAR Controller (SVC) voltages for Displacement Power Factor correction.

8.3 Implementation of Voltage-Source-Converter Type Matrix
Converter under the Dyadic Matrix Converter Theory Control

(Chapter 7, Appendices D, E, F, G, and H)

The Voltage-source-converter type matrix converter, has been implemented using three identical voltage-source-converter units, each rated at 1 kVA. The control circuit is a combination of analog and digital integrated circuit elements. The simulation and laboratory results, reported in chapter 7, have given experimental proof to:

- (1) the correctness of the Dyadic Matrix Converter Theory, and
- (2) the capability of the voltage-source converters to function as a matrix converter.

Experimental results also show that it is feasible to operate a variable ac motor drive with:

- (1) Unity Displacement Power Factor on the ac supply side, and
- (2) Field Vector Control on the motor side.

8.4 Suggestions for Future Work

The dyadic matrix converter theory developed in chapters 2-5, is a complete and effective analytical means for the design of matrix converters. It not only covers all the transformation matrix structures already discovered by the researchers, but also leaves more cases open for exploration.

The voltage-source-converter type matrix converter still has room for some improvements in the following areas:

- (1) The elimination of the dc and very low-frequency components in the side-1 branch currents;
- (2) Implementation of the closed-loop control systems; and
- (3) DSP-based implementation of the control unit.

Even though the natural application of the voltage-source-converter type matrix converter is in the area of ac motor drives, it has the potential capability of being used as a phase shifter thanks to the flexibility provided by the γ -control. It can also be used as a Variable-Speed Constant-Frequency (VSCF) power generating unit.

PROPERTIES OF [P]_{2x2}-MATRIX WITH

$$p_{11} = p_{22} = 0, p_{12} \neq 0 \text{ AND } p_{21} \neq 0$$

This appendix studies the properties of the $[P]_{2\times 2}$ -matrix having the following structures:

(a)
$$p_{11} = p_{22} = 0$$
 and $p_{12} = p_{21} = P_f$

$$\begin{bmatrix} P \end{bmatrix}_{2 \times 2} = P_f \begin{bmatrix} 0 & 1 \\ 1 & 0 \end{bmatrix} \tag{A-1}$$

(b)
$$p_{11} = p_{22} = 0$$
 and $p_{21} = -p_{12} = P_f$

$$[P]_{2\times 2} = P_f \begin{bmatrix} 0 & -1 \\ 1 & 0 \end{bmatrix}$$
 (A-2)

(c) $p_{11} = p_{22} = 0$ and $p_{12} \neq \pm p_{21}$

$$[P]_{2\times 2} = \begin{bmatrix} 0 & p_{12} \\ p_{21} & 0 \end{bmatrix}$$
 (A-3)

The structure given in (A-1), results in sine functions at $(\omega_1 + \omega_2)$ in the [H]matrix. The expressions for \underline{e}'_{1dq} , $[R_1']$, $[L_1']$, and $[G_1']$, from (3-17) - (3-20) of chapter

3 become:

$$\underline{e}'_{1dq} = \frac{1}{P_f} \begin{bmatrix} e_{1q} \\ e_{1d} \end{bmatrix} \tag{A-4}$$

$$\left[R_1'\right] = \frac{1}{P_f^2} \left[R_1\right] \tag{A-5}$$

$$\left[L_1'\right] = \frac{1}{P_f^2} \left[L_1\right] \tag{A-6}$$

$$\left[G_1'\right] = -\frac{1}{P_f^2} \left[G_1\right] \tag{A-7}$$

As seen, upon referring to side-2, the d-axis and q-axis components of \underline{e}_{1dq} have been divided by P_f and misplaced, i.e., \underline{e}_{1dq} has been divided by P_f and rotated through $\left(\pi/2 - \tan^{-1}\left(e_{1q}/e_{1d}\right)\right)$. The resistances and the inductances have been divided by P_f and the reactances have been divided by P_f^2 and gone through complex conjugation.

The structure of (A-2), leads to sine functions at $(\omega_1 - \omega_2)$ in the [H]-matrix. The referred quantities can be found from (3-17) - (3-20) of chapter 3 as:

$$\underline{e}'_{1dq} = \frac{1}{P_f} \begin{bmatrix} e_{1q} \\ -e_{1d} \end{bmatrix} \tag{A-8}$$

$$\left[R_1'\right] = \frac{1}{P_f^2} \left[R_1\right] \tag{A-9}$$

$$\left[L_1'\right] = \frac{1}{P_f^2} \left[L_1\right] \tag{A-10}$$

$$\left[G_1'\right] = \frac{1}{P_f^2} \left[G_1\right] \tag{A-11}$$

As seen, sic -1 source voltage is divided by P_f and rotated by $-\pi/2$, when referred to side-2. The resistances, inductances, and reactances are only divided by P_f^2 .

The more general structure of (A-3) results in sine functions at both $\omega_1 + \omega_2$ and $\omega_1 - \omega_2$ in the [H]-matrix. From (3-17) - (3-20), the referred quantities are:

$$\underline{e}'_{1dq} = \begin{bmatrix} \underline{e}_{1q} \\ \overline{p}_{21} \\ \underline{e}_{1d} \\ \overline{p}_{12} \end{bmatrix}$$
 (A-12)

$$\begin{bmatrix} R_1' \\ P_{21}' \end{bmatrix} = \begin{bmatrix} \frac{R_1}{p_{21}^2} & 0 \\ 0 & \frac{R_1}{p_{12}^2} \end{bmatrix}$$
(A-13)

$$[L_1'] = \begin{bmatrix} \frac{L_1}{p_{21}^2} & 0\\ 0 & \frac{L_1}{p_{12}^2} \end{bmatrix}$$
 (A-14)

$$\left[G_{1}^{\prime}\right] = -\frac{1}{p_{12} p_{21}} \left[G_{1}\right]$$
 (A-15)

[H]-MATRIX OF M. VENTURINI AND A. ALESINA'S MATRIX CONVERTER [46, 47]

The [H]-matrix proposed by M. Venturini and A. Alesina is:

$$[H] = \frac{1}{3} a_1 \begin{bmatrix} 1 + 2qCD(0) & 1 + 2qCD(-4\pi/3) & 1 + 2qCD(-2\pi/3) \\ 1 + 2qCD(-2\pi/3) & 1 + 2qCD(0) & 1 + 2qCD(-4\pi/3) \\ 1 + 2qCD(-4\pi/3) & 1 + 2qCD(-2\pi/3) & 1 + 2qCD(0) \end{bmatrix} \\ + \frac{1}{3} a_2 \begin{bmatrix} 1 + 2qCS(0) & 1 + 2qCS(-2\pi/3) & 1 + 2qCS(-4\pi/3) \\ 1 + 2qCS(-2\pi/3) & 1 + 2qCS(-4\pi/3) & 1 + 2qCS(0) \\ 1 + 2qCS(-4\pi/3) & 1 + 2qCS(0) & 1 + 2qCS(-2\pi/3) \end{bmatrix}$$

$$(B-1)$$

where

$$CD(x) = \cos[(\omega_1 - \omega_2)t + x]$$
 (B-2)

$$CS(x) = \cos[(\omega_1 + \omega_2)t + x]$$
 (B-5)

$$a_1 = \frac{1}{2} \left[1 + \tan \phi_1 \cdot \cot \alpha \phi_2 \right] \tag{B-4}$$

$$a_2 = 1 - a_1 = \frac{1}{2} [1 - \tan \phi_1 \cdot \cot \alpha \phi_2]$$
 (B-5)

and

$$q = \frac{V_2}{V_1} \tag{B-6}$$

 ϕ_1 and ϕ_2 being the displacement angle of the current with respect to the voltage on side-1 and side-2, respectively, and V_1 and V_2 being the rms values of the voltages on side-1 and side-2, respectively.

The constant scalars in the elements of the [H]-matrix do not play any role in the transformations, as explained in subsection 2.4.1.5 of chapter 2. The $[P]_{2x2}$ - matrix corresponding to the [H]-matrix of (B-1) is of the form given in (3-26), i.e., a general diagonal structure:

$$[P]_{2\times 2} = \begin{bmatrix} p_{11} & 0 \\ 0 & p_{22} \end{bmatrix}$$
 (B-7)

with

$$p_{11} = (a_1 + a_2)q (B-8)$$

and

$$p_{22} = (a_1 - a_2)q (B-9)$$

From (B-4) and (B-5),

$$a_1 + a_2 = 1$$
 (B-10)

and

$$a_1 - a_2 = 2 a_1 - 1 = 2 \tan \phi_1 \cdot \cot \alpha \phi_2$$
 (B-11)

Therefore, the elements of the [P]-matrix will be:

$$p_{11} = q \tag{B-12}$$

and

$$p_{22} = 2 q \tan \phi_1 \cdot \cot \alpha \phi_2 \tag{B-13}$$

As seen, there are two control degrees of freedom and therefore only for passive networks on side-2, displacement power factor control and UDPF condition on side-1 together with real power control can be achieved.

[H]-MATRIX OF L. HUBER AND D. BOROJEVIC'S MATRIX CONVERTER [70]

The [H]-matrix used by L. Huber and D. Borojevic is:

$$[H] = m \begin{bmatrix} \cos\left(\omega_{2}t - \varphi_{2} + \frac{\pi}{6}\right) \\ \cos\left(\omega_{2}t - \varphi_{2} + \frac{\pi}{6} - \frac{2\pi}{3}\right) \\ \cos\left(\omega_{1}t - \frac{2\pi}{3}\right) \end{bmatrix} \begin{bmatrix} \cos\left(\omega_{1}t - \varphi_{1}\right) \\ \cos\left(\omega_{1}t - \frac{2\pi}{3}\right) \\ \cos\left(\omega_{1}t - \varphi_{1} - \frac{4\pi}{3}\right) \end{bmatrix}^{T}$$
(C-1)

where ϕ_1 and ϕ_2 are the phase angles of the side-1 phase current and the side-2 phase voltage, respectively, and m is a constant scalar.

The $[P]_{2\times 2}$ -matrix corresponding to the [H]-matrix of (C-1) is of the form given in (3-62), i.e., a general full structure:

$$[P]_{2\times2} = P_{f1} \begin{bmatrix} \cos\gamma_1 & \sin\gamma_1 \\ -\sin\gamma_1 & \cos\gamma_1 \end{bmatrix} + P_{f2} \begin{bmatrix} \cos\gamma_2 & \sin\gamma_2 \\ \sin\gamma_2 & -\cos\gamma_2 \end{bmatrix}$$
 (C-2)

with

$$P_{f1} = P_{f2} = \frac{3}{4} m \tag{C-3}$$

$$\gamma_1 = \varphi_2 - \varphi_1 \tag{C-4}$$

and

$$\gamma_2 = -(\varphi_1 + \varphi_2) \tag{C-5}$$

As seen, there are three control degrees of freedom and therefore even for active networks on side-2, displacement power factor control and UDPF condition on side-1 together with real power control can be achieved.

CLOSED-LOOP CONTROL OF THE DC BIAS VOLTAGE ON SIDE-2

According to (6-41), the dc bias voltages on side-2 do not interfere with the frequency changing. Therefore, only the SVC part of the transformation matrix, [H], of (6-29), i.e., $[H_{\varphi}]$ given by (6-31), will be used here in the analysis and the design of the dc bias voltage control loop.

When $[H] = [H_{\varphi}]$, the side-2 voltages will consist of dc components only, i.e., in Fig. 6-1, $v_{2a} = v_{2b} = v_{2c} = V_{dc}$. In this case, no current will flow through the loads, i.e., $i'_{2a} = i'_{2b} = i'_{2c} = 0$. The equivalent circuit diagram of Fig. 6-4, can then be simplified to that of Fig. D-1.

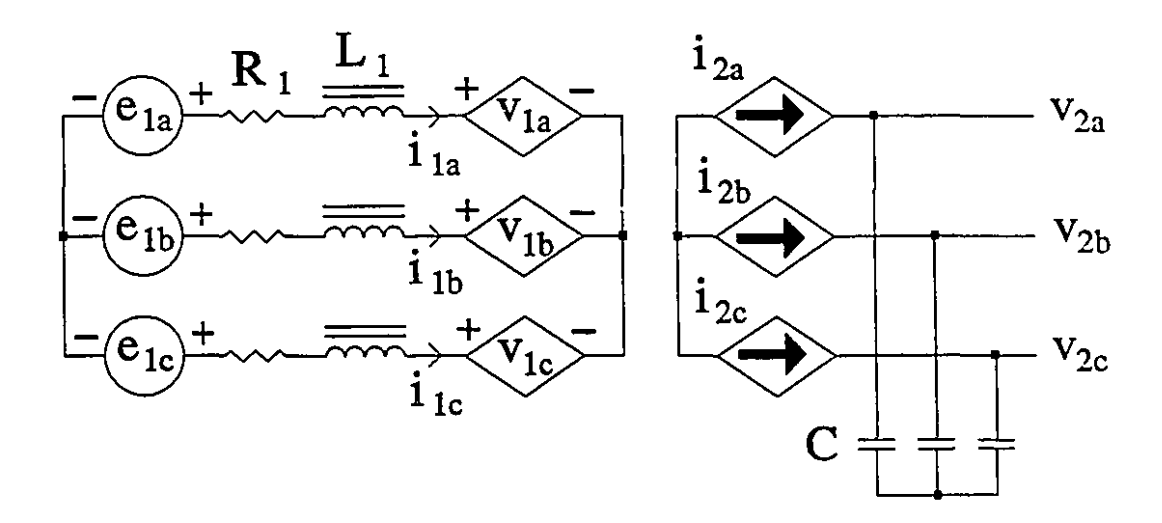


Fig. D-1 Equivalent circuit diagram of Fig. 6-4 simplified for the case of pure dc voltages on side-2.

The differential equations describing the system of Fig. D-1 are:

$$\frac{di_{1a}}{dt} = \frac{1}{L_1} \left(e_{1a} - R_1 i_{1a} - v_{1a} \right)
\frac{di_{1b}}{dt} = \frac{1}{L_1} \left(e_{1b} - R_1 i_{1b} - v_{1b} \right)
\frac{di_{1c}}{dt} = \frac{1}{L_1} \left(e_{1c} - R_1 i_{1c} - v_{1c} \right)$$
(D-1)

$$\frac{dv_{2a}}{dt} = \frac{1}{C} i_{2a}$$

$$\frac{dv_{2b}}{dt} = \frac{1}{C} i_{2b}$$

$$\frac{dv_{2c}}{dt} = \frac{1}{C} i_{2c}$$
(D-2)

and the voltage and current transformation equations are:

$$\begin{bmatrix} v_{1a} \\ v_{1b} \\ v_{1c} \end{bmatrix} = \frac{1}{6} \begin{bmatrix} m_{aa} & m_{ab} & m_{ac} \\ m_{ba} & m_{bb} & m_{bc} \\ m_{ca} & m_{cb} & m_{cc} \end{bmatrix} \begin{bmatrix} v_{2a} \\ v_{2b} \\ v_{2c} \end{bmatrix}$$
 (D-3)

$$\begin{bmatrix} i_{2a} \\ i_{2b} \\ i_{2c} \end{bmatrix} = \frac{1}{6} \begin{bmatrix} m_{aa} & m_{ba} & m_{ca} \\ m_{ab} & m_{bb} & m_{cb} \\ m_{ac} & m_{bc} & m_{cc} \end{bmatrix} \begin{bmatrix} i_{1a} \\ i_{1b} \\ i_{1c} \end{bmatrix}$$
(D-4)

where the matrix of normalized modulating signals is:

$$\begin{bmatrix} m_{aa} & m_{ab} & m_{ar} \\ m_{ba} & m_{bb} & m_{bc} \\ m_{ca} & m_{cb} & m_{cc} \end{bmatrix} = \begin{bmatrix} \cos(\omega_1 t + \varphi) & \cos(\omega_1 t + \varphi) \\ \cos(\omega_1 t + \varphi - 2\pi/3) & \cos(\omega_1 t + \varphi - 2\pi/3) & \cos(\omega_1 t + \varphi - 2\pi/3) \\ \cos(\omega_1 t + \varphi - 4\pi/3) & \cos(\omega_1 t + \varphi - 4\pi/3) & \cos(\omega_1 t + \varphi - 4\pi/3) \end{bmatrix}$$
(D-5)

If the source voltages e_{1a} , e_{1b} , and e_{1c} , and the source currents i_{1a} , i_{1b} , and i_{1c} are of the forms:

$$e_{1a} = E_{1m} \cos \omega_1 t$$

$$e_{1b} = E_{1m} \cos (\omega_1 t - 2\pi/3)$$

$$e_{1c} = E_{1m} \cos (\omega_1 t - 4\pi/3)$$
(D-6)

$$i_{1a} = I_{1m} \cos(\omega_1 t + \eta_1)$$

$$i_{1b} = I_{1m} \cos(\omega_1 t + \eta_1 - 2\pi/3)$$

$$i_{1c} = I_{1m} \cos(\omega_1 t + \eta_1 - 4\pi/3)$$
(D-7)

after substituting (D-5) in (D-3) and (D-4) and substituting the resulting equation and (D-6) and (D-7) in (D-1) and (D-2) and expanding and equating the coefficients of $\sin \omega_1 t$ and $\cos \omega_1 t$ on both sides of the equations and simplifying, the following system of nonlinear equations results:

$$\frac{d\eta_{1}}{dt} = \frac{-M_{\phi}V_{dc}}{2L_{1}I_{1m}}\sin(\varphi - \eta_{1}) - \frac{E_{1m}}{L_{1}I_{1m}}\sin\eta_{1} - \omega_{1}$$

$$\frac{dI_{1m}}{dt} = \frac{-M_{\phi}V_{dc}}{2L_{1}}\cos(\varphi - \eta_{1}) + \frac{E_{1m}}{L_{1}}\cos\eta_{1} - \frac{R_{1}}{L_{1}}I_{1m}$$

$$\frac{dV_{dc}}{dt} = \frac{M_{\phi}I_{1m}}{4C}\cos(\varphi - \eta_{1})$$
(D-8)

The nonlinear system of (D-8) is of the general form:

$$\dot{\underline{x}} = f(\underline{x}, \underline{u}) \tag{D-9}$$

where \underline{x} and \underline{u} denote the vectors of state variables and the control inputs, respectively, and \underline{x} stands for the vector of the time derivatives of the state variables. The linearized system will be:

$$\Delta \dot{\underline{x}} = \frac{\partial f}{\partial x}|_{*} \Delta \underline{x} + \frac{\partial f}{\partial u}|_{*} \Delta \underline{u}$$
 (D-10)

where $\Delta \underline{x}$ and $\Delta \underline{u}$ are the vectors of the state variables and control inputs of the perturbed system, and $\partial f/\partial \underline{x}|_{\bullet}$ and $\partial f/\partial \underline{u}|_{\bullet}$ are the Jacobians of the system with respect to the state variables and the control inputs, respectively, evaluated at steady-state.

The steady-state equations are obtained from (D-8) by putting the left-handsides of all three equations equal to zero. For any feasible steady-state value of η_1^* and V_{dc}^* , the corresponding steady-state values: I_{1m}^* , ϕ^* , and M_{ϕ}^* can then be found.

The third equation in (D-8), with $dV_{dc}/dt = 0$, yields:

$$\cos(\varphi^* - \eta_1^*) = 0 \implies \varphi^* - \eta_1^* = -\frac{\pi}{2}$$
 (D-11)

This is nothing but the condition for the steady-state in the side-2 dc bias voltage discussed in chapter 4. Substituting (D-11) in the second equation of (D-8), with $dI_{1m}/dt = 0$,

$$I_{1m}^* = \frac{E_{1m}}{R_1} \cos \eta_1^* \tag{D-12}$$

 M_{φ}^{*} can be found from the first equation in (D-8), with $d\eta_1/dt = 0$:

$$M_{\phi}^{*} = \frac{2E_{1m}}{V_{dc}^{*}R_{1}} \left(R_{1}\sin\eta_{1}^{*} + \omega_{1}L_{1}\cos\eta_{1}^{*} \right)$$
 (D-13)

For $M_{\varphi}^* = 0$,

$$\eta_1^* = \tan^{-1}\left(-\frac{\omega_1 L_1}{R_1}\right) \tag{D-14}$$

This is the natural side-1 displacement angle without any correction. To give a lead to η_1^* , i.e., to make the value of the parenthesis in (D-13) a bigger positive number,

a bigger positive M_{φ}^* should be chosen. To give a lag to η_1^* , beyond the natural value at $M_{\varphi}^* = 0$, the value of the parentheses in (D-13) should become negative. Therefore, a negative M_{φ}^* should be chosen.

Using the steady-state values given by (D-11)-(D-13), the state-space representation of the linear incremental system corresponding to (D-8) can be found as:

$$\begin{bmatrix} \Delta \dot{\eta}_{1} \\ \Delta \dot{I}_{1m} \\ \Delta \dot{V}_{dc} \end{bmatrix} = \begin{bmatrix} -\frac{R_{1}}{L_{1}} & -\frac{\omega_{1}}{I_{1m}^{*}} & \frac{M_{\phi}^{*}}{2L_{1}I_{1m}^{*}} \\ \omega_{1}I_{1m}^{*} & -\frac{R_{1}}{L_{1}} & 0 \\ -\frac{M_{\phi}^{*}V_{dc}^{*}}{4C} & 0 & 0 \end{bmatrix} \begin{bmatrix} \Delta \eta_{1} \\ \Delta I_{1m} \\ \Delta V_{dc} \end{bmatrix}$$

$$+ \begin{bmatrix} 0 & \frac{V_{dc}^{*}}{2L_{1}I_{1m}^{*}} \\ -\frac{M_{\phi}^{*}V_{dc}^{*}}{2L_{1}} & 0 \\ \frac{M_{\phi}^{*}I_{1m}^{*}}{4C} & 0 \end{bmatrix} \begin{bmatrix} \Delta \phi \\ \Delta M_{\phi} \end{bmatrix}$$

$$(D-15)$$

where I_{1m}^{\bullet} and M_{ϕ}^{\bullet} are given in (D-12) and (D-13), respectively.

The block diagram of the closed-loop control system that regulates the side-2 dc bias voltage is shown in Fig. D-2. The arrangement of Fig. D-2 together with a

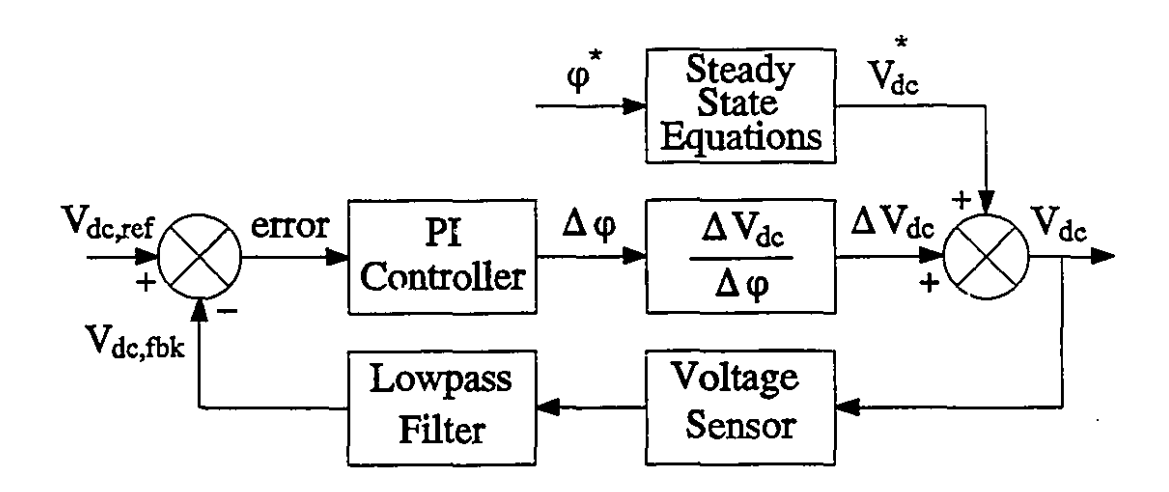


Fig. D-2 Closed-loop control system of side-2 dc bias voltage.

positive M_{φ} can be used to cause a leading effect η_1 . In case it is desired to add a lag to the side-1 displacement angle beyond the natural value given by (D-14) that occurs at M_{φ} = 0, a negative M_{φ} should be used. In this case, the error signal shown in the block diagram of Fig. D-2 must be inverted so that the control loop can regulate the dc bias voltage on side-2.

Since during the normal operation of the matrix converter, the side-2 voltages contain both ac and dc components, the dc component should be separated in order to obtain $V_{dc,fbk}$ for the control loop of Fig. D-2. The method used in digital simulation and laboratory implementation is illustrated in Fig. D-3. Since the ac components of v_{2a} , v_{2b} , and v_{2c} constitute a balanced 3-phase system, the average of the three side-2 voltages is simply V_{dc} . The low-pass filter is used to attenuate the

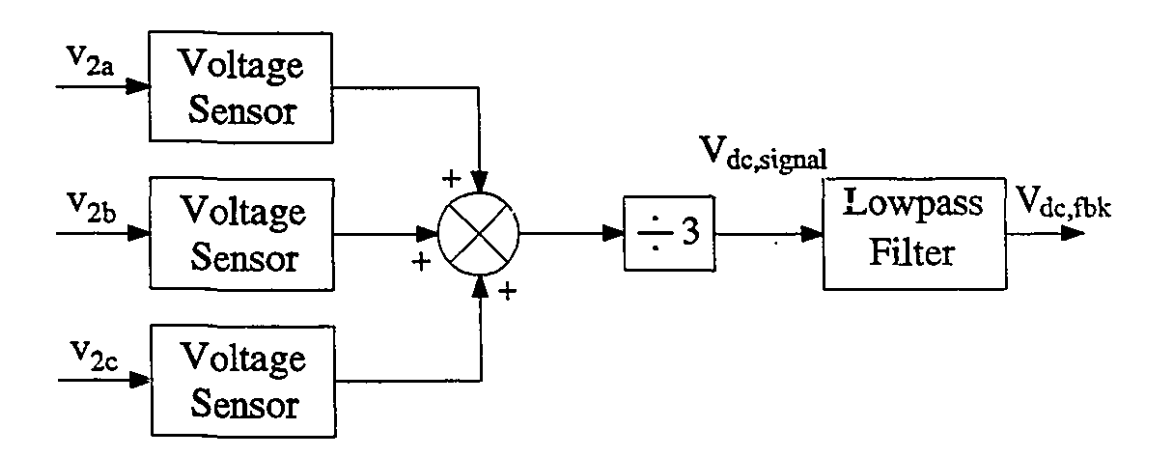


Fig. D-3 Derivation of the side-2 dc bias voltage signal by averaging the three side-2 voltages.

switching harmonics in the $V_{de,signal}$ and therefore is a very small filter having minimized effect on the performance of the control loop. Note that if V_{de} is to be found by filtering the side-2 voltage of one of the voltage-source converters, a big filter should be used and stability problems might arise. The first-order low-pass filter was designed with the dc-gain of 1 and the break-frequency of 1675 Hz. The PI-controller was designed with the proportional coefficient, K_p , of 0.05 and the integral coefficient, K_i , of 4. The detailed circuit diagrams of the dc voltage control loop are given in Appendix E.

IMPLEMENTATION OF: VOLTAGE-SOURCE-CONVERTER TYPE MATRIX CONVERTER

E.1 Introduction

The voltage-source-converter type matrix converter (Figs. 6-1), introduced in chapter 6, has been successfully implemented in the laboratory using three existing identical BJT voltage-source converter modules, each rated at 1kVA. In this Appendix, the power and the control circuits of the matrix converter will be described briefly.

Fig. E-1 shows an overall view of the complete experimental set-up. The control circuitry is shown in Fig. E-2. Figs. E-3 to E-14 show the detailed circuit

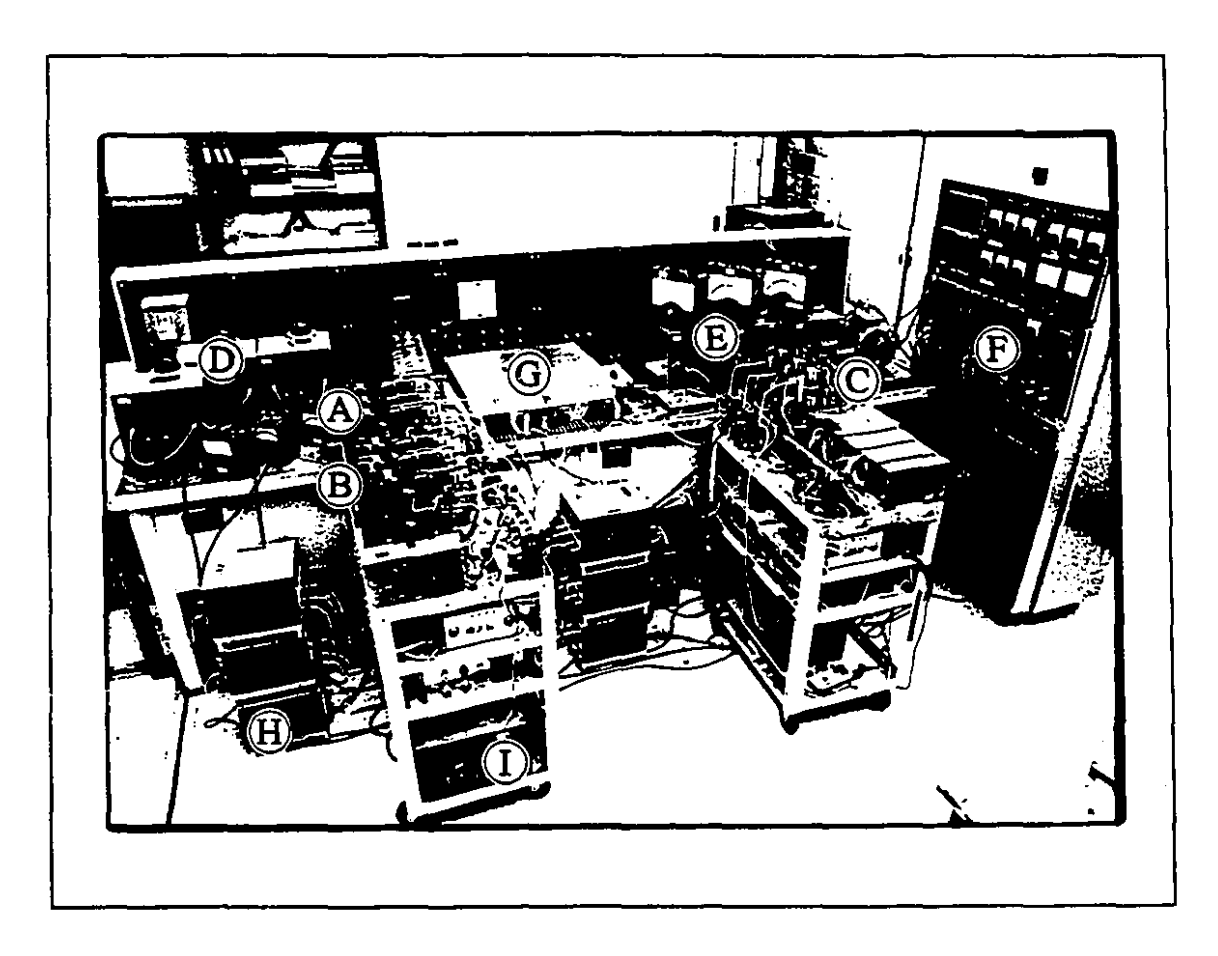


Fig. E-1 Overall view of the experimental set-up for the systems of Fig. 6-1 and 6-7:

- (A) Voltage-source converter (a), (B) Voltage-source converter (b),
- (C) Voltage-source converter (c), (D) Side-1 inductors, (E) Passive load, (F) Active load, (G) Control unit, (H) Trapping transformers, and (I) Side-2 capacitor.

diagrams of the system.

E.2 Power Circuit and Snubber Protection

The power circuit of a BJT voltage-source converter unit and the snubber

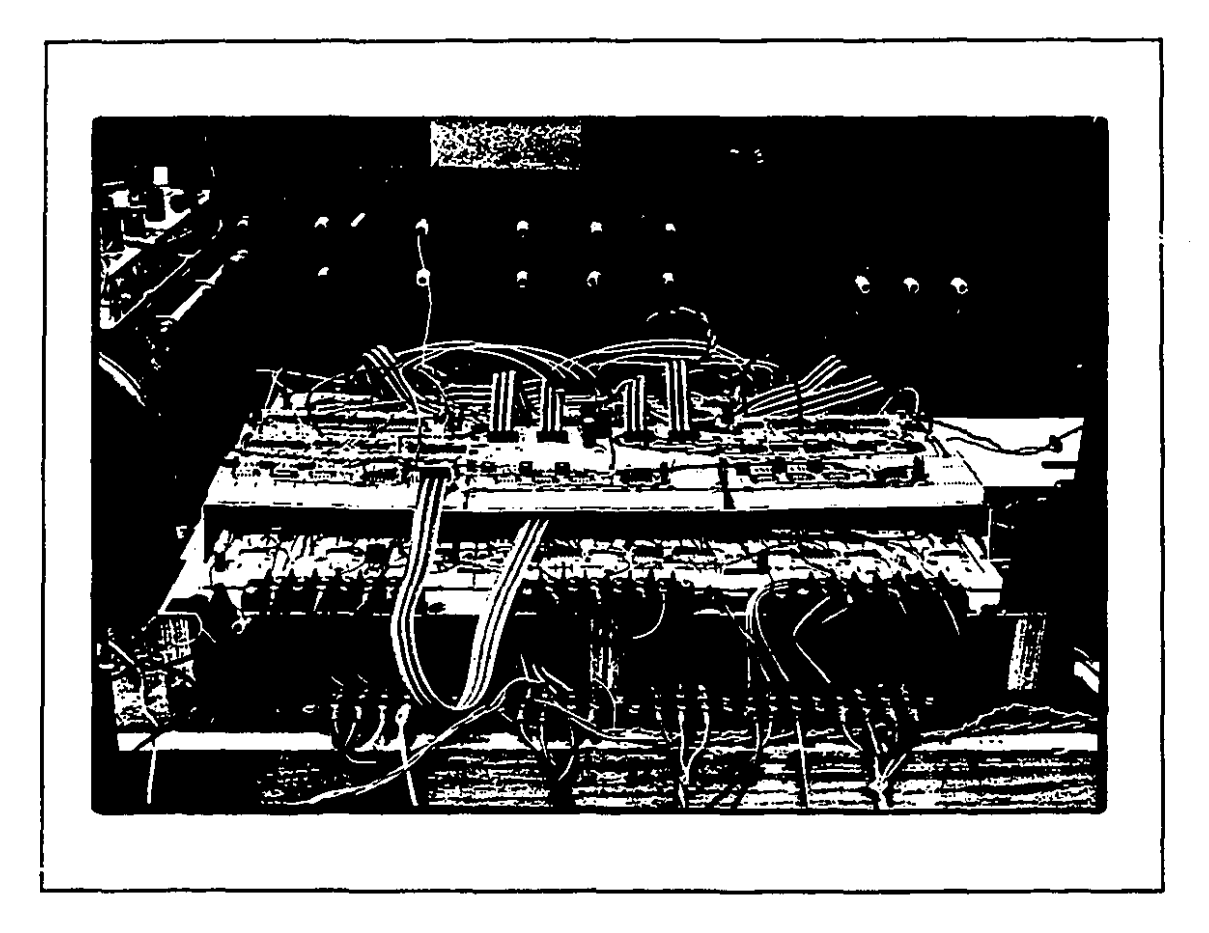
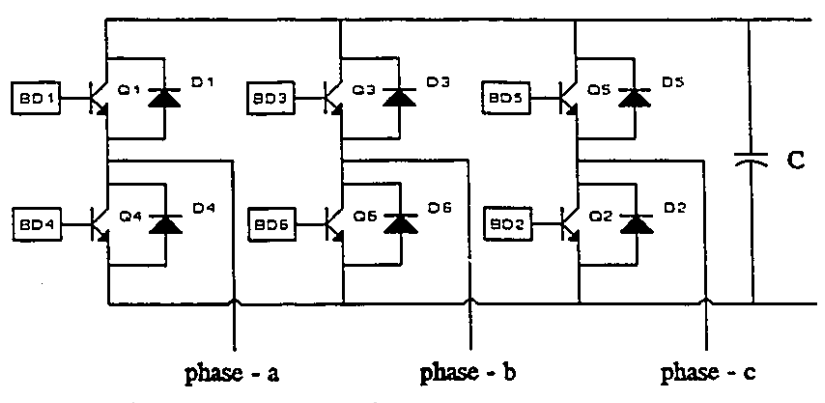


Fig. E-2 Control unit.

protection circuit for one leg are shown in Fig. E-3. For more details, please refer to Ref. [82].

E.3 Base Driver for the BJT Switches

Fig. E-4 shows the base driver unit used to drive the BJT switches of the voltage-source converter modules. A detailed description of the base driver unit can be found in Ref. [82].



Three - phase voltage - source converter

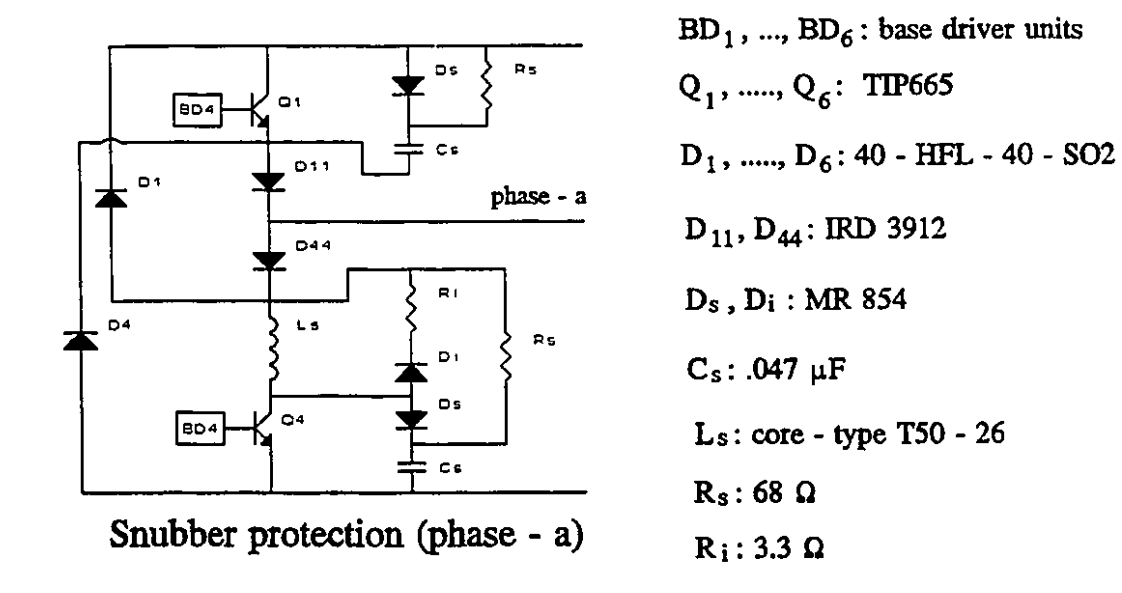


Fig. E-3 Power circuit and snubber protection scheme.

E.4 Gating Signal Generation and Interlock Circuit

There are totally nine modulating signals corresponding to the nine legs of the three voltage-source converters of the matrix converter of Fig. 6-1. These modulating signals are generated in the control circuit described in section E.6.

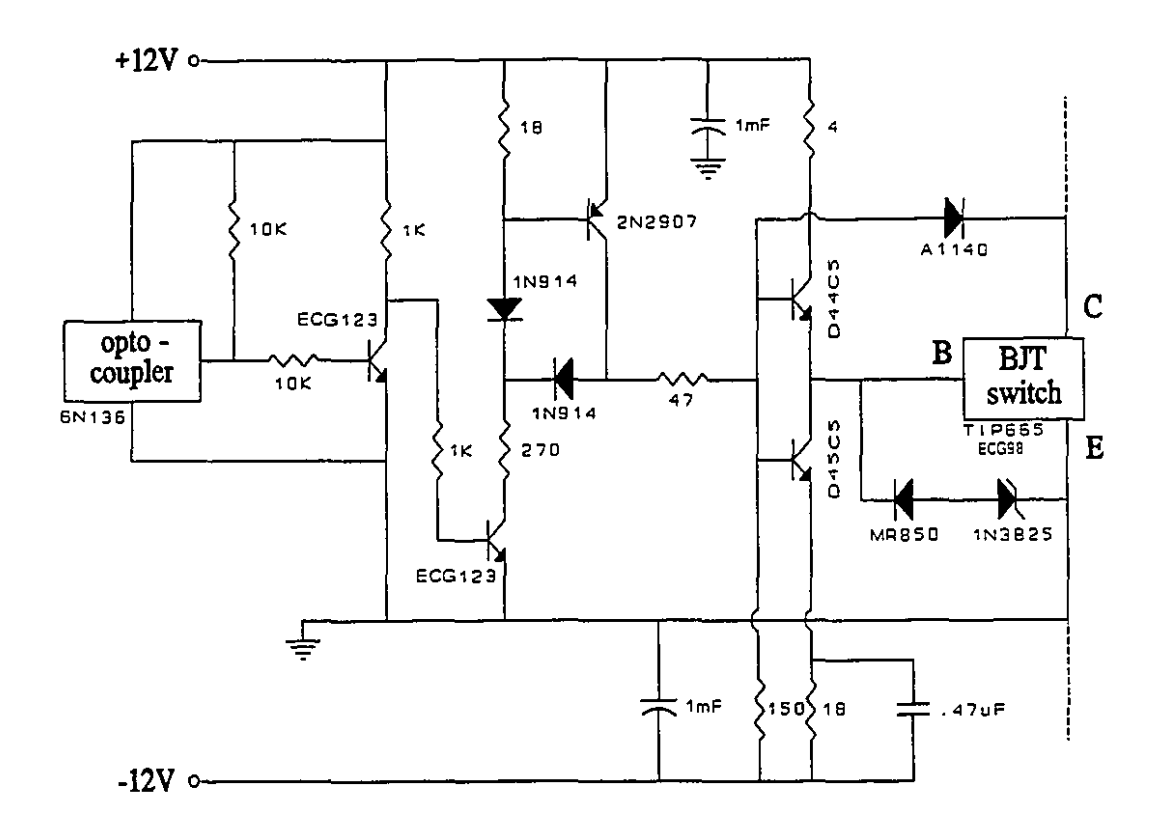
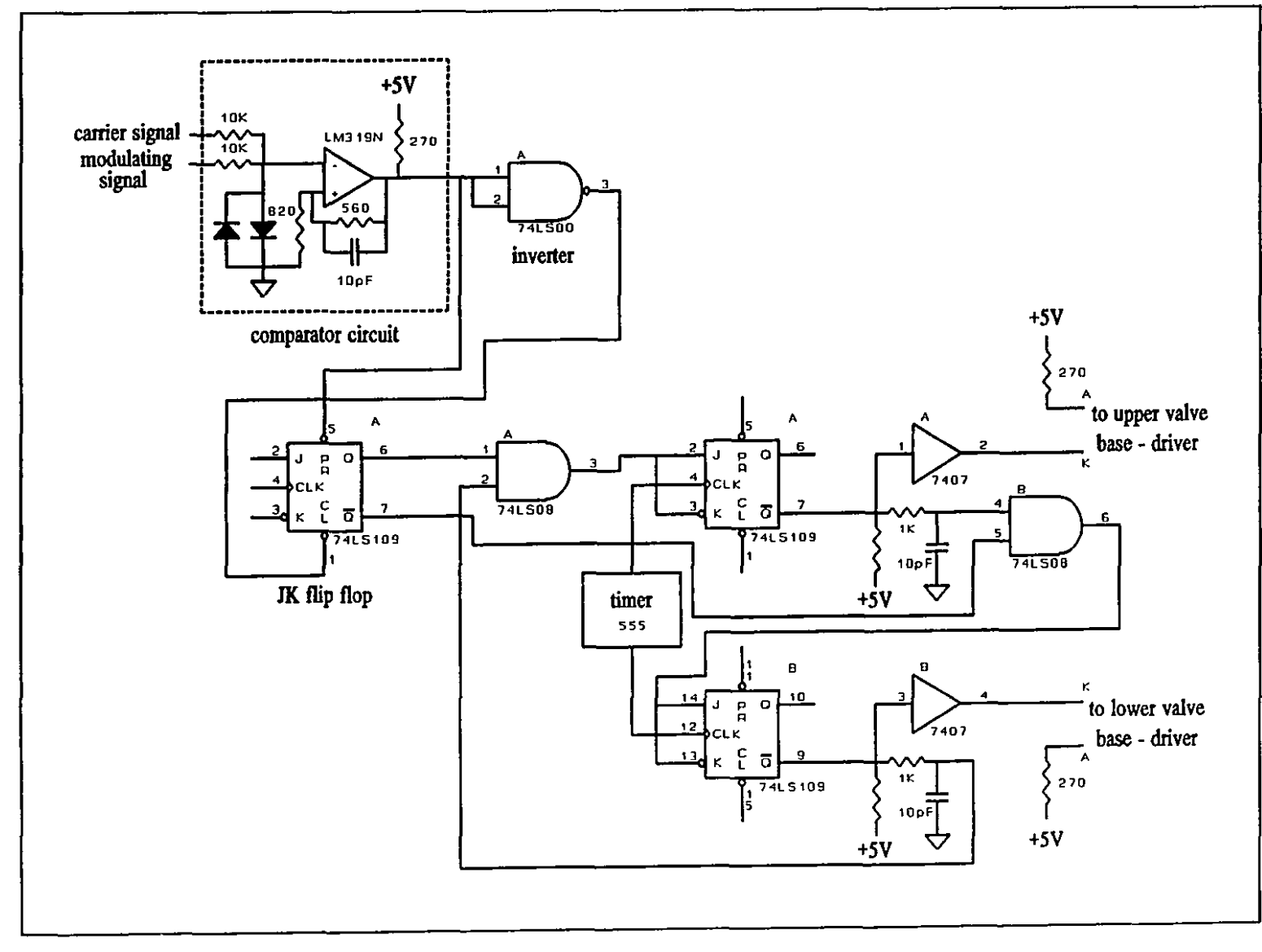


Fig. E-4 Base driver unit for the BJT switches used in the power circuit.

Fig. E-5 shows the gating signal generator and the interlock circuit for the two switches of one converter leg. First, the modulating signal is compared with the triangular carrier signal. The logic signal thus produced and its complementary signal can theoretically be used as the gating signals of the two switches in one converter leg. But, because of the switching transients, the ON-states of the two switches in one leg might overlap. This is a hazardous situation since the dc terminals of the voltage-source converter are short-circuited in this way and the switches might be destroyed by the resulting high current. The interlock circuit (Fig. E-5) causes a delay between

188



Gating signal generator and interlock circuit.

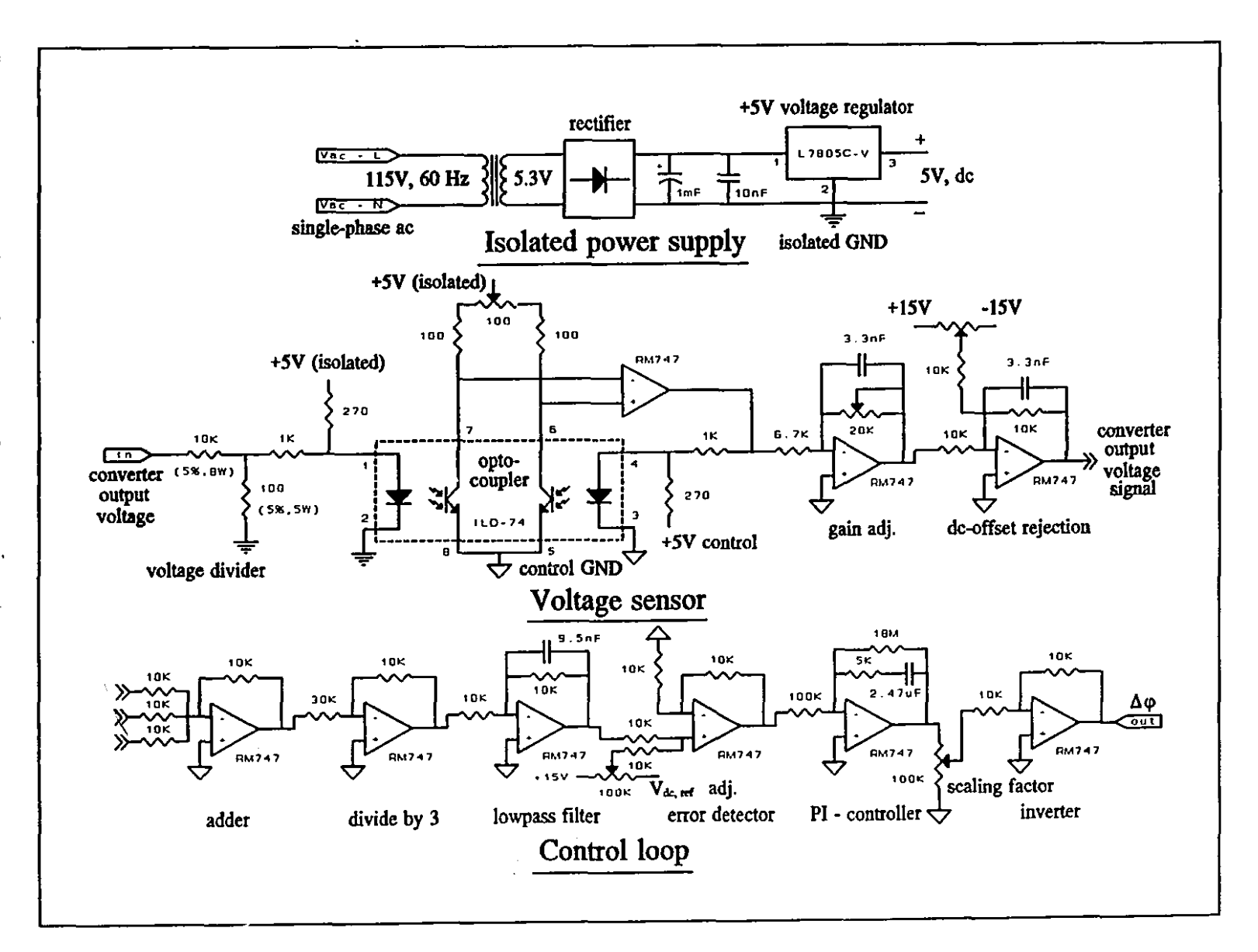
the OFF-command to one of the two switches in a converter leg and the ON-command to the other switch in the same leg, thus assuring that the two switches are never ON at the same time. The delay is adjustable by the period of the clock pulse generated by the timer (555). More details may be found in Ref. [82].

E.5 Side-2 DC Bias Voltage Control System

Fig. E-6 shows the detailed circuit diagram of the dc bias voltage control system described in Appendix D. In Fig. E-6, three parts can be distinguished: (1) the isolated +5V power supply, (2) the voltage sensor, and (3) the control loop circuitry.

Employing hall-effect voltage sensors is associated with a considerable amount of delay. Therefore, this kind of voltage sensors are not appropriate for sensing the side-2 voltages of the voltage-source converter modules of the matrix converter which are composed of dc and ac components. Instead, a different voltage sensor with optical isolation [83] has been used, as shown in Fig. E-6. The +5V isolated power supply is dedicated to the voltage sensor circuit.

To derive the side-2 dc bias voltage, the outputs of the three voltage sensors measuring the side-2 voltages of the three voltage-source converters are averaged. The ac components, comprising a three-phase symmetrical system are cancelled out in this way and the dc bias voltage signal remains. A low-pass filter removes the switching ripples and the result is the dc bias voltage feedback signal for the comparison with the reference. The averaging method used to derive the dc bias voltage has a significant advantage over the method of filtering one of the three side-



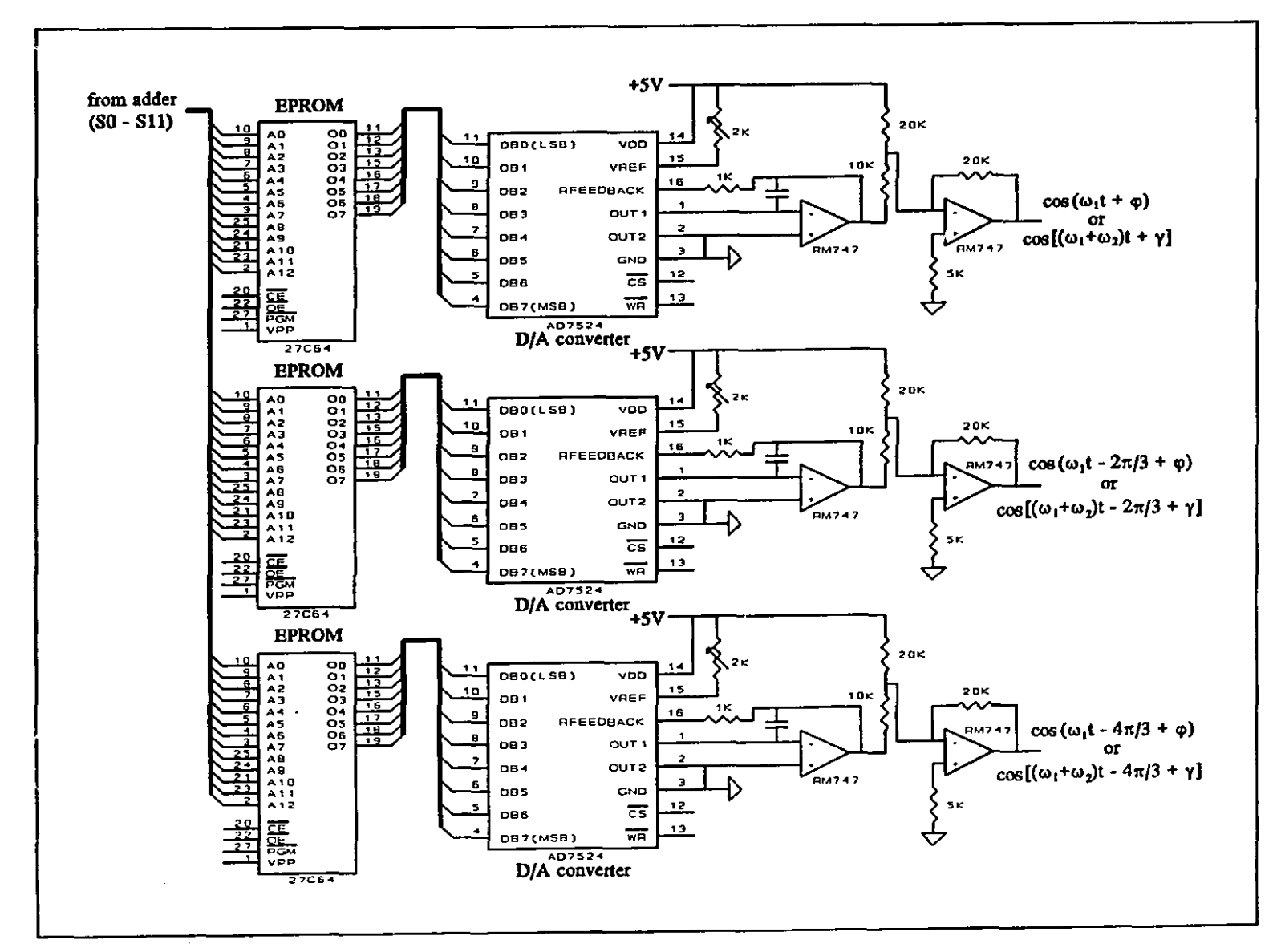
2 voltages. In fact, in the latter case, the filter should be big enough to be able to remove the ac component at ω_2 , while in the former case a very small filter will be adequate since only the switching ripples have to be filtered out. A small filter is less likely to create any stability problems.

The error resulting from the comparison of the dc bias voltage feedback and the reference signals, is fed to a PI-controller and the output of the controller is the incremental change in φ which controls the phase angle of the SVC terms in the [H]-matrix or the modulating signals of the matrix converter, to keep the dc bias voltage regulated at the desired level.

E.6 Modulating Signals Generation

Each of the nine modulating signals is composed of two (2) parts: (1) a cosine function at angular frequency ω_1 with the multiplier M_{ϕ} and the phase angle $\phi + x$, where x = 0, $-2\pi/3$, $-4\pi/3$, and (2) a cosine function at angular frequency $\omega_1 + \omega_2$ with the multiplier M_f and the phase angle $\gamma + x$, where x = 0, $-2\pi/3$, $-4\pi/3$. Full periods of the waveforms of the three-phase balanced cosine functions are stored in two sets of three EPROMs (Fig. E-7). The EPROMs have 12-bit address buses and 8-bit data resolution. One set of EPROMs is dedicated to the cosine functions at ω_1 and the other to the cosine functions at $\omega_1 + \omega_2$. The frequency of the cosine function that can be read out of an EPROM is determined by the speed at which the

APPENDIX E

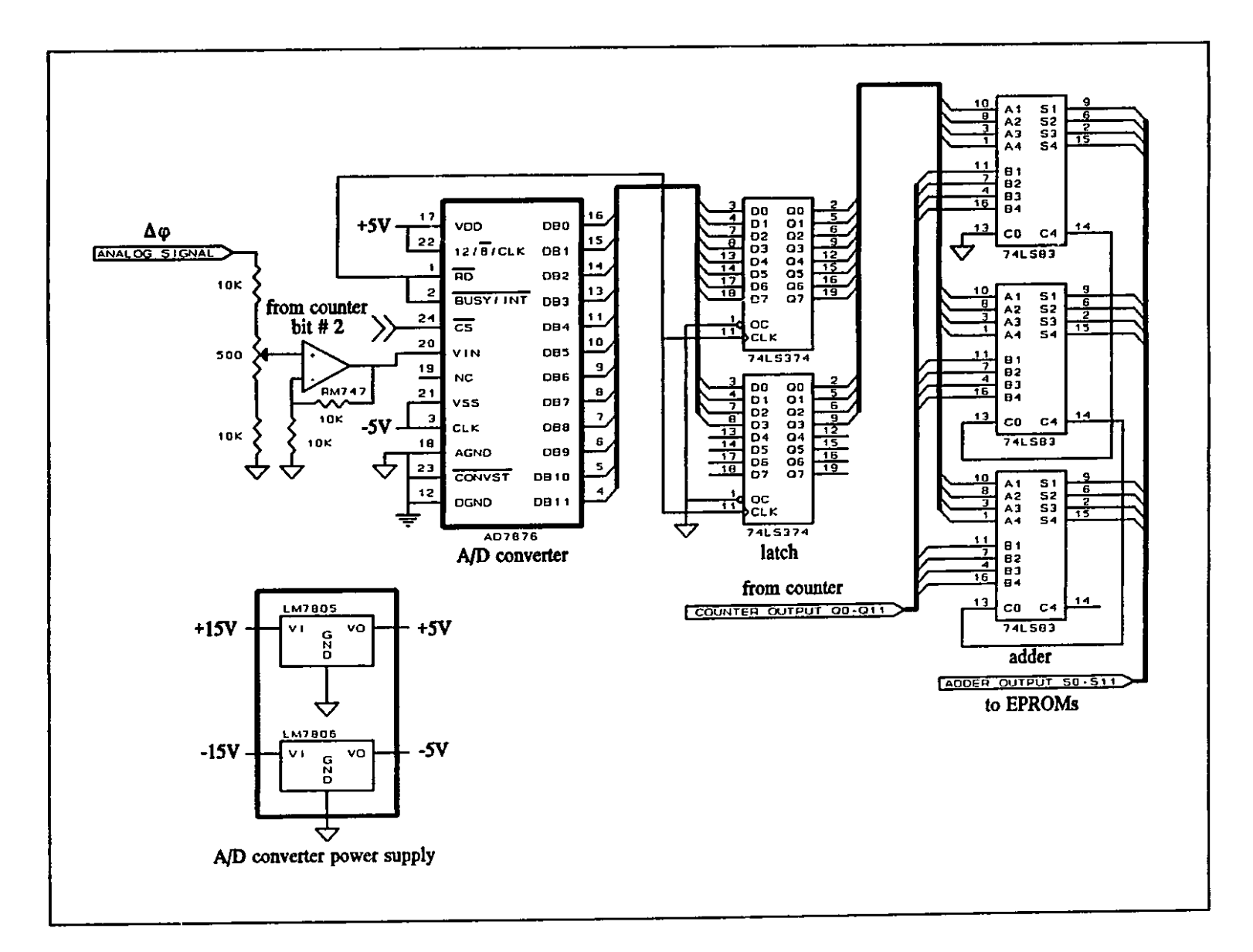


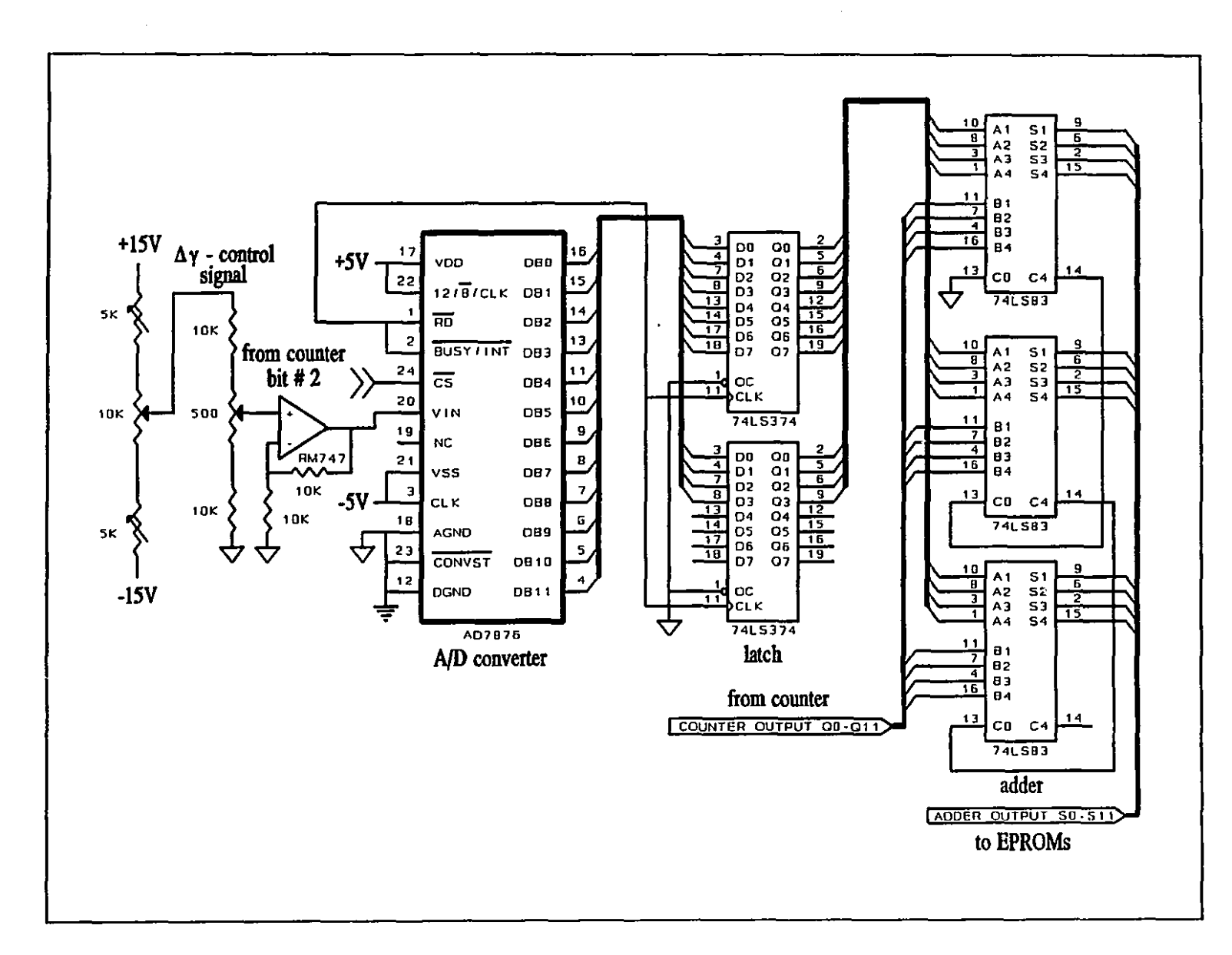
addresses are swept. Each EPROM is followed by a Digital-to-Analog (D/A) converter. The result is two sets of three-phase balanced cosine functions at ω_1 and $\omega_1 + \omega_2$, as shown in Fig. E-7. In order to introduce the phase angles φ and γ in the cosine functions at ω_1 and $\omega_1 + \omega_2$, respectively, binary adders have been used. As shown in Fig. E-8 and E-9, two binary numbers equivalent to the analog signals of $\Delta \varphi$ and $\Delta \gamma$ are produced using A/D converters. These binary numbers are then added to the outputs of the counters dedicated to ω_1 and $\omega_1 + \omega_2$, respectively. The counters and the synchronization circuits will be described later in section E.7.

In the laboratory implementation, $\Delta \varphi$ -signal is produced by the dc bias voltage control loop (Fig. E-6) and $\Delta \gamma$ -signal is manually adjusted. The output of the binary adders of Fig. E-8 and E-9 are input as addresses to the EPROMs for the cosine waveforms at ω_1 and $\omega_1 + \omega_2$, respectively (Fig. E-7).

Finally, the cosine functions at ω_1 and $\omega_1 + \omega_2$ are multiplied by the factors M_{ϕ} and M_f , respectively, as shown in Fig. E-10. M_{ϕ} is adjusted to control the phase angle of the side-1 source currents with respect to the side-1 source voltages, while M_f is used to control the magnitude of the ac component of the side-2 voltages. The complete modulating signals: $\nu_{\text{mod},aa}$, ..., $\nu_{\text{mod},cc}$ are derived by adding selected pairs of the cosine functions at ω_1 and $\omega_1 + \omega_2$.

APPENDIX E

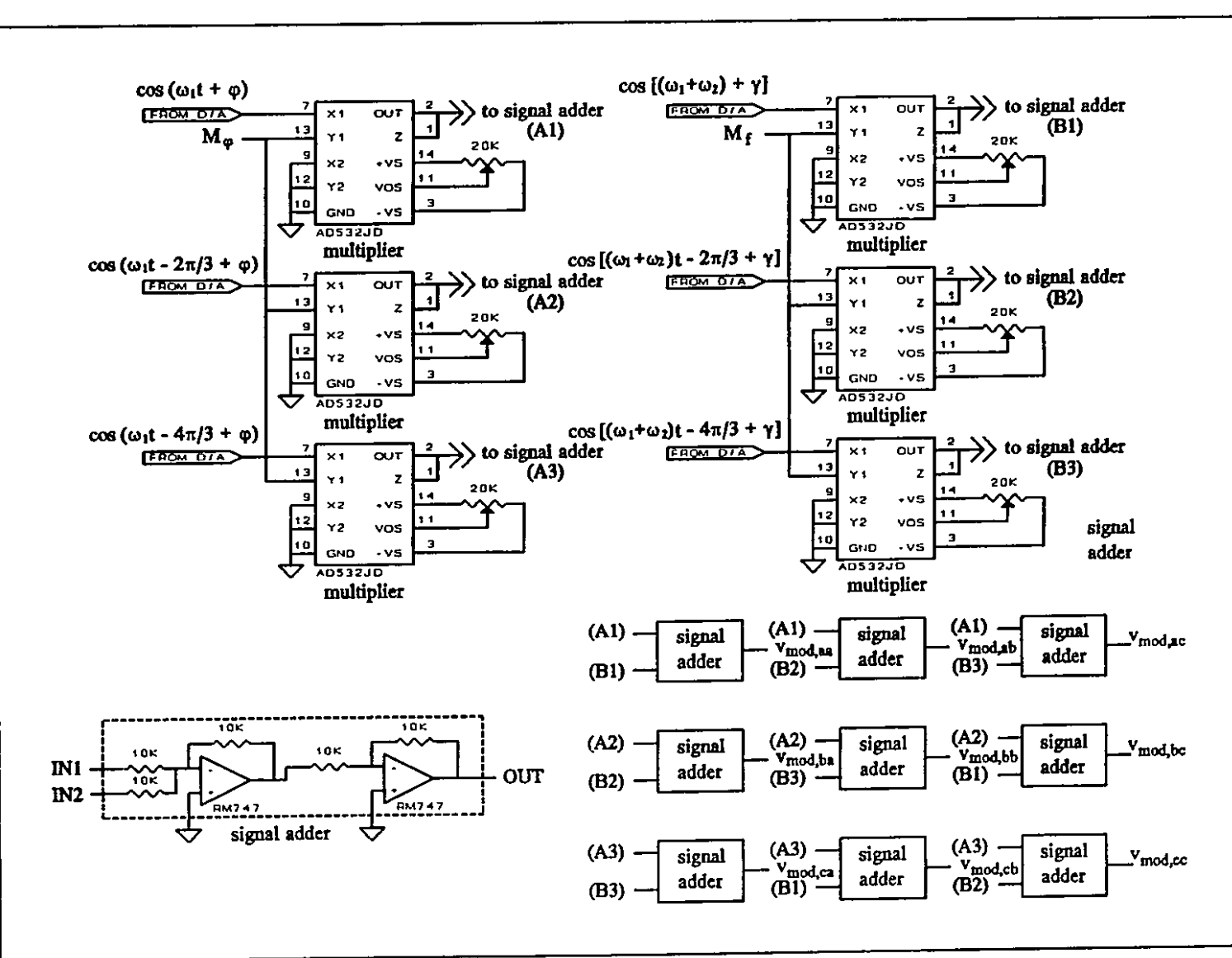




A/D converter, latch, and adder for γ -control.

196

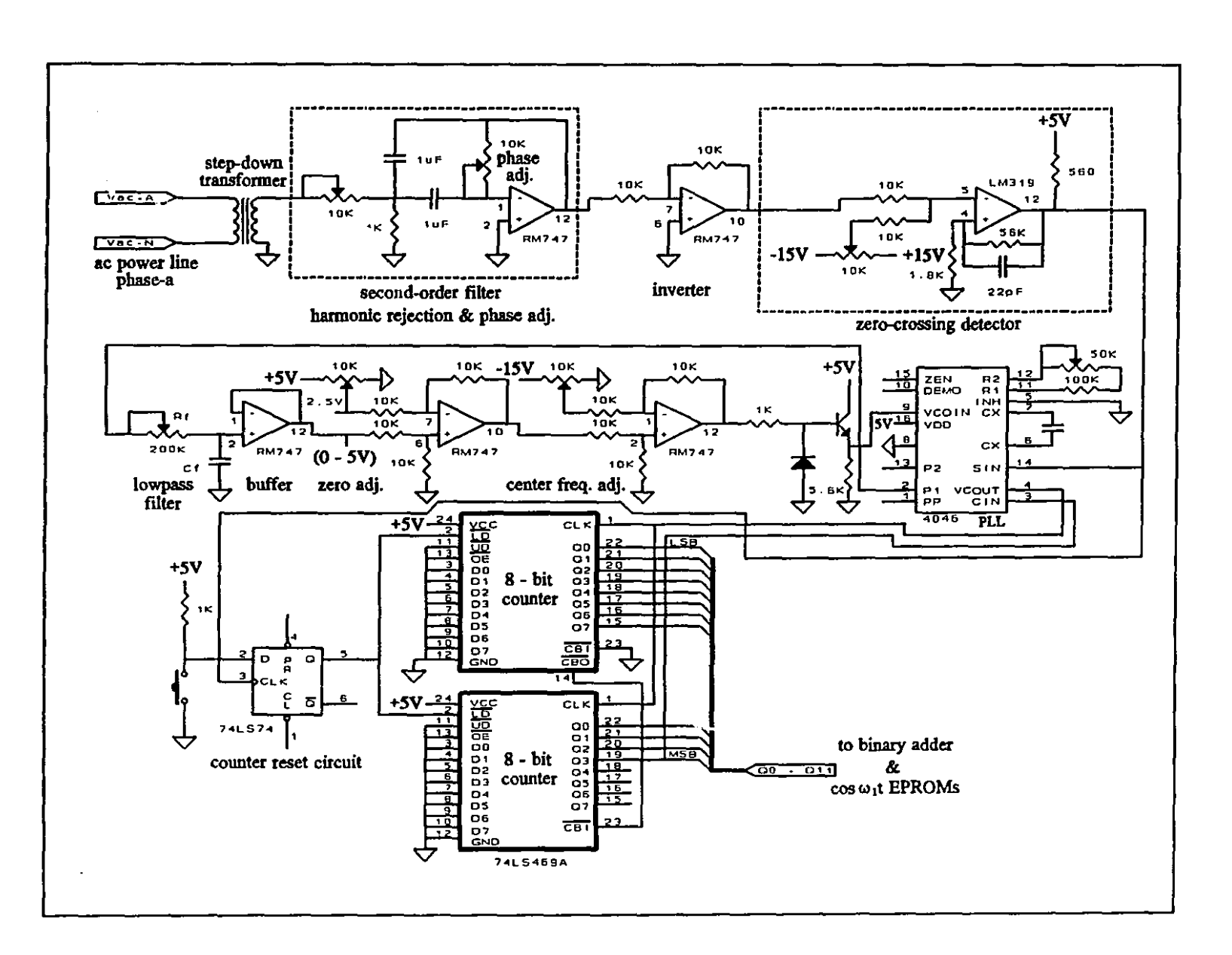




E.7 Synchronization Circuits

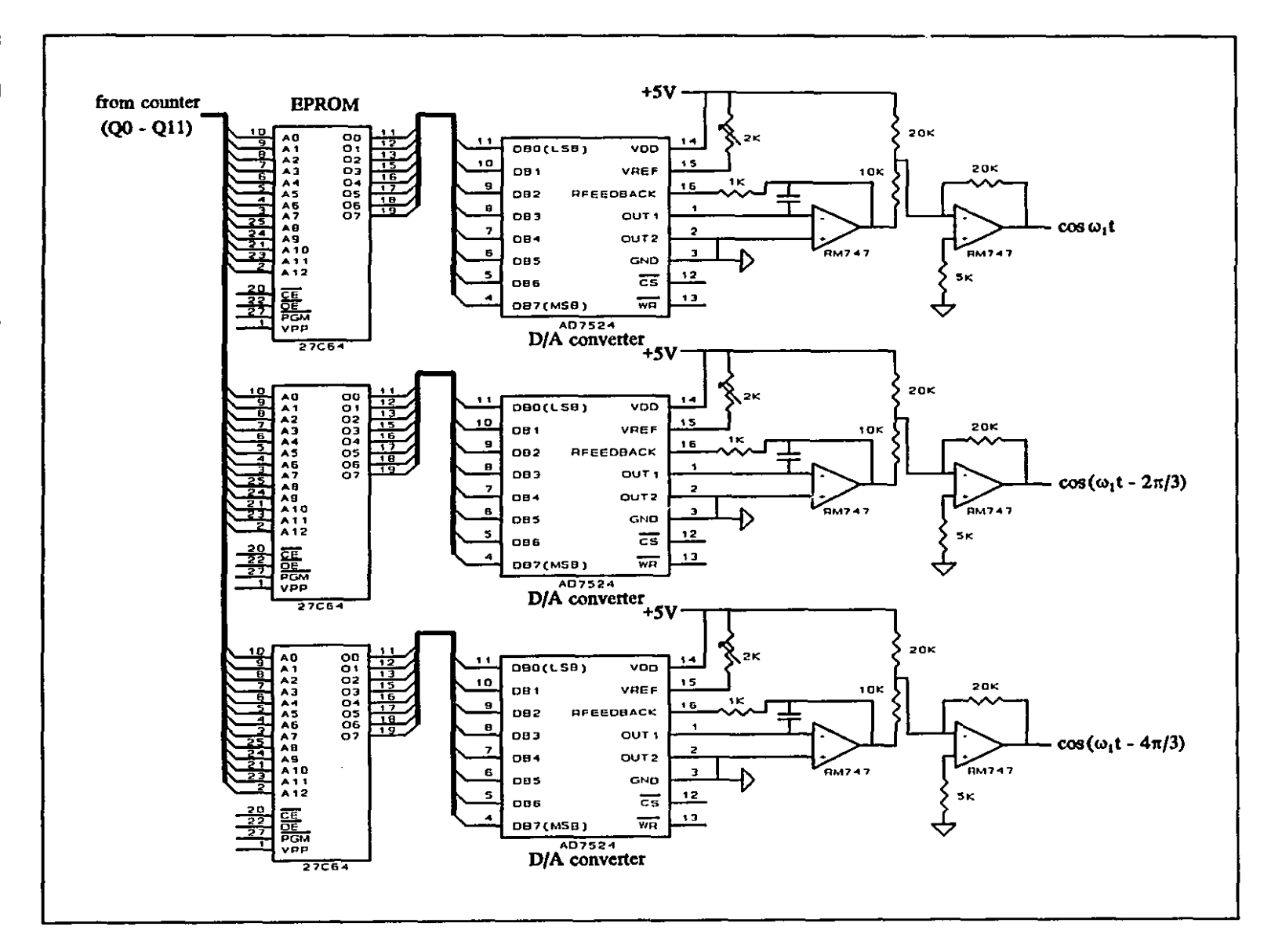
In order for the phase angle φ to be meaningful, a certain reference for the $\cos(\omega_1 t + \varphi + x)$ waveforms, $(x = 0, -2\pi/3, -4\pi/3)$, has to be specified. In the laboratory implementation, the side-1 source voltage e_{1a} has been chosen as the reference. It is assumed that $e_{1a} = E_{1m} \cos \omega_1 t$. In order to have a $\cos \omega_1 t$ -signal in phase with e_{1a} , the voltage e_{1a} has been stepped-down using a transformer, as shown in Fig. E-11. To compensate for the distortion and the phase angle introduced by the transformer, an adjustable second-order filter is used [83]. Then the digital synchronization signal is derived using a zero-crossing detector [83], the phase-lockedloop circuit is shown in Fig. E-11. The synch, signal just derived, and the MSB of the 12-bit counter are phase-compensated and the resulting signal goes through an R-C lowpass filter and the filtered signal is used as the VCO control signal which adjusts the CLK frequency of the counter to make the MSB of the counter have the same frequency as the synch. signal. There is a potentiometer for center-frequency adjustment which makes the MSB of the counter have the desired frequency ω_1 at VCO input equal to $V_{DD}/2$ [83].

The outputs of the 12-bit counter of Fig. E-11 are used as addresses for the EPROMs shown in Fig. E-12, in which full periods of waveforms of three-phase balanced cosine functions are stored. The EPROMS are followed by D/A converters



APPENDIX E IMPLEMENTATION OF ...

APPENDIX E



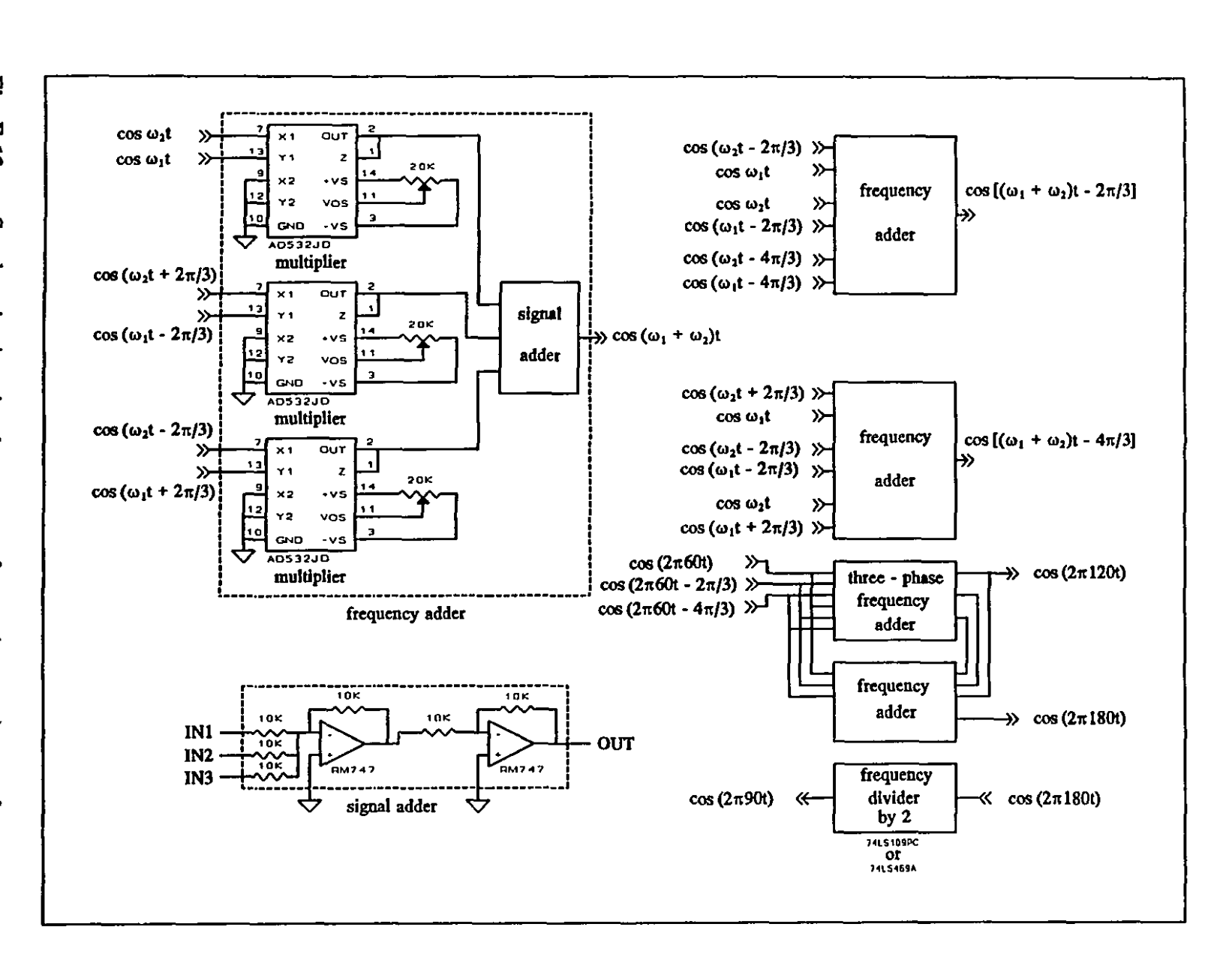
and the result is the waveforms $\cos(\omega_1 t + x)$, where $x = 0, -2\pi/3, -4\pi/3$. The $\cos \omega_1 t$ -signal can be made in phase with e_{1a} with the adjustment of the potentiometer named zero adj. in Fig. E-11. The outputs of the 12-bit counter of Fig. E-11 are also used in the binary adders of Fig. E-8.

In order for the angle γ to be meaningful, a reference for the $\cos[(\omega_1 + \omega_2)t + \gamma + x]$ waveforms, $(x = 0, -2\pi/3, -4\pi/3)$, should be specified. Using the $\cos(\omega_1 t + x)$ waveforms, $(x = 0, -2\pi/3, -4\pi/3)$, derived in Fig. E-12, and $\cos(\omega_2 t + x)$ waveforms, $(x = 0, -2\pi/3, -4\pi/3)$, the waveforms of $\cos[(\omega_1 + \omega_2)t + x]$, $(x = 0, -2\pi/3, -4\pi/3)$, can be derived as shown in Fig. E-13. Since in the laboratory implementation, three distinct side-2 frequencies: $f_2 = 30$, 60, and 120 Hz were of interest for testing purposes, the method of derivation of $\cos 2\pi 90t$, $\cos 2\pi 120t$, and $\cos 2\pi 180t$ is illustrated in Fig. E-13.

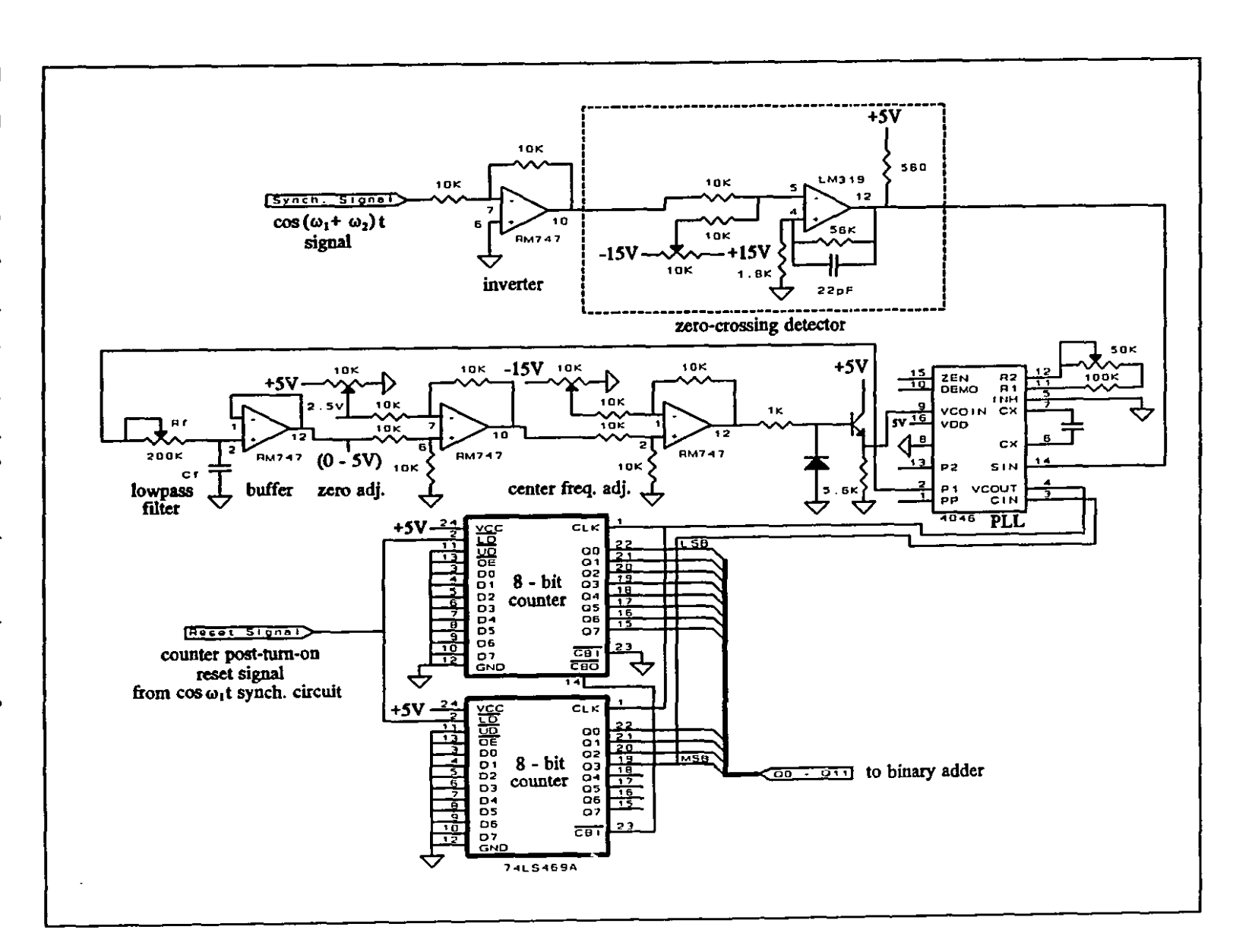
Finally, $\cos(\omega_1 + \omega_2)t$ -signal, derived in Fig. E-13, is used to synchronize the 12-bit counter of Fig. E-14 in the same way that was explained for the case of Fig. E-11. The outputs of the 12-bit counter of Fig. E-14 are input to the binary adders of Fig. E-9.



201



APPENDIX E



PARAMETERS OF THE SYSTEM OF FIG. 6-1

 E_{1r} = rms value of e_{1a} , e_{1b} , and e_{1c} = 10 V;

 $R_{s1} = 0, R_{s2} = 0.8 \Omega;$

 $L_{sI} = 0, L_{s2} = 6.6 \text{ mH};$

 $f_1 = 60 \text{ Hz};$

 $C = 50 \,\mu\text{F};$

 $R_2 = 2.42 \Omega;$

 $L_2 = 40 \text{ mH};$

 f_{i} = triangular carrier frequency = $21 \times f_{1}$ = 1260 Hz.

PARAMETERS OF THE SYSTEM OF FIG. 6-7

 E_{1r} = rms value of e_{1a} , e_{1b} , and e_{1c} = 10 V;

 $R_{sI} = 0, R_{s2} = 0.8 \Omega;$

 $L_{s1} = 0, L_{s2} = 6.6 \text{ mH};$

 f_1 = side-1 frequency = 60 Hz;

 $C = 50 \,\mu\text{F};$

 $R_2 = 1.86 \,\Omega;$

 $L_2 = 31.25 \text{ mH};$

 f_t = triangular carrier frequency = $21 \times f_1$ = 1260 Hz.

APPENDIX H

PARAMETERS OF TRANSFORMERS T_{aa}, ..., T_{cc}

$$L_o = 1.82 \text{ H } (X_o = 686.19 \ \Omega \ @ 60 \text{ Hz});$$
 $R_o = 9177.64 \ \Omega;$
 $L = 0.0045 \ \text{H};$
 $R = 0.28 \ \Omega;$
 $n_1/n_2 = 1;$

Rated Voltage = 220 V;

Rated Power = 1 kVA.

REFERENCES

- [1] L. Gyugyi and B.P. Pelly, "Static Power Frequency Changers: Theory, Performance, and Applications", New York: John Wiley & Sons Inc., 1976.
- [2] N. Mohan, T.M. Undeland, and W.P. Robbins, "Power Electronics: Converters, Applications, and Design", New York: John Wiley & Sons Inc., 1989.
- [3] S.I. Khan, P.D. Ziogas, and M.H. Rashid, "Forced Commutated Cycloconverters for High-Frequency Link Applications", *IEEE Trans. Ind. Appl.*, Vol. IA-23, No. 4, pp. 661-672, July/Aug 1987.
- [4] L.A. Hazeltine, "An Improved Method of and Apparatus for Converting Electric Power", British Patent No. 218.675, Jan. 4, 1926.
- [5] M. Schenkel, "Eine Unmittelbare Asynchrone Umrichtung für Niederfrequente Bahnnuetze", *Electric Bahnen*, No. 8, pp. 69-73, 1932.
- [6] Von Issendorff, "Der Gesteuerte Umrichter", Wiss. Veröff. Siemens, No. 14, pp. 1-31, 1935.
- [7] H. Rissik, "Mercury Arc Current Converters", Sir Isaac Pitman & Sons, 1935.
- [8] H. Rissik, "The Fundamental theory of Arc Converters", Chapman & Hall, 1939.
- [9] R.D. Jessee and W.J. Spaven, "Constant-Frequency AC Power Using Variable Speed Generation", *AIEE Trans. Appl. Ind.*, No. 78, Part II, pp. 411-418, 1959.
- [10] K.M. Chirgwin and L.J. Stratton, "Variable-Speed Constant-Frequency Generator System for Aircraft", *AIEE Trans. Appl. Ind.*, No. 78, Part II, pp. 304-310, 1959.
- [11] S.C. Caldwell, L.R. Peaslee, and D.L. Plette, "The Frequency Converter Approach to a Variable Speed Constant Frequency System", AIEE Conf.

- Paper, CP 60-1076, August 1960.
- [12] D.L. Plette and H.G. Carlson, "Performance of a Variable-Speed Constant-Frequency Electrical System", *IEEE Trans. Aerospace*, Vol. AS-2, pp. 957-970, April 1964.
- [13] D.A. Fisk, "VSCF for High Quality Electrical Power and Reliability", ASME

 Aviation and Space Division Conference Paper, June 16-19, 1968.
- [14] D.L. Lafuze, "VSCF Starter Generator", IEEE-PESC Conf. Rec., 1974.
- [15] C.J. Amato and R.B. Diczhazy, "Lower Order Distortion Terms in Frequency Converters", *IEEE Nat. Aerospace Elect. Conf. Rec.*, May 10-12, 1965, pp. 165-172.
- [16] C.J. Amato, "Sub-Ripple Distortion Components in Practical Cycloconverters", Suppl. IEEE Trans. Aerospace, pp. 98-106, June 1965.
- [17] R.A. Van Eck, "Frequency Changer Systems Using the Cycloconverter Principle", *IEEE Trans. Appl. Ind.*, pp. 163-168, May 1963.
- [18] A. Heck and M. Meyer, "A Static Frequency-Changer Fed Squirrel-Cage Motor Drive for Variable Speed and Reversing", Siemens Rev., No. 11, 401-405, Nov. 1963.
- [19] A. Schönung, "Varying the Speed of Three-Phase Motors by Means of Static Frequency Changers", *Brown Boveri Rev.*, Vol. 51, No. 8/9, pp. 540-554, 1964.
- [20] J.C. Guyeska and H.E. Jordan, "Cycloconverter Adjustable Frequency Drives", *IEEE Textile Ind. Conf.*, Oct. 1-2, 1964.
- [21] J.C. Guyeska and H.E. Jordan, "Static AC Variable Frequency Drive", Nat. Elect. Conf. Rec., 1964, Vol. 20, pp. 358-365.
- [22] M. Brown and W.T. Harvey, "A Variable Frequency Supply for Ind. Motors", Appl. Large Ind. Drives Conf. Rec., London, England, May 5-7, 1965, pp. 120-123.

- [23] L.J. Lawson, "Precisely Controlled Three-Phase Squirrel Cage Ind. Motor Drives for Aerospace Applications", Suppl. IEEE Trans. Aerospace, pp. 93-97, June 1965.
- [24] C.J. Amato, "Variable Speed with Controlledc Slip Induction Motor", *IEEE Ind. Static Power Conversion Conf. Rec.*, Nov. 1-3, 1965, pp. 181-185.
- [25] W. Slabiak and L.J. Lawson, "Optimizing Control Systems for Land Vehicles", *IEEE Ind. Static Power Conversion Conf. Rec.*, Nov. 1-3, 1965, pp. 186-189.
- [26] L. Abraham, J. Foster, and G. Schliephake, "AC Motor Supply with Thyristor Converters", *IEEE Trans. Ind. Gen. Appl.*, Vol. IGA-2, No. 5, pp. 334-340, Sep./Oct. 1966.
- [27] L.J. Lawson, R.P. Borland, and C.G. Puchy, "Optimal Control System Performance of an AC Electric Vehicular Wheel Drive", S.A.E. Trans., Vol. 75, pp. 672-680, 1967.
- [28] L.J. Lawson and W. Slabiak, "A Thyristor Drive for High Performance Land Vehicles", *Nat. Elect. Conf. Rec.*, 1966, Vol. 22, pp. 271-276.
- [29] P. Bowler," The Application of a Cycloconverter to the Control of Induction Motors", *Power Applications of Controllable Devices Conf.*, London, England, Nov. 10-11, 1965, IEEE Pub. No. 17, pp. 137-145.
- [30] W. Slabiak, "An AC Electric Individual Wheel Drive System for Land Vehicles", S.A.E. Trans., Vol. 75, pp. 664-671, 1967.
- [31] E. Reimers and C.J. Amato, "Performance Characteristics of a Controlled Slip Induction Motor Drive", (Abstract) *IEEE Pub. 34C36, IGA 1^{st.} Annual Meeting Conf. Rec.*, Oct. 3-6, 1966, Page 499.
- [32] E.A.E. Rich, "Concepts of Gearless Ball-Mill Drives", *IEEE Trans. Ind. Gen. Appl.*, Vol. IGA-5, No. 1, pp. 13-17, Jan./Feb. 1969.
- [33] E. Bläuenstein, "The First Gearless Drive for a Tube Mill", Brown Boveri Rev.,

- Vol. 57, No. 3, pp. 96-105, March 1970.
- [34] J. Langer, "Static Frequency Changer Supply System for Synchronous Motors Driving Tube Mills", *Brown Boveri Rev.*, Vol. 57, No. 3, pp. 112-119, March 1970.
- [35] H.U. Würgler, "The World's First Gearless Mill Drive", *IEEE Trans. Ind. Gen. Appl.*, Vol. IGA-6, No. 5, pp. 524-527, Sep./Oct. 1970.
- [36] H. Betz, "Neu-Ulm System -Tie Frequency Changer, An Installation for Supply to the German Federal Railway", *AEG-Telefunken Prog.*, No. 1, pp. 22-26, 1974.
- [37] E.R. Hill and C.L. Ivey, "Cycloconverter Powered Yankee Dryer", *IEEE Pulb and Paper Ind. Tech. Conf. Rec.*, 1974.
- [38] L. Gyugyi, "Power Frequency Changer with Controllable Input Displacement Factor", U.S. Patent No. 3,707,665, Dec. 26, 1972.
- [39] L. Gyugyi, "Unity Input Displacement Factor Frequency Changers", U.S. Patent Nos. 3,707,666 and 3,707,667, Dec. 26, 1972.
- [40] B.D. Bedford, "Versatile Cycloconverter Power Converter Circuit", U.S. Patent No. 3,742,336, June 26, 1973.
- [41] L. Gyugyi, "Static Power Conversion Arrangement and Method", U.S. Patent No. 3,858,105, Dec. 31, 1974.
- [42] L. Gyugyi, "Electrical Power Generating Arrangement and Method Utilizing an Induction Generator", U.S. Patent No. 3,832,625, Aug. 27, 1975.
- [43] L. Gyugyi, "Generalized Theory of Static Power Frequency Changers", Ph.D. Thesis, University of Salford, 1970.
- [44] B.R. Pelly, "Thyristor Phase-Controlled Converters and Cycloconverters", John Wiley & Sons, 1971.

- [45] W. McMurray, "The Theory and Design of Cycloconverters", The MIT Press, 1972.
- [46] M. Venturini and A. Alesina, "The Generalized Transformer: A New Bidirectional Sinusoidal Waveform Frequency Converter with Continuously Adjustable Input Power Factor", *IEEE-PESC Conf. Rec.*, 1980, pp. 242-252.
- [47] M. Venturini, "A New Sine Wave In, Sine Wave Out Conversion Technique Eliminates Reactive Elements", Seventh National Solid-State Power Conversion Conf. Rec., 1980, pp. E3-1-E3-15.
- [48] P.D. Ziogas, S.I. Khan, and M.H. Rashid, "Some Improved Forced Commutated Cycloconverter Structures", *IEEE Trans. Ind. Appl.*, Vol. IA-21, No. 5, pp. 1242-1253, Sep./Oct. 1985.
- [49] S. Miwazawa, F. Nakanura, and N. Yamada, "A New Method for Developing the Control Scheme of a CVVF Cycloconverter", *IEEE Trans. Ind. Elect.*, Vol. IE-33, No. 3, pp. 304-308, Aug. 1986.
- [50] G.M. Brown and B. Szabados, "A Flexible Hybrid-Firing Controller for Cycloconverter Devices", *IEEE Trans. Ind. Elect.*, Vol. IE-33, No. 3, pp. 297-303, Aug. 1986.
- [51] N.K. Sharda, R. Mulchandani, and R. Arochiasamy, "Microprocessor Control of Cycloconverter: Techniques for Implementation and Testing", *IEEE Trans. Ind. Elect.*, Vol. IE-33, No. 3, pp. 281-291, Aug. 1986.
- [52] L.A. Dessaint, H. Nakra, G. Olivier, and D. Mukhedkar,"A Multimicroprocessor-Based Controller for a Static Frequency Changer", IEEE Trans. Ind. Elect., Vol. IE-33, No. 3, pp. 292-296, Aug. 1986.
- [53] W.A. Hill and L. Mischke, "Control Strategy for an Icebreaker Propulsion System", *IEEE LAS Conf. Rec.*, 1989, Part I, pp. 692-698.
- [54] I. Kawaguchi, H. Ikeda, S. Kaga, Y. Ogihara, M. Matsukawa, and S. Tada,

- "Suppression of Harmonics Resonance Using Active Filter in Cycloconverter System", *International Power Electronics Conference (IPEC) Conf. Rec.*, 1990, pp. 809-816.
- [55] R. Hagmann, "AC-Cycloconverter Drives for Cold and Hot Rolling Mill Applications", *IEEE LAS Conf. Rec.*, 1991, Vol. II, pp. 1134-1140.
- [56] W.A. Hill, E.Y.Y. Ho, and I.J. Neuzil, "Dynamic Behavior of Cycloconverter System", *IEEE Trans. Ind. Appl.*, Vol. 27, No. 4, pp. 750-755, July/Aug. 1991.
- [57] H. Hakata, S. Tatara, R. Kurosawa, C.P. Lemone, and H. Hosoda, "Application Strategies for AC Rolling Mill Drives", *IEEE-LAS Conf. Rec.*, 1991, pp. 1141-1147.
- [58] S.I. Khan, M.H. Rashid, and P.D. Ziogas, "Analysis and Design of Improved Three to Single Phase Cycloconverter", *IEEE-IECON Conf. Rec.*, 1988, pp. 603-610.
- [59] P.D. Ziogas, S.I. Khan, and M.H. Rashid, "Analysis and Design of Forced Commutated Cycloconverter Structures with Improved Transfer Characteristics", *IEEE Trans. Ind. Elect.*, Vol. IE-33, No. 3, pp. 271-280, Aug. 1986.
- [60] A. Alesina and M. Venturini, "Analysis and Design of Optimum-Amplitude Nine-Switch Direct AC-AC Converters", *IEEE Trans Power Elect.*, Vol. 4, No. 1, pp. 101-112, Jan. 1989.
- [61] J. Oyama, T. Higuchi, E. Yamada, and T. Lipo, "New Control Strategy for Matrix Converter", *IEEE-PESC Cof. Rec.*, 1989, pp. 360-367.
- [62] N. Burány, "Safe Control of Four-Quadrant Switches", *IEEE LAS Conf. Rec.*, 1989, Part I, pp. 1190-1194.
- [63] L. Huber, D. Borojevic, and N. Burany, "Voltage Space Vector Based PWM Control of Forced Commutated Cycloconverters", *IEEE-IECON Conf. Rec.*,

- 1989, Vol. I, pp. 106-111.
- [64] C.L. Neft and C.D. Schauder, "Theory and Design of a 30-hp Matrix Converter", *IEEE Trans. Ind. Appl.*, Vol. 28, No. 3, pp. 546-551, May/June 1992.
- [65] L. Huber, D. Borojevic, X.F. Zhung, and F.C. Lee, "Design and Implementation of a Three-Phase to Three-Phase Matrix Converter with Input Power Factor Correction", I SE-APEC Conf. Rec., 1993, pp. 860-865.
- [66] A. Ishiguro, K. Inagaki, M. Ishida, S. Okuma, Y. Uchikawa, and K. Iwata, "A New Method of PWM Control for Forced Commutated Cycloconverters Using Microprocessors", *IEEE-IAS Conf. Rec.*, 1988, pp. 712-721.
- [67] G. Roy and G.E. April, "Direct Frequency Changer Operation Under a New Scalar Control Algorithm", *IEEE Trans. Power Electron.*, Vol. 6, No. 1, pp. 100-107, Jan. 1991.
- [68] A. Ishiguro, T. Furuhashi, and S. Okuma, "A Novel Control Method for Forced Commutated Cycloconverters Using Instataneous Values of Input Line-to-Line Voltages", *IEEE Trans. Ind. Elect.*, Vol. 38, No. 3, pp. 166-172, June 1991.
- [69] P. Tenti, L. Malesani, and L. Rossetto, "Optimum Control of N-Input K-Output Matrix Converters", *IEEE Trans. Power Electron.*, Vol. 7, No. 4, pp. 707-713, Oct. 1992.
- [70] L. Huber and D. Borojevic, "Space Vector Modulation with Unity Input Power Factor for Forced Commutated Cycloconverters", *IEEE IAS Conf. Rec.*, 1991, Vol. I, pp. 1032-1041.
- [71] D.G. Holmes and A. Lipo, "Implementation of a Controlled Rectifier Using AC-AC Matrix Converter Theory", *IEEE Trans. Power Electron.*, Vol. 7, No. 1, pp. 240-250, January 1992.

- [72] D.G. Holmes, "A Unified Modulation Algorithm for Voltage and Current Source Inverters Based on AC-AC Matrix Converter Theory", *IEEE Trans. Ind. Appl.*, Vol. 28, No. 1, pp. 31-40, Jan./Feb. 1992.
- [73] W.H. Kwon and G.H. Cho, "Analysis of Static and Dynamic Characteristics of Practical Step-Up Nine-Switch Matrix Converter", *IEE Proceedings-B*, March 1993, Vol. 140, No. 2, pp. 139-146.
- [74] L.A. Zadeh and C.A. Desoer, "Linear System Theory", McGraw Hill, 1963.
- [75] H.K. Messerle, "Dynamic Circuit Theory", Pergamon Press, 1965.
- [76] B.K. Bose, "Power Electronics and AC Drives", pp. 307-313, Prentice-Hall, 1986.
- [77] D.W. Novotny and R.D. Lorenz, "Introduction to Field Orientation and High Performance AC Drives", IEEE IAS Conf. Tutorial Course, 1986.
- [78] B.T. Ooi, S.Z. Dai, and X. Wang, "Solid-State Series Capacitive Reactance Compensators", *IEEE Trans. Power Delivery*, Vol. 7, No. 2, pp. 914-919, April 1992.
- [79] M. Kazerani and B.T. Ooi, "Direct AC-AC Matrix Converter Based on Three-Phase Voltage-Source Converter Modules", *IEEE-IECON Conf. Rec.*, 1993, Vol. II, pp. 812-817.
- [80] M. Kazerani and B.T. Ooi, "Feasibility of Both Vector Control and Displacement Factor Correction by Voltage-Source Type AC-AC Matrix Converter", *IEEE-IECON Conf. Rec.*, 1994, Vol. 1, pp.434-439.
- [81] B.T. Ooi and M. Kazerani, "Application of Dyadic Matrix Converter Theory in Conceptual Design of Dual Field Vector and Displacement Factor Controls", IEEE-IAS Conf. Rec., 1994, Vol. II, pp. 903-910.
- [82] J.W. Dixon, "Boost Type PWM Rectifiers for High Power Applications", M.Eng. Thesis, McGill University, June 1988.

[83] X. Wang, "Advances in Pulse Width Modulation Techniques", Ph.D. Thesis, McGill University, March 1993.